Effect of Rare-earth Doping on Structural, Magnetic and Electric properties of Transition Metal Ferrite Nanoparticles

A THESIS SUBMITTED IN PARTIAL FULFILLMENT FOR THE DEGREE OF

DOCTOR OF PHILOSOPHY

In

SCHOOL OF PHYSICAL AND APPLIED SCIENCES

GOA UNIVERSITY

By

Mr. MANOJ D. SALGAOKAR

School of Physical and Applied Sciences

Goa University

Goa-403206

September 2023

Effect of Rare-earth Doping on Structural, Magnetic and Electrical properties of Transition Metal Ferrite Nanoparticles

A THESIS SUBMITTED IN PARTIAL FULFILLMENT FOR THE DEGREE OF

DOCTOR OF PHILOSOPHY

In

SCHOOL OF PHYSICAL AND APPLIED SCIENCES

By

Mr. MANOJ D. SALGAONKAR

PROF. R. S. GAD

RESEARCH GUIDE

School of Physical and Applied Sciences

Goa University

Goa-403206

September 2023

DECLARATION

I, Manoj Demu Salgaonkar hereby declare that this thesis entitled **"Effect of Rare-earth Doping on Structural, Magnetic and Electrical properties of Transition Metal Ferrite Nanoparticles"** represents the work carried out by me and that it has not been submitted, either in part or full to any other University or Institution for the award of any research Degree.

Place: Taleigao Plateau, Goa. Mr. Manoj Demu Salgaonkar

Date: 21 - 09 - 2023 (Candidate)

CERTIFICATE

I hereby certify that the above Declaration of the candidate, Manoj Demu Salgaonkar is true and the work carried out under my supervision.

Prof. R. S. Gad
Research Guide
School of Physical and Applied Sciences,
Goa University, Goa.

ACKNOWLEGEMENT

I wish to express my sincere gratitude to my guiding teacher, Prof. Rudraji B. Tangsali (former Guide) and Prof. Rajendra S. Gad for introducing a current research topic of ferrite nanoparticles and encouraging me to pursue research work. The continuous guidance provided during my entire research period comprising of time span in experimental work and data analysis immensely helped me in achieving the set goals and logical conclusions.

I express my deepest gratitude to my Prof. Rudraji B. Tangsali for encouraging, enlightening with words of motivation, immense support and timely suggestion offered by him during my research period.

I also express my gratitude to my Prof. Rajendra S. Gad for continuous support, encouragement and valuable suggestion during my research period.

I am thankful to Prof. Ramesh Pai, SPAS, Goa University for his valuable suggestion and continuous evaluation. I extend thanks to Prof. Uma Subramanian, SPAS, Goa University for suggestion and evaluation.

I am grateful to Dr. Pranav P. Naik, Assistant Professor at SPAS, Goa University for his Co-operation and valuable guidance in analyzing the experimental data.

I thank

1. All the teaching and non-teaching staff of SPAS, Goa University for their co-operation and facilities throughout my research work.
2. Prof. V.M.S. Verenkar and research scholars Dr. Prajyoti Gauns Dessai, Ms. Mangala Sawal from School of Chemical and Applied Sciences, Goa University for extending immense help in VSM and AC Susceptibility facilities, for my research experiments.
3. Dr. Sunil Kumar Singh, Director of NIO, Dauna-paula, Goa and Mr. Girish Prabhu for availing x-ray diffraction (XRD) facility.

4. Dr. M. Ravichandran, Director of NCAOR , Vasco - da-Gama and Ms Sahina Gazi for availing Scanning Electron Microscope (SEM) facility.

I thank Mr Rajendra V. Kanekar , my teacher, mentor and adviser. I am greateful to my senior researchers Dr. Girish Kundaikar, Dr Manoj Kotwale, Dr. Jaison Joseph for their support and suggestions during my research period.

I thanks all my research colleagues Dr. Elain dias, Dr. Manjunath Nayak, Dr. Bhargav Alvani, Dr. Kapil Y. Salkar, Dr. Vaishali Gaonkar Dessai, Chetana Gaonkar, Dr. Rukma Nevgi, Samiksha Malik, Dr. Jeyakanthan, Mr. Santhosh kumar Bandaru, Mr. Pravin kumar Pinapati, Mr. Yatin Dessai for all happy moments during my research period.

I like to thanks my colleagues at St. Xavier's College, Dr. Nelson Lobo, Dr. Benedict Soares, Dr. Bosco Lawrence, Mr. Pradeep V. Morajkar and Mrs. Avani Talkatkar for their kind support in academics activities during my research period.

I thank God for helping me to keep cool temperament, positive attitude and showering blessings on me. Last but not the least, I wish to thanks my parents, Wife, Son and my friends being patients with me during the period of my research.

THANK YOU All

Mr. Manoj D. Salgaonkar

Dedicated to my Father

Late Shri Demu Keshav Salgaonkar

&

My family and well wishers

LIST OF ABBREVIATION

nm	nanometer
STM	Scanning Tunneling Microscope
DMS	Dilute Magnetic Semiconductor
AC	Alternating Current
DC	Direct Current
BE	Binding Energy
EMF	Electromotive Force
MRI	Magnetic Resonance Imaging
YIG	Yttrium Iron Garnet
FTIR	Fourier Transform Infrared Spectroscopy
EDS	Energy Dispersive Spectroscopy
RF	Radio Frequency
REE	Rare Earth Element
SD	Single Domain
MD	Multi Domain
SP	Super Paramagnetism
NTA	Nitrilo Triacetic Acid
RT	Room Temperature
ZFC	Zero Field Cooled
FC	Field Cooled
RKKY	Ruderman -Kittle- Kasuya-Yoshida

TABLE OF CONTENTS

LIST OF TABLES

LIST OF FIGURE

CHAPTER 1

PREFACE

1.1 Introduction

In recent years, the research trends have been focused on nanoscience and nanotechnology due to its immense potential and wide applications in almost all the fields of science and technology. Nanoscience promises in near future many breakthroughs that will bring revolution in the field of technology advances in the different areas of applications. Some applications are in use, some of them are in developing stage and some will take time to reach in the hands of end users. There are challenges before the technologist to develop suitable tools and hardware that will meet the requirements of nano level research. The materials with nanostructures are the nanomaterials having nanoscale dimensions i.e. between 1nm to 100 nm. If one of the dimension of a three dimensional structure falls in the range of nano scale, the structure is known as a quantum well and two of the dimensions are at nano scale are called as a quantum wire. The structure is a quantum dot for all three dimensions in nano range [1, 2]. The properties observed in nanomaterials are different as compared to the bulk materials [3]. In nano materials, the reduction in the size of the material has broken the size barrier below which the quantisation of energy for the electrons is relevant. Even for the reduction of size of a material from macro to micro level the quantisation effect is not dominant but when size of nano range is reached, the effect becomes dominant.

These materials show different properties as compared to what they show on macro scale. The second effect is, as the size of the material is reduced the relative surface area becomes larger. The material structure changes drastically that result into increase in catalytic activity and chemical reactivity. These are the two effects that are dominant at the nanoscale and responsible for novel applications [4, 5].

Nanoscience is the study of phenomena and manipulation of material at the nanoscale and is an inter disciplinary field that focuses on the nanoscale blending of fields such as physics, chemistry, biology, engineering, computer science and more. It is the world of atoms, molecules, macromolecules, quantum dots and macromolecular assemblies that is governed by surface and quantum effects. The nano materials are synthesised either by way of a top down approach or a bottom up approach. In top down approach is one in which bulk material size is reduced to nanoscale level where as in bottom up approach larger structure is grown by atom by atom or molecule by molecule [6].

The great physicist Richard Feynman was the first to put forward the concept of 'Nano-technology' in his talk "There is plenty of room at the bottom" at an American Physical Society meeting at Caltech on December 29, 1959. Further he described a process byaz which the ability to manipulate individuals atoms and molecules might be developed, using one set of precise tools to build and operate another proportionality smaller set, so on, down to the needed scale [6]. Tokyo Science University Professor Norio Taniguchi defined the term of nano-technology as "Nano-technology mainly consists of the processing, separation, consolidation, and deformation of materials by one atom or one molecule". Later these ideas were explore by Dr.Eric Drexler, who promoted the technological significance of nano-scale phenomena and devices through his talk and his books. The invention of the scanning tunnelling microscope (STM) and cluster science in the year 1980's made the beginning of nanotechnology and Nanoscience. This development resulted in the discovery of fullerenes in 1986 and followed by carbon nanotubes, the synthesis and properties of semiconductor nano-crystal and metal oxides nanoparticles of quantum dots. The nanotechnology applications in the field of medicine are diagnostics, cancer-killing micro-bubbles, drug delivery, tissue engineering, etc. The other fields are filtration, reduction of energy consumption, solar cells, recycling of batteries catalysis, semiconductor and optoelectronic devices displays, quantum computers, aerospace, construction, nano-coatings, household, optics, textiles, agriculture, sports etc [7].

1.2 Origin of Magnetic Material

Magnetic materials are present all around us. Magnetic materials are widely used in variety of technological applications such as power generation, communication sensors, data storage and retrieval etc. The field of magnetism was developed mainly due to the efforts and dedication of many people's who contributed for the understanding of the basic of this phenomenon. The term magnetism came into existence in 470 B.C. The Greeks found that some kind of stones shows unusual property to attract iron pieces. These stones were called loadstone and have chemical formula Fe_3O_4. Later, William Gilbert produced artificial magnets by rubbing iron pieces against loadstones but recognition was received when first electromagnet was made soon after the discovery of Hans Christian Oersted that an electric current produces magnetic field [8, 9].

In present technology progress, the magnetic material finds lot of applications. The suitability of a magnetic material for particular application depends on the magnetic properties such as magnetization, coercivity, and remanence. The permanent magnet, hard ferrites, rare earth dope transition metal ferrite like Sm-Co ferrite, Nd-Fe-B ferrites find different industrial applications. Soft magnetic materials having high saturation magnetization, permeability and low energy dissipation are used in electrical engineering for production, transportation and usage of electrical energy. The soft magnets also find use in telecommunication and electronics [10, 11]. Magnetic materials are used in wide variety of applications such as data storage in audio and video tapes, digital data storage in ferrite memory core, hard disc, floppy disc etc. The recent advances in the magnetic materials are towards advance technologies such as Giant magneto-resistive materials, Diluted Magnetic semiconductor (DMS). The DMS are the class of materials usually used in spintronics, microelectronics where in both spin and charges on electron are utilized [12, 13]. Based on the type of semiconductor compound used for spintronics materials could produce devices that can perform functions such as storage, detection, logical and communication capabilities on single matrix as a multifunctional device. Due to the multifunction capability of DMS materials [14], they are attracted by many researchers. Thus, the magnetic materials are essential part of revolution and will play leading role in the forthcoming technologies. Ferrite nanoparticles, comprised of diverse metal oxide compounds, particularly iron oxides (Fe_3O_4 and γ-Fe_2O_3), and have garnered significant attention across diverse domains due to their distinct characteristics and promising potential applications. Ferrite nanoparticles exhibit robust magnetic traits arising from their inherent composition.

These nanoparticles can be facilely manipulated through external magnetic fields, rendering them beneficial in endeavours such as magnetic separation, targeted drug delivery, and the formulation of contrast agents for magnetic resonance imaging (MRI). The potential of ferrite nanoparticles in environmental remediation has been explored. They can effectively eliminate contaminants from water and soil through processes like adsorption or catalytic degradation, thereby contributing to the amelioration of pollution issues.

1.3 Magnetic Properties in the Materials

The matter is made up of atoms which in turn consist of protons, electrons and neutrons. Electrons have motion around the nucleus with constant speed and carry a negative electrical charge. The motion of an electron produces magnetic field and the strength of this field is called magnetic moment of the electron. The magnetism in the material arises due to the spin and orbital motion of the electrons in the atom. These motions of electrons give rise to spin and orbital magnetic moment. The magnetic behaviour of the materials are decided by magnetic parameters such as magnetic field (H), magnetic fluxdensity (B), susceptibility (χ) and is measured using magnetic quantity calledmagnetization (M). The relations between the magnetic quantities are given in equation 1.1, 1.2 and 1.3 below.

$$B = \mu o\ \bar{H}+M \tag{1.1}$$

$$M = \chi\mu o\ \bar{H} \tag{1.2}$$

$$\chi = \bar{M} / \bar{H} \qquad 1.3$$

The constant μo is called the permeability in free space and Susceptibility (χ) is defined as magnetization per unit magnetic field.

1.3.1 Classification of Magnetic Materials

The material can be classified into different categories depending on the values and order of susceptibility.The types of ordering moments are shown in figure 1.1. The nature of material can be Diamagnetic, Paramagnetic, Ferromagnetic, Anti-Ferromagnetic, Ferrimagnetic, Super-Paramagnetic [8].

1.3.1.1 Diamagnetic

The material in which atom or ion has only paired electrons, the total magnetic moments becomes zero as added spin and orbital moment's acts as the nullifier. The susceptibility for such material is negative. Examples of some diamagnetic materials are copper, silver, gold, zinc, mercury [15].

1.3.1.2 Paramagnetic

The material in which atom or ion has one or more unpaired electrons, possesses a magnetic moment. There is no interaction between adjacent magnetic moments; the interaction is with the external magnetic field and has a small positive value of susceptibility which follows curie law. Here calcium, sodium, aluminium, magnesium are some of the examples of paramagnetic materials [15]. The susceptibility is inversely proportional to temperature and given by equation 1.4.

$$\chi = \frac{C}{T} \qquad 1.4$$

Where T is the absolute temperature and C is called curie constant. The variation of susceptibility with temperature is as shown in fig.1.1

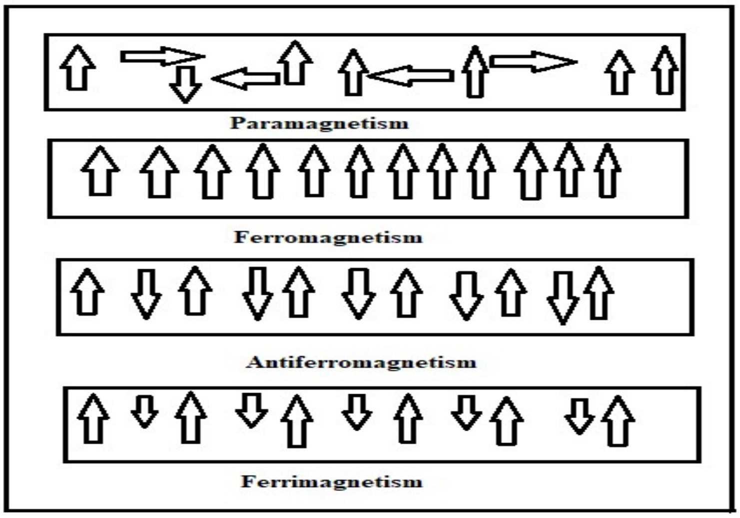

Fig.1.1: various types of ordering magnetic moments

1.3.1.3 Ferromagnetic

There is a strong interaction between adjacent magnetic moments which tends toaligned them parallel to one another, such material has a large positive value of susceptibility. At above certain critical temperature called Curie temperature ferromagnetic material become paramagnetic and follows Curie- Weiss law. The magnetic moments are ordered below and above Curie temperature show paramagnetic character since it losses magnetic ordering [16]. Examples of ferromagnetic materials are Fe, Co and Ni. The other elements are alloys employing transition metal or rare elements are ferromagnetic due their incomplete 3d and 4f shells. The variation of susceptibility with temperature is as shown in fig.1.2 (b).

1.3.1.4 Anti-ferromagnetic

If the interaction between neighbouring magnetic moments may lead to an antiparallel alignment resulting in a vanishing of a moment at 0 K. Above a certain temperature called Neel temperature, the material becomes paramagnetic and follow the Curie – Weiss law [8]. Examples are MnO, Nio, FeO etc. The variation of susceptibility with temperature is as shown in fig.1.2 (c)

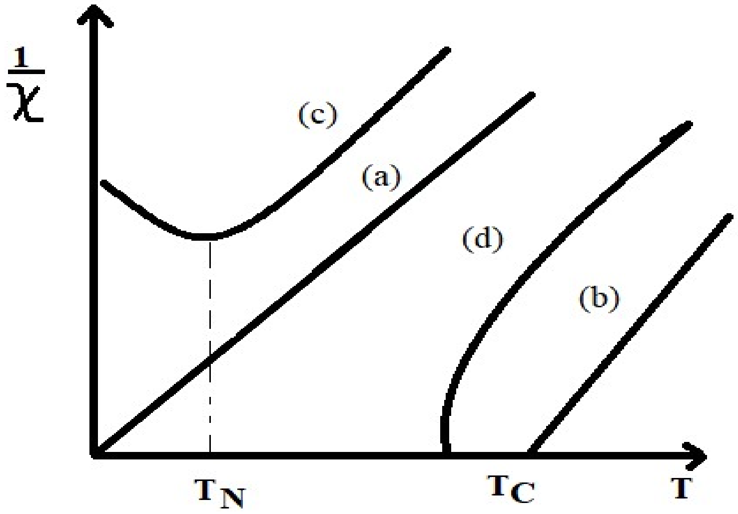

Fig.1.2: Variation of inverse susceptibility verses temperature for (a) Paramagnetic, (b) Ferromagnetic, (c) Anti-ferromagnetic and (d) Ferrimagnetic.T_N and T_C Neel and Curie temperature respectively.

1.3.1.4 Ferrimagnetic

The materials exhibit spontaneous magnetization due to antiparallel alignment between two magnetic sub-lattices. The net magnetization may be due to the two sublattice are of different types with different number of magnetic ions or the two sublattice of different crystallographic sites, also may be occupied either by the same type or different types with different number of magnetic ions. Above certain temperature called Neel temperature, a ferrimagnetic material becomes a paramagnetic material and the temperature i. Examples of ferrimagnetic materials are $NiFe_2O_4$, $CoFe_2O_4$, Fe_3O_4 etc. The variation of susceptibility with temperature is as shown in fig.1.2 (d)

1.4 Materials Studied in the Present Work

The studies deals with three different types of rare- earth elements doped with cobalt ferrites. The rare earth elements are Neodymium, Gadolinium and Dysprosium. The structural aspects, magnetic and electrical properties of these materials have been studied. The work deals with understanding of structural changes, alteration of magnetic and electrical properties of rare earth elements substituted in cobalt ferrites. The work has been discussed in chapter 4, 5 and 6 in details.

1.4.1 Ferrites

Ferrites are the class of ceramic materials that are composed of iron oxide (Fe_2O_4) combined with one or more other metallic oxides. Magnetite or ferrous ferrites is naturally occurring ferrites. They are known for their unique magnetic properties that find wide range of applications in electronic devices and industries. Ferrites are classified as hard or soft, depending on their magnetic characteristics. Hard ferrites have high coercivity i.e. it retain magnetization even in the absence of an external magnetic field. Hence used in permanent magnets, magnetic recording media, microwave devices etc. It is known as ceramic magnets since exhibit high resistance to demagnetization and can be operated for wide range of temperatures. In the case of soft magnets, they have low coercivity, which means it can be easily magnetized and demagnetized. They are used in transformers, inductors, electromagnetic interference suppression devices and high frequencies applications. Ferrites posses several desirable properties like high electrical resistivity, good thermal stability and corrosion resistance which are suitable for the applications in telecommunications, power electronics, data storage, magnetic sensors etc.

1.4.2 Classification of Ferrites

Ferrites are classified based on various factors such as composition, crystal structure, magnetic properties, applications etc. Ferrites can be classified namely into three main classes i.e. Spinel ferrites, Hexa ferrites and Garnet type ferrites. The classifications are also depending on cations distribution to these crystal structures that brings alteration in their properties.

1.4.2.1 Spinel Ferrites

In spinel ferrites, the general formula is represented as AB_2O_4, where A and B represent different metal ion [18]. The A is a tetrahedral site occupied by divalent metal ions such as nickel (Ni), cobalt (Co), and zinc (Zn) while the B is octahedral site occupied by trivalent metal ions like iron (Fe), aluminium (Al) [19]. The oxygen ions fill in the space between the metal ions. The crystal structure of spinel ferrites consist of cubic lattice with oxygen ions forming an orderly arrangement [20]. The A site ions are formed by four oxygen ions and B site ions are surrounded by six oxygen ions. This arrangement creates a spinel structure.

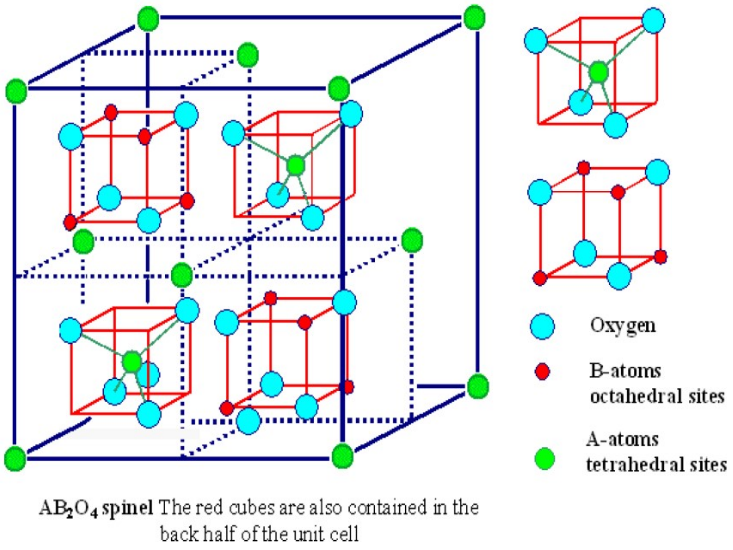

Fig1.3: Spinel structure of unit cell shows the tetrahedral sites and the octahedral site [17]

1.4.2.2 Spinel Ferrites Classification

Spinel ferrites can be further classified based on the composition of the metal occupying the A and B sites. The variety of metal ions and composition can be used to modify the properties of spinel ferrites for a wide range of applications such as magnetic devices, electronics, telecommunications, etc [2, 21-22]. The classifications of spinel ferrites are

- Normal Spinel Ferrites

In these ferrites, The A-site is occupied by divalent metal ions such as Mg^{+2}, Zn^{+2}, Mn^{+2}, etc and the B-site is occupied by trivalent metal ions like Fe^{+3}. Examples include magnesium ferrites ($MgFe_2O_4$), Zinc ferrites ($ZnFe_2O_4$), etc [1, 8, 23].

- Inverse Spinel Ferrites

In these ferries, The A-site is occupied by trivalent metal ions like Fe^{+3}, Al^{+3} and the B-site is occupied by a mixture of divalent and trivalent metal ions such as Fe^{+2}/Fe^{+3}.examples includes nickel zinc ferrites ($Ni_{0.5}Zn_{0.5}Fe_2O_4$), aluminium ferrites($AlFe_2O_4$) [1, 8 ,23].

- Mixed Spinel Ferrites

These ferrites are composed of a mixture of different metal ions at both the A and B sites with a general formula of $A_{1-x} B_xFe_2O_4$ The composition can be varied to suit the properties of the ferrite for specific applications. The nickel manganese ferrite ($NiMFe_2O_4$), cobalt zinc ferrites ($Co_{0.5}Zn_{0.5}Fe_2O_4$) are the examples of mixed ferrites [1, 8, 23].

1.4.2.3 Hexa Ferrites

These ferrites are known as hexagonal ferrites or ferrite magnets and are a specific class of ferrites materials that have a hexagonal crystal structure. They are composed of iron oxide (Fe_2O_4) combined with other metal oxides like barium (Ba) or strontium (Sr). They are known for their excellent magnetic properties like high coercivity and are used in wide variety of applications. The hexa ferrites are represented by the general formula

$MFe_{12}O_{19}$, where M represents divalent metal ions like barium (Ba), Strontium (Sr), lead (Pb). The properties and characteristics of hexa-ferrite depend on the specific metal ion used in the formula. The hexa-ferrites crystal structure often referred as magneto-plumbite structure. These crystal structures are the alternating layers of Fe^{+3} and O^{-2} ions with former ions occupy tetrahedral and octahedral sites within the crystal lattice. The examples includes like barium hexa-ferrite ($BFe_{12}O_{19}$), strontium hexa-ferrite ($SrFe_{12}O_{19}$), lead hexa-ferrite ($PbFe_{12}O_{19}$). They possess excellent magnetic properties which are useful in the applications where high magnetic performance and resistance to demagnetization are required. They show high magnetic anisotropy, chemical stability, coercivity, remanence and good temperature stability. They find widespread use in various applications like permanent magnets, microwave devices, magnetic recording and other technological fields where strong magnetic materials are required.

1.4.2.4 Garnet-type Ferrites

Also known as garnet ferrites are a class of ferrites materials that exhibit a crystal structure similar to that of natural garnets. It consist of iron oxide (Fe_2O_3) combined with other metal oxides such as yttrium(Y), aluminium (Al) or gadolinium (Gd). Some common types of garnet-types ferrites are yttrium iron garnet (YIG). The chemical formula is $Y_3Fe_5O_{12}$. The YIG is characterized by its high electrical resistivity and unique magnetic properties such as low magnetic damping, high magnetic permeability. They are used in various fields such as microwave devices, magnetic sensors, magneto-optical devices and telecommunications.

1.4.3 Cobalt Ferrites

Now a day's Spinel ferrites are of great importance to the fundamental science as it addresses relationship between a crystal structure and its magnetic properties. Crystal chemistry shows that the chemical formula; internal structure and physical properties are interrelated to one another. Among a spinel ferrite, cobalt ferrite has emerged as a most promising material due to its properties like mechanical hardness, high coercivity, excellent chemical stability, high magneto crystalline anisotropy and moderate saturation magnetization [25, 26]. Cobalt ferrite has face centre cubic structure and belonging to Fd3m space group [27, 28] with two sub-lattices inter-penetrating. The two sub-lattices are tetrahedral A site, octahedral B site and exhibits inverse spinel structure.

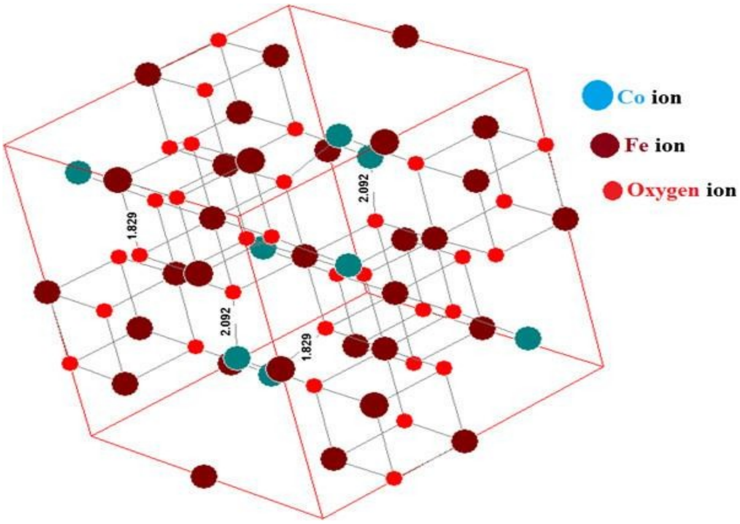

Fig.1.4: unit cell of cobalt ferrite [24]

Cobalt ferrite has face centre cubic structure and belonging to Fd3m space group [27, 28] with two sub-lattices inter-penetrating. The two sub-lattices are tetrahedral A site, octahedral B site and exhibits inverse spinel structure. The magnetic properties depend on the Co^{+2} ions and the distribution of cations between A and B sites. The preparation method, ionic radius, is responsible for cation distribution between A and B sites. The composition, methods of preparations, particle size, morphology, exchange interaction between tetrahedral site and octahedral site are the factors responsible for alteration of the properties of cobalt ferrites [2, 29, 30]. Cobalt ferrites find applications in a wide range of fields due to its unique magnetic properties such as magnetic storage media in the production of magnetic tapes and disk drives [31], magnetic sensors like gas sensors and magnetic field sensors [32-34], catalysts in chemical reactions due to their magnetic and structural properties, biomedical applications like drug delivery systems [35, 36], hyperthermia, cancer treatment, etc.

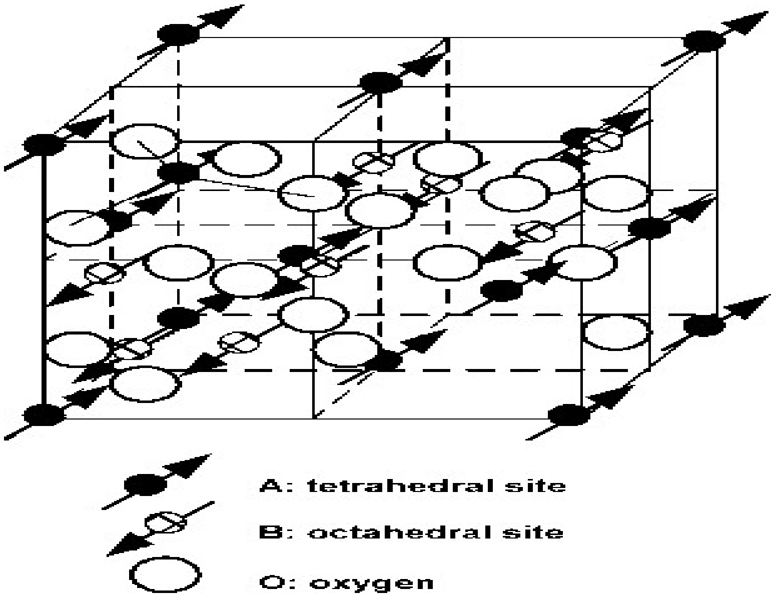

Fig.1.5: Spin structure of the cobalt ferrite [37]

1.4.4 Rare Earth Elements

Rare earth elements (REEs) are a group of 17 chemical elements in the periodic table. The lanthanides series consist of 15 elements from lanthanum to lutetium and other two elements as scandium and yttrium. The name rare earth elements, they are not actually rare in the earth's crust but they are widely dispersed and found in low concentrations mixed with other elements, making their extraction and recovery challenging. Hence they are found in a few countries around the world. Rare earth exhibit unique properties like a magnetic, luminescent, catalytic, high temperature characteristics. Rare earth have diverse applications in modern technology that include permanent magnets in electric motors, generators, hard disk drives, magnetic resonance imaging (MRI) machines, electronics devices, lighting devices such as energy efficient fluorescent lamps, compact fluorescent lamps (CFLs) and as light emitting diodes. They are also used as catalyst in industrial processes like petroleum refining, automotive exhaust systems and for the defence aerospace equipment like missile guidance system, radar system and communication devices.Rare earth is the special class of materials due to its 4f electrons and when doped with spinel ferrites alter the properties of the material [38].

1.4.5 Rare Earth Doped Ferrites

Rare earth elements are good Electrical insulators with high Electrical resistivity. Different workers have tried different ideas to enhance the performance of Ferrites materials. One of the popular ideas is, doping the ferrite material with rare earth ions of different types. By Synthesing rare earth dope ferrites affects the structural disorder and lattice strain of the ferrite material, thereby increasing the electrical and magnetic parameters [39, 40]. The concentration of rare earth in doped ferrites play important role to describe the electrical and magnetic properties of ferrites [41], 4fn electronic state of rare earth is responsible for these characteristics [42]. The electrical conductivity and the magnetic properties of ferrites are governed by the Fe – Fe interaction (spin coupling of the 3d electrons). By introducing rare earth ions into a spinel lattice, the RE-Fe interaction appears (3d – 4f coupling), responsible for change in behavior of these ferrites. The electron configuration f^0 (f- orbital are unoccupied), f^7 (half of the f- orbital are occupied) and f^{14} (f- orbital are occupied) of REE's are considered as more stable than the other configurations.

1.5 Literature survey

In depth review of large number of papers are available in the subject area shows that most of the works carried out have prepared the materials using Sol-gel method, co-precipitation method, citrate precursor technique, micro-emulsion method and plasma synthesis method [43- 50][26-33]. The researchers have done investigative studies on electrical and magnetic properties of these materials.

S. Burianova et. al. studied Surface spin effects in La-doped $CoFe_2O_4$ nanoparticles prepared by micro-emulsion route and found that doped particles are 5 nm in diameter where as the undoped nanoparticles are 26 nm using the similar preparation method. The coercivity values strongly depend on particle size. The surface effects in the La-doped samples are confirmed by Mossbauer spectroscopy [51]. The investigation to improved electrical and dielectric properties of La-doped Co ferrite is done by K. Bharathi et.al. [52]. It is found that the $CoFe_{1.925}La_{0.075}O_3$ indicates the cubic inverse spinel phase with a small amount of $LaFeO_3$ as an additional phase. Temperature dependent of electrical resistivity indicates two distinct regions which have two types of conduction mechanism i.e. the small polaron and variable-range hopping mechanisms are operative in the 220 to 300 K and variable-range hopping mechanisms 160 K to 220 K temperature regions respectively. The lattice parameters, dielectric constant and resistivity show higher value for doped cobalt ferrite than the pure cobalt ferrite. K. Sharma et.al.investigated synthesis and structural impurity effect of La on Cobalt ferrite [53]. The average particle size obtained for Co-ferrite is 52 nm and for La doped Co ferrites is 50 nm. Structural result indicates that the size decreases for La doped particles where as strain and lattice parameter increases. Further R. S. Yadav et. al. studied influence of La^{3+} on structural, magnetic, dielectric, electrical and modulus spectroscopic characteristics of single phase $CoFe_{2-x}La_xO_4$ nanoparticles [54]. They found that the SEM images shows formation of spherical nanoparticles with grain size of 10 –50 nm. VSM measurement revealed the saturation magnetization decreases with La^{3+} substitution, where as coercivity showed anomalous behavior. The dielectric constant and ac conductivity increases with increase of La^{3+} substitution, where as dielectric loss tangent exhibits anomalous behavior. Pengn et. al. [55] studied the magnetic properties of gadolinium-doped $CoFe_2O_4$ nanoparticles using hydrothermal synthesis and revealed that at the room temperature magnetic field versus magnetization measurements confirmed a strong influence of gadolinium doping on the saturation magnetization and coercivity. E. Pervaiz et.al.studied influence of Rare Earth (Gd^{3+}) on

structural, gigahertz dielectric and magnetic studies of cobalt ferrite using sol-gel auto combustion technique and found that average crystallite sizes ranges from16 nm - 25 nm, as calculated from Scherrer's formula and Williamson Hall plots. Room temperature DC electrical resistivity decreases (x = 0.025) and then increases up to x = 0.1. Magnetic studies done by VSM showed that magnetization (Ms) decreases for low concentration (x = 0.0, 0.025) and increases for higher Gd^{3+} concentration(x = 0.05, 0.075, 0.1) [56]. C V Ramanan et. al. studied Gadolinium-substitution induced effects on the structure and AC electrical properties of cobalt ferrite. He found that at any given frequency, the electrical conductivity decreases with increasing Gd concentration. The activation energy increases from 0.564 to 0.668 eV with increasing Gd content [57]. Zhao et. al. explored synthesis and characterization of gadolinium doped cobalt ferrite nanoparticles with enhanced adsorption capability for Congo Red and found that the average particle size gradually decreases from 13 nm to 8 nm with doping content. VSM analysis showed the saturation magnetization and coercivity decreases with Gd^{3+} ions. Exhibits super paramagnetic behavior gradually [58]. Md. T. Rahmanstudied Impedance spectroscopic characterization of gadolinium substituted cobalt ferrite ceramic synthesized by solid state ceramic method and revealed that the electrical resistivity decreases with increase in temperature. The resistivity increases with increase in Gd content. Impedance spectroscopy analysis under a wide range of frequency and temperature showed that the real part (Z) and imaginary part (Z') of the impedance decreases with increasing frequency [59]. Q. Lin et.al. studied the structural and magnetic properties of gadolinium doped $CoFe_2O_4$ nano ferrites and found that the average crystallite size decreases with the substitution of Gd^{3+} ions. Room temperature Mossbauer spectra of $CoGd_xFe_{2-x}O_4$ displayed ferrimagnetic behavior. The saturation magnetization decreases and the coercivity increases with substitution of Gd^{3+} ions [60].

V. S. Puli et. al. worked on Chemical bonding and magnetic properties of gadolinium (Gd) substituted cobalt ferrite. He found that for higher values of Gd content, secondary ortho-ferrite phase is formed. The substitution of Gd increases the saturation magnetization and decreases at higher Gd content ($x \geq 0.3$). Coercivity increases with increase in Gd^{3+} content and it is attributed to magnetic anisotropy in the ceramics [61]. R. P. Pant studied finite size effect on Gd^{3+} doped $CoGd_xFe_{2-x}O_4$ ($0.0< x<0.5$) particles and found that XRD data revealed there is the minor shift in the peak position. The crystallinity decreases with an increase in Gd^{3+} ion concentration and changes the structural parameters. Super-paramagnetic behavior of these particles has been observed with EPR spectroscopy [62]. Md. T. Rahman et.al and M. Vargas et. al. studied structural characteristics, electrical conduction and dielectric properties of gadolinium substituted cobalt ferrite. They found that the dielectric constant increases for temperature greater than 550° C. Dielectric constant of a sample is enhanced compared to pure CoFe2O4. Activation energy of the dielectric relaxation is calculated using Arrhenius equation varies from 0.564 to 0.668 (± 0.003) eV with increasing x values from 0.0 to 0.4 range. The resistivity and activation increases with increase in Gd content [63]. M. S. Khandekar et. al. studied nano crystalline Ce doped $CoFe_2O_4$ as an acetone gas sensor and found that in the temperature range of 200 – 450°C, the gas response of ferrite materials to gases like liquefied petroleum gas (LPG), acetone, ethanol and ammonia was investigated. The sensor response was found to be sensitive and selective towards acetone as compared to other gases. It is observed that Ce (4 wt %) strongly influenced the response and the operating temperature of the sensor material, thus can serve as acetone-sensing sensors [64]. M. Kaiser et.al. studied the influence of Ce substitution on structural, magnetic and electrical of cobalt ferrite nanoparticles and found that the minimum particle size of 18 nm was obtained for Ce^{3+} (x= 0.06). VSM measurements showed that the coercivity and magnetization values are strongly dependent on Ce^{3+} content and particle size. The conduction mechanism used cation-anion-cation interactions over the octahedral B-site [65]. G. Chandra, R.C. Srivastava and K Ashokan studied structural and magnetic properties of cerium doped cobalt ferrite nanoparticles and revealed that the crystallite size varies from 10 nm to 40 nm depending on the sintering temperature of the specimen. VSM study shows the ferrimagnetic nature of the cobalt ferrite nanoparticles. Saturation magnetization increases from 35 to 84 emu /gm as the sintering temperature varies from 300 to 900 ^{o}C for pure cobalt ferrite [66]. R. Sharma et.al. and others studied augmenting the catalytic activity of $CoFe_2O_4$ by substituting rare earth cations into the spinel structure. They found that the enhancement in activity of x = 0.1 and x = 0.4 for Ce and La doped $CoFe_2O_4$ respectively was correlated to the octahedral site preference of rare earth metal ions, reduces band gap and enhances surface area. This work announces the prominent role of RE metal ions in photo-fenton activity enhancement [67]. C. Yang et.al. studied Rare earth ions doped polyaniline/cobalt ferrite nano-composites via a novel coordination-oxidative polymerization-hydrothermal route: preparation and microwave-absorbing properties. They found that the composites mainly showed nano fibers with a diameter of 70 nm and a length longer than 2μm. The surface of composites was uniformly covered with numerous nano particles with an average size of 10 – 20 nm. Microwave absorption properties of polyaniline $CoRE_xFe_{2x}O_4$ nano composites doped with La ion were found to be better than those doped with Ce and Y ions [68]. F. A.

Kalam Khan et .al. and others studied Pr^{3+} doped $CoFe_2O_4$. A highly efficient, magnetically recoverable and reusable catalyst for one-pot four-component synthesis of multi substituted pyrroles. They found that the catalyst was easily recoverable using magnet and could be reused without a significant loss of catalytic activity. Even after five runs for the reaction, the catalytic activity of Pr^{3+} doped $CoFe_2O_4$ was almost the same as that of the freshly used catalyst [69]. S.Xaviers et.al. investigated effect of neodymium substitution on structural and magnetic properties of cobalt ferrite nanoparticles prepared through the sol- gel technique and found that the FTIR spectrum analysis indicates the substitution of Fe^{3+} ions on octahedral sites by Nd^{3+}ions. The TEM micrograph revealed nanoparticles are roughly spherical and slightly agglomerated. The saturation magnetization and coercivity decreases with increase in neodymium content [70]. S. Abbas et.al. studied enhanced electrical properties in Nd doped cobalt ferrite nano particles and found that the crystallite size was found to be 29 nm. The DC resistivity as a function of temperature showed direct dependence on temperature and inverse dependence on the concentration of Nd dopants. The material has potential for resistive random access memory application [71]. S. Rohilla et.al investigated the structural and optical properties of Nd doped cobalt ferrite and revealed that the crystallite size in range of 25 - 32 nm. Structural studies suggested that the mixed ferrite could be used as high density magnetic recording, permanent magnets, magnetic fluids, catalysis, and photo-magnetic materials [72]. R. S. Yadav et. al. worked on impact of Nd^{3+} in $CoFe_2O_4$ spinel ferrites nanoparticles on cation distribution, structural and magnetic properties. They found that the impact of Nd^{3+} on cation distribution of Co^{2+} and Fe^{3+} at octahedral and tetrahedral sites in spinel ferrite cobalt ferrite nanoparticles was investigated by X-ray photoelectron spectroscopy. Room temperature magnetization measurements showed that the saturation magnetization and coercivity increase with addition of Nd^{3+} substitution in cobalt ferrite [73]. M. M. Rashad et. al. studied magnetic properties of nano-crystalline Sm-substituted $CoFe_2O_4$ synthesized by citrate precursor method and observed that at low temperatures 400 – 600°C, Sm doped sample formed the broad peaks of cobalt ferrite phase and resulted in the formation of cubic cobalt spinel ferrites. $SmFeO_3$ phases were observed at high temperatures from 800 to 1000°C. The average crystallite sizes are in the range of 8 nm - 86 nm. The saturation magnetization and coercive field are strongly dependent on the calcinations temperature. The saturation magnetization was decreased by increasing the Sm content and increased by increasing the calcinations temperatures from 400 to 800°C [74]. F. Falsafi et.al. and others worked onSm-doped cobalt ferrite nanoparticles: A novel sensing material for conductometric hydrogen leak sensor. They found that to check applicability of the Sm-doped Co-ferrite for hydrogen leak sensing, a simple conductometric sensor has been fabricated and tested. The electrical behavior of the sensor has been recorded by exposure to hydrogen and some interfering gases. The results showed that the sensor developed is promising for the detection of hydrogen leak as it possesses good sensitivity, stable behavior and fast response recovery [75]. P. K.Gaikwad et.al. studied electrical properties of samarium substituted cobalt ferrite. The Electrical conductivity was investigated from two probe technique in the temperature range 300K to 850K. Plots of log ρ (Ω m) v/s 1000/T K^{-1} reciprocal of temperature show a transition near the Curie temperature. Activation energy and D.C. electrical resistivity both are decreasing with substituted Sm^{3+} rare earth ions in cobalt ferrites and activation energy in the paramagnetic region is more than that of ferrimagnetic region [76]. R. N. Panda et. al. studied magnetic properties of nano-crystalline Gd- or Pr- substituted $CoFe_2O_4$ synthesized by the citrate precursor technique. They found that the crystallite size of the materials in the range of 6.8 nm - 87.5 nm. TG techniques revealed formation of spinel ferrite phase at 220°C. The room temperature saturation magnetization of the ferrite materials decreases with the crystallite size. In rare – earth doped cobalt ferrite, coercivity increases due to the single ion anisotropy of the rare earth ions present in the crystals [77]. A. K. Nikumbh et. al. studied structural, electrical, magnetic and dielectric properties of rare-earth substituted cobalt ferrites nanoparticles synthesized by the co-precipitation method. They found that the particle size in the range 36.1 to 67.8 nm. The temperature variation of the electrical conductivity showed definite breaks, which corresponds to ferrimagnetic to paramagnetic transitions. The thermoelectric power for all compound are positive over the whole range of temperature [78].

M. A. Khan et. al. impacts of Tb substitution at cobalt site on structural, morphological and magnetic properties of cobalt ferrites synthesized via double sintering method. They found that the saturation magnetization was found to exist in the range of 63 – 67 emu /gm and coercivity in the range of 405 – 435 Oe. The substituting of terbium in cobalt ferrites substantially decreases the coercivity and remanence. The smaller values of coercive field suggest that these materials are useful in high density data storage devices [79]. R. C. Kambale et. al. studied low temperature synthesis of nano crystalline Dy^{3+} doped cobalt ferrite for structural and magnetic properties and found that SEM demonstrated the fine clustered particles with an increase of average grain size with Dy^{3+} content. Room temperature magnetization measurements showed that the saturation magnetization and hysteresis losses (coercivity) decreases with Dy^{3+} content, which implies that these materials may be applicable for magnetic data storage and recording media [80]. Z. Karimi et. al. investigated magnetic and structural properties of nano sized Dy doped cobalt ferrite nanoparticles synthesized by Co- precipitation method. The crystallite size obtained is 15nm and room temperature saturation magnetization decreases with dopent, but the residual magnetization and coercivity of ferrite were increases by 50 and 150% with dysprosium. For undoped cobalt ferrite, the anisotropy constant is equal to 19.1 erg /gm and was increased to 45.2 erg /gm by doping 0.05 dysprosium. Introducing dopants into the lattice led to a decrease in Curie temperature [81]. H. Kumar et. al. studied FTIR and electrical study of dysprosium doped cobalt ferrite nano particle sample - $CoFe_{2-x}Dy_xO4$ (x = 0.00, 0.05, 0.10, 0.15) using different sintering temperatures (300°C, 500°C, 700°C, and 900°C). They found that FTIR showed two absorption bands corresponds to the tetrahedral and octahedral sites, which indicate formation of spinel structure of the sample. The sample sintered at 300°C, the dielectric constant is almost unchanged with the frequency at concentrations of x = 0.00 and 0.05. The samples are sintered at 500°C (x = 0.10, 0.15), 700°C (x = 0.05, 0.10, and 0.15), and 900°C (x = 0.05, 0.10) and it is observed that the dielectric constant increases for the undoped cobalt ferrite sintered at temperature 500°C, 700°C, and 900°C. The value of electrical resistivity of the materials varies from 105 to 109 Ω -cm [82]. R. S. Yadav et. al. worked on magnetic properties of dysprosium-doped cobalt ferrite nanoparticles synthesized by starch-assisted sol-Gel Auto-combustion method and found that the nano sized particles of 5nm −15 nm with spherical morphology. The crystallite size and foreign phase $DyFeO_3$ affect the magnetic properties of cobalt ferrite nanoparticles. The X-ray photoelectron spectroscopy (XPS) analysis confirmed the presence of Co^{2+} at the octahedral as well as the tetrahedral site in the $CoFe_{2-x}Dy_xO_4$ (x = 0.05) nanoparticles [83].The study of H.S. Mund et.al. is on spin and orbital magnetization in Dy- and Gd-doped Co ferrite using magnetic compton scattering. They found that the doped and undoped $CoFe_2O_4$ showed a decrease in spin moment. The decrease in spin moment is on the basis of migration of Co^{2+} ions from octahedral to tetrahedral sites (supported by XPS). As compared to Gd^{3+}ions, Dy^{3+} ions has smaller ionic radii and larger magnetic moment that result to larger magnetic moment in Dy doped $CoFe_2O_4$ [84]. S. Amiri et.al. investigated magnetic and structural properties of RE doped Co-ferrite (RE=Nd, Eu and Gd) nano-particles synthesized by co-precipitation and found that the crystal size is about 22 nm for Gd – Co ferrite. The FTIR measurements between 350 and 4000 cm^{-1} confirmed the intrinsic cation vibrations of the spinel structure. The RE ion increases both vibration frequencies and bond strength. The highest magnetic coercivity and the loop area correspond to the Gd – Co ferrite, making useful for hyperthermia treatment. The Curie point decreased by the RE ions and has lowest value for Nd–Co ferrite [85]. Sanchez et. al. studied dielectric and complex impedance properties of tetravalent Hf^{+4} integrated cobalt ferrite. They found that :- XRD patterns for Hf -incorporated CFO confirm the formation of spinal phase, in addition to the small amount of HfO_2 monoclinic .The lattice constant were found to increase from 8.374 Å (x = 0.000) to 8.391 Å (x = 0.200). SEM imaging analysis indicates that Hf resides at the grain boundaries for CFO-Hf. The dielectric constant of CFO-Hf is independent of temperature (T< 450°C) [86]. L. Kumar et.al. Effect of Ho^{3+} substitution on the cation distribution, crystal structure and magnetocrystalline anisotropy of nanocrystalline cobalt ferrite found that the XRD (Rietveld) shows that Ho^{3+} ion has a strong preference for octahedral sites (B-sites). The lattice constants, magnetocrystalline anisotropy constant, coercivity and saturation magnetization decrease with the Ho^{3+} concentration up to x= 0.05. Crystallite size decreases with the Ho^{3+} concentration. The magnetic properties are strongly affected by surface effect rather than cation distribution. The samples with a low concentration of Ho^{3+} reveal that there is tendency of the material to show soft ferrimagnetic character [87]. M. U. Islam et. al. explored the structural and magnetic properties of holmium substituted cobalt ferrites synthesized by chemical co-precipitation method They found that XRD showed a second phase of $HoFeO_3$ along with the spinel phase. Saturation magnetization (Ms) and coercivity increases with Ho^{3+} substitution. Sample fallow Curie–Weiss law up to the Curie temperature. Above the Curie temperature it shows paramagnetic behavior. The increase in coercivity suggests that the material can be used for applications in perpendicular recording media [88]. A. M. Pachpinde et. al. study on Ho^{3+} doped CoFe2O4 nanoparticles: A highly efficient, magnetically recoverable and reusable catalyst for one-pot three-component synthesis of 2,4,5 -triaryl-1H-imidazoles They found that An efficient Ho^{3+} doped $CoFe_2O_4$ catalyst can be easily separable using magnet and reused with almost the same catalytic activity. The proposed method is advantageous due to its simplicity, high yield, and short reaction time, ease of separation and reusability of the magnetic catalyst [89].

R. N. Bhowmik et. al. Mechanical alloyed Ho^{3+} doping in $CoFe_2O_4$ spinel ferrite and understanding of magnetic nano domains They found that the magnetic grains showed single domain or pseudo-single domain behaviour below a critical annealing temperature1050^{0}C and above this temperature the grains become multi-domain. The transformation in the magnetic behaviour of the material was noted at about 1050^{0}C. The Ho doped $CoFe_2O_4$ nanograins retained soft ferromagnetic nature and T_C is independent of grain size variation [90]. S.G. Kakade investigated dielectric, complex impedance, and electrical transport properties of Erbium (Er^{3+}). Ion-substitute dm Nano crystalline, Cobalt-Rich Ferrite ($Co_{1.1}Fe_{1.9-x}Er_xO_4$) and found that CFEO materials crystallize in a spinel cubic structure for $x \leq 0.10$. The formation of ortho-ferrite secondary phase was noted for $x \geq 0.15$. Semiconducting behavior and small polaron conduction mechanism were evident in electrical transport properties of CFEO materials. The results presented are helpful for utilizing these materials in magneto electric sensors and high-frequency electromagnetic devices [91] P. Sateesh et.al. studied structural and ambient/sub-ambient temperature magnetic properties of Er-substituted cobalt ferrites synthesized by sol-gel assisted auto combustion method. The X-ray diffraction (XRD) confirmed the presence of the spinel phase and additional ortho-ferrite phase for higher compositions. The XRD spectra and the TEM micrographs indicated that the crystallite size of 120 - 200 nm. The magnetization curves show an increase in saturation magnetization (M) and coercivity (H). Er-substituted cobalt-ferrites have higher cubic anisotropy constant [92]. Y. Cedeno- Mattei et. al. worked on effect of rare earth doping on magnetic properties of cobalt Ferrite Nano crystals. They found that the nano crystal in the range of 10 nm – 20 nm. The room temperature coercivity increases from 3.8 kOe to 5.0 kOe (close to max value of 5.3 kOe). Mossbauer spectroscopy revealed presence of super paramagnetic particles in the powder [93]. M. L. Kahn investigated synthesis and magnetic properties of $CoFe_2O_4$

spinel ferrite nanoparticles doped with lanthanide ions Sample - $CoLn_{0.12}Fe_{1.88}O_4$ nanoparticles; Ln = Ce, Sm, Eu, Gd, Dy, Er. They found that X- ray diffraction (Rietveld refinement) revealed particle mean size of 20 nm. The blocking temperature for Ce, Gd, Dy increases and less specular for Sm, Eu, Er. The coercivity increases for Gd and Dy, Saturation magnetization and remanence shows higher value for Ce, Dy, Er. The temperature dependence of the magnetic Susceptibility is studied [94]. L. Ben tahar et. al. Magnetic properties of $CoFe_{1.9}RE_{0.1}O_4$ nanoparticles (RE = La, Ce, Nd, Sm, Eu, Gd, Tb, Ho) prepared in polyol. They found that the low-temperature saturation magnetization and coercivity increases with RE^{3+} ions - maximum values were found for Gd^{3+} and Eu^{3+} [95]. M. K. Shobana and others studied structural properties on the yttrium-doped cobalt ferrite powders synthesized by sol – gel combustion method and found that the mean crystallite size obtained in the range of 20 -70 nm. HR-SEM confirmed the cubic morphology of the prepared sample. The measured mean crystallite size is in good agreement with the XRD patterns. In addition, the elemental composition was confirmed by EDAX and FTIR [96]. S. R. Naik et. al. investigated change in the magneto structural properties of rare earth doped cobalt ferrites relative to the magnetic anisotropy. They found that X-ray photoelectron spectroscopy (XPS) confirmed the presence of metal ions in the required valence state. Strong L-S coupling from Co^{2+} ions in the octahedral lattice is responsible for blocking temperature in the individual compounds. Lattice distortion of the doped ferrite and transfer of Co^{2+} from octahedral to the tetrahedral site is responsible for magnetic properties of compound [97]. Woo chul Kim et.al. studied magnetic properties of Y-, La-, Nd-, Gd-, and Bi-doped ultrafine $CoFe_2O_4$ spinel grown by using a sol-gel method. They found that Y-, Gd-, and Bi-doped samples fired at and above 923K have only a single cubic spinel structure and behave ferrimagnetically, but in La- and Nd-doped samples a-Fe_2O_3 phase were observed at and above 1123K. The magnetic behavior of $CoFe_{1.9}Nd_{0.1}O_4$ spinel powders fired at and above 923K shows that an increase of the annealing temperature yields a decrease of the coercivity and an increase of the saturation magnetization [98] C. Virlan et.al. studied rare earth metals influence on the heat generating capability of cobalt ferrite nano particles. They found that the potential study of rare earth doped cobalt ferrite nano particles application in cancer treatment through hyperthermia. The crystallite sizes are in average 15 nm - 25 nm for all samples, visibly smaller for Dy doped samples. The specific adsorption rate varies similar to coercivity and saturation magnetization for Dy and Gd doped samples and opposite for Yb doped samples (average crystallite size exceeding 20 nm). A maximum increase of 26% was found for 0.05 Dy content and a smaller increase for Gd doped samples. All samples exhibit heat generating capability promising for applications in hyperthermia treatment [99].

The findings shows that there are wide fluctuations in several results of resistivity, dielectric constant, dielectric loss, saturation magnetization, coercivity, hysteresis loss, etc. which are to be related to different rare-earth doping and their concentrations [34 - 51]. However several of these workers have not done extensive wide ranging study on rare-earth doped Cobalt ferrite nanoparticles (references as listed above). Therefore it is proposed to carry out detailed investigations on $CoFe_{2-x}Re_xO_4$ by varying x as well as Re (rare-earth element) in a systematic manner.

1.6 Aim and Objectives of the Research Work

The literature review of large number of research publication concludes that majority of the researcher have prepared a few samples with single dopant with high concentration to study the properties of the material. An elaborative investigation is necessary to understand the effect of varying rare earth concentration from very low magnitudes to higher magnitudes to establish a concrete relation between the dopent concentrations and the properties of host ferrite material. To fill up this void to some extent, three different large series with varying rare earth dopant and low concentrations will be prepared in order to study, understand and investigate novel properties in these materials.

The investigations of rare earth doped transition metal ferrites such as Gd^{+3} doped $CoFe_2O_4$, Nd^{+3} doped $CoFe_2O_4$ and Dy^{+3} doped $CoFe_2O_4$ were prepared using auto – combustion method to study their structure, magnetic and electric properties. Nanoparticles $CoFe_{2-x}Gd_xO_4$ (x = 0.00, 0.02, 0.04, 0.06, 0.08, 0.10), $CoFe_{2-x}Nd_xO_4$(x = 0.00, 0.02, 0.04, 0.06, 0.08, 0.10) and $CoFe_{2-x}Dy_xO_4$ (x = 0.00, 0.02, 0.04, 0.06, 0.08, 0.10) using auto combustion method of sample preparation were synthesizeed. The findings, explanation to results and conclusion are presented in the theses.

1. Synthesis of $CoFe_{2-x}Re_xO_4$ by varying x as well as REE (rare-earth element) nanoparticles using simple preparative method.
2. Characterization using X-ray spectroscopy, Fourier transforms infrared spectroscopy, scanning electron microscope (SEM), EDX.

3. Particle size estimation using transmission electron microscopy, scanning electron microscopy.
4. Investigation of magnetic properties of rare earth doped using vibrating Sample magnetometer (VSM, SQUID).
5. Investigation of electrical properties such as D.C. resistivity, dielectric constant, dielectric loss.
6. Co-relating the various observed properties to doping concentrations and particle size of the materials.

The outcome of the research work will be published in form of papers that are presented in conferences and international journals. The work would result in addition of vital information and useful knowledge in the field of nano-magnetic research.

1.7 Organization of Thesis

The thesis has been written into seven chapters are as follows:

- ✓ **Chapter 1: Preface**

The chapter includes introduction to nanomaterials, origin of magnetic materials ferrites, spinel ferrites, magnetic nanomaterials, rare earth elements. Also focuses on topics such as cobalt ferrites, rare-earth doped ferrites and comprehensive theory review on research work published by researchers on rare earth doped cobalt ferrites.

- ✓ **Chapter 2: Preparation of RE doped Cobalt ferrite materials**

In this chapter information on different methods of sample preparation used by various researchers to prepare nanomaterials have been described. A comprehensive procedure of auto combustion synthesis method to prepare rare-earth doped ferrites is discussed.

- ✓ **Chapter 3: Characterization and Measurement Techniques**

Instruments and various methods of investigation used for characterization, magnetic properties and electrical properties have been discussed. The basic principles and the standard procedure used to utilize these sophisticated instruments are mentioned.

- ✓ **Chapter 4: Effect of Gd^{+3} doping on Structural, Magnetic and Electrical properties of $CoFe_2O_4$ Nanoparticles.**

The rare-earth Gd doped cobalt ferrites were prepared using auto combustion method having chemical formula for the material as $CoFe_{2-x}Gd_xO_4$ for (x= 0.00, 0.02, 0.04, 0.06, 0.08, 0.10). This chapter includes the results obtained on Gadolinium doped cobalt ferrites using various Characterization techniques such as X-ray diffraction (XRD), Fourier transform infrared spectroscopy (FTIR), Scanning electron microscope (SEM), Transmission electron microscope (TEM) and Energy dispersive spectroscopy (EDS). The chapter also includes the results obtained from magnetic and electrical investigations carried out on Gadolinium doped cobalt ferrites.

- ✓ **Chapter 5: Effect of Nd^{+3} doping on Structural, Magnetic and Electrical properties of $CoFe_2O_4$ Nanoparticles.**

The structural characterization, magnetic and electrical properties of Neodymium doped cobalt ferrites are investigated in this chapter. The characterization techniques such as X-ray diffraction (XRD), Fourier transforms infrared spectroscopy (FTIR), Scanning electron microscope (SEM), Transmission electron microscope (TEM) and Energy dispersive spectroscopy (EDS) are used to study the structural properties of $CoFe_{2-x}Nd_xO_4$ nanopaticles. The hysteresis curve and parmeters associated with this curve has been studied.The electrical properties such as dielectic constant and dielectric loss as fuction of frequency and temperature, resistivity property has been explore for $CoFe_{2-x}Nd_xO_4$ samples.

- ✓ **Chapter 6: Effect of Dy^{+3} doping on Structural, Magnetic and Electrical properties** of **$CoFe_2O_4$ Nanoparticles.**

In this chapter, we delve into the examination of Neodymium-doped cobalt ferrites, focusing on their structural characterization, as well as their magnetic and electrical attributes. To accomplish this, we employ a range of characterization techniques, including X-ray diffraction (XRD), Fourier transform infrared spectroscopy (FTIR), Scanning electron microscopy (SEM), Transmission electron microscopy (TEM), and Energy-dispersive spectroscopy (EDS) to scrutinize the structural properties of $CoFe_{2-x}Dy_xO_4$ nanoparticles. The investigation of the hysteresis curve and its associated parameters has been studied. Furthermore, we explore the electrical characteristics, specifically the dielectric constant and dielectric loss as functions of frequency and temperature, along with the resistivity properties exhibited by the $CoFe_{2-x}Dy_xO_4$ samples.

- ✓ **Chapter 7: Conclusion**

This chapter is focused on entire work of investigation and the results obtained. The research work on Gd^{+3} doped Cobalt ferrite, Nd^{+3} doped Cobalt ferrite and Dy^{+3} doped Cobalt ferrites on structural, magnetic and electric properties are summarized. The comparative study of these series for magnetic properties are explore in this chapter. A future scope in this field of research work is included in this chapter.

References:

[1] R. Valenzuela, magnetic Ceramics. Cambridge press, 1994.

[2] B. Vishwanathan, V.R.K. Moorthy, Ferrite Materials: Science and Technology Springer, Berlin, 2, 1990.

[3] G.S. Chaddha, University physics, Narosa publisher, 2015.

[4] S. S Sanjay, A. C. Pandey, A Brief Manifestation of Nanotechnology, (2016) 47-63.

[5] Alagarasi, Inroduction to nanomaterials, (2011)1-76.

[6] Poorvi Dutta, Sushmita Gupta, Understanding of Nanoscience and Technology,Global Publishing house, New Delhi,2006.

[7] K. K. Choudhary, Nanoscience and Technology, Narosa publishing house, 2018.

[8] B. D. Cullity, Introduction to Magnetic Materials, Addison Wesley publishing company, 1972.

[9] Mills A.A. The Loadstones: History, physics and formation Ann. Sci. 61,273- 319.

[10] R. C. O'Handley, Modern Magnetic Materials (Wiley-Interscience Publication, New York, 2000.

[11] E. du Trmolet de Lacheisserie, D. Gignoux and M. Schlenker (Eds.), Magnetism: Materials andApplications Springer, 2003.

[12] S. A. Wolf, D. D. Awschalom, R. A. Buhrman, J. M. Daughton, S. von Molnar, M. L.Roukes, A. Y. Chtchelkanova and D. M. Treger, Science 294 (2001) 1488.

[13] G. A. Prinz, J. Magn. Mater. 200,(1999), 57.

[14] S. S., Sarma D. D., Sanvito S, Nano Lett. 2,(2002), 605.

[15] M. S. Vijaya, G. Rangarajan, Materials Science, McGraw-Hill Publicompany limited, New Delhi (1999-2000).

[16] D. Jiles, Introduction to Magnetism and Magnetic Materials; Chapman Hall, London, 1990.

[17] K. E. Sickafus, J. Wills, J. Am. Ceram. Soc. 82, 3279, 1999.

[18] O. Muller and R. Roy, Crystal Chemistry of Non-Metallic Materials, Springer Verlag, Berlin, 1974.

[19] E. C Snelling "Soft Ferrites, Properties and applications", Bitterworth and Co. (Publishers) Ltd, London (1988).

[20] Vladimir Sepelak and Klara Tkacova, Acta MontanisticaSlovaca, Rocnik2, (1997), 266-272.

[21] I. C. Heck, Magnetic Materials and their Applications, Butterworth& Co. Pub. Ltd, London, 1974).

[22] A. Goldman, Modern Ferrite Technology, Van-Nostrand Reinhold, New York, 1990.

[23] E T Lacheisserie, D Gignoux and M Schlenker, New York, Springer, 2006.

[24] Lawrence Kumar, Pawan Kumar, Amarendra Narayan and ManoranjanKar International NanoLetters 3(2013) 1.

[25] Veena G E, Al-Omari I A, Malini K A, Joy P A, Sakthi K D, Yasuhiko Y and Anantharaman M R 2008 J.Magn.Magn.Mater.321 1092

[26] Cedeno – mattei Y and Perales-Perez O 2009 Microelectronics Journal 40, 673.

[27] F. S.Galasso, Structure and Properties of Inorganic Solids, pergapress, Oxford, 1970.

[28] R. W. G. Wyckoff, Crystal Structures: Miscellaneous InorgCompounds, Silicates and basic structural information Vol.4, 2nd ed. (Interscience Publishers, New York, 1968, pp. 540.

[29] Gul I H, Abbasi A Z, Amin F, Anis-ur-Rehman M and Maqsood A, J.Magn. Magn. Mater. 311494, 2007.

[30] K. J. Standley. Oxide Magnetic Materials, 2^{nd}edi. 1972.

[31] M. P. Horvath, J. Magn. Magn Mater, 215, (2000)171-183.

[32] Nikalje AP (2017) Nanotechnology and its Applications in Medicine. Med chem5: 081-089.

[33] Rasheed SAP, Jude M, Suresh K, Dey S, Sunil H, et al.,Nanotechnology and Its Applications in Dentistry. International Journal of Advanced Health Sciences 2: 1-10, 2019.

[34] Shrivastava S, Dash D (2013) Applying Nanotechnology to Human Health: Revolution in BiomedicaSciences. J Nanotech 1-15.

[35] Sasmita Mohapatra , Smruti R. Rout, Swatilekha Maiti , Tapas K. Maiti and Asit B. Panda, "Monodisperse mesoporous cobalt ferrite nanoparticles: synthesis and application in targeted delivery of antitumor drugs" J. Mater. Chem., 21 (2011), 9185.

[36] Abhishek NigamS, J. Pawar, Structural, magnetic, and antimicrobial properties of zinc doped Magnesium ferrite for drug delivery applications Ceramics International Volume 46, Issue 4, Pages 4058-406 drug delivery10 March 2020.

[37] Daliya S. Mathew and Ruey-Shin Juang, Chemical EngineeringJournal 129, (2007), 51.

[38] V. Zepf, Rare Earth Elements, Springer Theses,DOI: 10.1007/978-3-642-35458-8_2, Springer- Verlag Berlin Heidelberg 2013.

[39] E. E. Sileo, S.E. Jacobo, Physica B 354, (2004), 241.

[40] Fuxiancheng, ChunshengLiao,junfeng kuang, Xu Zhigang,ChnhuaYan,Liang Yaochen, HaibinZhao, Zh. U. Liu,J.Appl. Phys, 85, 2782 -2786, 1999.

[41] K. V. Kumar, D. Ravinder (2002), Electrical conductivity of Ni–Zn–Gd ferrites, Mater. Lett, Vol. 52, pp. 166– 168.

[42] A. Maqsood, Phase transformations in $Ho_2Si_2O_7$ ceramics, J. Alloys. Compd, Vol. 471, pp.432 - 434, 2009.

[43] C.S.kim, Y.S. Yi,K. T.Park,H. Namgung,J.G.Lee, growth of ultrafine Co-Mn ferrite and Magnetic properties by sol-gel method,journal of applied physics 85 5223-5225(1999).

[44] A.Hutlova, D. Niznasky, J. L. Rehspringer, C.Estournies, M. Kumoo,High coercive fieldfor Nanoparticles of $CoFe_2O_4$ in amorphous silica sol-gel, jounal of advanced materials 15, 1622-1625 , 2003.

[45] C. Murugesan and G. Chandrasekaran, R. S. C. Adv., 5, 73714-73725, 2015.

[46] T.A.S. Ferreia, J.C Waerenborgh, M.H.R.M. Mendonca, M.R. Nunes, F.M. Costa, Solid State Sciences 5, 383, 2003.

[47] N.Rezlescu, E. Rezlescu, C. Pasnicu, M.L. Craus, Effect of rare earth Ions on some Properties of a nickel-zinc ferrite, Journal of physics; Condensed Matter 6 (1994) 5707-5716.

[48] Y.I. Kim, C.S.Lee, Synthesis andcharacterization of $CoFe_2O_4$, physica B 337, 42-51, 2003.

[49] V A. Mumtaz,K.Maaz,B.Janjua, S.K. Hasanain,m.f. Bertino, Exchange bias and vertical shift in $CoFe_2O_4$ nanoparticles, Journal of Magnetism magnetic materials 313, 920070, 266- 272, 2007.

[50] V. Pillai, D.O.shah, Synthesis of high coercivity cobalt ferrite particles using water-in-oil Microemulsion, journal of Magnetism and Magnetic Materials 163,243-248,1996.

[51] Simona Burianova, Jana PoltierovaVejpravova,Petr Holec, Jiri Plocek, and DanielNiznansky ,JOURNAL OF APPLIED PHYSICS 110, 073902,2011.

[52] K. Kamala Bharathi and C.V. Ramana, Journal of materials research, Vol. 26, issue 4,pages 584- 591 , 2011.

[53] Krishna hari Sharma and Pankaj Sharma (OPTOELECTRONICS AND ADVANCED MATERIALS, RAPID COMMUNICATIONS Vol. 7, No. 11-12,pages 887-890, November- December 2013.

[54] Raghvendra Singh Yadav, Ivo Kuřitka, Jarmila Vilcakova, Jaromir Havlica, Lukas Kalina, Pavel Urbánek, Michal Machovsky, Milan Masař, Martin Holek, Zeitschrift :Jounal of materials science: materials in electronics, Ausgabe 12, 2017.

[55] Jian hongPengn ,MirabbosHojamberdiev , Yunhua Xu , Baowei Cao, Juan Wang, HongWu,Journal of Magnetism and Magnetic Materials 323,133,138, 2011.

[56] Erum Pervaiz and I H Gul, Journal of Physics: conferenceseries, volume 439, 012015, 2013.

[57] Md.T. Rahman, C.V.Ramanan, Ceramics International, volume 40, Issue 9, Pages 14533 – 14536, 2014.

[58] Xiruo Zhao , Wei Wang, Yajun Zhang , Sizhu Wu, Feng Li , J. Ping Liu, chemical engineering journal, volume 250, pages 164-174, 2014.

[59] Md. T. Rahman and C. V. Ramana, Journal of applied physics116, 164108, 2014.

[60] Qing Lin, Jinpie Lin, Yun He, Ruijun Wang, Jianghui Dong, Journal of Nanomaterials – Special issue Volumme2015, article no. 8, 2015

[61] Venkata Sreenivas Puli, Shiva Adi reddy, C.V. Ramana, Jounals of alloys and compounds, Vol.644, 470-475, 2015.

[62] R.P. Pant, Manju Arora, Balwinder Kaur, Vinod Kumar, Ashok Kumar, Journal of Magnetism and Magnetic Materials 322, 3688–3691, 2010.

[63] Md. T. Rahman, M. Vargas, C.V. Ramana, Journal of Alloys and Compounds 617, 547–562, 2014.

[64] M. S. Khandekar, N. L. Tarwal,I. S. Mulla and S. S. Suryavanshi, Ceramics international, volume 40,issue 1,part A, page 447-452,2014.

[65] Hashhash A., Kaiser M., titel -Influence of Ce substitution on .Magnetic and Electrical of cobalt ferrite Nanoparticles, NASA Astrophysics data system ADS.

[66] Grish Chandra, R.C. Srivastava and K. Ashokan (1st Internationa Congress on Computer, Electronics, Electrical and Communication Engineering, ICCEECE2014, IPCSIT, vol.59, 2014.

[67] Rimi sharma,S. Bansal and Sonal Singhal (RSC advances ,issue 75, 2016 [68] Chunming Yang, Junjun Jiang,XiaohuaLiu,ChengjieYin,Cuifen Deng, Journal of Magnetism and Magneetic materials 404,45-52,2016.

[69] Firoz A. Kalam Khan, Amol M. Pachpinde, Mallinath M. Langade, Kishan S. Lohar, Sunil M.Patange, Omprakash G. Bhusnure, Jaiprakash N. Sangshettia ,Iranian Journal of Catalysis 6(4), 333-338 , 2016.

[70] Sheena Xavier, Smitha Thankachan, Binu P Jacob and E M Mohammed, The Royal Swedish Academyof Sciences, Physica Scripta, Volume 87,No.2,2013.

[71] S. Abbas, A. Munir, F. Zahra and M. A. Rehman, IOP Conf. Series: Materials Science and Engineering 146, 012027, 2016.

[72] Sunil Rohilla, Pinki Rani, Navneet Kumar, National Conference on Recent innovations in Applied Sciences and Humanities' NCASH Vol. 4 , issue 10, 2015)

[73] Yadav, Raghvendra Singh; Havlica, Jaromir; Masilko, Jiri; Kalina, Lukas; Wasserbauer, Jaromir, NASA Astrophysics data system ADS.

[74] M. M. Rashad, R.M. MoamedH.El-shall (IOSR – JAP e -ISSN: 2278 – 4861.Volume 7, Issue 3 Ver. III, PP21-25 , May. - Jun. 2015.

[75] Frarhad Falsafi, Behrooz Hashemi, Shahid Beheshti, Ali Mirzaei, Giovanni Neri. j. ceramint, 10.035, 2016.

[76] Pravin K. Gaikwad, S. S. Sawant and K. M. Jadhav (JAAST: MaterialScience (Special Issue) Vol. 1|Issue 2|Page 35-37 Dec.2014.

[77] R.N. Panda, J.C. Shihab, T.S. Chinb (Journal of Magnetism and Magnetic Materials 257, 79–86, 2003.

[78] A. K. Nikumbh, R.A. Pawar, D. V. Nighot, G.S. Gugale, M. D. Sangale, M. B. Khanvilkar, A.V. Nagawade (Journal of Magnetism and Magnetic Materials355, 201–209, 2014.

[79] Muhammad AzharKhan, M.JavidurRehman, Khalid Mahmood, Irshad Ali, Majid Niaz Akhtar, Ghulam Murtaza, Imran Shakir, Muhammad Farooq Warsi, Ceramics International 10.0333, 2014 .[80] R.C. Kambale, K. M. Song, Y.S. Koo and N.H. Hur, Journal of Applied Physics 110, 053910, 2011.

[81] Karimi Z., Mohammadifar Y., Shokrollahi H., Asl, Sh. Khameneh, Yousefi, Gh.; Karimi, L. NASA Astrophysics Data System ADS,01-06- 2014.

[82] Hemaunt Kumar and Co-workers, (Journal of Nanoscience Volume 2014, Article ID 862415s, 2014).

[83] Raghvendra Singh Yadav and Co-workers (J Supercond Nov.Magn 28:2097–2107, 2015.

[84] H. S. Mund, Jagrati Sahariya, R. J. Choudhary, D. M. Phase, Alpa Dashora, M. Itou,Y. Sakurai, and B. L. Ahuja, APPLIED PHYSICS LETTERS 102, 232403 ,2013.

[85] S. Amiri, H. Shokrollahi, Journal of Magnetism and Magnetic Materials, Volume 345, Pages 18-23, 2013.

[86] Sanchez, Luis, (NASA Astrophysics data system ADS).

[87] Lawrence Kumar and Manoranjan Kar, Journal of Experimental Nanoscience, Vol. 9, No 4, 362–374, 2014.

[88] M.U. Islam, M. Ishaque, Hasan M. Khan, Muhammad Naeem Ashiq, M.U. Rana,Journal of Magnetism and Magnetic Materials,Volume 324,Issue 22, November 2012, Pages 3773-3777.

[89] A. M. Pachpinde, Firoz A. Kalam Khan, K. S. Lohar, M. M. Langade and Jaiprakash N.Sangshetti, Journal of Chemical and Pharmaceutical Research, 7(6), 950-956, 2015.

[90] I. Panneer Muthuselvam, R.N. Bhowmik (Journal of Magnetism and Magnetic Materials 322, 767–776, 2010.

[91] Sandip G. Kakade, Yuan-Ron Ma, Rupesh S. Devan, Yesh D. Kolekar, and C. V. Ramana J. Phys. Chem. C, 120 (10), pp 5682–5693, 2016.

[92] PrathapanSateesh; Jayaraman, TanjoreV, Varaprasadarao, Eswara K.; Das, Dibakar, NASA Astrophysics data system ADS, 2014-07-14.

[93]Y. Cedeno-Mattei, O. Parales-Perez, C.Osorio-Cantilo and O.N.C.Uwakweh (NSTI- Nanotech,ISBN 978-1-4398-1782-7,vol. 1,2009.

[94] Myrtil L. Kahn and Z. John Zhang *(*Applied physics letters vol.78 no.23 4 June 2001.

[95] L.BenTahar, M. Artus, S. Ammar, L. S. Smiri, F. Herbst, M.-J. Vaulay,V. Richard, J-M Grenèche, F Villain, F Fievet 9 (Journal of Magnetism and Magnetic Materials, Volume 320, Issue 23, Pages 3242-3250, 2008.

[96] M. K. Shobana, Hoon Kwonb, Heeman Choe (Journal of Magnetism and Magnetic Materials 324, 2245–2248, 2012.

[97] S.R. Naik and A.V. Salkar, Journal of Material chemistry, issue 6, 2012.

[98] Woo Chul Kim, Seung Wha Lee, Sam Jin Kim, Sung Hyun Yoon, Chul Sung Kim, Journal of Magnetism and Magnetic Materials 215-21, 217-220, 2000.

[99] Constantin Virlan, Georgiana Bulai, Ovidiu Florin Caltun, Rolf Hempelmann, Aurel Pui, Ceramic International, 04, 121, 2016.

CHAPTER 2

Preparation of Rare Earth doped Ferrites Materials

2.1 Introduction

The synthesis of the material plays an important role in the material research. In order to develop novel methods of synthesis, the research has been carried out across the globe to meet recent development in science and technology [1]. Scientific research insists on development of nanomaterials with variation to provide improved properties for the efficient performance. So method of material preparation have crucial role on the performance [2]. The various synthesis methods are developed by the researcher to prepare rare earth doped nano material ferrites and successfully employed. The rapid development in new areas of computer technology, electronic engineering and medicine was possible due to the nano particle ferrite technology.

The matter at the scale of one billionth of a meter is term as nanoparticles and is associated with nanotechnology. The researchers were attracted to nanoscale particles as they exhibit new inherited properties which are not observed at bulk solid level. As we move from bulk material to nano material level, there is a change in the size and the shape of particles including properties. There are two main methods for the preparation of nanoparticles: 1. Bottom- Up and 2.Top-to-Down. In Bottom-Up method, the building of larger objects from smaller building blocks like molecules or their constituents' atoms where as Top-to-Down method involves breaking up of bulk matter into smaller particles called nano particles [3]. The Bottom-Up method is considered as chemical method of synthesing which is more reliable for producing purity crystalline mono-phase nanoparticles. In Top-to-Down method, the bulk matter is down sized to nanometre scale called nano particles using lithographic techniques or etching, milling [4]. These two methods have their own advantages and disadvantages. The former method has more advantages like covalent bond holding a molecule is stronger, gives rise to quality of nanoparticles material.

2.2 Different Methods to Synthesis of Ferrite Nanomaterials

Ferrite nanomaterials have attracted many researchers due to its scope in the technological device applications. The practical applications include magnetic fluids, magnetic storage, permanent magnet etc. The researchers have utilized wide variety methods to prepare ferrites nanomaterials such as solid state synthesis, sol-gel method, co-precipitation method, precursor method, hydrothermal process, reverse micelle method, plasma synthesis, Sonochemical method, Chimie -Douce method, combustion method [5- 16]. Since each method has its own advantage and disadvantage, the selection method depends upon the type of ferrite material and the particular properties which are required for its applications. The methods are explained in a processing steps with some common raw materials used in different methods. In some the methods are explained on the basis of flow chart in way the raw material process.

2.2.1 Solid State Synthesis / Conventional Ceramic Method

The solid state synthesis is the oldest method which is used to prepare the polycrystalline material. The raw material used in this method is mineral oxides or carbonates that are thoroughly mixed with appropriate stoichiometric ratio. The grinding, crushing and milling of mixed raw materials and then calcinated to about 700 to 1000^{O}C temperatures for 5- 9 hours in air. After calcinations, again milling is done in order to breakdown the agglomerates to improve compaction and thermal reactivity, so as to reduce the particle size further. Sometimes instead of dry milling, a wet milling is preferred to improve particle size. The mill powder is then pressed in pallets or torroids and final sintering is done under control of atmosphere at about 1200 to 1400^{O}C. The Ni-Zn ferrites are prepared using conventional method [17]. Rahman et. al. prepared Gd substituted $CoFe_2O_4$ [18] , V S Puli et.al. prepared Gd substituted $CoFe_2O_4$ [19] and H S Mund et.al. reported RE doped $CoFe_2O_4$ [20]. The time of milling affects size distribution, coercivity, magnetization, chemical composition and morphology of the nanoparticles. The disadvantages in this method are that it needs high temperature, poor homogeneity. The monitoring progress of reaction is difficult and completion of reaction is decided by trial and error method. As the procedure of ceramic method is costly, time consuming and also particle showing large size distribution. The flow chart of method is shown in figure 2.1 below.

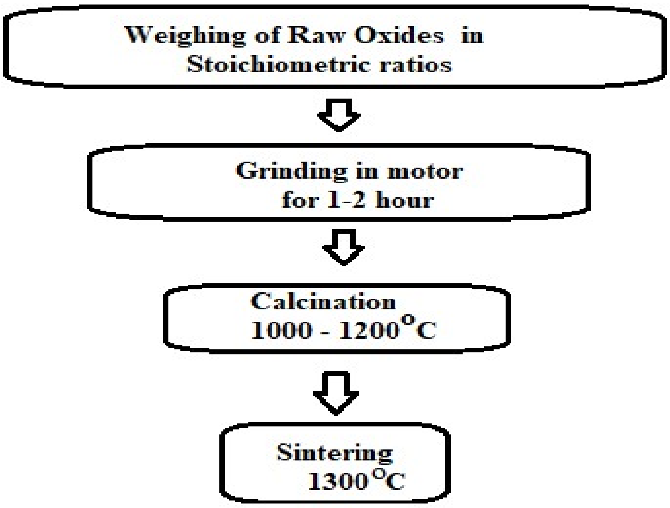

Fig.2.1: Flow chart for Solid State reaction method.

2.2.2 Co-precipitation Method

The required metal cations are taken in form of a common medium such as hydroxide, carbonates, oxalate format etc which gets co-precipitated. The precipitation reactions involved separation of the nucleation and growth of the nuclei. This precipitates are consequently calcinated at a suitable temperatures to give the final product in nano powder. The precipitates settled down at the bottom of a flask, and then it is filtered and washed number of times with water or solvents to remove impurities. After drying in air, the product is calcinated to obtained final crystal structure. The better solubility of the precipitates gives high homogeneity and yields low particle size. However this synthesis required special conditions and special precursor reactions. Also it is essential to control the solution concentration, pH, temperature and mixture, so as to obtain the end product with innovative properties [21-27]. The main problem in this method is the emission of fumes during reaction and incorporation of impurities in synthesized compounds.

2.2.3 Hydrothermal Process

In this process a nanosize crystal of complex compound is synthesize under high temperature and pressure conditions and it is based on the solubility of a compound in hot water under high pressure. The facts that numerous oxides are soluble in an alkali solution, this method is suitable to prepare ferrite material. The method allows the re-crystallization of the powder and to control the grain size and shapes. Along with water, compound is also mixed with polar and non polar solvents and the pH of the solution is adjusted. Then solution is put in autoclave vessel and temperature is raised to build pressure in the vessel. The reaction time is adjusted to get nano crystallite of a particular compound. The adjustment of reaction time we get to know from our experience. The crystals settle down in the vessel are filtered out and washed with water or organic solvents, dried in the air, and then calcined to obtain purified crystalline powder. The advantages of this method includes low synthesis temperature, nanosize powder production, ultrafine particle size distribution, single phase, particle morphology control, high density, high purity, low porosity and environmental friendly. The researchers have used this method to synthesis nano size crystallites of ferrites [28-30].

2.2.4 Reverse Micelle Method

Reverse micelle method is used for the production of nanoparticles. Wet chemical method is carried out in reverse micelle, where quantity of water is enclose by surfactant molecules in an access volume of oil which offers good control over size and morphology of the nano particle. In this process surfactant molecule keep particles separated and restrict the particle growth which maintains control on size and shape of the particles. The surfactant molecule is use to make the aqueous droplet sizes stable in a hydrocarbon medium. In the aqueous portion, metal salt precursors are transformed from hydrocarbon state by a reactant. So the structure of the surfactant and the size produces a material with the wide range of grain sizes. The precipitation of the metal is influenced by the pH and the electrochemical potential of the solution, so the initial ratio of metal in precursors is modified to account for reduction of metals in the precipitate and to fire the sample. In this route molar ratio of water is used to control micelle size which is selected to yield a fine particle size in nano meter range. The amount of precursor solution to be used depends on the volume of aqueous solution and the particle size to be determined. The metal salt solution is then added to ammonia solution with constant stirring, the reaction is allowed to proceed until particle flocculation is induced by adding methanol. The particles are collected using centrifugation and washed by methanol, followed by methanol water solution to remove un-reacted ions. Finally, material is dried under vacuum and fired at high temperature in inert atmosphere to obtain the required product [31-34].

2.2.5 Precursor Method

The method is used for degradable compound of metals and the mix metals to synthesize with thermal treatment to produces require oxides. Homogeneous, pure oxide material and Ultra fine particles are generated from precursor. The researchers have employed a wet chemical method to synthesis ferrites for water soluble salts of desirable metals. The method is also known for the production of large surface area, homogeneous, low porosity and smaller size particles. The different methods are used for the production of ferrites nanoparticles and utilization from manufacturer point of view depends on the cost and purity of initial raw materials [35 -37].

2.2.6 Sol-gel Method

Sol gel method is used in preparation of inorganic oxides. It is a wet chemical method which involves physical as well as chemical process like hydrolysis, polymerization, gelation (solidification after freezing), condensation, drying, dehydration and densification. In this process the viscosity variation occurs at particular points in the sequence of steps. A sudden increase in the viscosity will result in the formation of gel, hence the name sol-gel for this method. Inorganic or oregano -metallic precursor are used in the synthesis of inorganic oxides. The advantages of the sol-gel method are good homogeneity, purity, processing in low temperature, and uniform phase distribution in complex system, better size, control on morphology and preparereration of crystalline / non crystalline materials.

The process involved in sol-gel method is at first solution is transform into a di-phasic gel like system consisting of solid and liquid phase. In some processes in order to form gel, excess liquid is removed and remaining liquid undergoes drying process, that result in shrinkage and densification. The rate at which solvent is removed tells about porosity. The process is then followed by poly-condensation and sintering of dried product that gives changes in structural and mechanical properties [38- 46].

2.2.7 Sonochemical Method

In this method the chemical reaction of molecules starts when it is exposed to powerful ultrasound radiation of frequency range from 20 KHz – 10 MHz. In this technique, the selected metal complex precursor's solution is exposed to fixed frequency sound waves. As the sound waves propagates in alternates rarefaction and compression, with certain threshold vapour pressure which causes cavities to form, grow and implode. This process involves the formation, growth and bubbles in liquid to collapses and the phenomenon is called acoustic cavitations. The method is used to prepare different kinds of amorphous magnetic nanomaterials of metal, metal alloy, oxide, ferrite, and nitride, also upgraded to produce core shell type materials [47].

2.2.8 Plasma Synthesis

Plasma synthesis is the most efficient technique to prepare nano powder samples. In this method a RF induction plasma torch of 50 KW at 3 MHz is used to produce crystalline nanomaterials. In stoichiometric proportion, a high power ball milled element powder with size less than 10 microns is used as metal ions in the plasma. The plasma gas as argon, and the mixture of argon and hydrogen gas as a plasma stream gas are used in the techniques. The process starts with a precursor powders are injected through plasma stream using an argon gas which acts as a carrier gas. Once the induction plasma is generated in the reactor, a high pressure air is injected as an oxidizer. Since this method involves complex system, the preparation of sample is tedious work. [51-54]

2.2.9 Chimie- Douce Method

The difficult synthesis made possible in this method and is quite peculiar. The method is an addition to the precursor method of sample preparation. The reactions in precursor method takes place at lower temperature such as below 500 ^{O}C compared to solid state reaction, so the phases thus formed are in metastable state according to the thermodynamics theory. Often the new phases that are formed have unusual structures but fascinating properties. In order to obtained a stable structure it is calcined at higher temperature. This method was originated from French researcher, hence the term Chimie-Douce method [55] of sample preparation.

The process involves with intercalation in which ions are inserted in the existing structure that leads to the decrease in cations of the host material using electrochemical method. The reverse of intercalation can also be done using electrochemical method.

The next step after intercalation is dehydration or removal of hydroxide group which is done using usual heating method and maintaining temperature below $500^{O}C$. Finally, the crystallite sizes of specimen are obtained by calcinations at different temperatures. It is observed that size depends on calcinations temperature which also affects particle size, Curie temperature, permeability, saturation magnetization, dielectric properties and resistivity.

2.3 Synthesis Of Rare Earth Doped Cobalt Ferrite Nanoparticles Material Using Thermal Combustion.

The one which is simple, reliable, quick and cost effective for the preparation of nano particles material is combustion method. The previous reports shows that researcher has employed combustion method for the preparation of Mn-Zn ferrite nanoparticles which is monophasic, better particle size distribution and having fascinating structural, magnetic and electrical properties. The process of synthesis involves several steps in which the metal salts are of AR grade having type I / II are taken in stoichiometric proportion along with complexing agent and fuel for combustion. The mixture is dissolved in the distilled water to get clear solution, free from any residues. Then the mixture solution is subjected to magnetic stirring at conventional temperature to obtain reduction in the volume. The reduced volume solution is further subjected to higher temperature heating to convert it to dry mass. As the dry mass dries completely, then triggers the auto combustion process. Finally powder is obtained at the end of the combustion method which is high quality product having ultra fine size particle distribution. This powder is utilized to study structural, magnetic and electric properties.

In current investigation three series of rare earth doped cobalt ferrite crystalline nanoparticles material prepared i.e. Gadolinium doped cobalt ferrites, Neodymium doped cobalt ferrites and Dysprosium doped cobalt ferrites using combustion synthesis.

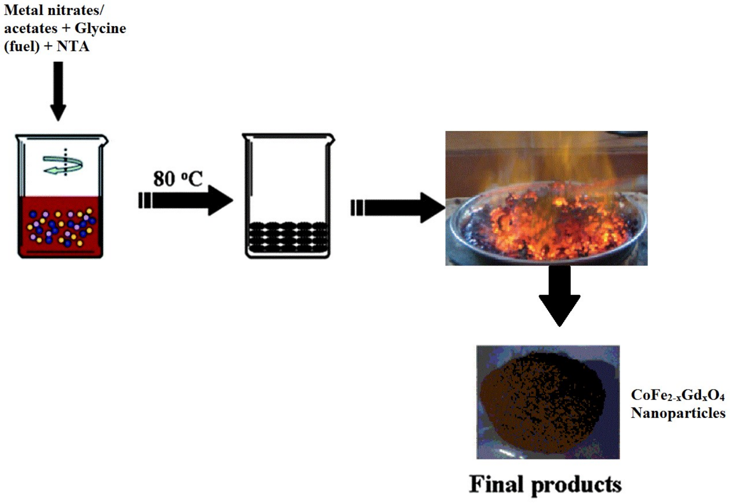

Fig.2.2: Steps involved in the preparation of rare earth doped cobalt ferrites using combustion method.

The chemical formulae and the doping concentration of materials are as follows:

i) $CoFe_{2-x}Gd_xO_4$ with concentration $x = 0.00, 0.02, 0.04, 0.06, 0.08, 0.10$.
ii) $CoFe_{2-x}Nd_xO_4$ with concentration $x = 0.00, 0.02, 0.04, 0.06, 0.08, 0.10$.
iii) $CoFe_{2-x}Dy_xO_4$ with concentration $x = 0.00, 0.02, 0.04, 0.06, 0.08, 0.10$.

The metal salt taken in stoichiometric ratio to prepare rare earth doped cobalt ferrites nano particles:

i) $CoFe_{2-x}Gd_xO4$ (Gadolinium doped Cobalt Ferrite), Cobalt (II) Nitrate, $Fe(NO_3)_39H_2O$, Gadolinium Nitrate, Nitrilotriacetic acid (NTA) [$C_6H_9NO_6$] and Glycine [$NH_{2.}CH_{2.}COOH$]

ii) $CoFe_{2-x}Nd_xO_4$ (Neodymium doped Cobalt Ferrite), Cobalt (II) Nitrate, $Fe(NO_3)_39H2O$, Neodymium (III) acetate hydrate [$Nd(CH_3CO_2)_3.xH2O$], Nitrilotriacetic acid (NTA) [$C_6H_9NO_6$] and Glycine [$NH_{2.}CH_{2.}COOH$]

iii) $CoFe_{2-x}Dy_xO_4$ (Dysprosium doped Cobalt Ferrite), Cobalt (II) Nitrate, $Fe(NO_3)_39H2O$, Dysprosium Nitrate, Nitrilotriacetic acid (NTA) [$C_6H_9NO_6$] and Glycine [$NH_{2.}CH_{2.}COOH$]

The metal salts as mentioned above were taken in stoichiometric ratio where Nitrilotriacetic acid as a complexing agent and Glycine as a fuel to burn mixture in the process of combustion method. The metal salts were mixed in 300 ml double distilled water and dissolved using magnetic stirrer at 80^OC temperature to obtain a clear homogeneous solution. This solution is then heated on the magnetic stirrer at 100^OC for the reduction of volume to form thick solution and to trigger auto combustion method. The solution was then transferred on a shallow plate kept on a heater. The solution was stirred constantly to avoid the bulging effect due to temperature gradient in the content. The continuous heating of the solution makes it bulging paste into a thick dry mass which then self ignites producing a residue powder. The residue powder which is obtained in the combustion method is the final ultrafine powder sample which is used for various characterization techniques of a sample [56-58].

References:

[1] Poorvi Dutta, Sushmita Gupta, Understanding of Nanoscience and Technology, Global publishing house, New Delhi,2006.

[2] N. Kaur, M. Kaur, Processing and Application of Ceramics, 8 (3), 137–143, 2014.

[3] K. K. Choudhary, Nanoscience and Technology, Narosa publishing house, 2018.

[4] R. Lane, B. Craig and W. Babcock, Amtiac, vol 6, 31, (2002).

[5] M. Rozman and M. Drofenik, J. Am. Ceram. Soc.78, 2449, 1995.

[6] D.S. Mathew, R.S. Juang, Chemical Engineering Journal 129 (2007) 51–65.

[7] A. Kale, S. Gubbala, R. Misra, Journal of Magnetism and Magnetic Materials 277 (2004), 350–358.

[8] S. Komarneni, E. Fregeau, E. Breval and R. Roy, J. Am.Ceram. Soc.,71(1988), C26.

[9] A. Goldman and A. M. Laing., J. Phys. Coll. 4 (1977), C1 297.

[10] A. Attaie, M. R. Piramoon, I. R. Harris, C. B. Ponton, J. Mater. Sci. 30, (1995), 5600.

[11] M. Seki, T. Sato and S. Usui, J. Appl. Phys. 63 (1988) 1424.

[12] A. Thakur and M. Singh, Ceram. Int. 29 (2003) 505

[13] C.F. Zhang, X.C. Zhong, H.Y. Yu, Z.W. Liu, D.C. Zeng, Physica B: Condensed Matter 404 (2009) 2327–2331.

[14] L. Nalbandian, A. Delimitis, V.T. Zaspalis, E.A. Deliyanni, D.N. Bakoyannakis, E.N. Peleka, Microporous and Mesoporous Materials 114 (2008) 465–473.

[15] P.P. Hankare, R.P. Patil, U.B. Sankpal, S.D. Jadhav, K.M. Garadkar, S.N. Achary, Journal of Alloys and Compounds 509 (2011) 276–280.

[16] A.S. Teja, P.Y. Koh, Progress in Crystal Growth and Characterization of Materials, 55,(2009) 22–45.

[17] S. Zahi, M. Hashim, A.R. Daud, Synthesis, magnetic properties and microstructure of Ni–Zn ferrite by sol–gel technique, J. Magn. Magn. Mater. 308(2), 177–182 (2007)

[18] Md. T. Rahman and C. V. Ramana, Journal of applied physics116, 164108, 2014.

[19] Venkata Sreenivas Puli, Shiva Adireddy, C.V. Ramana, Jounals of alloys and compounds, Vol.644, 470-475, 2015.

[20] H. S. Mund, Jagrati Sahariya,R. J. Choudhary, D. M. Phase, Alpa Dashora, M. Itou,Y. Sakurai and B. L. Ahuja, APPLIED PHYSICS LETTERS 102, 232403, 2013.

[21] Krishna hari Sharma and Pankaj Sharma (OPTOELECTRONICS AND ADVANCED MATERIALS, RAPID COMMUNICATIONS Vol. 7, No. 11-12,pages 887-890, November -December 2013.

[22]Sunil Rohilla , Pinki Rani , Navneet Kumar, National Conference on Recent innovations in Applied Sciences and Humanities' NCASH Vol. 4, issue 10, 2015.

[23]R.P. Pant, Manju Arora, Balwinder Kaur, Vinod Kumar, Ashok Kumar, Journal of Magnetism and Magnetic Materials 322, 3688–3691, 2010.

[24] A. K. Nikumbh, R.A. Pawar, D. V. Nighot, G.S. Gugale, M. D. Sangale, M. B. Khanvilkar, A.V. Nagawade (Journal of Magnetism and Magnetic Materials355, 201–209, 2014.

[24] Karimi Z., Mohammadifar Y., Shokrollahi H., Asl, Sh. Khameneh, Yousefi, Gh.; Karimi, L. NASA Astrophysics Data System ADS,01-06- 2014.

[25] S. Amiri, H. Shokrollahi, Journal of Magnetism and Magnetic Materials Volume 345, Pages 18-23, 2013.

[26] M.U. Islam, M. Ishaque, Hasan M. Khan, Muhammad Naeem Ashiq, M.U. Rana,Journal of Magnetism and Magnetic Materials,Volume 324, Issue 22, November 2012, Pages 3773-3777.

[27] Constantin Virlan , Georgiana Bulai, Ovidiu FlorinCaltun , Rolf Hempelmann , Aurel Pui, Ceramic International, 04, 121, 2016.

[28] Saif Ul Haque, Kallol Kumar Saikia, G.Murgesan and S. Kalainathan, Journal of Alloys and compounds, Vol.701, pages 612-618, 2017.

[29] Jianhong Pengn, Mirabbos Hojamberdiev , Yunhua Xu , Baowei Cao, Juan Wang ,HongWu ,Journal of Magnetism and Magnetic Materials 323,133,138, 2011.

[30] Xiruo Zhao , Wei Wang, Yajun Zhang , Sizhu Wu, Feng Li , J. Ping Liu, chemical engineering journal, volume 250, pages 164-174,2014.

[31] Myrtil L. Kahn and Z. John Zhang, Applied physics letters vol.78 no.23 4 June 2001.

[32] D. Kim, M. Miyamoto, and M. Nakayama, Journal of Applied Physics, 100 (2006).

[33]J. Chandradass, M. Balasubramanian, Dong Sik Bae, Hern Kim, Materials and Manufacturing Processes, 12 (2012), 1290-1294, 46.

[34] B. A. Smith, Jin Z. Zhang, Alan Joly, Jun Liu., Physical Review B, 62 (2000).

[35] M. M. Rashad, R.M. MoamedH.El- shall (IOSR – JAP e -ISSN: 2278 4861.Volume 7, Issue 3 Ver. III, PP21-25, May. - Jun. 2015.

[36] R.N. Panda, J.C. Shihab, T.S. Chinb (Journal of Magnetismand Mag netic Materials 257, 79 – 86, 2003.

[37] Lawrence Kumar and Manoranjan Kar, Journal of Experimental Nanoscience, Vol. 9, No.4, 362–374, 2014.

[38] S.R. Naik and A.V. Salkar, Journal of Material chemistry, issue 6, 2012.

[39] M.K. Shobana, HoonKwonb, Heeman Choe, Journal of Magnetism and Magnetic Materials 324, 2245–2248, 2012.

[40] Prathapan Sateesh; Jayaraman,Tanjore V., Varaprasadarao, Eswara K.; Das, Dibakar, NASA Astrophysics data system ADS, 2014-07-14.

[41] Sandip G. Kakade, Yuan-Ron Ma, Rupesh S. Devan, Yesh D. Kolekar, and C. V. Ramana J. Phys. Chem. C, 120 (10), pp 5682–5693, 2016.

[42] Erum Pervaiz and I H Gul, Journal of Physics: conference series, volume 439, 012015, 2013.

[43] Yadav, Raghvendra Singh; Havlica, Jaromir; Masilko, Jiri; Kalina, Lukas; Wasserbauer, Jaromir, NASA Astrophysics data system ADS.

[44] Sheena Xavier, Smitha Thankachan, Binu P Jacob and E M Mohammed, The Royal Swedish Academyof Sciences, Physica Scripta, Volume 87,No.2,2013.

[45] Rimi sharma,S. Bansal and Sonal Singhal (RSC advances ,issue 75, 2016.

[46] Raghvendra Singh Yadav, Ivo Kuřitka, Jarmila Vilcakova, Jaromir Havlica, Lukas Kalina, Pavel Urbánek, Michal Machovsky, Milan Masař, Martin Holek, Zeitschrift :Jounamaterials science: materials in electronics, Ausgabe 12, 2017.

[47] S.H. Jung, E. Oh, K.H. Lee, Y. Yang, C.G. Park, W. Park, S.H. Jeong, Crystal Growth Des, 8 (2008) 265–269.

[48] A.E.Kandjani, M.F. Tabriz, B. Pourabbas, Material Research Bulletin, 43 (2008) 645–654.

[49] L. B. Arruda, Douglas M.G. Leite, Marcelo O. Orlandi, Wilson A. Ortiz, Paulo Noronh Lisboa-Filho, Journal of Supercondtivity and Noval Magnetism, 26 (2013) 2515–2519.

[50] R.S. Yadav, P. Mishra, A.C. Pandey, Ultrasonic Sonochemical, 15 (2008) 863–868.

[51] Z. Tugut, Ph. D. Thesis CMU 2000.

[52] M. I. Boulos, J. High Temp. Chem. Processes 1 (1992) 401.

[53] S. Son et al., J. Appl. Phys., 91 (10), (2002), 7589.

[54] S.Yamamoto, N. Tanamachi, H. Kurisu, M. Matsuura and K. Ishida, 21 Aa I-6 digest 8th Int. Conf.on ferrites Kyoto Japan.

[55] A. R. West, Solid state chemistry and its applications, John Wiley and sons (1984).

[56] A. Thakur and M. Singh, Ceram. Int., 29, (2003), 505-511.

[57] A. D'souza, Deepak Kumar, M. Chatim, V. Naik, Pranav P. Naik, R. B Tangsali, Advanced Science Letters, Volume 22, Number 4, April 2016, pp.773-779(7).

[58] Pranav P. Naik, R.B. Tangsali, S.S. Meena, S.M. Yusuf, Materials Chemistry and Physics 191, 2017, 215-224.

CHAPTER 3

Characterization and Measurement Techniques

3.1 Introduction

Once the material samples are prepared, it has to be characterized in order to study the structure and properties of the materials. The research methodology plays role to investigate sample material formation and correlates its various properties involved by controlling their associated parameters. The advance technology and instrumentation allows the analysis of the materials and to extract novel information on structural morphology and the properties underlying this morphology. The data information obtained from modern instruments and techniques allows us to know the formation and confirmation of the sample. Once the sample is formed, the next step is the measurement of material properties using different types of sophisticated instruments. This chapter describes the characterization techniques and instruments used in collection and analysis of data for material samples.

The analytical techniques, the equipments and the procedure of various experimental techniques utilized for characterization, measurement of magnetic and electrical properties of rare earth doped cobalt ferrite nano particles are discuss. The chemical composition of material samples are $CoFe_{2-x}Gd_xO_4$, $CoFe_{2-x}Nd_xO_4$ and $CoFe_{2-x}Dy_xO_4$ (x= 0.00, 0.02, 0.04, 0.06, 0.08, 0.10).

3.2 Characterization Techniques

The characterization of the material sample reveals structure and provides information on processing stages, properties and performance of the material. The structure of a material is considered as atomic structure or arrangement of micro/macro structure that influences how the atoms are bonded together. This information allows us to categorised materials into metals, ceramics, and polymers and helps us to draw general conclusion related to their mechanical properties and physical behaviour of the materials. The characterization describes the features such as composition and structure of a material which are significant in providing information related to materials like electrical, thermal and mechanical properties. The characterization processes is usually achieved by allowing some form of probe to interact with sample under study and are used to explore crystal structure, particle size, size distribution, porosity, density, morphology, chemical composition etc.

The characterization methods used in present work are X-ray diffraction (XRD), Fourier Transform Infra red Spectroscopy (FTIR), Scanning Electron Microscopy (SEM), Transmission Electron Microscopy (TEM) and Energy Dispersive Spectroscopy (EDS). These are the techniques employed to characterize the material sample which will provides qualitative as well as quantitative information.

3.2.1 X-ray Diffraction Spectroscopy

A technique used to study the crystal structure which explores crystal parameters like crystallite size, unit cell shape, defects, stresses and to identify unknown materials etc [1]. The interaction of X-rays with the crystalline substance gives a diffraction pattern, a unique characteristic of a crystalline solid that provides information of the structure, phase and purity of the material. In fact intensities and peak position in diffraction pattern gives information of the structure and phases of the material. A crystal might be regarded as a three dimensional diffraction grating for X-ray whose wavelength is comparable with the atomic spacing and hence diffraction pattern provides information about the regular arrangement of atoms in the lattice. The average crystallite size is most important parameter which influences physical and chemical properties of nano crystalline samples. Hence, X-ray plays important role in determination of average crystallite size of nano crystalline samples [2].

3.2.1.1 Bragg's Law

The materials are made up of periodic array of atoms and when X-ray scatters from such arrangement gives rise to diffraction effect that follows Bragg's law. This law shows relationship between the scattering angles, the wavelength of the radiation and the spacing between atomic planes. The distances between atomic planes depend on size and distribution of atoms. So XRD are used in the phase identification of the material [3-5].

When X-ray beam is incident on the crystal structure at a particular angle (θ), it gets reflected from atomic planes and the constructive interference in the crystalline material occurs when the path difference between reflected beams is integral multiple of X-ray wavelength [6]. The condition satisfied by Bragg's law and given as

$$n\lambda = 2d\sin\theta \qquad 3.1$$

where d is a spacing between two adjacent plane, λ is a wavelength of the X-ray, n is an integer which is equal to 1 (first order) and θ is known as a diffraction angel or a Bragg's angle. The diffractometer scanned sample at an angle of 2θ in all possible direction of the lattice due to its random orientation of the powder sample. The law states that the constructive interference of diffracted waves takes place only when the inter-planar path difference is integral multiple of the incident wave length (λ).

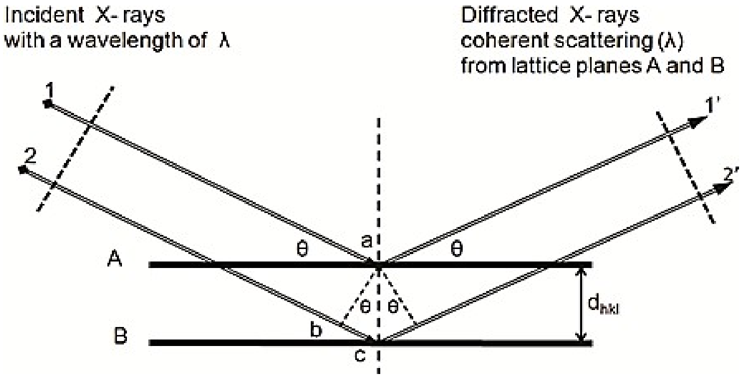

Fig.3.1: constructive interference from the parallel planes [7]

The measurement geometry used in X-ray diffraction instrument is Bragg-Brentano techniques [8-11] in which diffracted angle is 2θ that is the angle between incident beam and detector angle. The incident angle is always half of the detector angle. In these techniques, X-ray tube is fixed with the sample that rotates at θ° per minute and detector rotates at 2θ° per minute [12-14]. Each material has unique d–spacing, so by carefully inspecting d-spacing of diffracted peaks of a material allows one to identify the sample material. These d-spacing values of diffracted peaks are compared with the reference standard patterns to attain the identification of a sample material. The crystal system is divided into seven crystal structure using lattice parameters a, b, c corresponds to length of crystallographic unit cell and α, β, γ are the angles between the lattice parameters [15-19]. The figure 3.2 shows the lattice parmeters of a unit cell. The seven crystal systems are: 1.cubic 2. tetragonal 3.orthorhombic 4.hexagonal 5.trigonal / rhobhohedral 6. monoclinic 7. Triclinic.

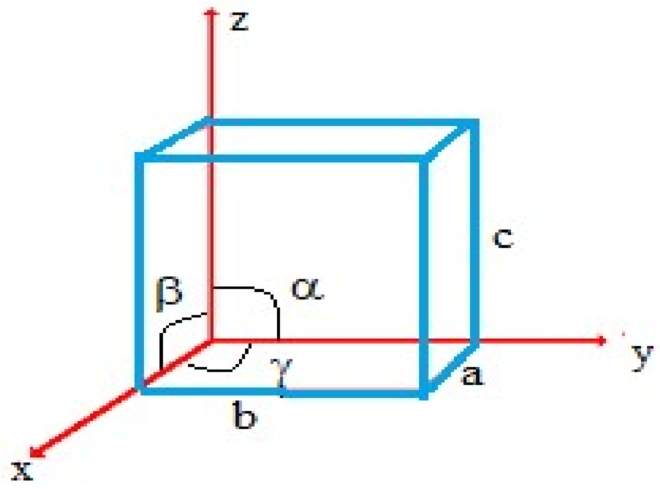

Fig. 3.2: Lattice parmeters of a unit cell.

3.2.1.2 Crystallite Size

It is known that for ultrafine particles, when the crystallite size decreases, the width of the diffraction peak increases. Therefore, XRD can be used to estimate average size of small crystallites, using the measured width of the peaks in the diffraction patterns. The formula used to estimate average crystallite size is Debye- Scherrer and is given by equation 3.2.

$$t = 0.89\lambda / \beta\cos\theta \qquad 3.2$$

where t is thickness of the crystallites in Å, λ is x-ray wavelength, θ is the diffraction angel 0.89 is the shape factor and β is the width of the diffraction peak (FWHM) [3].

3.2.1.3 Lattice Constant

The individual sample lattice constant of each peak was calculated using equation (3. 3) gien below.

$$a = d^* (h^2+K^2+l^2)^{1/2} \qquad 3.3$$

where h, k, l are called miller indices of a crystal plane and d is called interplanar distance. The accurate calculation is done using Nelson- Riley techniques. The function F (θ) is called Nelson-Riley function and it is expressed as (3.4)

$$F(\theta) = \tfrac{1}{2} [\mathrm{Cos}2\theta / \mathrm{Sin}\theta + \mathrm{Cos}2\theta/\theta] \qquad 3.4$$

In this method first calculate lattice constant ‘a’ of all the peaks and then plotted against F (θ). The accurate value of lattice constant is calculated using a least square fit method. The graph of lattice constant ‘a’ versus F (θ) (x-axis) with least square fit line intersect y-axis when f (θ) = 0, here the Y-intercept gives the actual value of a lattice constant [20].

3.2.1.4 X-ray Density (ρ_x)

The X-ray density is calculated from the equation (3.5) given below.

$$\rho_x = 8\,M / N_a{}^3 \qquad 3.5$$

where M ismolecular weight of the sample, N –Avogadro's number, a –lattice constant.

3.2.1.5 Porosity (P)

The porosity of sample can be calculated from the equation (3.6).

$$P=(\rho_x-\rho_b/\rho_x) \qquad 3.6$$

Where ρ_b – mass density measured using Archimedes principle and ρ_x is X-ray density.

3.2.1.6 Preparation of Sample Material for Powder X-ray Diffraction

A finely grinded sample powder of approximately 0.5gm was use for obtaining X-ray pattern for preparing rare dope cobalt ferrite sample material. The materials under investigations are rare earth doped transition metal ferrites such as Gd doped $CoFe_2O_4$, Nd doped $CoFe_2O_4$ and Dy doped $CoFe_2O_4$.

Fig.3.3: Rigaku X-ray diffractometer, SPAS, Goa University.

Rigaku diffractometer with target cu-kα, λ = 1.5148 Å was used for the phase confirmation of the sample material over the 2θ range from 20^o - 80^o in a steps of 0.02 and scan rate of 2^o per minute.

3.2.2 Fourier Transform Infra-red Spectroscopy (FTIR)

Infrared Spectroscopy is a technique used in the field of research and industrial purposes as one of the tool for a measurement, control and to maintain a quality check. The method helps us to identify chemical functional group present in the sample material by matching its spectrum with known reference spectrum. In crystalline solids a local symmetry, ordering phenomenon in spinel and to locate Fe^{2+} ions in the sample is usually determine by IR spectroscopy. IR region of spectrum is spread from wavelength of 0.75 – 300 μm. The region is further divided into following sub-regions: near infra-red region (0.7 – 2.5 μm), middle infra-red region (2.5 – 15 μm) and far infra-red region (14.3 – 50 μm) [21, 22]. The energy ranges for this three regions are 37 – 10 kcal / mole, 10 -1.0 kcal/mole and 1.0 -0.1 kcal/mole respectively. The middle IR region is used for the study of organic compounds. It is also express in terms of wave number with the unit of cm^{-1}. Since IR radiations do not have enough energy to induce electronic transition, hence the absorption is restricted to possible vibration and rotational states of a compound that deals with small energies. The absorption in infra red radiation depends on increasing the energy of vibration or rotation associated with the covalent bond in a molecule. If such an increase causes a change in the dipole moment of the molecule so as to absorb infrared radiation molecule must undergo a net change in dipole moment due to its vibrational or rotational motion. The molecules containing covalent bonds will show some degree of selective absorption in the infrared with the exception of diatomic species such as O_2, N_2, H_2, C_2 etc.

Fig.3.4: Shimadzu FTIR 8900 system, SPAS,Goa university.

The absorption of infra red radiation is characterized by the Bouger-Lambert-Beer law which states that absorbance of a material sample is directly proportional to the thickness of the sample and the concentration of the attenuating species in the material sample. IR presented by a plot of the % Transmission versus the wave number in cm^{-1}. A typical IR is recorded for the range of 5000 cm^{-1}- 100 cm^{-1} [23-25].

Stretching and bending are the two main types of molecular vibration that are associated with the compound. Whenever there is a change in inter atomic distance along the bond axis, the stretching mode is observed. The stretching mode shows symmetric or asymmetric motion. The change in bond angle occurs in bending and shows twisting, scissoring, wagging or rocking types of motion. The compound absorbs radiation in a specific frequency ranges and associate energy enhances above kinds of motion. This occurs when frequency of the IR absorption matches with the vibrational frequency of the molecule. The absorption gives rise to the absorption bands in IR spectrum [26-28]. The inspection of position, shape and the intensity of the absorption peaks of the IR spectrum reveal the details of the molecular structure of a sample [29, 30].

The basic idea in IR spectroscopy is to utilized two interfering beams of interferometer. If optical path difference between two inferring beams is change then each wavelength beam produces its own interference pattern. The radiation from the interferometer passes through the sample; either it transmutes or reflects to analyser and focussed on the detector. The signals from detector are amplified, converted to digital and transfers to a computer for Fourier transformation [31-33].

3.2.2.1 Sample Material Preparation for FTIR Spectroscopy

To record FTIR spectra of rare earth doped cobalt ferrite nanoparticles sample, first background spectrum has to be recorded. For background spectrum, 100 mg KBr powder is weighed and pressed into the pallet with the thickness of 1mm and radius of 6mm.The background spectrum is recorded on FTIR instrument and stored. Next the sample to run on FTIR spectra are weighed as 1-2 mg depending on the concentration, type of material and mixed with 100 mg of KBr powder. The mixtures were grinded properly and pressed into similar pallet to record FTIR spectra for rare earth doped cobalt ferrite.

3.2.3 Scanning Electron Microscope (SEM)

Instrument is used to obtained high resolution images to study the surface morphology of the sample material. The high resolution images are used to study shape of the object, chemical composition variation, spot chemical analysis using EDS, phases of crystalline structure. The images help to evaluate grain size, surface roughness, porosity, particle distributions, etc. SEM images focuses on surface processes rather than transmission which is used in TEM [34]. In SEM instrument a fine beam of energetic electrons exposed to the surface of the specimen which emits secondary electrons from the surface of specimen under observation. The two dimensional view of specimen topography is obtained.

Fig.3.5: Carl Zeiss EV018 scanning electron microscope assembly, Electronic Instrumentation, Goa University

The basic construction of scanning electron microscope consist of optical system, material mounting stag, secondary electron detector, display unit and control system to carry out various operation. The optical system is equipped with optical setup to generate probing electron and mounting stage for placing specimen. The detector is used to detect secondary electrons and display unit to monitor. The optical system comprises of electron gun, condenser lens and objective lens to produce electron probe. The space around the specimen is kept under high vacuum.

In the working of SEM, a source of electrons is focused in vacuum into a fine probe that is placed over the surface of the specimen. The electron beam passes through the scan coil and objective lens that deflect horizontally as well as vertically so that the beam scans the surface of the sample. As electrons beam penetrates a specimen, the number of interactions results that give rise to the emission of X-rays, Auger electrons, backscattered electrons and secondary electrons from the sample or through the surface. All the signals are then collected by detectors to form images of sample which has to be display on the monitor or the images can be printed. The secondary electron imaging shows the surface topography features where as backscatter electron image shows the spatial distribution of elements or compound within the top micron of the sample. The characteristics of X-rays are used for detecting composition of the sample material and to measure abundance of elements in the sample using EDS [35, 36].

3.2.3.1 Sample Material Preparation Of Scanning Electron Microscope

The sample material is first grounded into a fine particles powder using mortal. The quantity of 3 – 5 mg powder is weighed and then mixed with 50 ml of acetone. The mixture is sonicated for one hour and then the drop of sonicated solution was taken on thin gas cover-slips. The cover slips are exposed to gold sputtering process for about 90 seconds to improve the surface conductivity of the sample. These gold sputtering cover slips are mounted on specimen stage to obtain SEM images.

3.2.4 Transmission Electron Microscope (TEM)

Transmission electron microscopy is an imaging technique in which a beam produce by electron gun is focus onto a specimen using set of condenser lenses and is then magnified by projector lenses. These lenses makes an enlarge version to appear on a fluorescent screen or a layer of photographic film or to be detected by a CCD camera. The basic principle of operation uses electron beam in microscope instead of light. TEM is useful for determining size, shape and arrangement of the particle. The specimen used in TEM is useful for determination of lattice planes and atomic scale defects at nano level with the help of selected area using electron diffraction (SAED) techniques [37, 38]. The d-spacing between lattice planes of crystalline materials can be calculated from a SAED pattern using the relationship given below in equation (3.7).

$$dr = \lambda L \qquad 3.7$$

where L is a distance between the specimen and the photographic plate, λL is camera constant and r is the radius of diffracted rings.

It is easy to major r directly from the photographic plate and λL can be established from the instrument by calibrating it with a standard material such as Ag. The value of each d corresponds to a specific lattice plane and for a specific crystal structure. SAED pattern is useful in describing a crystal structure of a crystalline specimen and more helpful as compared to XRD instrument due to its detection limit.

3.2.4.1 Sample Material Preparation in TEM Measurement

For TEM measurement, the sample material was grounded finely and weighs 2-3 mg of sample. Using ultrasonic machine powder sample was dispersed in a suitable organic solvent like acetone/methanol. The drop of the solution is poured on Carbon coated TEM grids. The film formed on TEM grid is allowed to dry for 2 minutes. The extra solvent is removed using a blotting paper and sample film is placed in holder for the exposure of electron beam. Then TEM measurements are performed.

3.2.5 Vibrating Sample Magnetometer (VSM)

A vibrating sample magnetometer is used for the measurement of magnetic characteristics of different materials as a function of applied field at different temperatures and as a function of temperature at different applied field strengths. The working of vibrating sample magnetometer is based on the Faraday's law of induction, according to which a changing magnetic field produces an electric field. The data express as a function of varying magnetic field are used to determine the behavior of magnetic material. The sample in VSM device is vibrated in uniform magnetic field, and the induce voltage is detected by properly positioned set of coils, which is proportional to the magnetization of the material. The instrument allows precise magnetization measurement to be made as a function of magnetic field, temperature and crystallographic orientation.

These types of measurements find applications in the field of research and development, testing of production, quality and process control.The electric field generated by an alternating magnetic field in the pickup coil is in accordance with the Faraday's law of induction, and the current produced will be proportional to the magnetization of the sample. The induced current is higher for the greater magnetization [39- 41].

The Quantum Design Versa Lab's 3 Tesla vibrating sample magnetometer (VSM) is fastest and reliable with delicate DC magnetometer and is used in the magnetic measurement of the samples. The temperature of the sample can be varied between lower 50 K to higher 400 K and to achieve cryogenic temperature a cryogen free cry-cooler device is used. The niobium-titanium (Nb-Ti) superconducting solenoid placed in the cryostat vacuum provides magnetic field of 3T at 20 A current and is cooled by solid conduction. The magnetic shield is utilized to isolate magnetic noise in the system [42].

3.2.5.1 Sample Material Preparation for Vibrating Sample Magnetometer

The magnetic properties of rare earth doped cobalt ferrites sample materials are measured using Quantum Design Versa Lab's 3 Tesla vibrating sample magnetometer (VSM). Hysteresis measurement of a sample, the powder sample of 3 mg was wrapped in Teflon tape and placed on sample holder of the system. The contribution due to Teflon tape was eliminated in the data measurement. The magnetic moment measurement for Zero field cooled (ZFC) and Field Cooled (FC) was obtained on the same system. In ZFC magnetic measurement, initially sample was cooled down from room temperature to 50 K in the absence of magnetic field, and then magnetic moment of the sample was measured by increasing the temperature of the sample with constant applied magnetic field of 500 Oe. Similarly for FC magnetic data recording, the sample was cooled from room temperature to 50K with a constant magnetic field of 500 Oe and the data is recorded for rise in temperature. The entire measurement is automated and computer control through a software program. The software program is adjusted by feeding in the required parameters as per the user requirement.

3.2.6 D.C. Resistivity

The material in which resistivity varies over a large range of temperature like semiconductor, find applications in the field of sensors [43]. In ferrites materials, the electrical resistivity depends on the composition, micro structure and the preparatory condition [44]. The conduction mechanism in ferrites is different from that in conventional semiconductor and can be explained using electron hopping model [45, 46]. Ferrites material shows resistivity variation over wide range from 10^{-3} Ω cm to 10^{10} Ω cm [47].The variation is attributed to cations distribution at tetrahedral A site and octahedral B site along with hopping mechanism. The low value of resistivity is for dominance of divalent cations and high value for trivalent cations dominance at octahedral site with hopping between two sites.

In hopping model, a charge carrier jump from one cationic site to another since they are not free to move. As lattice vibrates, the probability of electron transfer is high as the ions come close enough to facilitate electron transfer. The conduction in this case is trigger due to the lattice vibrations. The carrier mobility shows temperature depends in conduction mechanism and is characterized by activation energy [48, 49].

The fixed voltage two probe techniques were utilized for the measurement of resistance. DC resistivity setup for measurement is shown in the figure 3.5. The temperature of the sample is measured using a calibrated thermocouple attached to the controller and the temperature is indicated on the monitor. The resistance of the sample is measured by varying the temperature and on increasing temperature thermal agitation of the electrons increases. The electrons acquire energy larger than band gap energy and hop into the conduction band. These electrons in conduction bands are called free electrons and vacancies existing in valence band are holes. Since more and more charge carriers move into conduction band as temperature increases, the resistivity of the semiconductor decreases.

Fig.3.6: Two probe D.C. resistivity setup with data acquisition system, SPAS, Goa University.

3.2.6.1 Sample material preparation for Resistivity measurement

Rare earth doped cobalt ferrites nanoparticles powder having chemical formula $CoFe_{2-x}RE_xO_4$ is pressed into pallets. The pallet thickness was ranging between 2 to 3 mm with a diameter of 6 mm .The palette was painted with silver paste on the both side to create good ohmic contact with the electrodes. The current variations over temperature were recorded for all the samples in the range from room temperature to 500^{O} C using two-probe resistivity set up.

3.2.7 Dielectric Measurement

The insulating nature of dielectric materials exhibits a property of electric polarization by virtue of which they modify the dielectric variation of the vacuum. A dielectric material when introduced into an electric field, the material gets polarized. In presence of electric field material is polarized, this phenomenon is known as dielectric polarization. The microscopic structure of the material is correlated to specific inductive capacity by Mossotti [50, 51] and Clausius [52] and Faraday introduce macroscopic feature of the insulator [53] which is called dielectric constant. According to Faraday's, dielectric is composition of conducting sphere in non conducting medium and showed the relation between the real part of the dielectric constant and the volume fraction occupied by the conducting particle in the dielectric by Clausius and Mossotti [54] .

Michal Faraday showed that if capacitor Co is filled with a dielectric material under vacuum then its value increases to C and the increase in capacitance is expressed in terms of electrical susceptibility χ as (3.8)

$$x = \frac{C-Co}{Co} = \frac{\Delta C}{Co} \qquad 3.8$$

Another term, dielectric permittivity ε_r defined as a ratio of capacitance C filled with dielectric material to Co capacitance in vacuum condition and given by equation 3.9.

$$\varepsilon_r = \frac{C}{Co} \qquad 3.9$$

The dielectric constant is dimensionless quantity and is a measure of extent to which the electric charge distribution in the material is distorted or polarized by applying an electric field.

In ferrites, materials show excellent dielectric at lower frequencies and for crystalline materials the dielectric constant is strongly dependent on applied frequencies. In designing microwave devices such as isolators, circulators etc., ferrites materials with high dielectric constants are used. The dielectric property of a material especially nano material depends on the method of preparation, chemical composition, grains structure or size and doping concentration.

Figure 3.7: Wayne Kerr precision component analyzer 6440B, School of Physical and Applied Sciences (SPAS), Goa University.

3.2.7.1 Dielectric Loss

The permittivity of a dielectric material, express as real and imaginary part and denoted as $\varepsilon^{'}$ and ε'' respectively. The imaginary part depicts energy lost during the passage of AC signal through the dielectric material. The real part of permittivity is called dielectric constant or relative permittivity and specifies a relation between the transmission of speed of AC signal and the capacitance of dielectric material. The imaginary part measures the amount of electric field loss in terms of heat which is dissipated during the polarization process in the passage of an alternating electric field known as dielectric loss and is given by following equation 3.10.

$$Tan\,\delta = \frac{\varepsilon^{''}}{\varepsilon^{'}} \qquad 3.10$$

The alignment in the dipoles in an electric field is responsible for the alteration in the frequency of dielectric constant and dielectric loss over a wide range of frequency. The relative permittivity of the material is connected with various processes that results into increase in polarization. In low frequency range due to ion conductivity influence the imaginary part of permittivity is suppressed. The alteration produced in permittivity is due to various factors like dipole relaxation. The application in microwave devices and radio frequency is depends on dielectric properties which are alter and affected by the position of ions due to lattice vibrations [55-57].

There are two types of losses occurs in the range of high frequencies, intrinsic and extrinsic loss that are associated with crystalline solids. The factors responsible for this are ionic masses, electric charge, and valence state of ion, spring constant of the bond; lattice imperfection etc. Intensive dielectric losses in solids are due to low frequency phonons and are dependent on the microwave field and phonon interaction cause to the relaxation of the phonon distribution function. The interaction between the charge defects and the microwave fields are the cause of extrinsic losses.

3.2.7.2 Sample Material Preparation for the Measurement of Dielectrics

Rare earth doped powder is pressed into the pallets of about 2 mm to 3 mm of thickness and the diameter of 12 mm. The pallets were painted with silver on both sides for good ohmic contact. Capacitance and dielectric loss is measured as a function of frequency over the range of 20 Hz to 3 MHz. Temperature dependence of capacitor and dielectric loss is measured. Capacitance and dielectric loss is recorded over the temperature range of 30°C to 500°C at ten different frequencies (20 Hz, 100 Hz, 500Hz, 1KHz, 5 KHZ, 10 KHz, 100 KHz, 500KHz, 1 MHz, 2 MHz, 3 MHz) for the experimenta samples using Wayne Kerr precision component analyzer 6440 system. Dielectric constant is determined using following equation (3.11).

$$\varepsilon_r = \frac{Cd}{\varepsilon_{0A}} \qquad 3.11$$

Here *C*- capacitance, *d*- thickness of pallet, *A*- area of pallet, ε_0 – the permittivity of the free space.

3.2.8 Thermo Power

In thermo power instrument, the two sides of a ferrites material are maintained at different temperature that produces a electromotive force (emf) i.e. thermo-emf which is measured in volts. The analysis of thermo power is useful in understanding the conduction mechanism in the semiconductor material due to its low mobility. The quantification of thermo-emf is simple and its sign provides important information regarding conduction mechanism in the material. The sign gives the information about conduction in the material whether it is electrons or holes. The measurement explores the behaviour of the material whether it is p type or n type. The main significance of thermo-emf techniques is that it allows calculating Fermi energy and carrier concentration values. The experimental set up of thermo-emf is shown in the figure 3.8. The experiment has upper contact point probe that forms a hot junction and the lower contact point probe is cold junction and the sample is place in between them [58 - 64].

Fig.3.8: Thermoelectric power setup, SPAS, Goa University

3.2.8.1 Sample Preparation for Thermo Power

Rare earth doped powder is pressed into the pallets having thickness of 2 mm to 3 mm and the diameter of 12 mm. The pallets are painted with silver paste on both sides for ohmic contact. The thermoelectric power measurement is recorded over the temperature range from room temperature to 500^{o}C in the steps of 5^{o}C.

3.2.9 A C Susceptibility

The investigation of AC susceptibility serves a twofold purpose: firstly, to as certain the Curie temperature of a sample particle, and secondly, to identify the particle type within the sample material. The classification encompasses three distinct particle categories: single domain (SD), multidomain (MD), and super-paramagnetism (SP). Utilizing a high-temperature AC susceptibility setup provided by ADEC Embedded Technology and Solutions Private Limited in Goa, India, the thermal dependency of normalized AC susceptibility for various ferrite samples is meticulously examined across a temperature spectrum spanning from room temperature to 600°C.

Through meticulous plotting of normalized AC susceptibility against temperature for all ferrite specimens, distinctive patterns emerged, facilitating the determination of the sample's particle characteristics. It was observed that particles with dimensions below 10 nanometers typically exhibit super-paramagnetic behavior, characterized by a consistent decline in susceptibility as temperature rises. Conversely, particles ranging from 10 to approximately 50 nanometers tend to display single domain attributes, resulting in a linear susceptibility increase with escalating temperature until a critical point corresponding to the Curie temperature [65-70].

3.2.9.1 Sample Material Preparation for AC Susceptibility Measurement

The 5 -7 mg powder is grinded properly and inserted in the glass test tube which in turn inserted in the AC susceptibility measurement set up supplied by ADEC embedded system and measurement of susceptibility is recorded from room temperature to 550^{O}C.

References:

[1] J. P. Srivastava, Elements of Solid State Physics, Prentice - Hall India, New Delhi (2001).

[2] C. B. Murray, C. R. Kagan, and M. G. Bawendi, Annu. Rev. Mater. Sci., 30, 545-550, 2000.

[3] R. Jenkins, An Introduction to X-ray Spectrometry, Wiley Heyden, London, Chapter 4, 1974.

[4] L.S. Birks, 'History of X-ray Spectro -chemical Analysis', American Chemical Society Centennial Volume, ACS, W ashington DC, 1 976.

[5] H.G. J. Moseley, Philosophical Magazine, 26, (1912)1024–1034.

[6] C. Kittel, Introducion to Solid State Physics, Seventh Edition, John Wiley & Sons Inc., Singapore, (1995).

[7] Simona Burianova, Jana PoltierovaVejpravova, Petr Holec, Jiri Plocek and Daniel Niznansk, Journal Applied Physics 110 (2011) 073902.

[8] L.S. Birks, 'History of X-ray Spectro-chemical Analysis', American Chemical Society Centennial Volume, ACS, Washington DC, 1976.

[9] Brady, B. John, Boardman, J. Shelby, Journal of Geo-science. Education, v. 43 (5) (1995), 471-476.

[10] M. Birkholz, C. Genzel, T. Jung, Journal of Applied Physics, **96,** 7202, 2004.

[11] Y. T. Prabhu, K. Venkateswara Rao, V. Sesha Sai Kumar, B. Siva Kumari, International Journal of Engineering and Advanced Technology (IJEAT), 2, 2249 – 8958, 2013.

[12] R. Jenkins, D. J. Haas, F. R.Paolini, Norelco Reporter, 18, (1971)1–16.

[13] C.L. Mallory, R.L. Snyder, Advances in X-Ray Analysis, 22, (1979)121–132.

[14] B. E. Warren, X-Ray Diffraction, Addison-Wesley, Reading, MA, (1969).

[15] B. D. Cullity, Elements of X-Ray Diffraction, Addison-Wesley, Reading, MA, miller, 1967.

[16] P. P. Naik, R. B. Tangsali, B. Sonaye, S. Sugur, Journal of Magnetism and Magnetic Materials, 385,377–385. Miller, 2015.

[17] A. L. Linsebigler, Guangquan Lu, John T. Yates Jr., Chem. Rev 95 (1995) 735–758.

[18] G. Vijayaprasath, R. Murugan, Y. Hayakawa, G. Ravi, Journal of Luminescence 178 (2016) 375–383.

[19] S.Taguchi, T. Tayagaki, Y. Kanemitsu, Materials Science and Engineering 6 (2009) 012029.

[20] A. K. M. Akther Hossaina, S.T.Mahmuda, M. Seki, T. Kawai and H.Tabata, J. Magn. Magn Mater, 312, (2007), 210-219.

[21] B. Stuart, Infrared Spectroscopy: Fundamentals and Applications Chichester: Wiley 2004.

[22] H.Gunzler, H. U. Gremlich, IR Spectroscopy: An Introduction Weinheim: Wiley 2002.

[23] Ratnamala Chatterjee, AnjaliVerma, Journal of Magnetism and Magnetic Materials, 306(2006) 313–320.

[24] B. Stuart, Infrared Spectroscopy: Fundamentals and Applications (Chichester: Wiley) 2004.

[25] H. Gunzler, H. U. Gremlich, IR Spectroscopy: An Introduction (Weinheim: Wiley) 2002.

[26] R. J. Bell, Introductory Fourier Transform Spectroscopy New York: Academic (1972).

[27] T. Vo-Dinh, Handbook of Spectroscopy, WILEY-VCH (2003).

[28] M. Vollmer, K-P Möllmann, The Physics Teacher, 46 (2008) 114–7.

[29] J. Kauppinen, Fourier Transforms in Spectroscopy Berlin: Wiley (2001).

[30] W. S. Lau, IR Characterization for Microelectronics, World Scientific (1999).

[31] E. D. Palik, Handbook of Optical Constants of Solids Boston, MA: Academic (1985).

[32] H. M Heise, J Fritzsche, H Tkatsch, F Waag, K Karch, K Henze, S Delbeck, J 71 Budde, European Journal of Physics, 34 (2013) 139–59.

[33] M Vollmer, K-P Möllmann, Infrared Thermal Imaging: Fundamentals, Research and Applications, Weinheim: Wiley (2010).

[34] J. Goldstein, Scanning electron microscopy and x-ray microanalysis, Kluwer Adacemic / Plenum Publishers, (2003), 689. 109.

[35] B. Voutou and E. C. Stefanaki, Physics of Advanced Materials Winter School, (2008).

[36] E. Suzuki, Journal of Microscopy, 208 (3), (2002), 153-157.

[37] G. Thomas, Transmission Electron Microscopy of Metals (John Wiley & Sons, Inc, New York, 1962).

[38] D. B. Williams and C. B. Carter, Transmission Electron Microscopy: A Textbook for Materials Science Vol. I-IV, (Plenum Press, New York, 1996).

[39] A. Hubert, R. Schäfer. Magnetic Domains, Springer-Verlag, Berlin Heidelberg, 1998.

[40] B. D. Cullity, C. D. Graham, Introduction to Magnetic Materials. John Wiley & Sons, New Jersey, 2009.

[41] O' Handley, R. C. Modern magnetic materials: principles and applications. John Wile & Sons, New York, 2000.

[42] Quantum Design's Versa lab 3 Tesla VSM user manual, part no. 1300-001, A0.

[43] D. Santosh Kumar and K. Chandra Mouli, International Journal of Nanotechnology and Applications, Volume 4, No.1 (2010) 51-59.

[44] Sangeeta Thakur and S. C. Katyal M. Singh, Applied Physics Letters, 91, (2007), 262501.

[45] A. A. Samokhvalov, A.G. Rustamov, Soviet Physics Solid state, 6,749, 1964.

[46] A. A. Samokhvalov, A.G. Rustamov, Soviet Physics Solid state, 7, (1965), 961.

[47] L. G. Van Uitert, Proc .I. R.E. 44 (1956) 1294.

[48] G. H. Jonker, J. Phys. Chem. Solids, 9, (1959), 165.

[49] E. J. W. Verwey and J. H. de Boer, Reauil Ches Travaux chimques des Phys. Bas (Czeckh), 55(1936) 531.

[50] "The NIST reference on fundamental physical constants" *Physics.nist.gov.* Retrieved 2011-11-08.

[51] O. F. Mossoti, Bibl. univ. modena6, (1847) 193.

[52] R. Clausius Vieweg. Braunschweigh Volume 2 (1879)

[53] M. Faraday, Phil. Trans 128:1 79 (1837)265.

[54] O. F. Mossoti, Mem. di Matheme.e.fisica in modena, 24(2) (1850)49.

[55] I. El Heda, Study of the structural, electrical, dielectric properties and transport mechanisms of Cu0.5Fe2.5O4 ferrite nanoparticles for energy storage, photocatalytic and microelectronic applications, Heliyon 9(2023) e 17403.

[56] A. J. Dekker, Solid State Physics, 148, 149.

[57] A.K. Jonscher, Dielectric relaxation in solids, 306.

[58] B. L. Gallagher and P. N. Butcher, Handbook on semiconductors, Amsterdam; Elsevier, 1 (1992) 721-816.

[59] C.M. Bandari and D.M. Rowe, Thermal conduction in semiconductors, Wiley Estern Ltd, New Delhi (1988).

[60] F.J. Blatt, P.A.Schroeder, C.L.Foiles and D. Greig, Thermoelectric power of metals, Plenum Press, New York, (1976).

[61] S.M. Puri, and T.H. Geballe, Semiconductors and Semimetals, Eds. R. K. Willardson and A. C. Beer, Academic Press, New York (1966) 203.

[62] B. L. Gallagher and P. N. Butcher, Handbook on semiconductors, Amsterdam; Elsevier, 1 (1992) 721-816.

[63] C.M. Bandari and D.M. Rowe, Thermal conduction in semiconductors, Wiley Estern Ltd, New Delhi (1988).

[64] F. J. Blatt, P.A.Schroeder, C.L.Foiles and D. Greig, Thermoelectric power of metals, Plenum Press, New York, (1976).

[65] M.A. Gabal, Y.M.A. Angari, F.A. Al-Agel, Cr-substituted Ni–Zn ferrites via oxalate decomposition: Structural, electrical and magnetic properties, J. Magn. Magn. Mater., 391 (2015) 108–115.

[66] I. Soibam, S. Phanjoubam, C. Prakash, Magnetic and Mössbauer studies of Ni substituted Li–Zn ferrite, J. Magn. Magn. Mater., 321 (2009) 2779– 2782.

[67] T. Prabhakaran, J. Hemalatha, Chemical control on the size and properties of nano NiFe2O4 synthesized by sol–gel autocombustion method, Ceram. Int., 40,(2014), 3315–3324.

[68] H. Das, N. Sakamoto, H. Aono, K. Shinozaki, H. Suzuki, N. Wakiya, Investigations of superparamagnetism in magnesium ferrite nano-sphere synthesized by ultrasonic spray pyrolysis technique for hyperthermia application, J. Magn. Magn. Mater., 392 (2015) 91–100.

[69] M. Mozaffari, J. Amighian, E. Darsheshdar, Magnetic and structural studies of nickelsubstituted cobalt ferrite nanoparticles, synthesized by the sol–gel method, J. Magn. Magn. Mater., 350 (2014) 19–22.

[70] S.G. Gawas, S.S. Meena, S.M. Yusuf, V.M.S. Verenkar, Anisotropy and domain state dependen enhancement of single domain ferrimagnetism in cobalt substituted Ni–Zn ferrites, New J. Chem., 40 (2016) 9275–9284.

CHAPTER 4

Effect of Gd^{+3} doping on Structural, Magnetic and Electrical properties of $CoFe_2O_4$ Nanoparticles.

4.1 Introduction

Nanoparticles have drawn the lots of attention due to the wide range of applications such as drug delivery, magnetic resonance imaging, hyperthermia treatment, data storage, catalysis, biomedical applications due to their sizes. The sizes can be manipulated and with appropriate molecules, the surface can be made functionalized for selective target.

Spinel structure material with transition metal cations of smaller ionic radii occupies octahedral and tetrahedral site are amazing in their behavior due to strong spin exchange interaction among the cations. Cobalt ferrite (CFO) exhibit an inverse spinel structure with a formula $(Fe)_A$ $(Co\ Fe)_B$, where A and B depicts tetrahedral and octahedral site respectively [1-5]. The cations distribution in tetrahedral and octahedral site sites is responsible for novel magnetic and electrical properties of the CFO [6-7]. Many researchers have drawn their attention to these materials due to its properties like high coercivity, resistivity, Curie temperature, chemical stability and mechanical hardness [8-12]. These properties makes the material potential candidate for use in different applications like high density recording media, transformer cores, sensors, actuators, microwave devices like isolators, circulators, RF circuit, high quality filters and as a electrode materials for Li batteries and solid oxide fuels [13- 15]. CFO system has been studied to explore its special magnetic behavior and to enhance properties by doping.

The performance of ferrites materials is further improved by doping material with rare earth ions of different types. The concentration of rare earth in doped ferrites and 4 fn electronic state of rare earth plays an important role to describe the electrical and magnetic properties of ferrites.

The performance and properties of ferrites material depends on the core material and preparation method adopted. In characterization of the material, to reveal structure of the material, one needs to know in details of processing stages, properties and performance of the sample material. The structure of the material may have atomic structure, atomic arrangement, macro/micro structure, which influences on bonding in atoms, that helps us to differentiates the material in categories like matters, ceramics and polymers. The characterization is achieved by interaction of some probe to interact with sample material. Once the material structure is reveled, the next stage is to investigate properties such as mechanical, thermal, optical, physical, and magnetic of the material using the sophisticated modern tools. The techniques like X-ray diffraction, Scanning electron microscopy, Transmission electron microscopy, and Electron dispersive spectroscopy, modern tools to investigate magnetic and electrical properties are being used to provide qualitative and quantitative information of the material. The properties of a structure can be change by altering compositions or processing or both. The knowledge of structure and composition of materials, gives idea about their use in appropriate applications.

In current chapter Gd doped cobalt ferrites sample has been investigated for structure as well as magnetic and electrical properties of the sample materials. The characterization methods such as XRD, SEM, TEM, FTIR, EDS are used for scrutinizing materials for crystal structure, crystallite size, lattice parameter, structural morphology and the chemical composition. The magnetic and electrical properties of the materials is also explored and presented in this chapter.

4.2 Structural Characterization

The sample materials used for characterization are Gd^{+3} doped cobalt ferrites with chemical formula as $CoFe_{2-x}Gd_xO_4$ (x = 0.00, 0.02, 0.04, 0.06, 0.08, 0.10). The characterization of material is essential due to various reasons such as understanding the material properties, ensuring quality control, optimizing performance, aiding material selection, troubleshooting failures and advancing research and development. The information is useful for designing and utilizing the material effectively and efficiently in the various industrial applications.

4.2.1 X-ray Diffraction Spectrum

X-ray diffraction pattern of samples with chemical formula $CoFe_{2-x}Gd_xO_4$(X=0.00, 0.02, 0.04, 0.06, 0.08, 0.10 are shown in fig 4.1

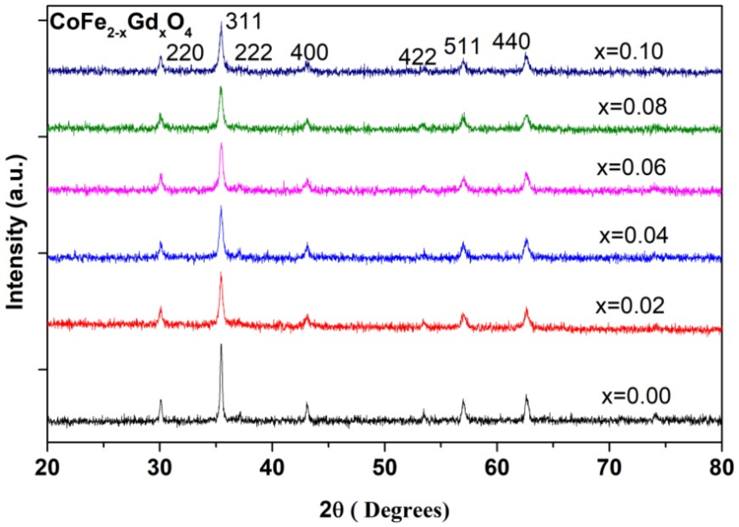

Fig 4.1: X-ray diffraction pattern for $CoFe_{2-x}Gd_xO_4$ (x = 0.00, 0.02, 0.04, 0.06, 0.08, 0.10)

Samples were characterised using XRD Rigaku X-ray diffractometer (Cu $K\alpha_1$= 1.5418 Å). The XRD pattern in which (311) exhibits as a major peak and all other peaks corresponds to spinel structure with no other impurities phases which indicates single phase cubic structured ferrites material formation.

XRD spectra of all compositions shows the formation of monophasic samples and was confirmed by indexing the maxima peaks as (220) ,(311) ,(222) ,(400) ,(422) ,(511) and (440) which specify the characteristic planes of single phase fcc cubic spinel structure (JCPDS Card no. 22-1086).

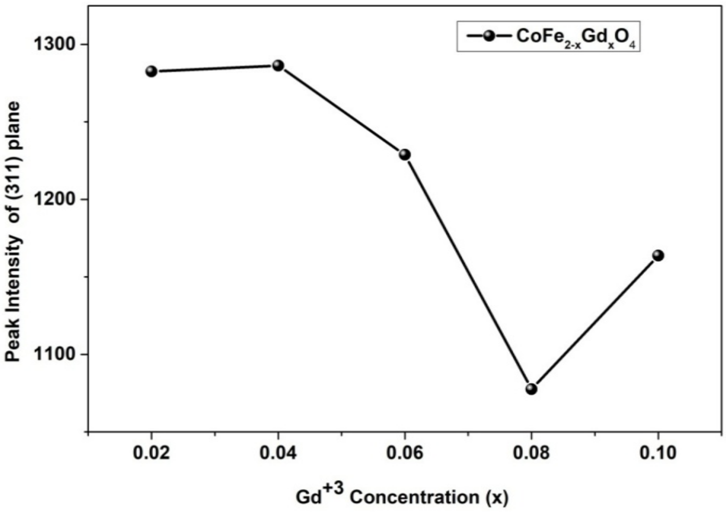

Fig, 4.2: Variation of peak intensity of (31 1) plane with Gd^{+3}Concentrations for $CoFe_{2-x}Gd_xO_4$.

The peak intensity variation of hkl value (311) plane with Gd^{+3} concentration for $CoFe_{2-x}Gd_xO$in fig 4.2 shows decreasing trend which indicates reduction in crystalline nature with increasing concentration of Gd^{+3} in the ferrites lattice and FWHM variation with Gd^{+3} concentrations increase indicates reduction in the crystallite sizes.

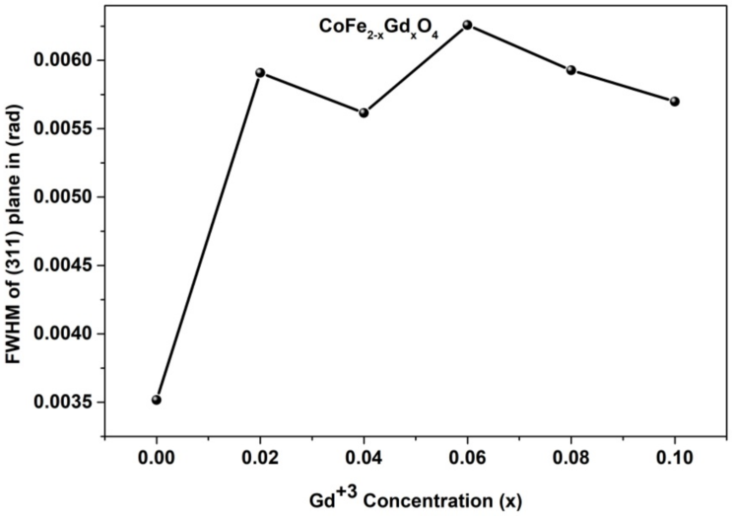

Fig, 4.3: Variation in FWHM of (311) plane with Gd^{+3} concentration for $CoFe_{2-x}Gd_xO_4$.

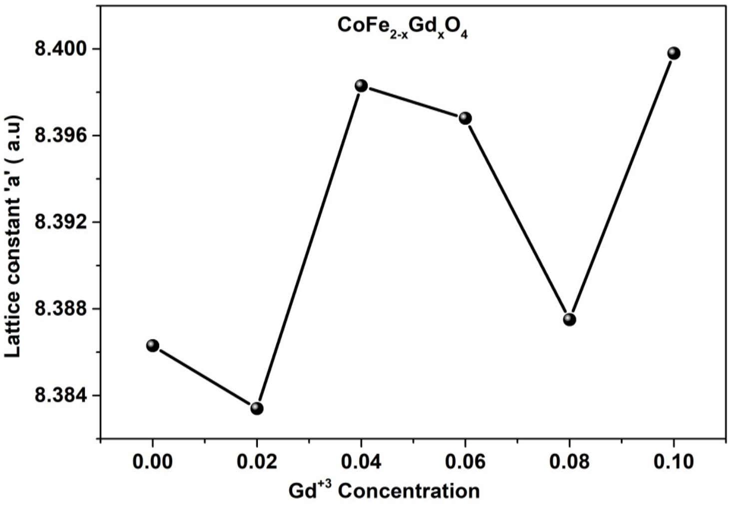

Fig. 4.4: Variation of lattice constant ‘a’ with Gd^{+3} concentrations for $CoFe_{2-x}Gd_xO_4$

The variation of lattice constant 'a' with concentrations of Gd^{+3} for $CoFe_{2-x}Gd_xO_4$ nanoparticles is shown in fig.4.4 Lattice constant increases from 8.3863 Å to 8.3998 Å as Gd^{+3} concentration increases from x= 0 to x= 0.10. The increase in lattice constant is due to replacement of larger ionic radii of Gd^{+3} (0.94 Å) by smaller ionic radii of Fe^{+3} (0.64 Å) at octahedral site. This causes expansion of octahedral sub lattice site which results in increase in lattice constant. [16]

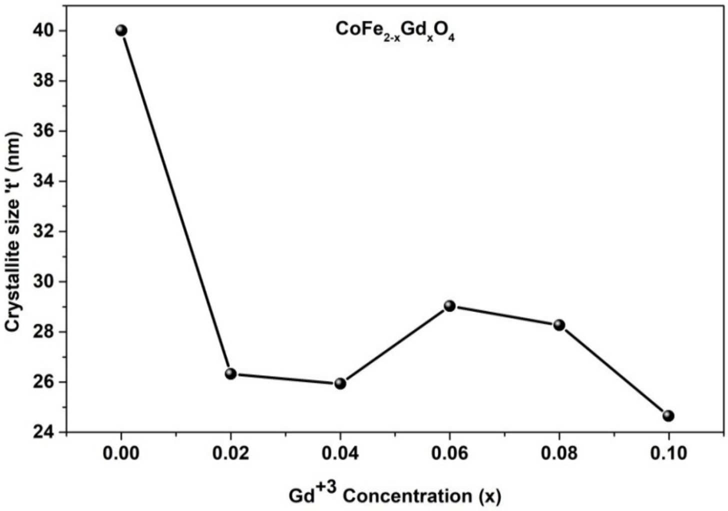

Fig, 4.5: Crystallite size Variation with Gd^{+3} concentrations for$CoFe_{2-x}Gd_xO_4$

The crystallite size variation with concentration of Gd^{+3} in the fig 4.5 shows that the crystallite size is found to decrease with increase in Gd^{+3} concentrations in the range from 40 nm to 21 nm. Nano particles do not exhibit identical crystallite size due to the rate of ferrites formation differs for different composition and for our different crystallite sizes [17]. The replacement of a larger ionic radii ion by smaller radii ion creates strain in the lattice. Also the presence of Co^{+2} ions with maximum electrostatic shielding by 3d electrons introduces an additional strain. This strain depends on different factors such as lattice defects, larger surface energy, and presence of impurities etc. The micro-strain arises due to larger surface energy involved in larger surface to volume ratio of the sample [18-19]. The decrease in crystallite size is due to inclusion of rare earth ions that develops lattice strain, which hinders the crystal growth and are responsible for reduction of crystallite size for such materials. It is noticed that substitution of Gd^{+3} in $CoFe_2O_4$ is restricted; as a result there is a reduction in crystallite size. The reason is Gd^{+3}- O^{-2} bond energy is more than the Fe^{+3}- O^{-2} bond energy, so it required more energy to incorporate Gd^{+3} ions in place of Fe^{+3} ions into octahedral site [20].

Table 4.1: Lattice constant and crystallite size for various concentrations of Gd^{+3}

Concentration 'x' of $CoFe_{2-x}Gd_xO_4$	**Lattice constant 'a' in Å**	**Crystallite size ' t' in nm**
0.0	8.3863	40
0.02	8.3834	26
0.04	8.3983	25
0.06	8.3968	29
0.08	8.3875	28
0.10	8.3998	24

The fig 4.6 shows that, x-ray density increases with Gd^{+3} concentrations.This can attributed to the fact that the density and atomic weight of Gd^{3+} is 7.90 gm /cm^3 and 157.25 gm respectively which is greater than that of Fe^{3+} (7.874 gm/cm^3, 55.845).

This behavior of enhancement in the X-ray density with increase in Gd^{+3} concentrations also supports effective incorporation of Gd^{+3} into $CoFe_{2-x}Gd_xO_4$ samples.

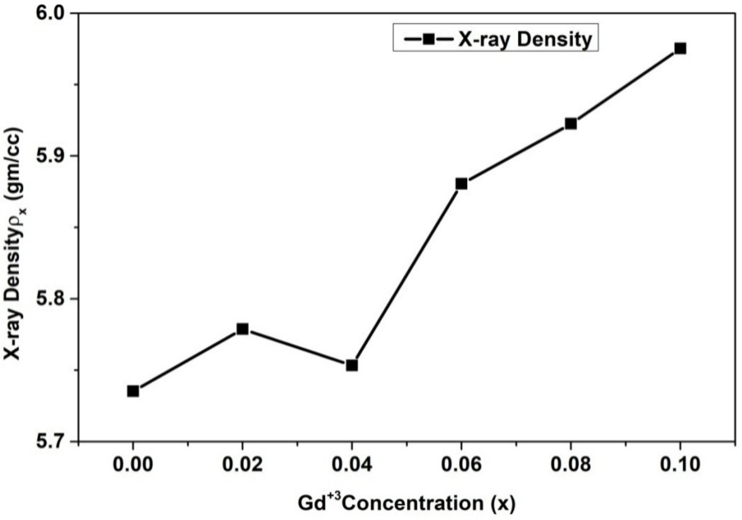

Fig.4.6: Shows FTIR spectra of pure and Gd^{+3} doped $CoFe_2O_4$nanoparticles samples.

The enhanced value of X-ray density may also be due to the improved molecular weight of the samples with Gadolinium ions. The x-ray density calculated using equation (4.1).

$$\rho x = \frac{8M_x}{N_a a^3} \qquad 4.1$$

Where M_x = molecular weight of the sample, *N*a - Avogadro's number (6.023×10^{23} atoms/mole) and 'a' is the lattice constant [21- 24].

The mass density 'ρ_M' increases with Gd^{+3} concentrations shown in fig 4.7. The mass density of ferrites can vary depending on specific dopants and its concentrations.

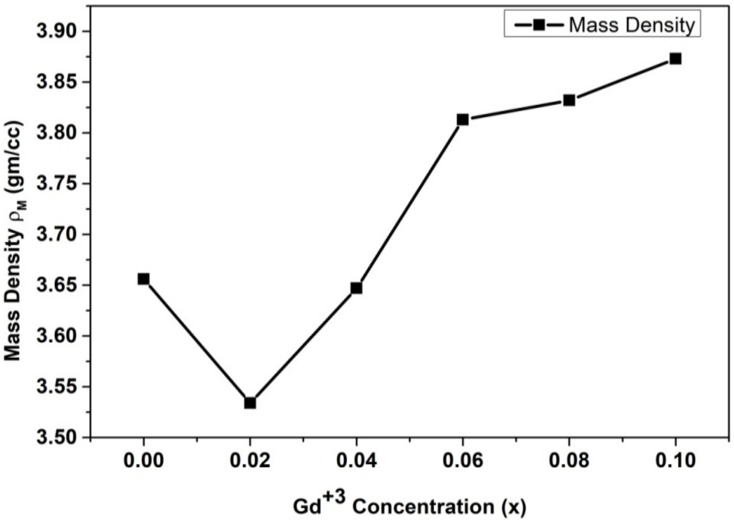

Fig. 4.7: Variation of mass density 'ρ_M' with Gd^{+3} concentrations for $CoFe_{2-x}Gd_xO_4$.

The mass density is typically expressed in units of grams per cubic centimeter (gm/cm^3) or kilograms per cubic meter (kg/m^3). For most ferrite materials, the mass density falls in the range of 4.9 to 5.2 g/cm^3, but can be lower or higher value depending on dopants atomic mass and concentrations. The porosity in the ferrites materials can be controlled during fabrication.To achieve a desire level of porosity the techniques used are sintering, hot pressing, Sol-gel method, etc.

The porosity of the material is calculated using equation (4.2).

$$P(\%) = \left[1 - \frac{\rho_M}{\rho_x}\right] \times 100 \qquad 4.2$$

Where ρ_{M}, ρ_x is the mass density and x-ray density of the sample respectively. Fig 4.8 shows the % porosityvariation with the concentration of Gd^{+3}.It is observed that initially % porosity increases and then decreases with increase in Gd^{+3} concentrations.

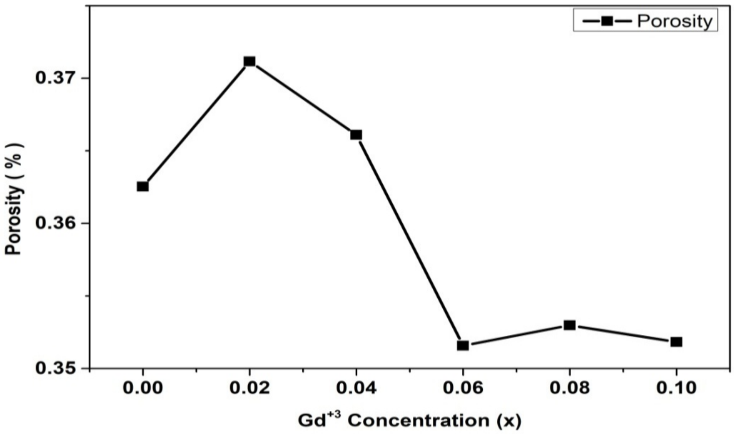

Fig. 4.8: Variation of porosity (%) with Gd+3 concentrations for $CoFe_{2-x}Gd_xO_4$.

4.2.2 Fourier Transform Infra red (FTIR) Spectroscopy

Two major absorption bands have been observed in the wave number range 390 – 700 cm^{-1} for all the samples as seen in fig 4.9.

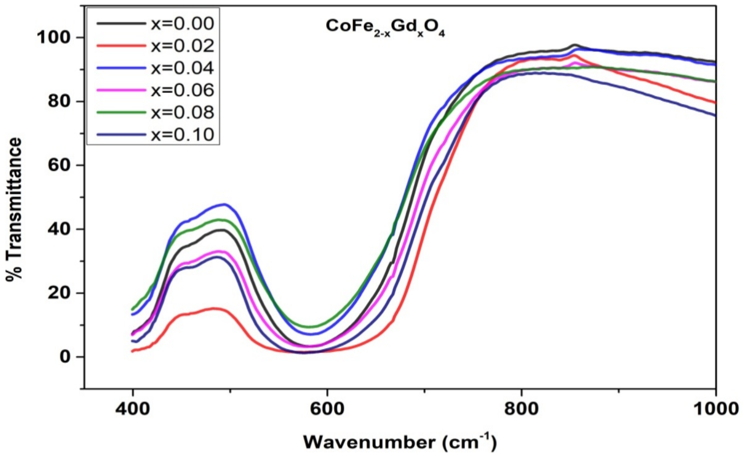

Fig. 4.9 : FTIR spectra of $CoFe_{2-x}Gd_xO_4$ nano particle

One band is observed at 390 cm^{-1}- 430 cm^{-1} which corresponds to stretching vibration of octahedral groups and other band at 560 cm^{-1}- 670 cm^{-1} corresponds to stretching vibration of tetrahedral groups [25]. The two absorption bands stated whrein, the lower frequency band is around 390cm^{-1} corresponds to the vibration of metal oxide bond at octahedral site and the one corresponding to higher frequency around 590 cm^{-1} indicates metal-oxygen vibration at tetrahedral site. These two absorption bands confirm the formation of spinel cobalt ferrites structure material.

4.2.3 Scanning Electron Microscopy (SEM)

The SEM images of pure Co ferrite, 4 % Gd doped and 10 % Gd doped cobalt ferrites are shown in the fig. 4.10 (a, b, c) respectively.

The surface morphological information of Co ferrite and Gd doped Co ferrite was obtained from SEM images. It is noticed from images that Co ferrites particles are spherical in shape, agglomerated and nano size. The nano particles large agglomerates are formed and this agglomeration increases with doping concentrations of Gd^{+3}. Further the clusters of grain boundaries in nano range are visible. The nano grains particles appears in spherical geometry shape. The extent of agglomeration increases with doping concentration of Gd^{+3} that may be due to the inclusion of Gd ions at octahedral site and also presence of surface charges with other type of forces [26]. The differences in undoped and doped samples were observed.

The surface morphological information of Co ferrite and Gd doped Co ferrite was obtained from SEM images.

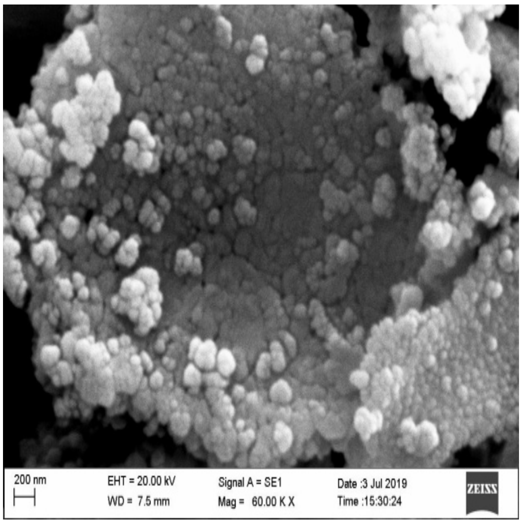

(a)

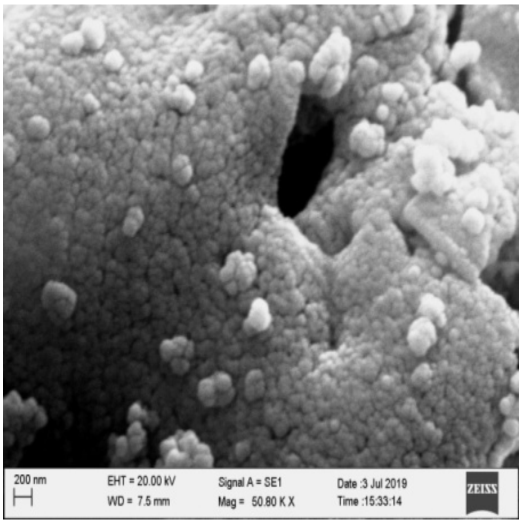

(b)

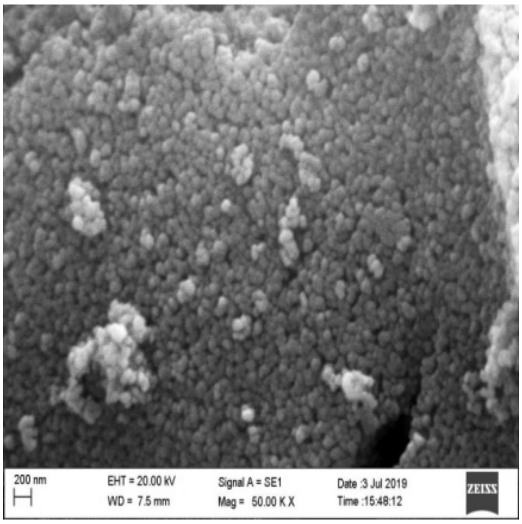

(c)

Fig.4.10: Scanning Electron Micrograph of (a) $CoFe_2O_4$, (b) $CoFe_{1.96}Gd_{0.04}O_4$and (c) $CoFe_{1.90}Gd_{0.10}O_4$

4.2.4 Energy Dispersive Spectroscopy

Energy dispersive spectroscopy analysis for Co ferrite and Gd doped Co ferrites samples.

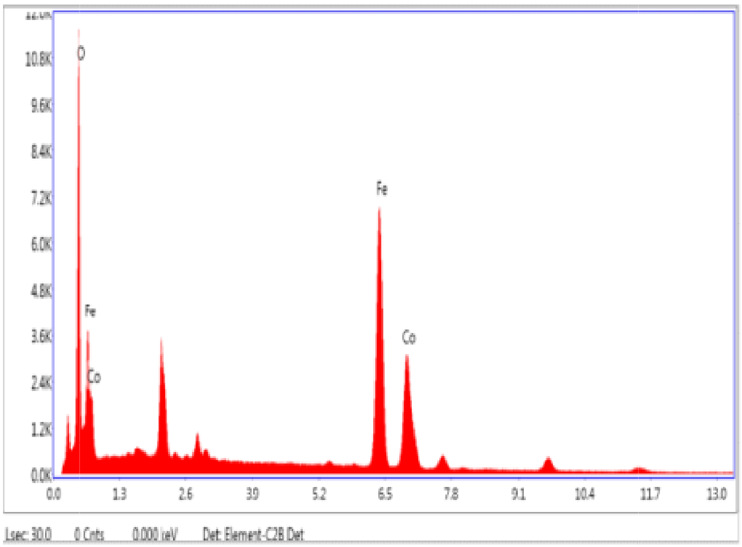

(a) $CoFe_2O_4$

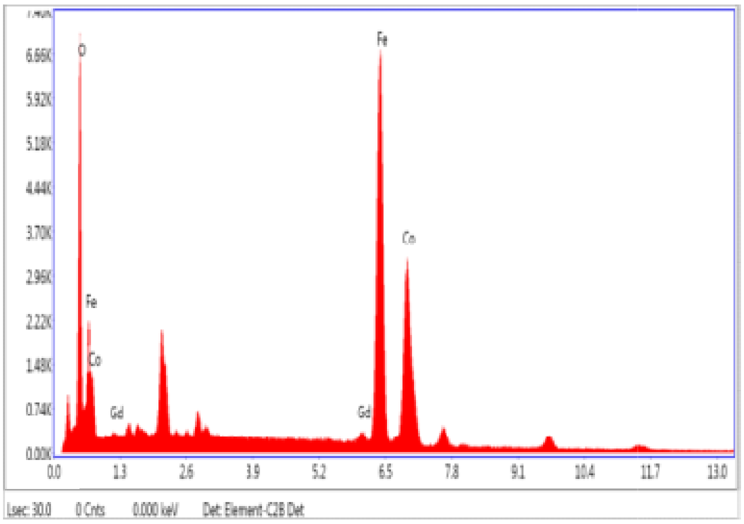

(b) $CoFe_{1.96}Gd_{0.04}O_4$

Energy dispersive spectroscopy analysis for Gd doped Co ferrites samples.

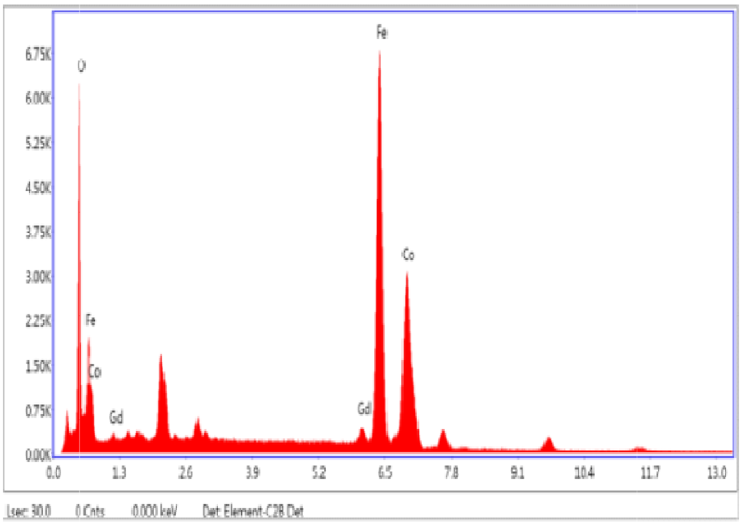

(c) $CoFe_{1.90}Gd_{0.10}O_4$

Fig.4.11: EDS analysis of (a) $CoFe_2O_4$ (b) $CoFe_{1.96}Gd_{0.04}O_4$ (c) $CoFe_{1.90}Gd_{0.10}O_4$.

Table 4.2: Experimental and calculated weight percentage value for (a) $CoFe_2O_4$ (b) $CoFe_{1.96}Gd_{0.04}O_4$ (c) $CoFe_{1.90}Gd_{0.10}O_4$

Composition	**$CoFe_2O_4$**		**$CoFe_{1.96}Gd_{0.04}O_4$**		**$CoFe_{1.90}Gd_{0.10}O_4$**	
of elements	**Exp%**	**Theo%**	**Exp%**	**Theo%**	**Exp%**	**Theo%**
Fe	54.15	47.61	45.44	45.86	54.79	43.35
Co	28.03	25.12	24.69	24.70	29.09	24.08
O	17.82	27.27	26.69	26.80	9.73	26.14
Gd	0	0	3.28	2.64	6.40	6.43
Total	100.00	100.00	100.00	100.00	100.00	100.00

The elemental composition of $CoFe_2O_4$ and Gd doped $CoFe_2O_4$ has been analyzed using energy dispersive spectroscopy analysis. The experimental and theoretical percentage compositions of elements in the samples are shown in Table 4. 2. The results confirms the presence of Co, Fe, Gd and O elements in the prepared samples and no other impurities are found within the experimental limit of EDS.

4.2.5 Transmission Electron Micrograph (TEM)

Transmission electron micrograph for $CoFe_{1.96}Gd_{0.04}O_4$ and $CoFe_{1.90}Gd_{0.10}O_4$ is shown in fig. 4.12. Since Gd^{+3} occupies octahedral site that produces strain in the lattice as well as grain boundaries due to its larger ionic radii which causes hindrance in grain growth, which results in the reduction of particle size.

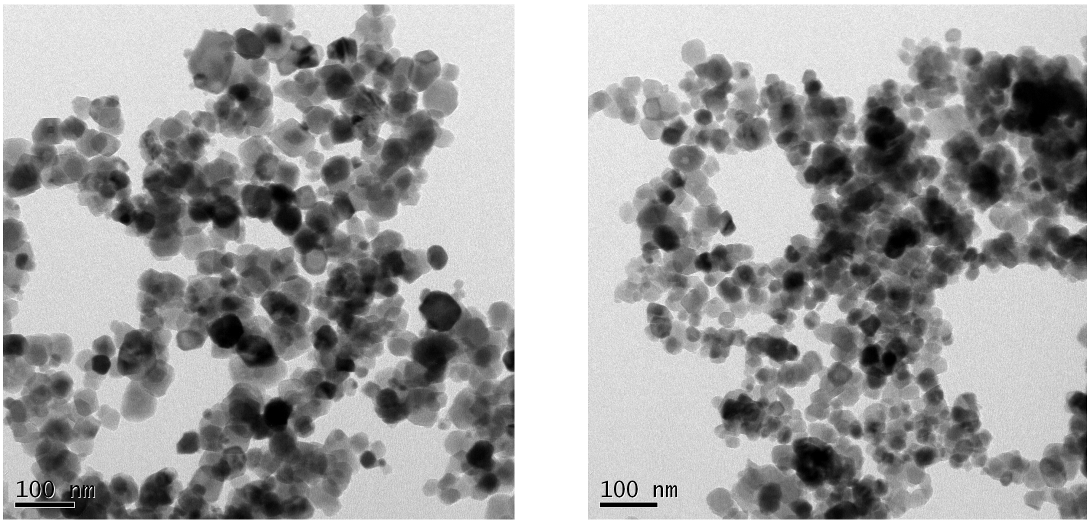

(a) (b)

Fig. 4.12: Transmission Electron Micrograph of (a) $CoFe_{1.96}Gd_{0.04}O_4$ and (b)$CoFe_{1.90}Gd_{0.10}O_4$

The micrographs show the agglomeration which indicates the strong magnetic nature of Gd^{+3} doped cobalt ferrites.

4.3 Magnetic Properties Study

The magnetic properties of samples materials are studied by considering its behaviors changes in presence of external magnetic fields. It has been found that pure cobalt ferrites and Gd^{+3} doped cobalt ferrites shows ferrimagnetic behavior. In the current chapter magnetic measurement studies such as hysteresis for pure and Gd^{+3} doped cobalt ferrites are explored. Also zero field cooled (ZFC) and field cooled (FC) measurement for constant field has been studied. AC susceptibility measurement to study a Curie temperature of samples has been investigated.

4.3.1 Vibrating Sample Magnetometer (VSM)

Quantum design's versa lab 3 tesla vibrating sample magnetometer (VSM) is used for the magnetic hysteresis loop measurement for cobalt ferrites and Gd^{+3} doped cobalt ferrites samples, the measurement are carried out for room temperature. The Fig. 4.13 shows the hysteresis loops of $CoFe_{2-x}Gd_xO_4$ (x = 0.00, 0.02, 0.04, 0.06, 0.08, 0.10) nanoparticles.

The saturation Magnetization (Ms), Coercivity (Hc) and remanence magnetization (Mr) are given in the table.4.13 It is observed that saturation magnetization decreases with increase in Gd^{+3} concentrations except for 10% Gd^{+3} doped Co ferrites sample. The magnetic properties of ferrites are influenced by cation distribution in the spinel lattice sites. As per Neel's sublattice model, three types of interactions i.e. A-A, B-B and A-B exists between tetrahedral site and octahedral site of spinel ferrites. Among these three interactions, A-B interaction is stronger than other two interactions [27, 28].

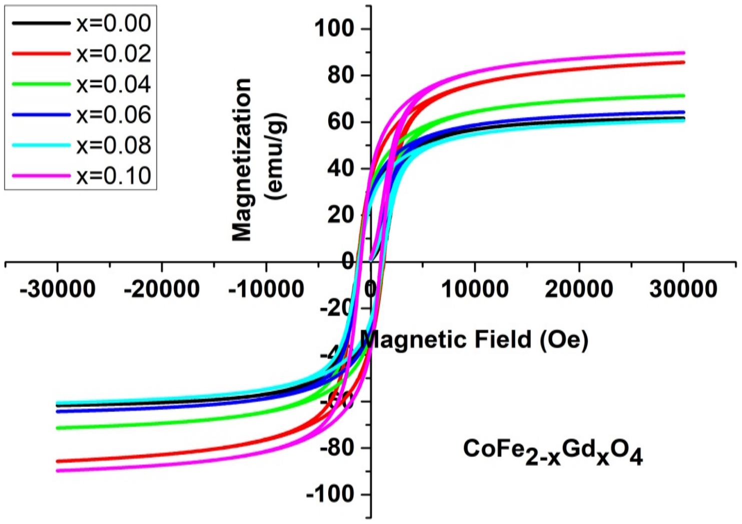

Fig. 4.13: Hysteresis loops for $CoFe_{2-x}Gd_xO_4$ (x = 0.00, 0.02, 0.04, 0.06, 0.08, 0.10) nanoparticles.

In rare earth doped ferrites, ion occupies octahedral sites due to its larger ionic radius. Also the magnetic moment originate from 4f electrons[29] for Gd^{+3} ions and at room temperature their magnetic dipole orientations are in disorder form, hence they contribute very small to net magnetization at room temperature [30,31]. Therefore doping of Gd^{+3} ions in cobalt ferrites lattices is equal to the substitution of non magnetic atom at B sites that result in the reduction of magnetization at B sites. The total magnetization of cobalt ferrites calculated from the difference of magnetization of B sites and A sites. The A-B interactions become weaker as a concentration of Gd^{+3} increases [32, 33]. Hence the magnetization decreases with increase in Gd^{+3} doping concentrations. The enhancement of saturation magnetization may be due to higher Gd^{+3} doping concentration, in which Co^{+2} ion immigrates in A site accompanied by equivalent Fe^{+3} ion moving from A site to B site. This migration decreases the concentration of Fe^{+3} ions in A site that results into the increase of saturation magnetization of 10% Gd^{+3} doped co ferrites. The factors are decrease in Yafetn- kittel angle θ_{YK} between moment of B sites [34] and surface effect [35] due to the surface disorder in which the number of spins increases at surface of rare earth doped ferrites as the crystallite size is reduced [36].

Table 4.3: Magnetic properties of $CoFe_{2-x}Gd_xO_4$: saturation magnetization (Ms), coercivity (Hc), remanent magnetization (Mr) and remanence ratio.

Concentrations 'x' of $CoFe_{2-x}Gd_xO_4$	**Ms (emu/g)**	**Hc (Oe)**	**Mr (emu/g)**	**Mr/Ms Ratio**
$CoFe_2O_4$	62.01	1186	27.89	0.450
$CoFe_{1.98}Gd_{0.02}O_4$	85.69	1263	33.58	0.392
$CoFe_{1.96}Gd_{0.04}O_4$	71.38	1158	30.21	0.423
$CoFe_{1.94}Gd_{0.06}O_4$	64.29	1140	28.36	0.441
$CoFe_{1.92}Gd_{0.08}O_4$	60.65	1036	24.73	0.408
$CoFe_{1.90}Gd_{0.1}O_4$	89.74	952	35.91	0.400

The variation of coercivity with Gd^{+3} concentrations are shown in the table 4.3. It is observed that coercivity decreases with Gd^{+3} concentrations. The pure Co ferrites shows coercivity of 1186 Oe and 2% Gd doped co ferrites sample shows coercivity of 1263 Oe, which then decreases to 952 Oe when Gd concentrations increases from x= 0.02 to x=

0.10. The coercivity trend of variation is due to the substitution of large ionic radii Gd^{+3} ion by Fe^{+3} ion in B sites, to compensate for this Co^{+2} ions migrated from B sites to A sites which decreases Co^{+2} cations at B sites. This reduces single Co^{+2} ion anisotropy that results in the reduction of the coercivity. The decrease in coercivity also related to crystallite size in the single domain region according to which coercivity decreases with decrease in crystallite size [37]. The equation that relates coercivity and crystallite size't' is given by $Hc = g - (h / t^{3/2})$ where g and h are constant. The remanent ratio or the loop squareness ratios (Mr/Ms) are presented in the table 4.3 shows on average decrease with increase in Gd^{+3} concentrations. It tells us the domains reorientation of magnetization itself to the easy nearer axis when magnetic field is removed [38]. The low value of remanent ratio indicates the particles interact magneto-statically [39, 40]. The remanent variation indicates the decrease in anisotropy with Gd doped Co ferrites samples and is similar to the coercivity.

4.3.2 ZFC and FC Measurement

Fig.4.14 shows the measurement of magnetization as a function of temperature inthe applied field of 500 Oe. The magnetic moment variation with change in the temperature from 50 K to 400 K is studied. The ZFC measurement was carried out as follows: first sample were cooled from 400 K to 50 K in the absence of magnetic field, then the samples is allowed to warm in presence of the applied magnetic field of 500 Oe and the measurement is carried out. In case of FC measurements the cooling and warming of the samples were done in the presence of the applied magnetic field and measurement was carried out during the warming of the sample.

From fig.4.14 shows that in ZFC measurement, the magnetization of the sample increases with increase in temperature from 50 K to 400 K, while in FC measurement there is a gradual decrease in magnetization as the temperature increases. The decrease in magnetization during FC measurement is due to thermal activation which randomizes the magnetization direction by lowering magnetic anisotropy that decreases the value of magnetization. In cooling of FC mode, the magnetic moments within the particles alien along the field direction which gives high magnetization value.

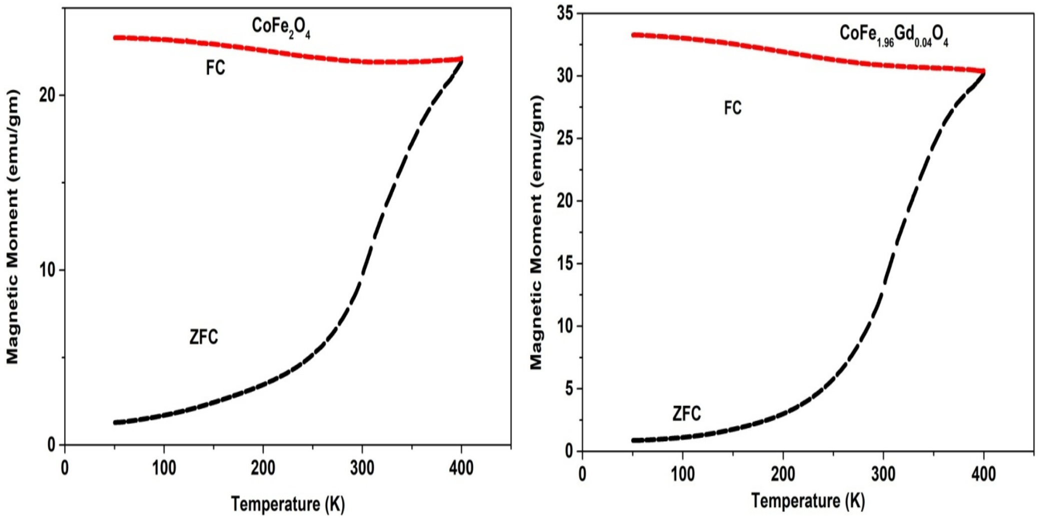

(a) (b)

Magnetic moment variation with temperature for $CoFe_{1.90}Gd_{0.10}O_4$

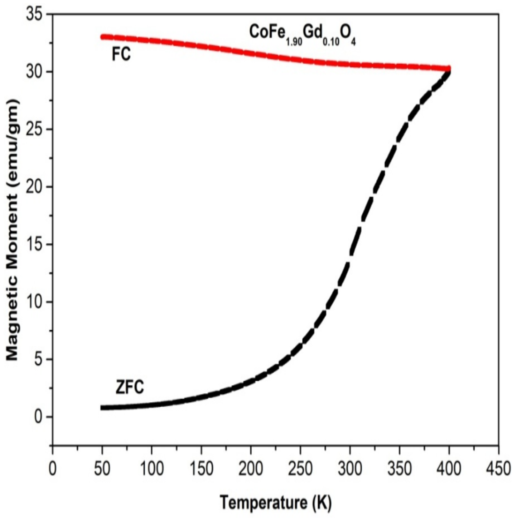

(c)

Fig.4.14: Variation of magnetic moment with temperature for x = 0.00, 0.04 and 0.10.

The temperature at which ZFC and FC curve coincides is called irreversibility temperature (T_{irr}) and in ZFC measurement the temperature at which magnetization reaches maximum value just before it decreases, is called blocking temperature (T_b) [41]. The blocking temperature and irreversibility temperature is found to decrease with increase in applied magnetic field. Both the temperatures relates to the blocking of larger particles in the sample. From the fig.4.14 it is seen that irreversibility temperature exits for the samples but blocking temperature is not observed. The blocking temperature for this sample may be above 400 K at 500 Oe. The reason may be the presence of larger number of bigger particles compared to average particles size in the sample. It is also been reported that agglomeration of particles may leads to increase in blocking temperature [42].

4.3.3. AC Susceptibility

The normalized AC susceptibility plot as the function of temperature for $CoFe_{2-x}Gd_xO_4$ is shown in fig. 4.15 Ac susceptibility refers to the measure of a materials response to an alternating magnetic field.

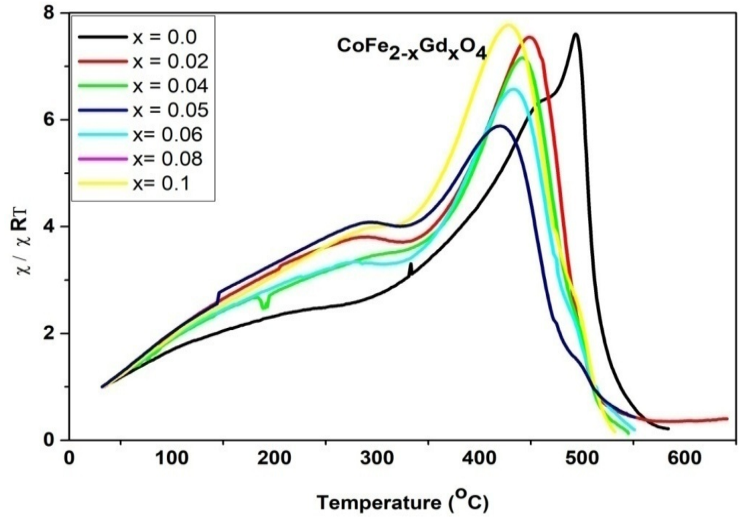

Fig. 4.15: The normalized AC susceptibility plot as the function of temperature for $CoFe_{2-x}Gd_xO_4$.

It is one of the important properties in the study of magnetic materials and provides valuable insights into the magnetic behavior. When the magnetic field is applied to a material, it causes the magnetic moment within the material to oscillate. AC susceptibility quantity measures how much materials magnetization changes in the response to this alternating magnetic field and represented as a function of the frequency of the applied AC magnetic field. The AC susceptibility provides valuable information about a material's properties like magnetic phase transitions, magnetic relaxation, super-paramagnetism (SP), magnetic anisotropy etc.

The study of AC susceptibility provides information about the domain type and the curie temperature of the ferrites. The ferrites material exhibits three types of domain such as single domain (SD), multi domain (MD) and super-paramagnetic (SP).

In multi domain, there are many small domains separated by walls in between and when grain size is of order of wall thickness, unable to support the wall are called single domain. The particles with size smaller than 10 nm exhibits super-paramagnetism nature. The fig.4.15 shows sharp fall in the normalized susceptibility at the particular temperature called Curie temperature. All the samples exhibit single Curie temperature that indicates ferrite samples are single phase without any impurity in it. The samples are single domain because as the temperature increases the magnetization increases, which reaches a maximum value and then there is a sharp fall just before Curie temperature Tc. The region between sharp increase in magnetization and sharp decrease just before Curie temperature, there is a hump in between is called Hopkinson’s hump and it is due to Hopkinson’s effect. Hopkinson effect is observed in nano- crystalline single domain particles. The Curie temperature of the samples obtained from AC susceptibility plot is given in the table 4.4.

Table 4.4:Sample concentration, crystallite size and Curie temperature.

Concentration 'x' of Sample Co $Fe_{2-x}Gd_xO_4$	**Gd Crystallite Size 't' in nm**	**Curie Temp 'T'$_C$ in ^OC**
0.00	40	531
0.02	26	527
0.04	25	525
0.06	29	522
0.08	28	519
0.10	24	512

It is seen from the table 4.4 that the Curie temperature of samples decreases with increase in concentration of Gd^{+3} and decrease in crystallite size. It is reported in literature that the variation in Curie temperature can be explain on the bases of variation in their particle size and lattice parameter [43-45]. Sample shows the MD type behavior with the mixture of SD grains. It is also reported that particle with smaller size and higher lattice constant shows higher Curie temperature [46]. But it is observed in our studies that larger particle size ferrites show higher Curie temperature.

AC susceptibility of ferrimagnetic materials is affected by both particle size and lattice constant. However, the relationship is highly complex and depends on the specific material, its crystal structure, the arrangement of magnetic sub-lattices, and the interactions between them.

4.4 Electrical Properties Study

Gadolinium (Gd^{+3}) doped $CoFe_2O_4$ are the special magnetic material that exhibits interesting electric and magnetic properties due to the presence of Gd^{+3} ions in the crystal structure. As we know Cobalt ferrites are ferrimagnetic materials, and Gd doping can further modify their electrical characteristics. The specific electrical properties of Gd^{+3} doped cobalt ferrites can vary depending on the doping level, sample preparation techniques, and measurement conditions. The optimization of these parameters is necessary to achieve desired electrical characteristics for specific applications. The study and exploration of these properties are still ongoing; more insights into their properties and potential applications are likely to emerge. The electrical properties of Gd^{+3} doped cobalt ferrites can be tailored by controlling the synthesis methods, annealing conditions, and the concentration of Gd^{+3} dopants. These materials find applications in the fields of electronics, telecommunications, sensors, and magnetic storage devices. The electrical properties such as resistivity, dielectric constant and dielectric loss variation with frequency/temperature, thermo-electric power of Gd^{+3} doped $CoFe_2O_4$ are discussed in the current chapter.

4.4.1 DC Resistivity

The variation of resistivity with temperature for Gd^{+3} doped $CoFe_2O_4$ with different concentrations of $Gd^{+3}$are shown in fig. 4.16. The electrical resistivity of Gd^{+3} doped ferrites typically follows a certain temperature dependent trends. The specific temperature dependence of resistivity can vary depending on the type and concentration of the dopants, the crystal structure, density, porosity and the microstructure of the material [47, 48].

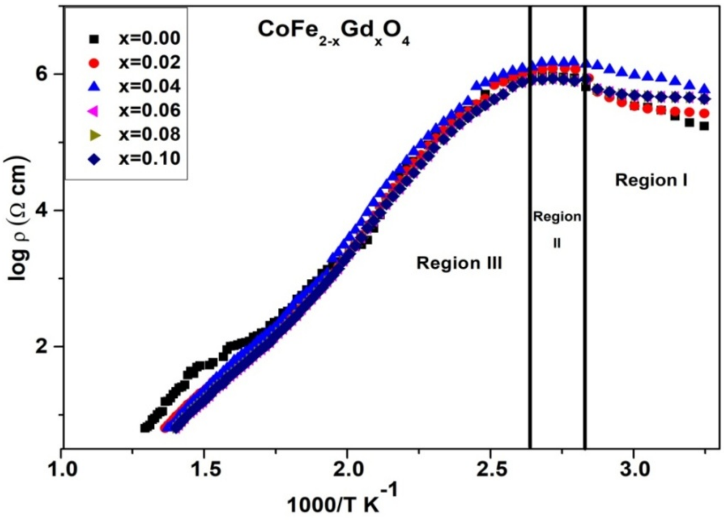

Fig. 4.16: Variation of dc resistivity with (1000/T) for $CoFe_{2-x}Gd_xO_4$ (x= 0.00, 0.02, 0.04, 0.05, 0.06, 0.08, 0.10).

The resistivity-temperature relationship of a material can provide valuable insights into its electrical behavior and the underlying physical processes. The DC resistivity study was carried out from room temperature to 773 K using two probe method and the plots of log ρ v/s 1000/ T K is shown in fig. 4.16 For many ferrite materials, including Cobalt ferrites, the resistivity typically decreases with increasing temperature which is the typical behavior of semiconductor. This behavior is associated with the increase in charge carrier mobility due to thermal activation. As the temperature rises, more charge carriers become available for conduction, leading to a lower resistivity. As it is seen from the fig.4.16 initially resistivity increases attains maximum, remains constant and then decreases with increase in applied temperature. The resistivity increases in region I from room temperature to 353 K ($80^{O}C$), remains constant in region II from 353K

($80^{O}C$) to 380 K ($107^{O}C$) and then deceases in region III from 380K ($107^{O}C$) to 773K ($500^{O}C$). The increase in resistivity in region I is attributed to presence of open pores, loose agglomeration and the entrapped moisture. As the temperature increases, moisture gets evaporated and till all the gets desorption it reaches end of region II in which resistivity remains constant. After desorption of all the moisture in region III, the resistivity fallows the normal trend shown by spinel ferrites i.e. it starts decreasing as temperature increases [49]. The conduction mechanism is based on the Verwey de Boer mechanism [50]. According to this mechanism, the conduction in ferrites is due to exchange of electrons between the ions of same element but existing with different valence state on the equivalent lattice site. With increase in temperature, the drift mobility of charge carriers leads to the decrease in resistivity [48, 51]. This can be explained as follows: when temperature increases, the vibration of lattice also increases which makes the ions come closer to each other that results in increase of probability of hopping on adjacent ions and thereby increasing the mobility of the charge carriers. The grains are good conducting and grains boundaries are poor conducting so increase in grain size leads to decrease in porosity. There is the relation between porosity and resistivity; increase in porosity gives rise in number of vacancies, scattering centers and pores of electrical charge carriers which increases resistivity [52, 53].

The Arrhenius equation is often applicable for describing the resistivity variation with temperature in materials due to thermally activated charge carriers. The activation energy (Ea) characterizes the dependence of resistivity on temperature, and it can be obtained from experimental data by plotting the natural logarithm of resistivity (log ρ)

as a function of the reciprocal of temperature (1 / T K) and fitting a straight line to the data. The Arrhenius equation is expressed as follows (4.3)

$$\rho = \rho_0 \cdot e^{Ea/KT} \qquad 4.3$$

ρ is the resistivity of the material at temperature T, ρ_0 is the resistivity at a reference temperature (T_0) (usually room temperature), Ea is the activation energy for conduction, which represents the energy barrier for charge carriers to move through the material, K is the Boltzmann constant and T is the absolute temperature in Kelvin.

It is also observed that as resistivity decreases with decrease in activation energy [54]. The decrease in activation energy is due to the redistributions of cations in octahedral site. The hopping of electrons is the main reason for conductivity, hence resistivity. In region III the resistivity decreases as transfer of Fe^{+3} ions from the tetrahedral site to octahedral site increases. It is known that the electron hopping between $Fe^{+2} \Leftrightarrow Fe^{+3}$ ions in octahedral sites are responsible for conduction. As the number of Fe ion increases and ultimately $Fe^{+2} \Leftrightarrow Fe^{+3}$ ion pairs, since the hopping of electrons between $Fe^{+2} \Leftrightarrow Fe^{+3}$ ions are responsible for electrical conduction, an increase in $Fe^{+2} \Leftrightarrow Fe^{+3}$ ions pairs increases the hopping of electrons and also electrical conductivity. Therefore electrical resistivity decreases in region III.

4.3.2 Dielectric properties

4.3.2.1 Dielectric constant variation with frequency

The frequency dependence of dielectric constant of pure cobalt ferrites and Gd^{+3} doped cobalt ferrites are measured at room temperature in the frequency range from 20 Hz to 3MHz.from The dielectric constant 'ε' was calculated using equation 4.4

$$\varepsilon = \frac{Cd}{\varepsilon_0 A} \qquad 4.4$$

Where C – capacitance, *d* - thickness of the pallet, *A*- area of pallet and ε_0 – permittivity of free space.

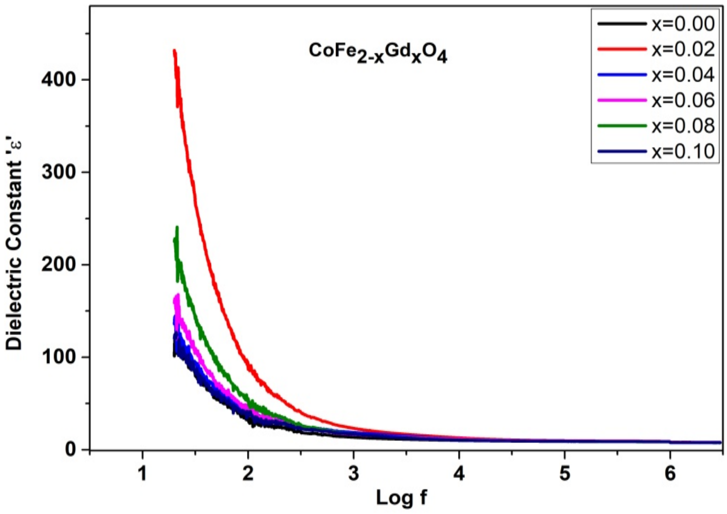

Figure 4.17: Variation of dielectric constant as a function of frequencywith Gd^{+3} concentrations

The variation of dielectric constant with frequencies for $CoFe_{2-x}Gd_xO_4$ with x = 0.00, 0.02, 0.04, 0.06, 0.08, 0.10 nanoparticles at room temperature. It is seen from Fig. 4.17

that the measured value of dielectric constant strongly dependent on the frequency of the applied field. It is observed that initially dielectric constant (Ɛ) decreases abruptly at low frequencies and at higher frequencies decrease is gradual and finally become constant for all Gd^{+3} doped Co ferrites samples. The decrease in dielectric constant at lower frequencies is the characteristic of the dielectric dispersion. The dispersion in dielectric constant is due to the Maxwell-Wagner's type of interfacial polarization model and is in agreement with Koop's phenomenological theory [55-57]. According to this model, the dielectric medium consists of conducting grains which are separated by poor conducting grains boundaries. In the presence of external applied field, the opposite polarity charge carriers moves inside the grains in opposite direction. These moving charges piles up at the poor conducting grain boundaries that acts as the wall. The presence of applied external electric field, the grain functions as an electric dipole, which is termed as space charge polarization or interfacial polarization. The space charge polarization shows high dielectric value for the samples at low frequencies [58 - 59]. The polarization mechanism in cobalt ferrites is similar to the conducting process [60], in which electron hopping between $Fe^{+2} \Leftrightarrow Fe^{+3}$ ions and hole hopping between $Co^{+2} \Leftrightarrow Co^{+3}$ ions, charge carriers, reaching the poor conducting grain boundaries and pile up due high resistance producing polarization. As the frequency of applied field increases a charge carriers cannot follow the frequency of the alternating applied electric field as a result polarization decreases [61]. Some literature reported [62] that increase in the dielectric constant could be due to the increasing number of Fe^{+3} ions at the octahedral site. This can be explained as follows: The doping of Gd^{+3} ions makes migration of Co^{+2} ions to tetrahedral site in order to relax strain and equal number of Fe^{+3} ions migrate from tetrahedral site to the octahedral site which increases the hopping of electrons between Fe^{+2}⇔Fe^{+3} ions in octahedral sites and increases dielectric constant. For some time dielectric decreases due to the limitation on the migration of Fe^{+3} ions from tetrahedral sites to octahedral sites, the number of Fe ions are decrease and also Fe^{+2}⇔ Fe^{+3} ion pairs. As a result availability of Fe^{+2}⇔Fe^{+3} ions and hopping electrons in between Fe^{+2}⇔Fe^{+3} decreases in octahedral sites that reduces the dielectric constant value.

4.4.2.2 Dielectric Loss Variation with Frequency

The variation of dielectric loss (tan δ) with frequencies for $CoFe_{2-x}Gd_xO_4$ with x = 0.00, 0.02, 0.04, 0.06, 0.08, 0.10 nanoparticles at room temperature is seen from figure 4.18.

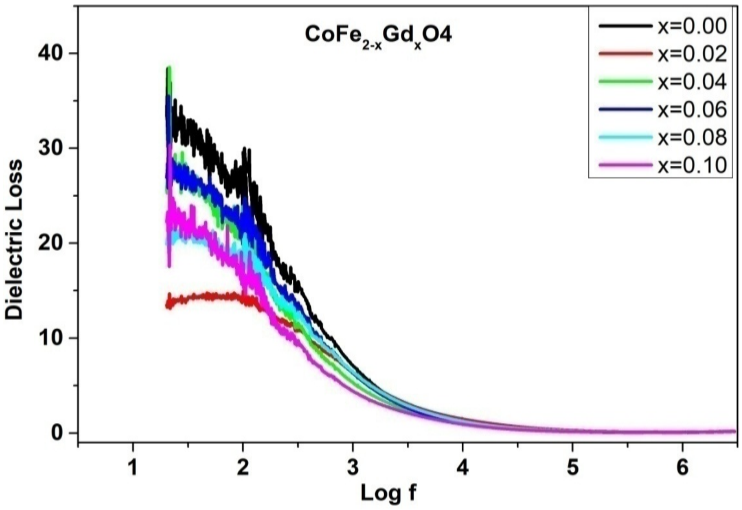

Figure 4.18: Variation of dielectric loss (tan δ) as a function of frequency

with Gd^{+3}concentrations.

The frequency dependence of dielectric loss of pure cobalt ferrites and Gd^{+3} doped cobalt ferrites are measured at room temperature in the frequency range from 20 Hz to 3MHz. It is seen from Fig. 4.18 that initially dielectric loss (tan δ) increase at very low frequency and as the frequency is increased further it decrease and finally become constant for all Gd^{+3} doped Co ferrites samples. The decreasing trend at higher frequency is similar to dielectric constant. The increase in dielectric loss is due to the limitation in an electronic exchange between Fe^{+2} ions and Fe^{+3} ions due to the lager ionic radii of Gd^{+3} as mentioned in resistivity. The decrease shown in dielectric loss tangent may be due to fine particle size results in increase of surface area along with Gd^{+3} ions which increases the amount of energy require for electronic exchange and is responsible for the dielectric loss. At high frequencies the electronic exchange cannot follow the frequency of applied alternating electrical field and results in the decrease of dielectric loss [63].

The dielectric loss exhibits dispersion with increasing frequency similar to dielectric permittivity and can be explained by Maxwell-Wagner's model [64]. The polarization lags behind applied alternating field due to the presence of defects and structural inhomogeinities in ferrites, hence results in dielectric loss [65]. The dielectric loss decreases with Gd^{+3} substitution and low value loss are observed for higher frequencies which indicate their potential applications in high frequency microwave devices.

4.4.2.3 Dielectric Constant Variation with Temperature as the Function of Frequency

Fig.4.19 shows the variation of dielectric constant of a material with frequency is very sensitive to temperature. The measurement of dielectric constant for all the samples was recorded at different frequencies from room temperature to $500^{O}C$. It is seen from the figure 4.19, all the samples shows peaks behavior in the lower temperature region from $40^{O}C$ to $90^{O}C$ for all the fruencies and then increases with increase in temperature. The structural investigation depicts that the crystallite size is dependent on the Co^{+2} content in the sample and co-relate the link between the particle size and the magnitudes of the peak height. The peaks are the relaxation peaks which are dependent on the frequency. The peaks are produced due to the relaxation time which is the time taken by the electrical dipole to orient in the direction of the applied field.

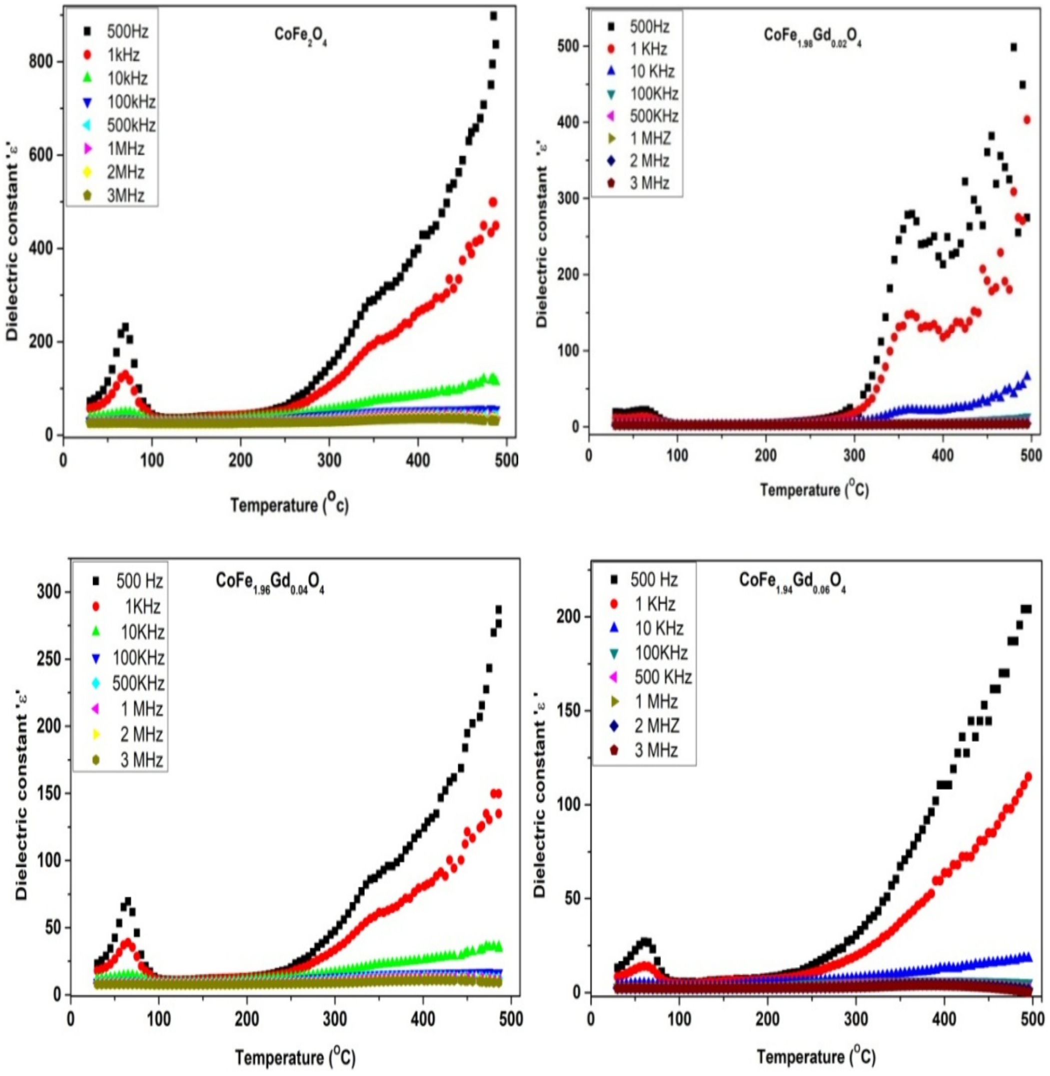

The variation of the dielectric constant (Ɛ) with temperaturefor $CoFe_{2-x}Gd_xO_4$

(x = 0. 00, 0.02, 0.04, 0.06) as a function of frequency.

The dielectric constant (Ɛ) Variation with temperaturefor $CoFe_{2-x}Gd_xO_4$ (x = 0.08, 0.1.0) as a function of frequency is shown below.

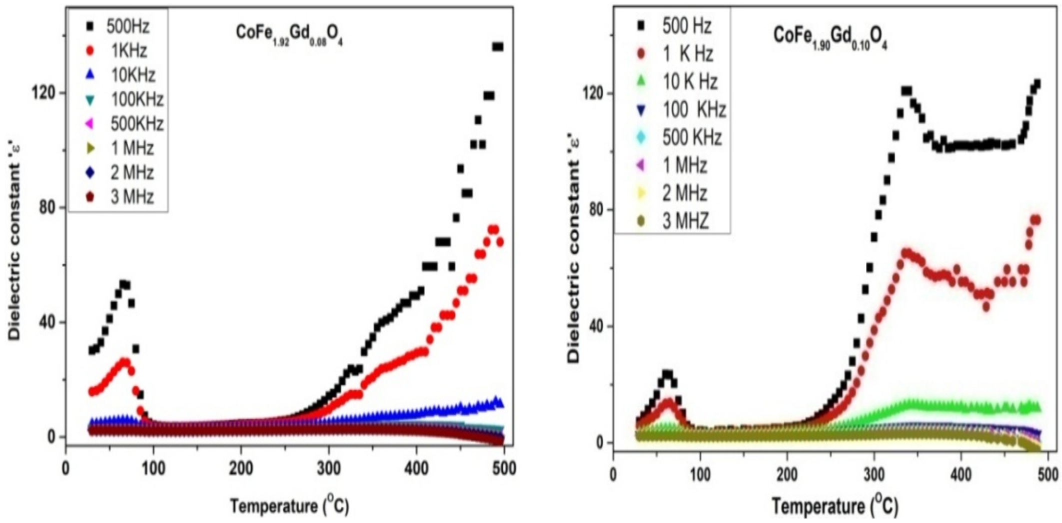

Fig.4.19: Variation of the dielectric constant (Ɛ) with temperaturefor $CoFe_{2-x}Gd_xO_4$ (x = 0. 00, 0.02, 0.04, 0.06, 0.08, 0.1) as a function of frequency.

When the frequency of the applied AC field matches with the frequency of the relaxation time, the resonance phenomenon occurs during which maximum energy transfer from the applied AC field takes place.

The dielectric constant 'ε' varies with temperature as the function of frequency shows peaks behavior between 40^{O}C to 90^{O}C temperature, relaxation peaks spread and height of dielectric constant decreases with increasing AC field frequency and finally becomes flat for high frequency of 500 KHz. The relaxation peaks at higher frequency and at lower temperature disappear due to charge carrier localization [66, 67]. As the temperature increases, the thermal energy increases which increases hopping rate of charge carrier's thereby increasing mobility in amplified form that increases the conductivity. There is augmentation of dipole polarization that depends on applied frequency [66, 68] and Co^{+2}content in the sample.

The dielectric constant decreases with increase in Gd^{+3} concentration in $CoFe_{2-x}Gd_xO_4$.This is due to the substitution of large ionic radii Gd^{+3} ions in octahedral sites which decreases Fe^{+3} ions at octahedral sites of samples. The Gd^{+3} ions at octahedral sites replace Fe^{+3} ions which reduces the rate of hopping of Fe^{+2} and Fe^{+3} ions. Hence polarization decreases with increase in Gd^{+3} content in the sample which reduces dielectric constant value.

4.3.2.4 Dielectric Loss Variation with Temperature as the Function of Frequency

The dielectric loss variations with temperature as the function of frequency are shown in the figures below. It is seen from the figure 4.20 behavior shown by dielectric loss is similar to the dielectric constant. The peaks in the lower temperature range are not prominent. In the crystalline material, when the dielectric polarization lag behind applied alternating field that results in dielectric loss which occurs due to grain boundary effect. The dielectric property in the case of nano-particle samples may depend on factors such as sample preparation method, structure, size of the crystallite, chemical composition and preparative conditions [68].

The dielectric loss variation with temperature as the function of frequency for $CoFe_{2-x}Gd_xO_4$ (x = 0.00, 0.02, 0.04, 0.06) is shown in the figure 4.20 below.

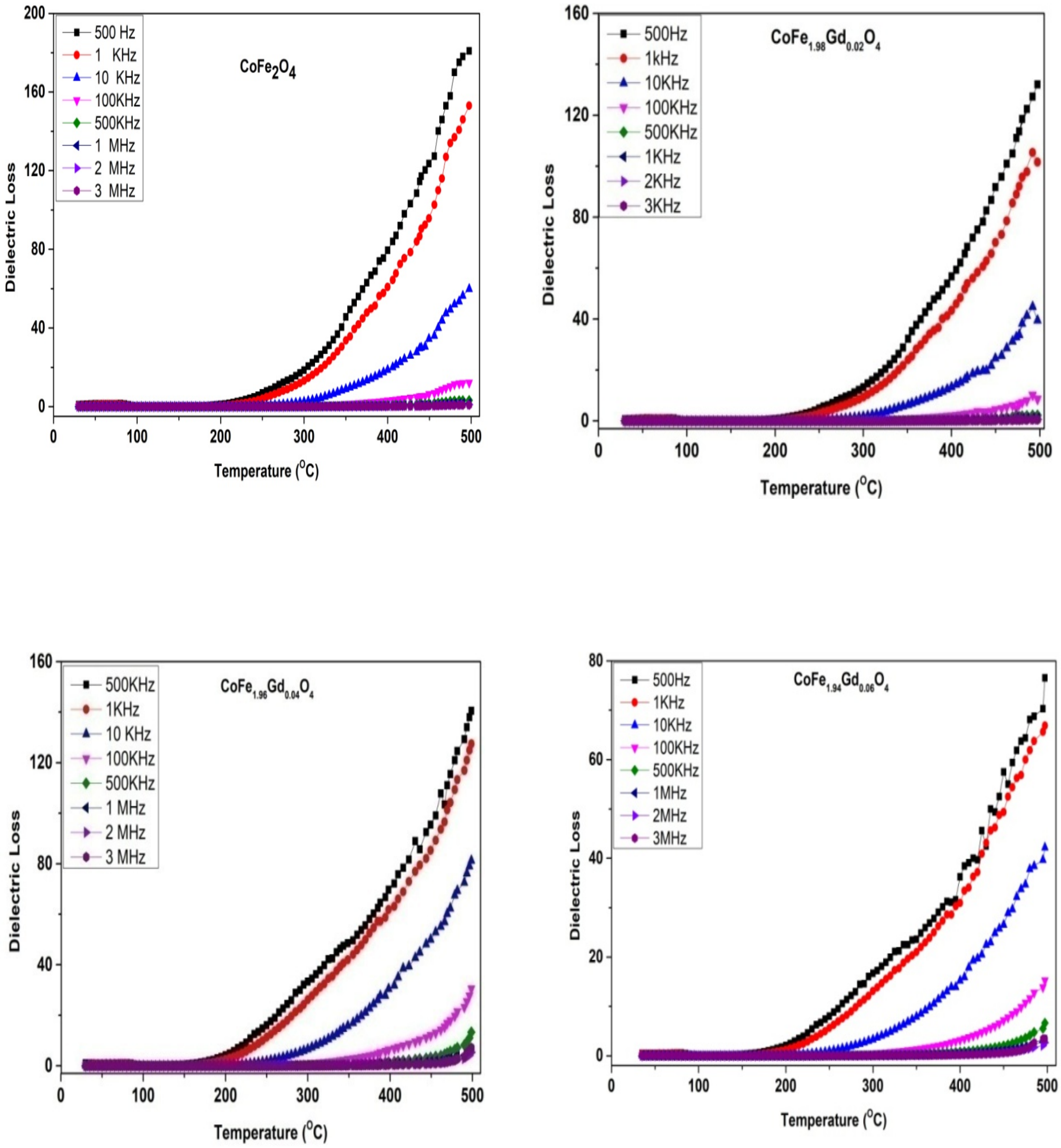

The variation of dielectric loss with temperature as the function of frequency for $CoFe_{2-x}Gd_xO_4$ (x = 0.08, 0.10) are shown in the figure 4.20 below.

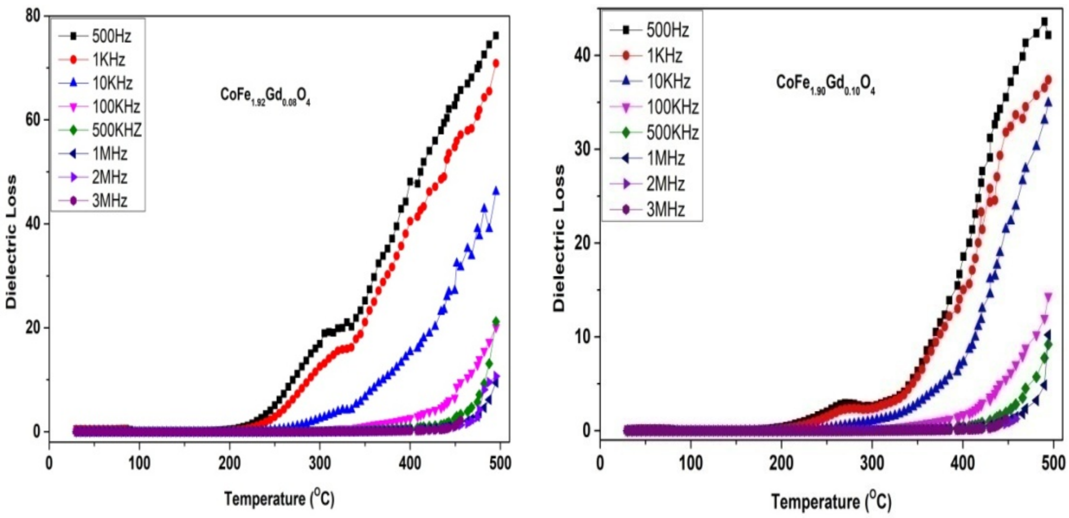

Fig.4.20: Variation of the dielectric loss (tanδ) for $CoFe_{2-x}Gd_xO_4$ (x = 0.00, 0.02, 0.04, 0.06, 0.08, 0.10) with temperatures as a function of frequency.

It is seen from the figure 4.20 behavior shown by dielectric loss is similar to the dielectric constant. The peaks in the lower temperature range are not prominent. In the crystalline material, when the dielectric polarization lag behind applied alternating field that results in dielectric loss which occurs due to grain boundary effect. The dielectric property in the case of nano-particle samples may depend on factors such as sample preparation method, structure, size of the crystallite, chemical composition and preparative conditions [68].

4.4.3 Thermoelectric Power

Thermoelectric power or seebeck coefficient of $CoFe_{2-x}Gd_xO_4$ (x = 0.00, 0.02, 0.04, 0.06, 0.08, 0.10) samples was measured in the range of room temperature to 500 ^{O}C. The fig.4.21 shows thermal variation of thermoelectric power of Gd^{+3} dope Cobalt ferrites samples. It can be seen that all the composition have positive thermo electric power at room temperature. As a temperature increases, the positivity of thermoelectric power decreases and changes to negative value at certain temperature which is observed for all the samples.

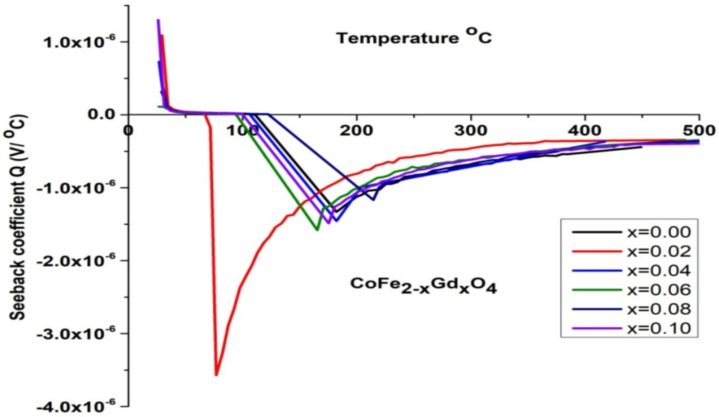

Fig. 4.21: Variation of thermoelectric power with temperature of $CoFe_{2-x}Gd_xO_4$ samples.

It is seen from fig.4.21 that samples shows p-type semiconductor behavior in low temperature region and n-type semiconductor in high temperature region. The p-type of conduction mechanism is due to hopping of holes between $Co^{+3} \Leftrightarrow Co^{+2}$ and n-type conduction mechanism in the sample is due to hopping of electrons between $Fe^{+2} \Leftrightarrow Fe^{+3}$ [69]. The transition from p-type to n-type supports the changes in concentration of Co^{+2}

and further predicts the conduction mechanism is due to hopping of electrons between Fe^{+2} and Fe^{+3}[70].

Table. 4.5: Transition temperatures T (p-n) of $CoFe_{2-X}Gd_xO_4$ samples.

Concentration 'x' of $CoFe_{2-x}Gd_xO_4$	**Transition Temperature T p-n (^OC)**
0.00	111
0.02	67
0.04	106
0.06	94
0.08	122
0.10	100

Table 4.5 provides the transition temperature Tp-n of each sample at which thermoelectric power changes from positive to negative i.e. p-type to n-type. The temperature T (p-n) varies in the range of 67^OC to 122^OC.

References:

[1] A.K. Giri, E. M.Kirkpatrick, P. Moongkhamklang, and S.A. Majetich, Applied Physics Letters 80 (2002) 2341-2343.

[2] S.J.Lee, C.C.H Lo, P.N.Matlage, S.H.Song, Y.Melikhov, J.E.Snyder, and D.C.Jiles Journal Applied Physics 102 (2007) 073910.

[3] K.Kamal Bharati, R.J. Tackett, C.E.Botez and C.V. Ramana Journal Applied Physics 109 (2011) 07A510.

[4] Simona Burianova, Jana PoltierovaVejpravova, Petr Holec, Jiri Plocek and Daniel Niznansk, Journal Applied Physics 110 (2011) 073902.

[5] K.Vasundhara, S.N. Achary, S.K. Deshpande, P.D. Babu, S. S. Meena and A.K. Tyagi, Journal of Applied Physics 113 (2013) 194101.

[6] A. K. Nikumbh, A.V. Nagawade, V.B.Tadke and P.P. Bakare, Journal of Materials Science 36 (2001), 653.

[7] G.D. Dwivedi, K.F.Tseng, C.L. Chan, P. Shahi, J. Lourembam , B.Chatterjee, A.K. Ghosh, H.D.Yang and Sandip Chatterjee, Physical review B 82 (2010) 134428.

[8] A.Franco, Jr., and F.C.e Silva, Applied Physics Letters 96 (2010) 172505.

[9] S.J.Lee, S.H.Song, C.C. Lo, S.T. Aldini and D.C. Jiles, Journal Applied Physics 101 (2007), 09C502.

[10] A.Franco Jr., F.L.A Machado, V.S.Zapf and F.W. Fabris, Journal Applied Physics 109 (2011) 07A745.

[11] S.P.Yadav, S.S.Shinde, A.A. Kadam and K.Y.Rajpure, Journal of Alloys and Compounds, 555 (2013) 330.

[12] Y. Cedeño Mattei, O. Perales-Perez, M.S.Tomar, F. Roman, P.M Voyles and W. G. Stratton, Journal Applied Physics 103 (2008) 07E512.

[13] A.V.R. Reddy, G. Ranga Mohan, D. Ravinder, B. S. Boyanov, Journal of materials science, 34 (1999) 3169.

[14] K.Kamala Bharathi and C.V. Ramana, Journal of Materials Research 26, (2011), 584.

[15] G. Dascalu, T.Popescu, M.Feder and O.F.Caltun, Journal of Magnetism and Magnetic Materials 333, (2013), 69. 56.

[16] Pranav P. Naik, R.B. Tangsali, S.S. Meena, S.M. Yusuf, Materials Chemistry and Physics, 191 (2017) 215-224.

[17] K.Velmurugan, V. S .K.Venkatachalapathy and S.Sendhilnathan, Materials research, 12, (2009), 529 - 534.

[18] J. A. Eastman, M. R. Fitzsimmons, L. J. Thompson, A. C. Lawson and R. A. Robinson, Nanostruct. Mater., 1, (1992), 465-470.

[19] D. Oleszak and P. H. Shingu, J. Appl. Phys., 79, (1996), 2975-2980.

[20] J. A. Dean, Lange's handbook of chemistry, McGraw-Hill, New York, 15th edn, 1998.

[21] C.Venkataraju, Applied Physics Research1 (No. 1) (2009) 41-45.

[22] M.M. Haque, M. Huq, M.A. Hakim, Indian J. Phys. 78A (3) (2004) 397-400.

[23]Emad M.M. Ewais, Mahmoud M. Hessien, Abdel-Hady A. El-Geassy, Journal of Australian Ceramic Society, 44 (1) (2008) 57-62.

[24] K. Rama Krishna, K. Vijaya Kumar, Dachepalli Ravinder, Advances in Materials Physics and Chemistry 2, (2012) 185-191.

[25] R. D. Waldron, Phys. Rev., 1955, 99, 1727.

[26] K. Manju, T. Smitha, D. S. Nair, E. K Aswathy, B. Aswathy, T Arathy, Binu, K. T. Krishna, Journal of Advanced Ceramics, 2015, 4(3): 199–205

[27] K. J. Standley, Oxide magnetic materials, Oxford University Press, 1972.

[28] G.K. Williamson, W. H. Hall, Acta Metal. 1 (1953), 22.

[29] W. J. Nellis, S. Legvold, Phys. Rev. 180, (1969) , 581.

[30] P. Kumar, S. K. Sharma, M. Knobel, J. Chand and M. Singh, J.Electroceram, 2011, 27, 51.

[31] J. Jing, L. Liangchao, X. Feng, J.Rare Earth. 25, (2007), 79.

[32] S. Singhal, S.K. Barthwal, K. Chandra K, J. Magn. Magn. Mater. 306 , (2006) 233.

[33]J. Jiang, Y.M. Yang, L.C. LiL, Physica B 399 (2007) 105.

[34] A.T. Ngo, P. Bonville, and M.P. Pileni, J. Appl. Phys. 89 (2001) 3370.

[35] K. Maaz, A. Mumtaz, S. K. Hasanain and A. Ceylan, J. Magn. Magn. Mater., 2007, 308, 289.

[36] R. H. Kodama, A. E. Berkowitz, J. E. J. McNiff and S. Foner, Phys. Rev. Lett., 1996, 77, 394.

[37] T.Sodaee, A. Ghasemi, R. Shoja Razavi, J Clust Sci 27 (2016)1239.

[38] G. Bottoni, D. Candolfo and A. Cecchetti, J. Appl.Phys. 81 (1997), 3794.

[39] S. Mukherjee, S. Pradip, A.K. Mishra, D. Das, Zn substituted NiFe2O4 with very high saturation magnetization and negligible dielectric loss synthesized via a soft chemical route, Appl. Phys. A 116, 389–393, (2014).

[40] M.A. Gabal, Y.M. Al Angari, F.A. Al-Agel, Cr-substituted Ni-Zn ferrites via oxalate decomposition. Structural, electrical and magnetic properties, J. Magn. Magn. Mater. 391, 108–115 (2015).

[41] L. Ben Tahar, L.S. Smiri, A.-L. Joudrier, M. Artus, F. Herbst, M.-J. Vaulay, S. Ammar, F. Fie´vet, Mater. Res. Bull. 42 (2007) 1888.

[42] S.S. Jadhav, S.E. Shirsath, B.G. Toksha, S.J. Shukla, K.M. Jadhav, Effect of cation proportion on the structural and magnetic properties of Ni-Zn ferrites nano-size particles prepared by co-precipitation technique, Chin. J. Chem. Phys. 21, 381–386 (2008).

[43] T. J. Shinde, A.B. Gadkari, P.N. Vasambekar, Magnetic properties and cation distribution study of nanocrystalline Ni-Zn ferrites, J. Magn. Magn. Mater. 333, 152–155, (2013).

[44] O.A. Li, C. R. Lin, H. Y. Chen, H. S. Hsu, K. Y. Shih, I.S. Edelman, K.-W. Wu, Y.T. Tseng, S.G. Ovchinnikov, J.S. Lee, Size dependent magnetic and magneto-optical properties of Ni0.2Zn0.8Fe2O4 nanoparticles, J. Magn. Magn. Mater. 408, 206– 212 (2016).

[45] V. Grimal, D. Autissier, L. Longuet, H. Pascard, M. Gervais, Iron, nickel and zinc stoichiometric influences on the dynamic magneto-elastic properties of spinel ferrites. J. Eur. Ceram. Soc. 26, 3687–3693, (2006).

[46] I. Szczygieł, K. Winiarska, A. Bieńko, K. Suracka, D. Gaworska Koniarek, The effect of the sol-gel autocombustion synthesis conditions on the Mn-Zn ferrite magnetic properties, J. Alloy. Compd. 604, 1–7, (2014).

[47] A.V. Humbe, A.C. Nawle, A.B. Shinde, K.M. Jadhav, Impact of Jahn Teller ion on magnetic and semiconducting behavior of Ni-Zn spinel ferrite synthesized by nitrate-citrate route, J. Alloy. Compd. 691, 343–354 (2017).

[48] I.H. Gul, W. Ahmed, A. Maqsood, Electrical and magnetic characterization of nanocrystalline Ni-Zn ferrite synthesis by co-precipitation route. J. Magn. Magn. Mater. 320, 270–275 (2008).

[49] P.P. Sarangi, S.R. Vadera, M.K. Patra, N.N. Ghosh, Synthesis and characterization of pure single phase Ni-Zn ferrite nanopowders by oxalate based precursor method, Powder Technol. 203, 348– 353, (2010).

[50] E.J.W. Verwey, Electronic conduction of magnetite (Fe3O4) and its transition point at low temperatures, Nature 144, 327–328 (1939).

[51] A.D. Sheikh, V.L. Mathe, Anomalous electrical properties of nanocrystalline Ni–Zn ferrite. J. Mater. Sci. 43, 2018–2025 (2008).

[52] A. Hajalilou, H.M. Kamari, K. Shameli, Dielectric and electrical characteristics of mechanically synthesized Ni-Zn ferrite nanoparticles, J. Alloy. Compd. 708, 813–826 (2017).

[53] M.A. Ali, M.M. Uddin, M.N.I. Khan, F.-U.-Z. Chowdhury, S.M. Haque, Structural, morphological and electrical properties of Snsubstituted Ni-Zn ferrites synthesized by double sintering technique, J. Magn. Magn. Mater. 424, 148–154, (2017).

[54] M. T. Rahman and C. V. Ramana, J. Appl. Phys., 2014, 116, 164108.

[55] J. C. Maxwell, Electricity and Magnetism, Oxford Univ. Press, London, 1973.

[56] C. G. Koops, Phys. Rev, 1951, 83, 121.

[57] S. Sharma, Kirti Nanda, R.S. Kundu, R. Punia and N. Kishore, Structural Properties, Conductivity, Journal of Atomic, Molecular, Condensate &Nano Physics, 2 (2015) 15–31.

[58]M. Mehedi Hassan, Arham S. Ahmed, M. Chaman, Wasi Khan, A.H. Naqvi, Ameer Azam, Materials Research Bulletin, 47 (2012) 3952–3958.

[59]C. Belkhaoui, Ramzi Lefi, NissafMzabi, Hichem Smaoui, Journal of Materials Science: Materials in Electronics, (2018).

[60] K. Iwauchi, Jpn. J. Appl. Phys., 1971, 10, 1520.

[61] N. Sivakumar, A. Narayanasamy, C. N. Chinnasamy and B. Jeyadevan, J. Phys.: Condens. Matter, 2007, 19, 386201.

[62] A. Rana, O. P. Thakur and V. Kumar, Mater. Lett., 2011, 65, 3191.

[63] R. S. Devan, B. K. Chougule, Journal of Applied Physics 101, (2007)014109.

[64] K.M. Batoo, S. Kumar, C.G. Lee, Alimuddin, Curr. Appl Phys. 9 (2009) 826.

[65] A.K. Singh, T.C. Goel, R.G. Mendiratta, O.P. Thankur, C. Prakash, J Appl Phys. 91 (2002) 6626–6629.[66]M. R. Bryce and Michael C. Petty, Nature 374 (1995) 771-776.

[67] S. Sagadevan, Kaushik Pal, Zaira Zaman Chowdhury, M. Enamul Hoque, J Sol-Gel Sci Technol, (2018).

[68] C. C. Naik, A. V. Salker, Journal of Materials Science: Materials in Electronics (2017).

[69] A. G Bhosale and B. K. Chougule Materials Letters 60, (2006), 3912-3915.

[70] D. Ravinder, P. Vijaya and B. Reddy, J. Magn.Magn.Mater, 263, (2003), 127- 133.

CHAPTER 5

Effect of Nd^{+3}doping on Structural, Magnetic and Electrical properties of $CoFe_2O_4$ Nanoparticles

5. 1 Introduction

The material composed of nano particles exhibit new and fascinating properties which depend under factor such as particle size, preparation method, atmospheric condition etc. The nano particles with particle size in the vicinity of 10 nm are always a challenge of immense potential to the researchers and technologists. The development of new methods for the nano particles preparation is welcome in the area of research. Initially an oxide were used for the preparation of nano-particles as the starting material and was limited to the ceramic method followed by grinding of material using ball mill techniques for long duration and with high speed. As the advancement of the research, newer methods were introduced and now chemical methods employ salts other than oxides that have motivated searching and developing a simple chemical method to prepare nano particles ferrites materials.

Magnetic materials play very important roles in a daily life [1]. Among different magnetic materials, the ceramic materials received special attention due to the chemical stability, ease of synthesis and a high electrical resistivity value. One of the important magnetic spinel material, cobalt ferrites which shows properties like high Curie temperature, hard magnetic properties, large magnetostrictive coefficient and saturation magnetization [2-5]. A small amount of rare earth element substitution in cobalt ferrites can affect the magnetic property as well as magnetic coercivity which make it suitable for different applications like hyperthermia treatment [6, 7]. Due to the localized nature of 4f electrons, rare earth elements possess large magnetic moments, large value of magneto crystalline anisotropy and high magnetostriction at low temperature. Since Nd has large ionic radii (0.0983nm), the substitution of Nd in the spinel structure leads to distortion of crystal structure [8] and change in coercivity [9]. Nanoparticles have a wide range of applications such as drug delivery, magnetic resonance imaging, data storage, catalysis, biomedical applications due to their sizes.

The qualitative and quantitative information of the material were investigated using techniques like XRD, Scanning electron microscopy, Transmission electron microscopy, and electron dispersive spectroscopy. The modern tools are used to explore magnetic and electrical properties of the material. Since the properties of a structure can be change by altering compositions or processes or both, the understanding of structure and composition of materials is essential to use the material in an appropriate application.

The structural investigation, magnetic and electrical properties of Nd doped cobalt ferrites sample are discussed in this chapter. The materials are characterized using methods such as XRD, SEM, TEM, FTIR, EDS and are used to study the crystal structure, crystallite size, lattice parameter, structural morphology, the chemical composition. Also the magnetic and electrical properties of the materials are explored.

5.2 Structural Characterization

The Nd^{+3} doped cobalt ferrites material with chemical formula as $CoFe_{2-x}Nd_xO_4$ ($x = 0.00, 0.02, 0.04, 0.06, 0.08, 0.10$) are characterized using various sophisticated instruments. The material is characterized in order to understand the properties which are useful in ensuring quality control, optimizing performance, aiding material selection, and advancing research and development. The information is useful for designing and utilizing the material effectively and efficiently in the various industrial applications.

5.2.1 X-ray Diffraction Spectrum

X-ray diffraction pattern of samples with chemical formula $CoFe_{2-x}Nd_xO_4$(X=0.00, 0.02, 0.04, 0.06, 0.08, 0.10 are depicted in fig 5.1

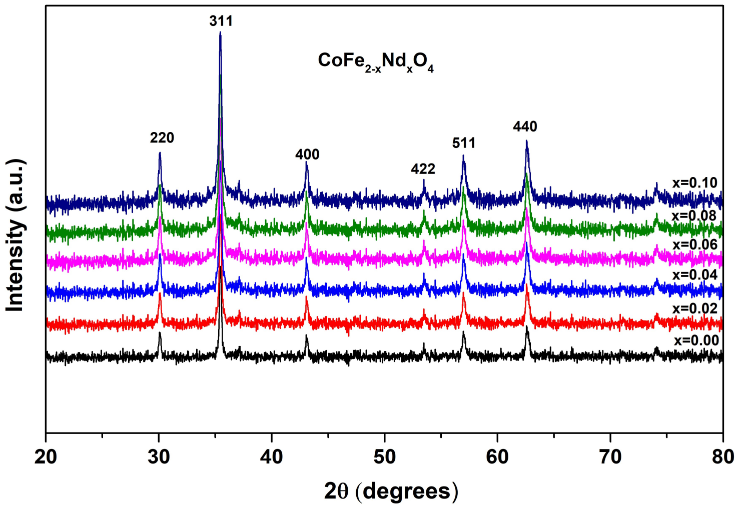

Fig 5.1: X-ray diffraction pattern for $CoFe_{2-x}Nd_xO_4$ (x = 0.00, 0.02, 0.04, 0.06, 0.08, 0.10)

Rigaku X-ray diffractometer (Cu $K\alpha_1$= 1.5418 Å) was used for the phase determination of samples with 0.02 step of 2θ in the range of 20^O- 80^O to obtain XRD pattern. The XRD pattern shows (311) as a major peak and all other peaks correspond to spinel structure with no other impurities are observed in all the diffraction patterns. XRD spectra of all compositions shows the formation of Monophasic samples and the prominent Bragg reflection was index as (220) ,(311) ,(222) ,(400) ,(422) ,(511) and (440); which specify the characteristic planes of single phase fcc cubic spinel structure (JCPDS Card no. 22-1086).

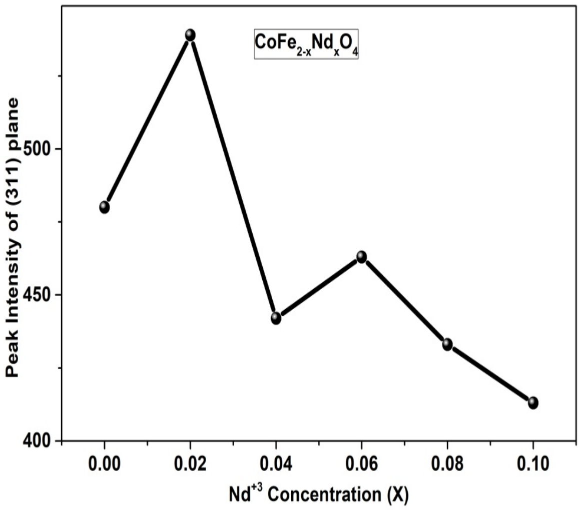

Fig. 5.2: Variation of peak intensity of (311) plane with Nd^{+3} concentration

for $CoFe_{2-x}Nd_xO_4$

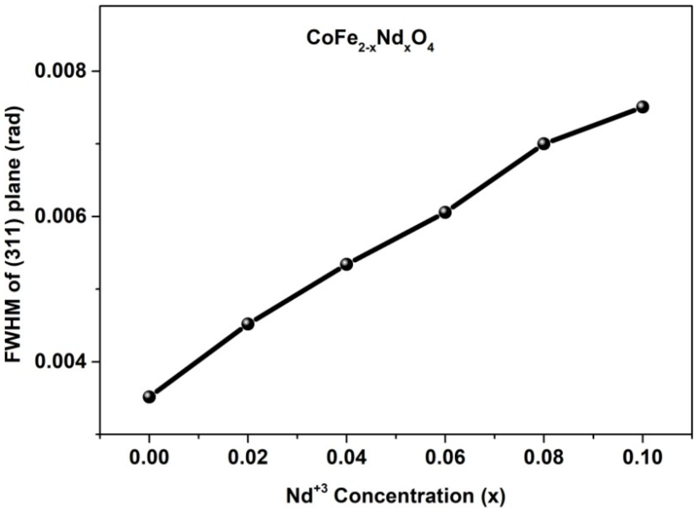

Fig. 5.3: Variation in FWHM of (311) plane with Nd^{+3} concentration for $CoFe_{2-x}Nd_xO_4$.

The peak intensity of (311) value plane varied with Nd^{+3} concentrations for $CoFe_{2-x}Nd_xO$ is shown in fig 5.2. It shows that initially intensity increases for low concentration and then decreases for higher Nd^{+3}concentration, overall it shows a decreasing trend which indicates reduction in crystalline nature with increasing concentration of Nd^{+3} in the ferrites lattice. The FWHM variation with Nd^{+3} concentrations increases, which indicates reduction in the crystallite sizes.

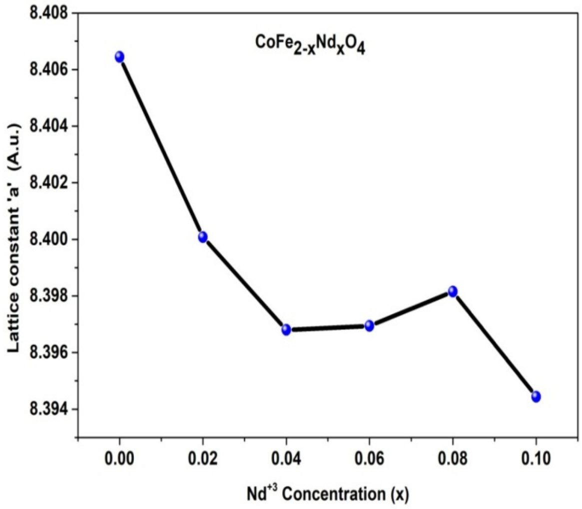

Fig, 5.4: Variation of lattice constant ‘a’ with Nd^{+3} concentrations for$CoFe_{2-x}Nd_xO_4$

The variation of lattice constant ‘a’ with concentrations of Nd^{+3} for $CoFe_{2-x}Nd_xO_4$ nanoparticles is shown in fig.5.4. It is observed that the lattice constant decreases from 8.4064 Å to 8.3944 Å as Nd^{+3} concentration increases from x = 0 to x = 0.10. The decrease in lattice constant is due to replacement of larger ionic radii of Nd^{+3}(0.983 Å) by smaller ionic radii of Fe^{+3} (0.64 Å) at octahedral site. This causes expansion of octahedral sub lattice site which results in increase in lattice constant [10].

The fig 5.5 shows thevariation of crystallite size with Nd^{+3}concentrations , the crystallite size is found to decrease with increase in Nd^{+3} concentrations in the range from 37 nm to 18 nm.

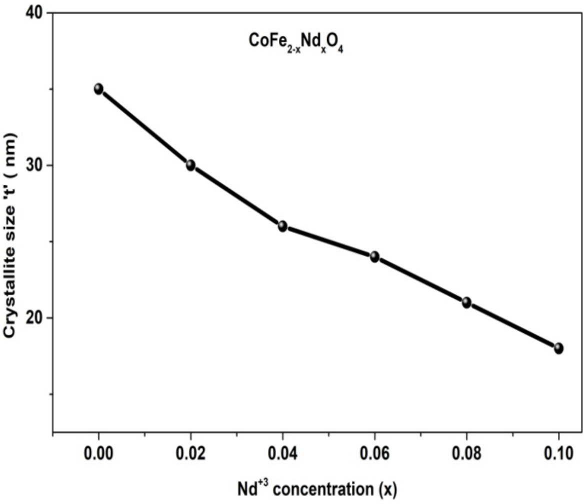

Fig, 5.5: Crystallite size Variation with Nd^{+3} concentrations for $CoFe_{2-x}Nd_xO_4$

Nano particles crystallite size is not identical due to the rate of ferrites formation differ for different composition and probability of favoring a different crystallite sizes [11]. The replacement of a larger ionic radii Nd^{+3} ion (0.0983 nm) by smaller radii Fe^{+3}ion (0.0645 nm) and Co^{+2} ion (0.0745 nm) at octahedral site [12-14] creates a strain in the lattice. Also the presence of Co^{+2} ions with maximum electrostatic shielding by 3d electrons introduces an additional strain. This strain depends on different factors such as lattice defects, larger surface energy, and presence of impurities etc. The micro-strain arises due to larger surface energy that results in larger surface to volume ratio of the sample [15-16]. The decrease in crystallite size is due to inclusion of rare earth ions developing lattice strain which hinders the crystal growth and are responsible for reduction for these materials. It is noticed that substitution of Nd^{+3} in $CoFe_2O_4$ is restricted; as a result there is a reduction in crystallite size. The reason is Nd^{+3}-O^{-2} bond energy is more than the Fe^{+3}- O^{-2} bond energy, so it required more energy to incorporate Nd^{+3} ions in place of Fe^{+3} ions into octahedral site [17].

Table 5.1: Lattice constant and crystallite size for various concentrations of Nd^{+3}.

Concentration 'x' of Nd^{+3} $CoFe_{2-x}Nd_xO_4$	**Lattice constant 'a' in Å**	**Crystallite size ' t' in nm**
0.0	8.4064	35
0.02	8.4001	30
0.04	8.3968	26
0.06	8.3970	24
0.08	8.3982	21
0.10	8.3944	18

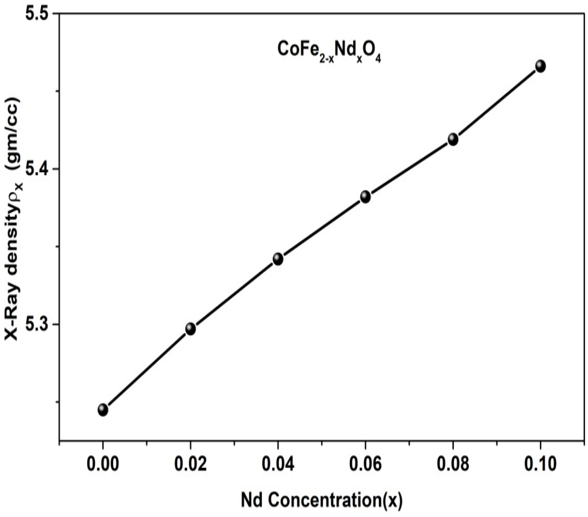

Fig, 5.6: Variation of X-ray density 'ρ_x' with Nd^{+3} concentrations for $CoFe_{2-x}Nd_xO_4$

X-ray density refers to the density of a material as measured using X-ray diffraction techniques. The fig 5.6 shows that x-ray density increases with Nd^{+3} concentrations. The changes in X-ray density when neodymium is doped into cobalt ferrites could be attributed to various factors, such as changes in crystal structure, atomic arrangement, and composition. This can attributed to the fact that the atomic weight of Nd^{+3} is 144.24 gm, which is greater than that of Fe^{3+} (55.845 gm). This behavior of enhancement in the X-ray density with increase in Nd^{+3} concentrations also supports effective incorporation of Nd^{+3} into $CoFe_{2-x}Nd_xO_4$ samples. The enhanced value of X-ray density may be also due to the improved molecular weight of the samples with neodymium ions. When neodymium (Nd) is doped into cobalt ferrites ($CoFe_2O_4$), it can lead to changes in the physical properties of the material, including its density.

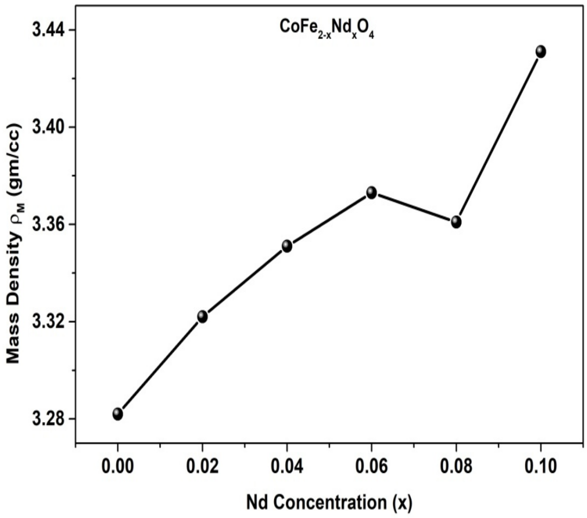

Fig. 5.7: Variation of mass density 'ρ_M' with Nd^{+3} concentrations for $CoFe_{2-x}Nd_xO_4$

Neodymium doping could potentially introduce disorder or lattice distortion into the cobalt ferrite structure, which might result in a change in the X-ray density. For example, if neodymium doping causes the lattice to expand or contract, the overall X-ray density of the material could decrease.Fig 5.7 shows mass density 'ρ_M' increases with Nd^{+3} concentrations. The mass density of ferrites can vary depending on specific dopants and its concentrations. The mass density is typically expressed in units of grams per cubic centimeter (g/cm³) or kilograms per cubic meter (kg/m³) [18-21]. For most ferrite materials, the mass density lies in the range of 4.9 to 5.2 g/cm³, but can be lower or higher value depending on dopants atomic mass and concentrations.

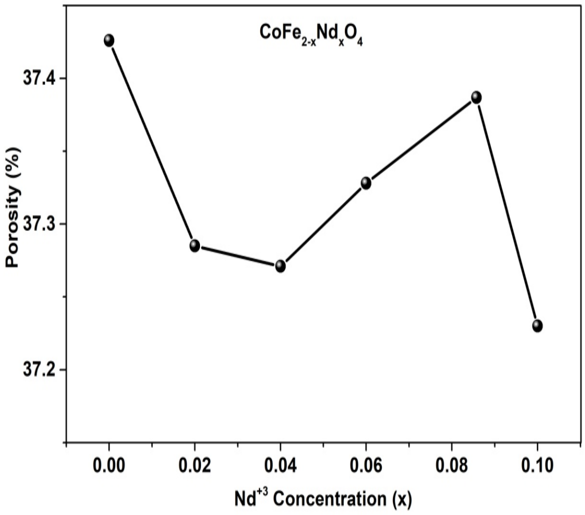

Fig. 5.8: Variation of porosity (%) with Nd^{+3} concentrations for $CoFe_{2-x}Nd_xO_4$

Generally, introducing dopants like neodymium into a material can influence its porosity, as dopants can affect the grain growth, sintering behavior, and overall microstructure of the material.The porosity in the ferrites materials can be controlled during fabrication. To achieve a desire level of porosity the techniques used are sintering, hot pressing, Sol-gel method, etc. The fig 5.8 shows the % porosity variation with the concentration of Nd^{+3}.It is observed that initially % porosity increases and then decreases with increase in Nd concentrations. The porosity of the sample helps in reduction of distortion losses and well separated particles can improve the transportation properties.

5.2.2 Fourier Transform Infra red (FTIR) Spectroscopy

Fig.5.9 Shows FTIR spectra of pure and Nd^{+3} doped $CoFe_2O_4$ nanoparticles samples. Two prominent bands are observed in the wave number range 370 – 700 cm^{-1} for all the samples. One band appear at lower wave number 370 cm^{-1}- 430 cm^{-1} are assigned to octahedral metal stretching vibration and other band appear at higher wave number at 560 cm^{-1}- 680 cm^{-1} corresponds to tetrahedral metal stretching vibration [22,24].

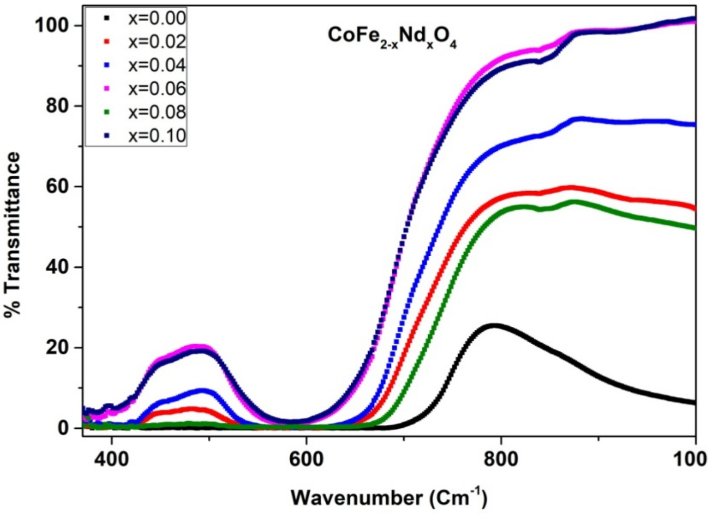

Fig. 5.9: FTIR spectra of $CoFe_{2-x}Nd_xO_4$ nano particles.

The two absorption bands are observed, the lower frequency band is about 390 cm^{-1} which corresponds to the vibration of metal oxide bond at octahedral site and the one corresponding to higher frequency is about 590 cm^{-1} indicates metal-oxygen vibration at tetrahedral site. These two absorption bands confirm the formation of spinel cobalt ferrites structure material. The difference in frequencies at octahedral and tetrahedral is due to the change in the bond length of (Fe^{+3}-O^{-2}) octahedral and tetrahedral site [25] and introducing Co^{+2} ion in octahedral and tetrahedral site.

It is known that the increase in site radius reduces the fundamental frequency and thus the central frequency should shift towards the lower frequency side. The increase in site radius maybe expected due to the replacement of smaller Fe^{+3} ions by larger Nd^{+3} ions. Vasant Naidu et. al. showed with addition of rare earth ions, absorption bad shift towards the higher frequency and attributed to increase in bond length at B site [26], and hence Rare earth occupies B site. M. M.Rashad et.al. reported the shift in band frequency towards higher wave number [27]. A.K. Nikumbh et.al. reported that no shift occur at A site band position but a B site band position, which shift towards the higher wave number shows the variation of Fe-O distance at B site. Bands undergo widening after doping [28].

5.2.3 Scanning Electron Microscopy (SEM)

The SEM images of pure co ferrite, 4% Nd doped and 10% Nd doped cobalt ferrites are shown in the fig.5.10 (a, b, c) respectively.

The surface morphological information of Co ferrite and Nd doped Co ferrite was obtained from SEM images. It is noticed from images that Co ferrites particles are spherical in shape, agglomerated and nano size. The nano particles large agglomerates are formed and this agglomeration increases with doping concentrations of Nd^{+3}. Further the clusters of grain boundaries in nano range are visible. The nano grains particles appears in spherical geometry shape. The extent of agglomeration increases with doping concentration of Nd^{+3}, may be due to the inclusion of Nd ions at octahedral site and also presence of surface charges with other type of forces [29]. The differences in undoped and doped samples are observed.

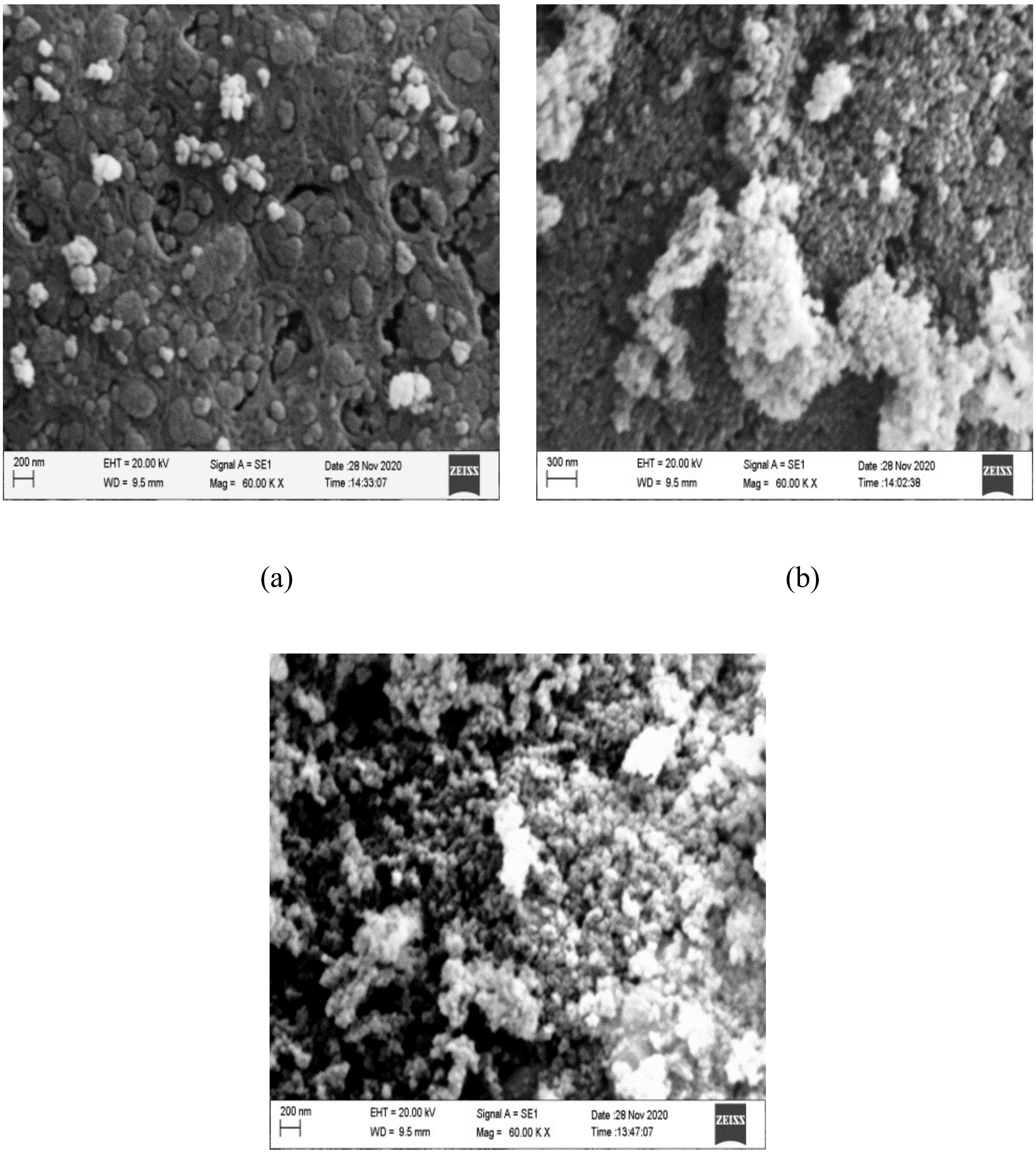

(a) (b)

(c)

Fig. 5.10: Scanning Electron Micrograph of (a) $CoFe_2O_4$, (b) $CoFe_{1.96}Nd_{0.04}O_4$ and (c) $CoFe_{1.90}Nd_{0.10}O_4$

5.2.4 Energy Dispersive Spectroscopy

Energy dispersive spectroscopy analysis for Co ferrite and Nd doped Co ferrites samples are shown in Fig.5.11. $CoFe_2O_4$ and Nd^{+3} doped $CoFe_2O_4$have been analyzed using energy dispersive spectroscopy analysis and the elemental composition depicted in table 5.2. The table shows the experimental and theoretical percentage composition of elements in the samples. The results confirms the presence of Co, Fe, Nd and O elements in the prepared samples and no other impurities are found within the experimental limit or resolution of EDS.

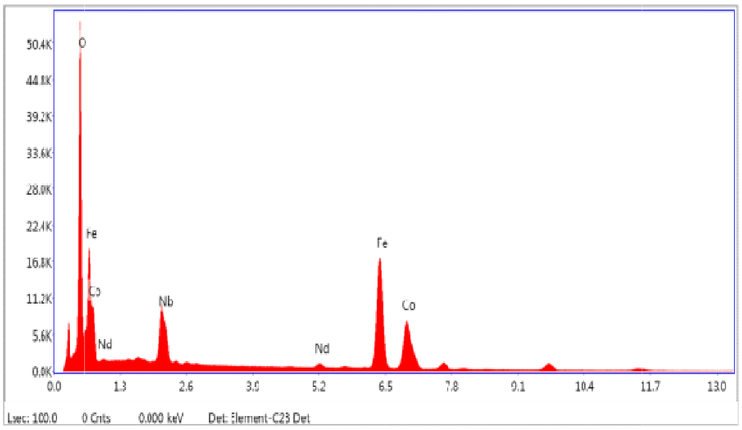

(a)$CoFe_2O_4$

EDS analysis of (b) $CoFe_{1.96}Nd_{0.04}O_4$ and (c) $CoFe_{1.90}Nd_{0.10}O_4$ shown below.

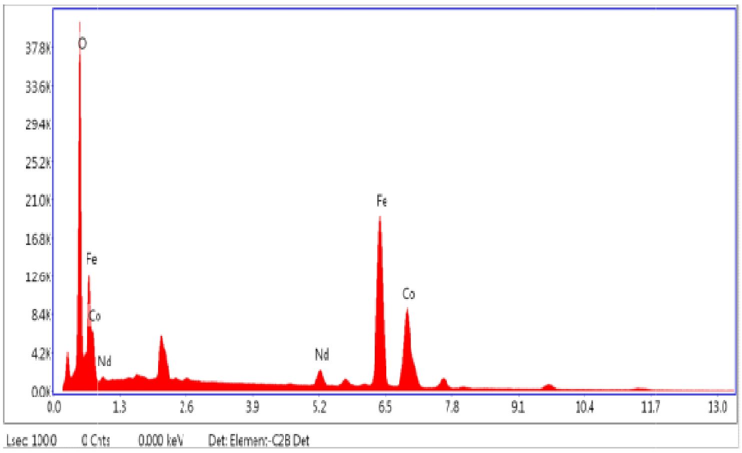

(b) $CoFe_{1.96}Nd_{0.04}O_4$

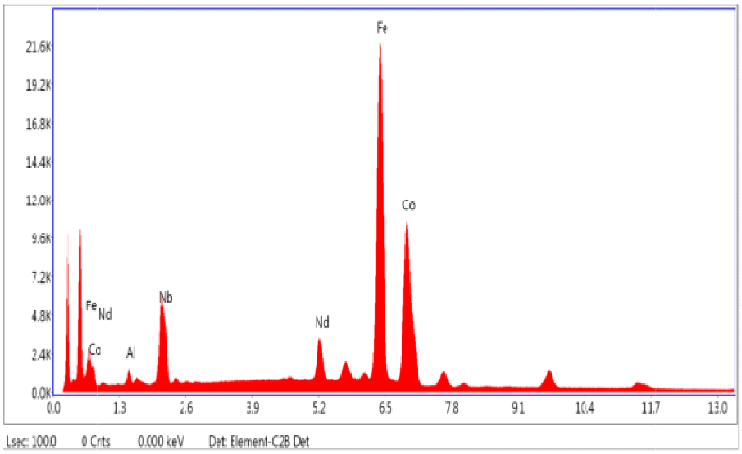

(c) $CoFe_{1.90}Nd_{0.10}O_4$

Fig.5.11: EDS analysis of (a) $CoFe_2O_4$ (b) $CoFe_{1.96}Nd_{0.04}O_4$ (c) $CoFe_{1.90}Nd_{0.10}O_4$

Table 5.2: Experimental and calculate weight percentage (a) $CoFe_2O_4$

(b)$CoFe_{1.96}Nd_{0.04}O_4$ (c) $CoFe_{1.90}Nd_{0.10}O_4$

Composition	**$CoFe_2O_4$**		**$CoFe_{1.96}Nd_{0.04}O_4$**		**$CoFe_{1.90}Nd_{0.10}O_4$**	
of Elements	**Exp%**	**Theo%**	**Exp%**	**Theo%**	**Exp%**	**Theo%**
Fe	49.88	47.61	47.32	45.97	47.77	43.59
Co	26.03	25.12	18.85	24.75	26.05	24.21
O	49.88	47.61	31.14	26.86	21.72	26.28
Nd	0	0	2.69	2.42	5.54	5.92
Total	100.00	100.00	100.00	100.00	100.00	100.00

5.2.5 Transmission Electron Micrograph (TEM)

Transmission electron micrograph for $CoFe_{1.96}Nd_{0.04}O_4$ and $CoFe_{1.90}Nd_{0.10}O_4$ is seen in fig.5.12. Since Nd^{+3} occupies octahedral site produces strain in the lattice as well as grain boundaries due to its larger ionic radii which causes hindrance in grain growth and is responsible for reduction of particle size.

The micrograph shows the agglomeration which indicates the strong magnetic nature of Nd^{+3} doped Cobalt ferrites.

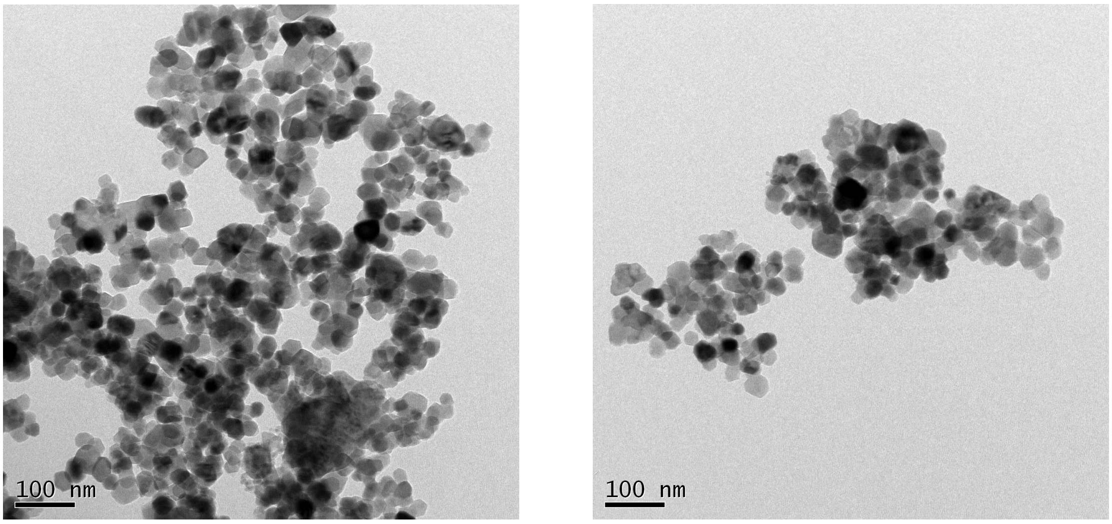

Fig. 5.12: Transmission Electron Micrograph of (a) $CoFe_{1.96}Nd_{0.04}O_4$ and (b) $CoFe_{1.90}Nd_{0.1}O_4$

5.3 Magnetic Properties Study

The magnetic behaviors properties of samples materials originate from the quantum couplings at the atomic level including electron spin coupling (S-S coupling), spin and angular momentum of electron orbital (L-S coupling) [30]. Each magnetic nanoparticles is considered to possess a single domain and hence magnetic properties are studied with changes in presence of external magnetic fields. It has been found that pure cobalt ferrites and Nd^{+3} doped cobalt ferrites shows ferrimagnetic behavior. The magnetic measurement studies such as hysteresis for pure and Nd^{+3} doped cobalt ferrites are explored. The study of zero field cooled (ZFC) and field cooled (FC) measurement for constant field has been investigated. Curie temperature of samples are explore using AC susceptibility measurement.

5.3.1 Vibrating Sample Magnetometer (VSM)

The magnetic loop measurement for Co ferrites and Nd doped ferrites samples are recorded on Quatum design's versa lab 3 tesla system.The Fig. 5.13 shows the hysteresis loops of $CoFe_{2-x}Nd_xO_4$ (x = 0.00, 0.02, 0.04, 0.06, 0.08, 0.10) nanoparticles.

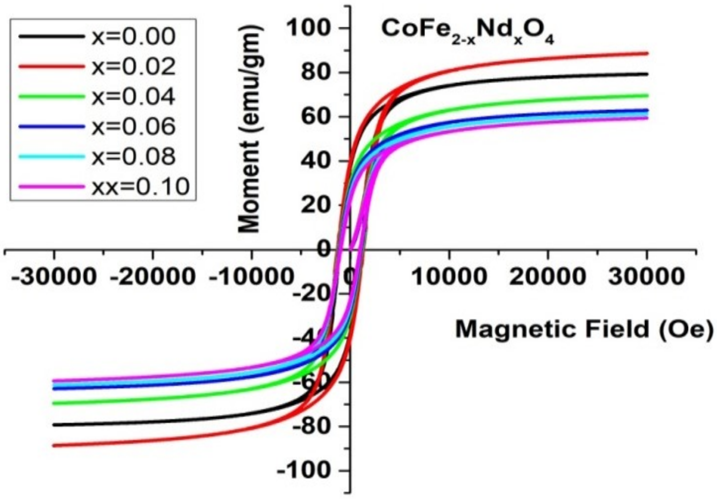

Fig. 5.13: Hysteresis loops for $CoFe_{2-x}Nd_xO_4$ (x = 0.00, 0.02, 0.04, 0.06, 0.08, 0.10) nanoparticles.

The saturation Magnetization (Ms), Coercivity (Hc) and remanence magnetization (Mr) are extracted from magnetization curve shown in fig.5.13 and values are listed in the table.5.3 It is observed that saturation magnetization decreases with increase in Nd^{+3} concentrations for Nd^{+3} doped Co ferrites sample. The value of Ms for Co ferrites is 79 emu/gm and the saturation magnetization value decreases from 89 emu/gm to 59 emu/gm for Nd doped samples when concentration of Nd^{+3} increases from x= 0.0 to x=

0.10. The magnetic properties of ferrites appear to be sensitive to cation distribution in the spinel lattice sites. The substitution of larger radii Nd^{+3} ions into octahedral sites can destroy the stability of original equilibrium distribution. As per Neel's sublattice model, three types of interactions i.e. A-A, B-B and A-B exists between tetrahedral site and octahedral site of spinel ferrites. Among these three interactions, A-B interaction is stronger than other two interactions [31, 32]. The ion occupies octahedral sites in rare earth doped ferrites due to its larger ionic radius. Also the magnetic moment for Nd^{+3} ions originate from 4f electrons [33] and at room temperature their magnetic dipole orientations are in disorder form, hence they contribute very small to net magnetization at room temperature [34,35]. Therefore doping of Nd^{+3} ions in cobalt ferrites lattices is equal to the substitution of non magnetic atom at B sites that result in the reduction of magnetization at B sites. The total magnetization of cobalt ferrites calculated from the difference of magnetization of B sites and A sites. The A-B interactions become weaker as a concentration of Nd^{+3} increases [36, 37]. Hence the magnetization decreases with increase in Nd^{+3} doping concentrations. The bond angle in A-A and B-B interaction decreases where as in A-B interaction it increases which attributes to the decrease in magnetization. Also in ferrimagnetic ferrite structure, the magnetization of tetrahedral sublattice and octahedral sublattice are antiparallel to each other and ultrafine particles have non-collinear magnetic structure on the surface layer. The reduction in particle size tends to increase in non-collinear magnetic structure in which magnetic moment are not aligned with external magnetic field. Thus the increase in non-collinear structure decreases the saturation magnetization [38]. The enhancement of saturation magnetization may be due to higher Nd^{+3} doping concentration, in which Co^{+2} ion immigrates in A site accompanied by equivalent Fe^{+3} ion moving from A site to B site. This migration decreases the concentration of Fe^{+3} ions in A site that results into the increase of saturation magnetization for rare earth doped Co ferrites. Table 5.3 shows magnetic properties of $CoFe_{2-x}Nd_xO_4$: saturation magnetization (Ms), coercivity (Hc), remanent magnetization (Mr) and remanence ratio.

Table 5.3: The variation of coercivity with Nd^{+3} concentrations are shown in the table

Concentrations 'x' of sample $CoFe_{2-x}Nd_xO_4$	**Ms (emu/g)**	**Hc (Oe)**	**Mr (emu/g)**	**Mr/Ms Ratio**
$CoFe_2O_4$	79	1099	40	0.501
$CoFe_{1.98}Nd_{0.02}O_4$	89	1256	39	0.438
$CoFe_{1.96}Nd_{0.04}O_4$	70	1144	31	0.440
$CoFe_{1.94}Nd_{0.06}O_4$	63	1093	27	0.427
$CoFe_{1.92}Nd_{0.08}O_4$	61	1000	25	0.412
$CoFe_{1.90}Nd_{0.1}O_4$	59	992	20	0.342

The coercive field shows decreasing trend with increase in Nd^{+} concentration and itvaries from 1256 Oe to 992 Oe. The coercivity trend of variation is due to the substitution of large ionic radii Nd^{+3}ion by Fe^{+3} ion in B sites, to compensate for this Co^{+2} ions migrated from B sites to A sites which decreases Co^{+2} cations at B sites. This reduces single Co^{+2} ion anisotropy that results in the reduction of the coercivity. The decrease in coercivity also related to crystallite size in the single domain region according to which coercivity decreases with decrease in crystallite size [39]. The variation of coercivity can explained domain structure, critical diameter, strain, magneto crystallite anisotropy and shape anisotropy [40]. The remanent ratio or the loop squareness ratios (Mr/Ms) are presented in the table 5.3 shows average decrease with increase in Nd^{+3} concentrations[39]. The low value of remanent ratio indicates the particles interact magneto-statically [41, 42]. The remanent variation indicates the decrease in anisotropy with Nd^{+3} doped Co ferrites samples and is similar to the coercivity.

5.3.2 ZFC and FC Measurement

Fig.5.14 shows the measurement of magnetization as a function of temperature in the applied field of 500 Oe. The magnetic moment variation with change in the temperature from 50 K to 400 K was studied. The ZFC measurement was carried out as follows: first sample were cooled from 400 K to 50 K in the absence of magnetic field, then the samples is allowed to warm in presence of the applied magnetic field of 500 Oe and the measurement was recorded. In case of FC measurements the cooling and warming of the samples were done in the presence of the applied magnetic field and measurement was carried out during the warming of the sample. From fig.5.14 shows that in ZFC measurement, the magnetization of the sample increases with increase in temperature from 50 K to 400 K, while in FC measurement shows there is a gradual decrease in magnetization as the temperature increases. The decrease in magnetization during FC measurement is due to thermal activation which randomizes the magnetization direction by lowering magnetic anisotropy that decreases the value of magnetization. In cooling of FC mode, the magnetic moments within the particles alien along the field direction which gives high magnetization value. The temperature at which ZFC and FC curve coincides is called irreversibility temperature (T_{irr}) and in ZFC measurement the temperature at which magnetization reaches maximum value just before it decreases, is called blocking temperature (T_b) [43]. It is found that the blocking temperature Tb and irreversibility temperature (T_{irr}) is found to decrease with increase in applied magnetic field.

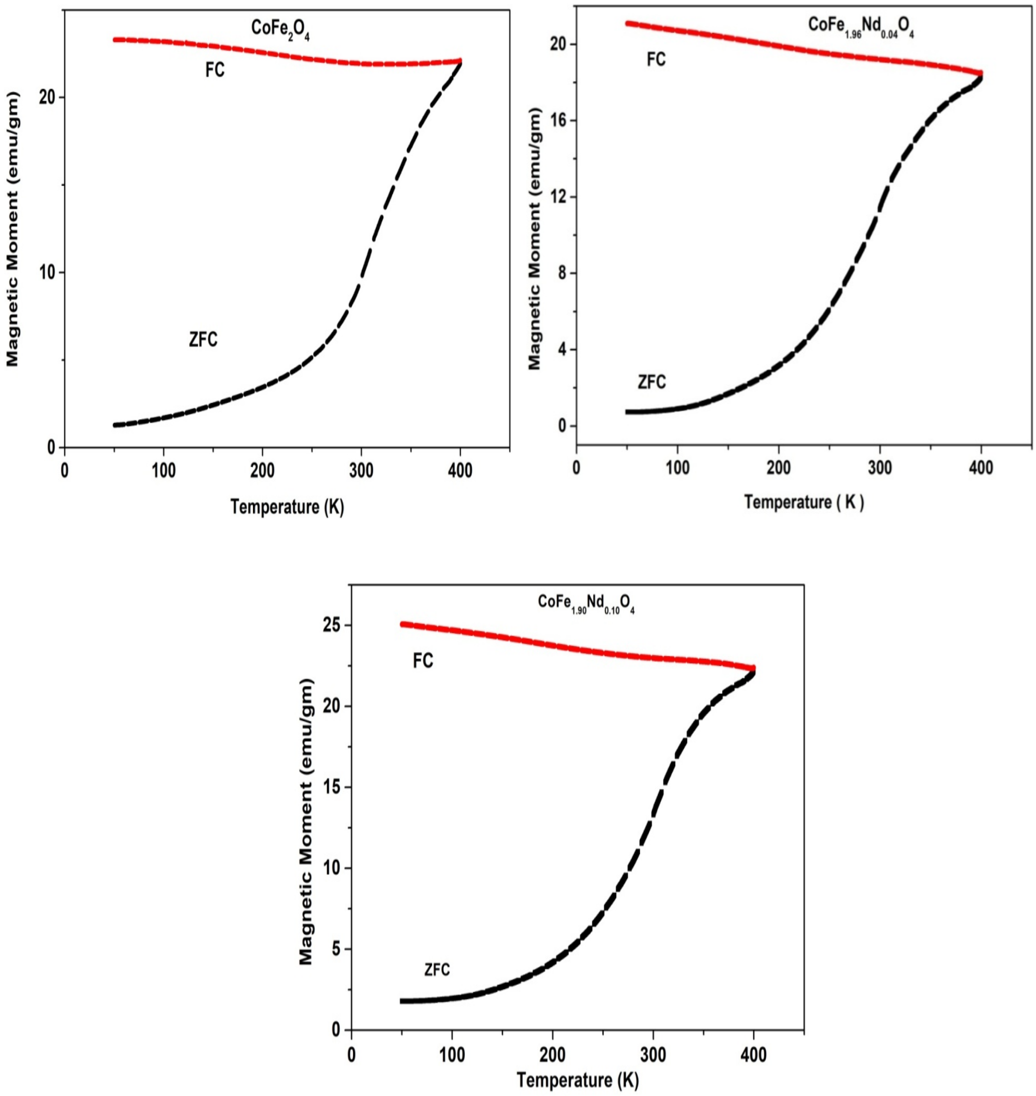

Fig.5.14: variation of magnetic moment with temperature (K) for $CoFe_{2-x}Nd_xO_4$ (x=0.00, x=0.04 and x =0.10)

Both the temperatures relates to the blocking of larger particles in the sample. From the fig.5.14 it is seen that the magnetic moment of particle sample found to increases with increase in the content of Nd^{+3}. The irreversibility temperature exits for the samples but blocking temperature is not observed. The blocking temperature for this sample may be above 400 k at 500 Oe. The reason may be the presence of larger number of bigger particles compared to average particles size in the sample. It is also been reported that agglomeration of particles may leads to increase in blocking temperature [44].The magnetic moment of the particle increases with the doping content.

5.3.2. AC Susceptibility

The normalized AC susceptibility plot shown in Fig.5.15 shows sharp fall in the normalized susceptibility at the particular temperature called Curie temperature.

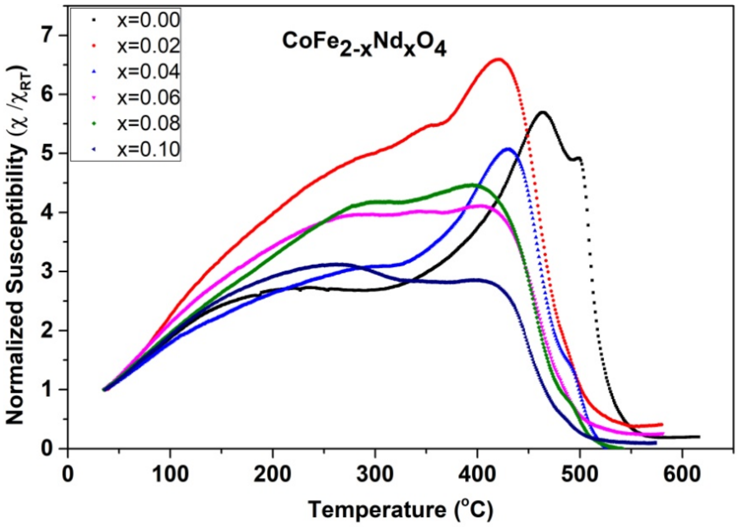

Fig.5.15: The normalized AC susceptibility plot as the function of temperature for $CoFe_{2-x}Nd_xO_4$

All the samples exhibit single Curie temperature that indicates ferrite samples are single phase without any impurity in it. The samples are single domain because as the temperature increases magnetization increases, reaches a maximum value and then there is a sharp fall just before Curie temperature Tc. The region between sharp increase in magnetization and sharp decrease just before Curie temperature, there is a hump in between is called Hopkinson's hump and it is due to Hopkinson's effect. Hopkinson effect is observed in nano- crystalline single domain particles. The Curie temperature of the samples extracted from AC susceptibility plot is given in the table 5.15

Table 5.4: Sample concentration, crystallite size and Curie temperature

Concentration 'x' of Sample Co $Fe_{2-x}Nd_xO_4$	**Nd Crystallite Size 't' in nm**	**Curie Temp T_C in ^{o} c**
0.00	35	549
0.02	30	539
0.04	26	525
0.06	24	504
0.08	21	500
0.10	18	497

It is seen from the Table: 5.4 that the Curie temperature of samples decreases with increase in concentration of Nd^{+3} and decrease in crystallite size. It is reported in literature that the variation in Curie temperature can be explain on the bases of variation in their particle size and lattice parameter [45-48]. Sample shows the SD type behavior with the mixture of MD grains. It is also reported that particle with smaller size and higher lattice constant shows higher Curie temperature [49]. But it is observed in our studies that larger particle size ferrites show higher Curie temperature.

AC susceptibility of ferrimagnetic materials is affected by both particle size and lattice constant. However, the relationship is highly complex and depends on the specific material, its crystal structure, the arrangement of magnetic sub-lattices, and the interactions between them.

5.4 Electrical Properties Study

Neodymium (Nd^{+3}) doped $CoFe_2O_4$ are the special type of magnetic material that combines the properties of Nd and Co ferrites to achieve specific magnetic and electrical properties due to the presence of Nd^{+3} ions in the crystal structure. As we know Cobalt ferrites are ferrimagnetic materials, and Nd doping can further modify their electrical characteristics. The specific electrical properties of Nd^{+3} doped cobalt ferrites can vary depending on the doping level, sample preparation techniques, and measurement conditions. The optimization of these parameters is necessary to achieve desired electrical characteristics for specific applications. The electrical properties such as dielectric, conductivity, ferroelectricity, magnetostriction, multiferroic behavior, semiconductor properties, and tuning properties can be altered by doping with rare earth element. The study and exploration of these properties are still ongoing; more insights into their properties and potential applications are likely to emerge. The electrical properties of Nd^{+3} doped cobalt ferrites can be tailored by controlling the synthesis methods, annealing conditions, and the concentration of Nd^{+3} dopants. These materials find applications in the fields of electronics, telecommunications, sensors, and magnetic storage devices. The electrical properties such as resistivity, dielectric constant and dielectric loss variation with frequency/temperature, thermo-electric power of Nd^{+3} doped $CoFe_2O_4$ are discussed in the current chapter.

5.4.1 DC Resistivity

The resistivity variation of Nd^{+3} doped $CoFe_2O_4$ with temperature for different concentrations of $Nd^{+3}$are shown in fig. 5.16

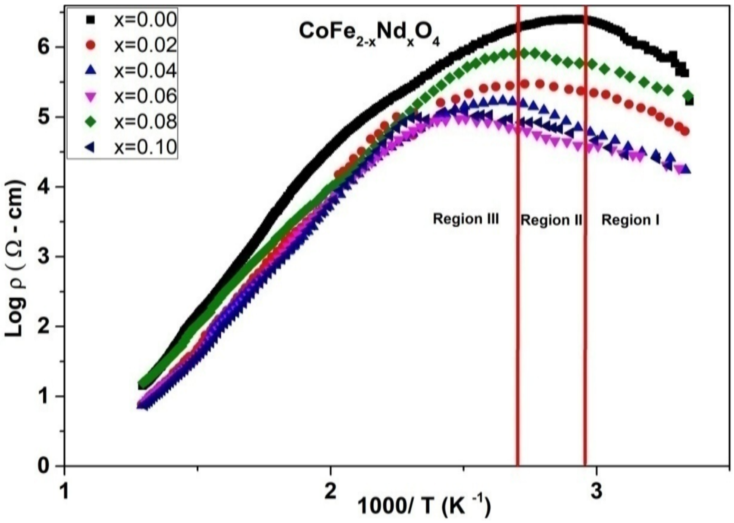

Fig. 5.16: Variation of dc resistivity with (1000/T) of $CoFe_{2-x}Nd_xO_4$

(x = 0.0 , 0.02 , 0.04 , 0.06, 0.08, 0.1)

The electrical resistivity of Nd^{+3} doped ferrites shows temperature dependent trends. The temperature dependence of resistivity depends on the crystal structure type, concentration of the dopants, density, porosity and the microstructure of the material [50, 51]. The resistivity- versus temperature of a material can provide information on electrical behavior and the physical processes associate with it. The DC resistivity measurement was carried from room temperature to 773 K using two probe method and the plots of log ρ versus 1000/ T K is depicted in Fig. 5.16 The resistivity typically decreases with increasing temperature for many ferrite materials, which is the similar behavior as shown by semiconductor material. In this type, the charge carrier mobility increases due to thermal activation. As the temperature rises, more charge carriers become available for conduction; result in the reduction of resistivity. The fig.5.15 shows that initial increase in resistivity and attains maximum value, remains constant and then shows decreasing trend with increase in applied temperature. The resistivity increases in region I from room temperature to 338 K ($65^{O}C$), remains constant in region II from 338K ($65^{O}C$) to 370 K ($97^{O}C$) and then deceases in region III from 380K ($97^{O}C$) to 773K ($500^{O}C$). In region I the increase in resistivity is attributed to presence of open pores, the entrapped moisture and loose agglomeration. As the temperature increases, moisture gets evaporated in region II where resistivity remains constant. In region III, desorption of all the moisture occurs and the resistivity follows the normal trend shown by spinel ferrites i.e. it starts decreasing as temperature increases [52]. The conduction mechanism is based on the Verwey de Boer mechanism [53]. According to this mechanism, the exchanges of electrons between the ions of different valence state of same element on the equivalent lattice site are responsible for conduction in ferrites. As a temperature increases, the drift mobility in charge carriers leads to the decrease in resistivity [51, 54]. This can be explained as follows: when temperature increases, the vibration of lattice also increases which makes the ions come closer to each other, that results in increase of probability of hopping on adjacent ions and thereby increasing the mobility of the charge carriers. The grains are good conducting and grains boundaries are poor conducting, so increase in grain size leads to decrease in porosity. The relation between porosity and resistivity; increase in porosity gives rise in number of vacancies, scattering centers and pores of electrical charge carriers which increases resistivity [55, 56].

The resistivity variations with temperature in materials with thermally activated charge carriers are describe using Arrhenius equation. The activation energy (Ea) characterizes the dependence of resistivity on temperature, and it can be obtained from experimental data by plotting the natural logarithm of resistivity (log ρ) as a function of the reciprocal of temperature (1/T K) and fitting a straight line to the data.

It is reported that resistivity decreases with decrease in activation energy [57] and the decrease in activation energy is attributed to redistributions of cations in octahedral site. Conductivity is due to the hopping of electrons, hence the resistivity. In region III the resistivity decreases as transfer of Fe^{+3} ions increases from the tetrahedral site to octahedral site. It is known that the electron hopping between $Fe^{+2} \Leftrightarrow Fe^{+3}$ ions in octahedral sites are responsible for conduction. As the number of Fe ion increases and ultimately$Fe^{+2} \Leftrightarrow Fe^{+3}$ ion pairs, since the hopping of electrons between $Fe^{+2} \Leftrightarrow Fe^{+3}$ ions are responsible for electrical conduction, an increase in $Fe^{+2} \Leftrightarrow Fe^{+3}$ions pairs increases the hopping of electrons and also electrical conductivity which results in decrease of electrical resistivity in region III.

5.4.2 Dielectric Properties

5.4.2.1 Dielectric Constant Variation with Frequency

The variation of dielectric constant with frequencies for $CoFe_{2-x}Nd_xO_4$ nanoparticles is depicted in figure 5.17. The frequency dependence of dielectric constant of pure cobalt ferrites and Nd^{+3} doped cobalt ferrites are measured at room temperature in the frequency range from 20 Hz to 3MHz.

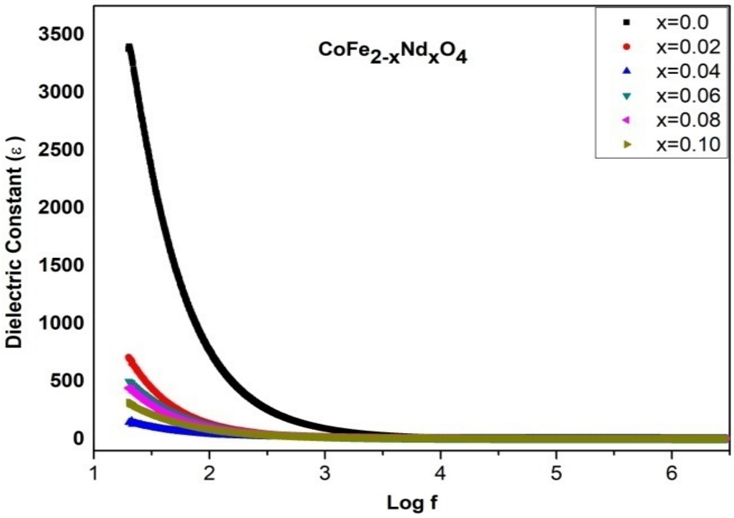

Figure 5.17: Variation of dielectric constant as a function of frequency with Nd^{+3} concentrations

It is seen from fig. 5.17 that the measured value of dielectric constant exhibit the inverse dependence on the frequency as reported for various ferrites. Initially dielectric constant (Ɛ) decreases abruptly at low frequencies, while decrease is gradual at higher frequencies and finally become constant for all Nd^{+3} doped Co ferrites samples. The decrease in dielectric constant at lower frequencies can be explained on the basis of Koop's phenomenological theory [58] and is the characteristic of the dielectric dispersion. The dispersion in dielectric constant is due to the Maxwell-Wagner's type of interfacial polarization model [59, 60]. According to this model, the dielectric structure is consider as inhomogeneous medium of two layers, of which one is conducting grains and the second is separated by poor conducting grains boundaries. In the presence of external applied field, the opposite polarity charge carriers moves inside the grains in opposite direction. These moving charges piles up at the poor conducting grain boundaries which acts as the wall. For the presence of applied external electric field, the grain functions acts as an electric dipole which is termed as space charge polarization or interfacial polarization. The space charge polarization occurring at interfaces enhances the dielectric value, thus shows high dielectric value for the samples at low frequencies [61- 62]. The polarization mechanism in cobalt ferrites is similar to the conducting process [63], in which electron hopping between $Fe^{+2} \Leftrightarrow Fe^{+3}$ ions and hole hopping between $Co^{+2} \Leftrightarrow Co^{+3}$ ions, charge carriers reaching the poor conducting grain boundaries pile up due to high resistance and produces polarization. As the frequency of applied field increases, charge carriers cannot follow the frequency of the alternating applied electric field; as a result polarization decreases [64]. Therefore, the dielectric value at higher frequencies decreases. Some literature reported [65] that increase in the dielectric constant could be due to the increasing number of Fe^{+3} ions at the octahedral site. This can be explained as follows: The doping of Nd^{+3} ions makes migration of Co^{+2} ions to tetrahedral site and hence to relax strain a equal number of Fe^{+3} ions migrate from tetrahedral site to the octahedral site. This increases the hopping of electrons between Fe^{+2}⇔Fe^{+3} ions in octahedral sites which is responsible for the increase in dielectric constant. Some time it shows decrease in dielectric due to the limitation on the migration of Fe^{+3} ions from tetrahedral sites to octahedral sites. The number of Fe ions decreases and also Fe^{+2}⇔ Fe^{+3} ion pairs. As a result availability of Fe^{+2}⇔Fe^{+3} ions and hopping electrons in between Fe^{+2}⇔Fe^{+3} decreases in octahedral sites that reduces the dielectric constant value.

5.4.2.2 Dielectric Loss Variation with Frequency

The figure 5.18 shows the variation of loss tangent (tan δ) with frequency for various neodymium concentrations nanoparticles. The frequency dependence of dielectric loss of pure cobalt ferrites and Nd^{+3} doped cobalt ferrites are measured at room temperature in the frequency range from 20 Hz to 3MHz. It is seen from fig. 5.18 that all the doped samples exhibit relaxations at specific frequencies and this dielectric relaxation occurs when the hopping frequency of charge carriers is approximately is equal to that of external applied field [66].

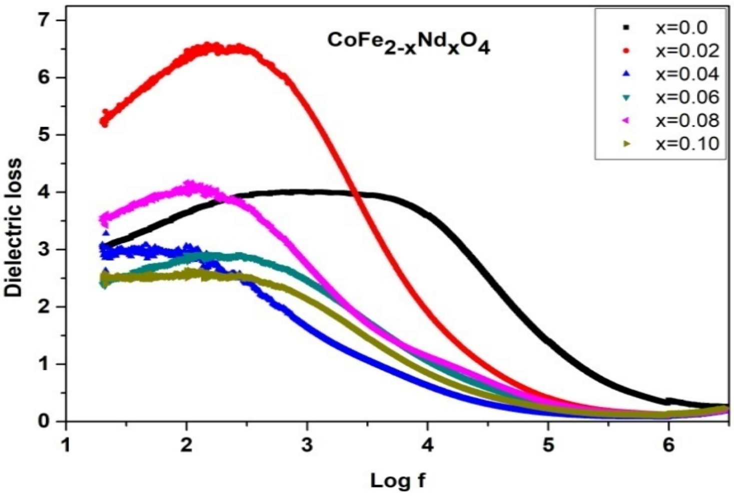

Figure 5.18: Variation of dielectric loss (tan δ) as a function of frequency with Nd^{+3} concentrations

As the frequency is increased further it decreases and finally become constant for all Nd^{+3} doped Co ferrites samples. The decreasing trend at higher frequency is similar to dielectric constant. The increase in dielectric loss is due to the limitation in an electronic exchange between Fe^{+2} ions and Fe^{+3} ions and is attributed to the lager ionic radii of Nd^{+3} as mentioned in resistivity. The decrease shown in dielectric loss tangent may be the fine particle size results in increase of surface area along with Nd^{+3} ions inclusion that increases the amount of energy require for electronic exchange which is responsible for the dielectric loss. At high frequencies the electronic exchange cannot follow the frequency of applied alternating electrical field and results in the decrease of dielectric loss [67].The dielectric loss exhibits dispersion with increasing frequency similar to dielectric permittivity and can be explained by Maxwell-Wagner's model [68]. The polarization lags behind applied alternating field due to the presence of defects, structural inhomogeinities in ferrites andhence results in dielectric loss [69]. The dielectric loss decreases with Nd^{+3} substitution and low value loss are observed for higher frequencies which indicate their potential applications in high frequency microwave devices.

5.4.2.3 Dielectric Constant Variation with Temperature as the Function of Frequency

It is seen from fig.5.19 the variation of dielectric constant of a material with frequency is very sensitive to temperature. The dielectric constant measurement for all the samples was recorded at different frequencies from room temperature to $500^{O}C$. From the fig. all the samples shows peaks behavior from $40^{O}C$ to $90^{O}C$ temperature regions for all the frequencies.

The structural investigation depicts that the crystallite size is dependent on the Co^{+2} content in the sample and co-relate the link between the particle size and the magnitudes of the peak height.

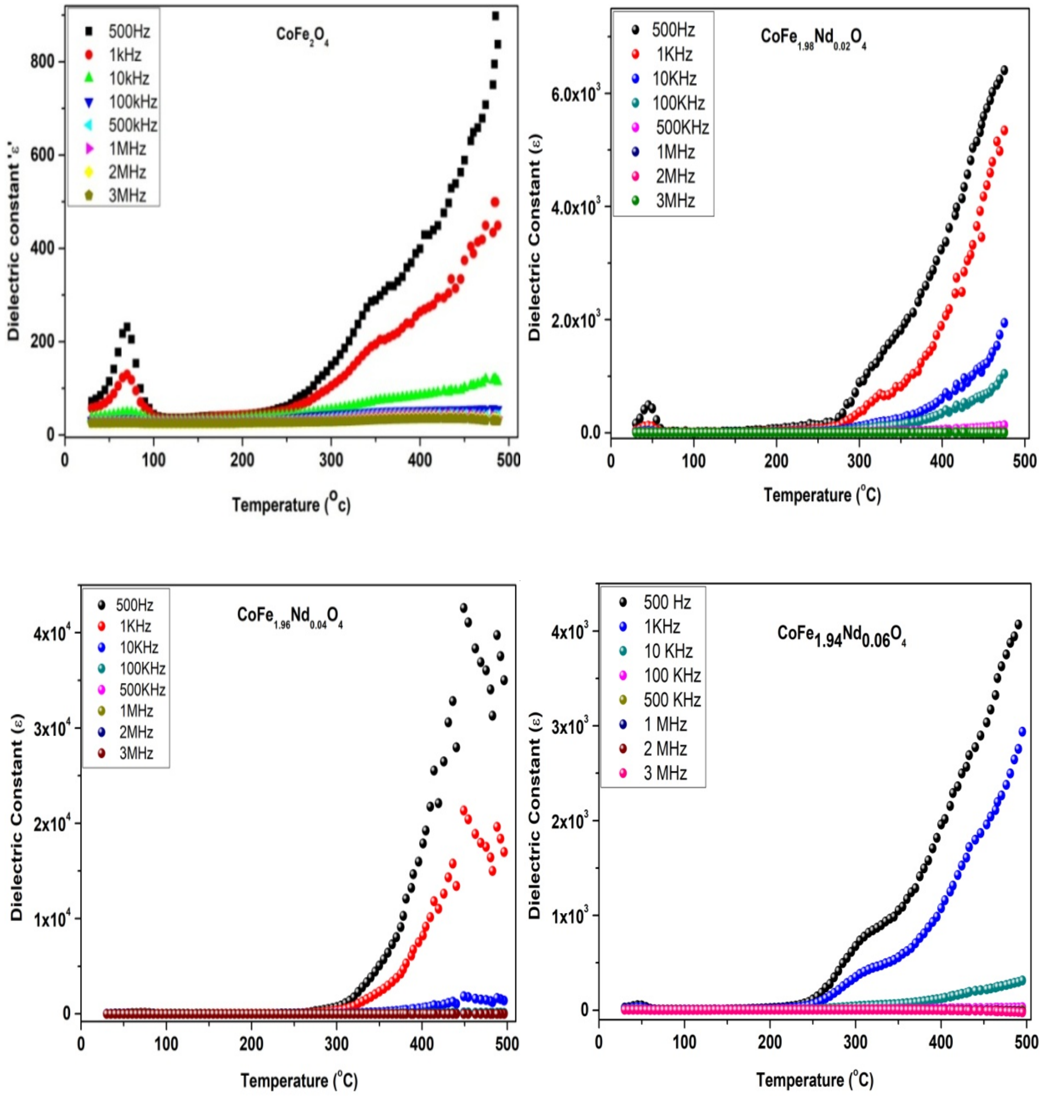

The variation of the dielectric constant (Ɛ) with temperaturefor $CoFe_{2-x}Nd_xO_4$ (x = 0. 00, 0.02, 0.04, 0.06) as a function of frequency.

The dielectric constant (Ɛ) Variation with temperaturefor $CoFe_{2-x}Nd_xO_4$ (x = 0.08, 0.10) as a function of frequency are shown fig. 5.19 below.

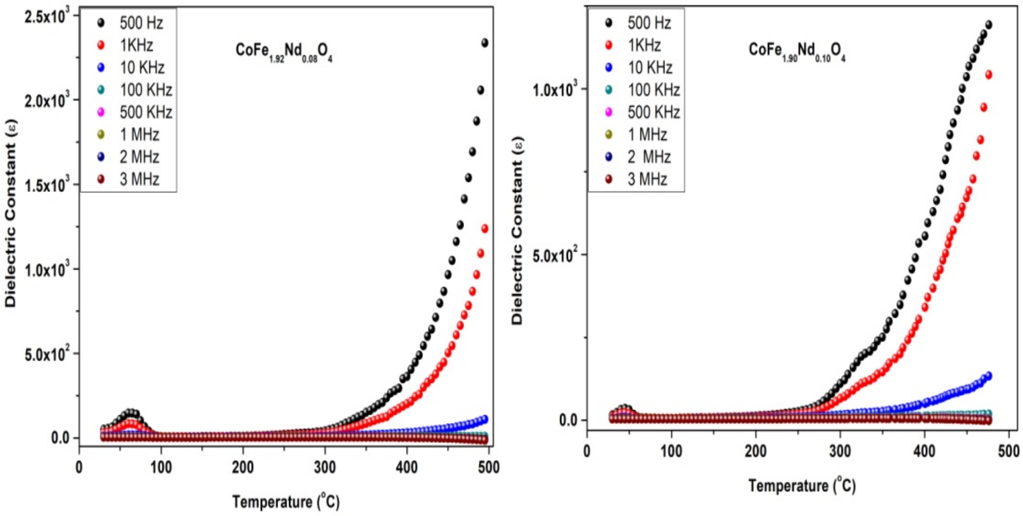

Fig.5.19: Variation of the dielectric constant (Ɛ) with temperaturefor $CoFe_{2-x}Nd_xO_4$ (x = 0. 00, 0.02, 0.04, 0.06, 0.08, 0.1) as a function of frequency.

The peaks are the relaxation peaks which are dependent on the frequency. The peaks are produced due to the relaxation time which is the time taken by the electrical dipole to orient in the direction of the applied field. When the frequency of the applied AC field matches with the frequency of the relaxation time, the resonance phenomenon occurs during which maximum energy transfer from the applied AC field. In dielectric constant 'ε' variation with temperature as the function of frequency shows peaks behavior between 40^{O}C to 90^{O}C temperature, relaxation peaks spread and height of dielectric constant decreases with increasing AC field frequency and finally becomes flat for high frequency of 500 KHz. The relaxation peaks at higher frequency disappear due to charge carrier localization [70, 71]. As the temperature increases, the thermal energy increases which increases hopping rate of charge carrier's thereby increasing mobility in amplified form which increases the conductivity. There is augmentation of dipole polarization that depends on applied frequency [70, 72] and Co^{+2}content in the sample.

The dielectric constant decreases with increase in Nd^{+3} concentration in $CoFe_{2-x}Nd_xO_4$.This is due to the substitution of large ionic radii Nd^{+3} ions in octahedral sites which decreases Fe^{+3} ions at octahedral sites of samples. The Nd^{+3} ions at octahedral sites replace Fe^{+3} ions which reduces the rate of hopping of Fe^{+2} and Fe^{+3} ions. Hence polarization decreased with increasing in Nd^{+3} content in the sample which reduces dielectric constant value.

5.4.2.4 Dielectric Loss Variation with Temperature as the Function Of Frequency

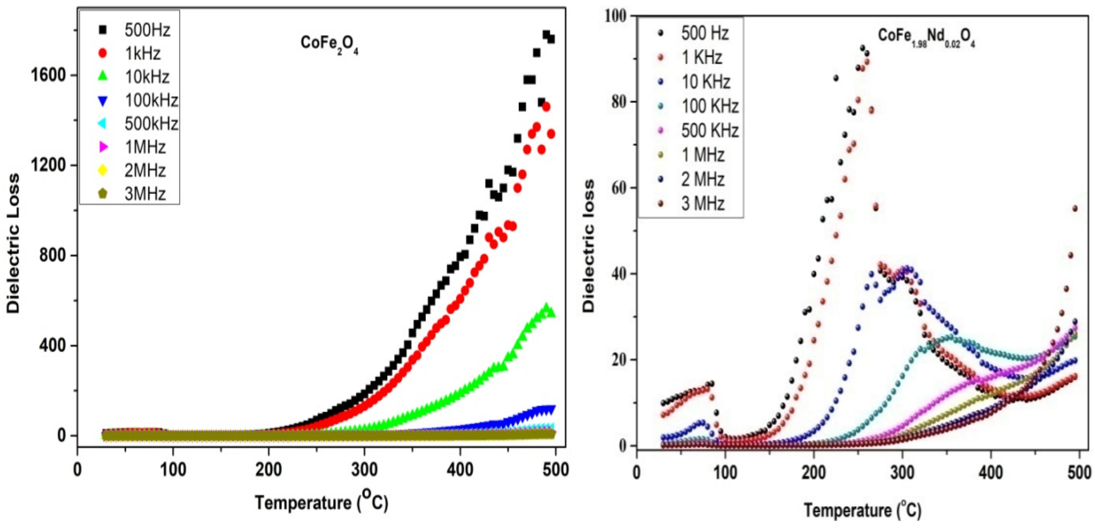

The variation of the dielectric loss with temperaturefor $CoFe_{2-x}Nd_xO_4$

(x = 0. 00, 0.02) as a function of frequency.

The dielectric loss variation with temperaturefor $CoFe_{2-x}Nd_xO_4$ (x = 0.08, 0.10) as a function of frequency.

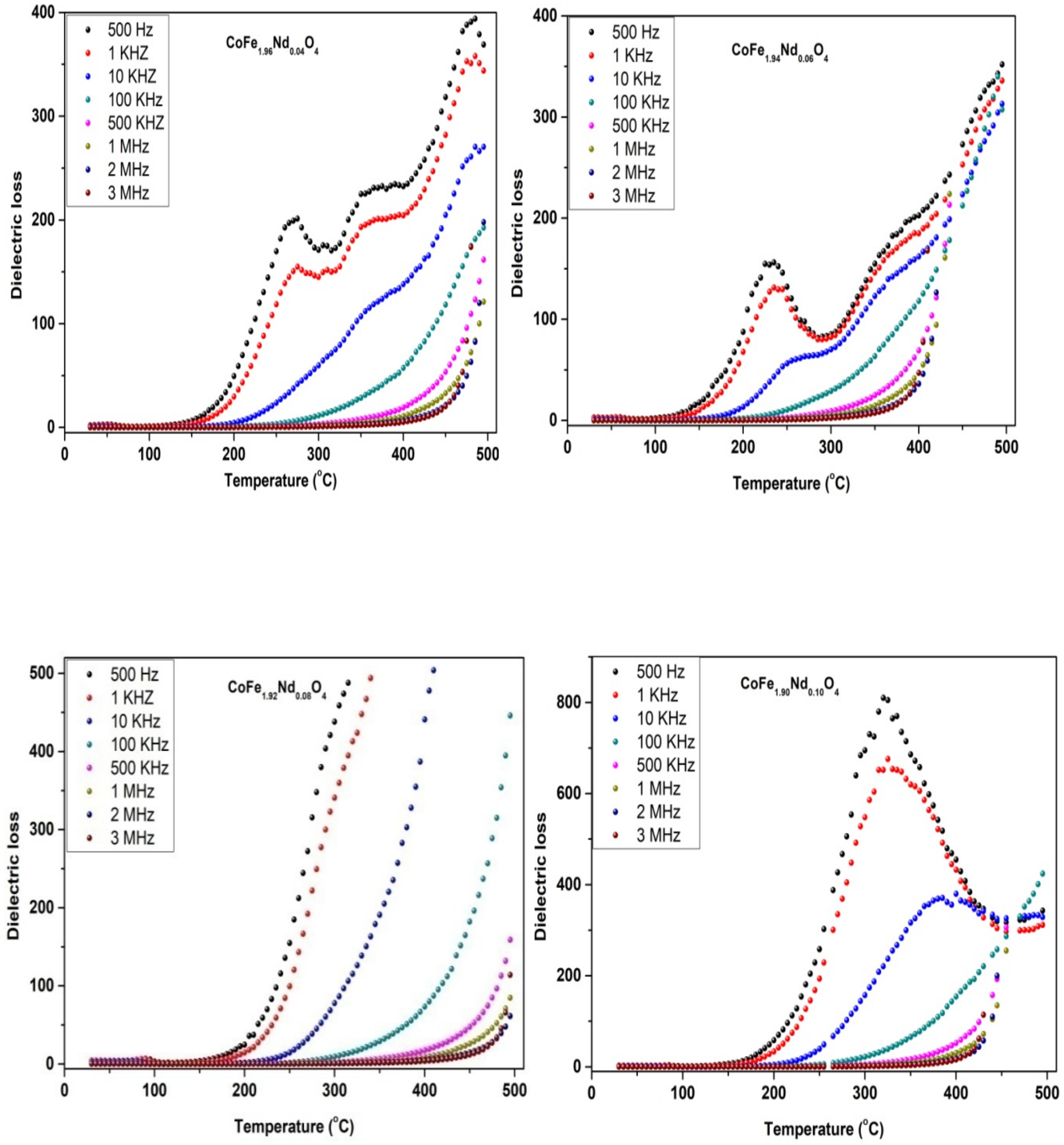

Fig.5.20: Variation of the dielectric loss (tan δ) with temperature for $CoFe_{2-x}Nd_xO_4$ (x = 0.00, 0.02, 0.04, 0.06, 0.08, 0.10) as a function of frequency.

The variation of loss tangent with temperature as the function of frequency is shown in fig.5.20. The behavior shown by dielectric loss is similar to the dielectric constant but the peaks in the lower temperature range are not prominent. The relaxation peak is due to the collective contribution from both p and n charge carriers and can be explain on the basis of Rezlescu model [73]. The electronic exchange between Fe^{+2} and Fe^{+3} and hole transfer between Co^{+2} and Co^{+3} in an octahedral site are responsible for such behavior. At the relaxation peak the jumping frequencies of localized charge carrier is almost equal to the frequencies of applied electric field and maximum transfer of energy occurs at this point. The sample shows low dielectric loss values at higher frequencies that shows the potential applications of these materials in high frequency micro-wave devices. The high dielectric loss in low frequency region is due to the high resistivity. In which more energy is required for electron exchange between Fe^{+2} and Fe^{+3}, where as in high frequency region corresponds to the low resistivity region which requires low energy for exchange of Fe ions at the octahedral sites. Thus in low frequency region dielectric loss is high and in high frequency region dielectric loss shows low value. In the crystalline material, when the dielectric polarization lag behind applied alternating field that results in dielectric loss which occurs due to grain boundary effect. The dielectric property in the case of nano-particle samples may depend on factors such as sample preparation method, structure, size of the crystallite, chemical composition and preparative conditions [72].

5.4.3 Thermoelectric Power

Thermoelectric power or seebeck coefficient of $CoFe_{2-x}Nd_xO_4$ with various concentrations of Nd samples was measured in the range of room temperature to 500^OC. It is seen from Fig.5.21 thermal variation of thermoelectric power of Nd^{+3} dope Cobalt ferrites samples and all the composition show positive thermo electric power at room temperature. As a temperature increases, the positivity of thermoelectric power decreases and changes to negative value at certain temperature and this was observed for all the samples.

It is depicted from fig.5.21 that samples shows p-type of semiconductor behavior in low temperature region and n-type of semiconductor in high temperature region. The p-type of conduction mechanism is due to hopping of holes between Co^{+3}⇔ Co^{+2} and n-type conduction mechanism in the sample is due to hopping of electrons between Fe^{+2}⇔ Fe^{+3} [74]. The transition from p-type to n-type supports the changes in concentration of Co^{+2} and further predicts the conduction mechanism is due to hopping of electrons between Fe^{+2} and Fe^{+3} [75].

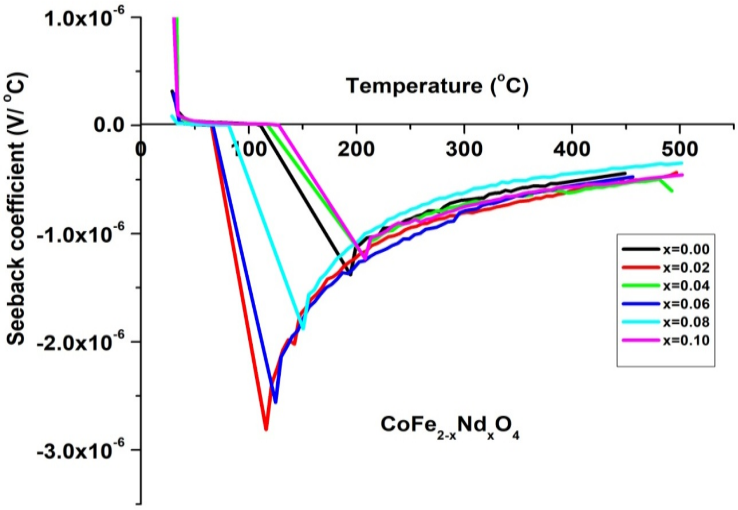

Fig. 5.21: Variation of thermoelectric power with temperature of $CoFe_{2-x}Nd_xO_4$ samples.

Table5.5: Transition temperatures T (p-n) of $CoFe_{2-X}Nd_xO_4$ samples.

Concentration 'x' of $CoFe_{2-x}Nd_xO_4$	**Transition Temperature T p-n (^OC)**
0.00	104
0.02	65
0.04	117
0.06	66
0.08	81
0.10	128

Table 5.5 provides the transition temperature Tp-n of each sample at which thermoelectric power changes from positive to negative i.e. p-type to n-type. The temperature T (p-n) varies in the range of 67^OC to 122^OC.

References:

[1] U. Jeong, X. Teng, Y. Wang, H. Yang, Y. Xia, Super paramagnetic colloids: controlled synthesis and niche applications, Journal of Advanced Materials 19 (2007) 33–60.

[2] H. Shokrollahi, K. Janghorban, Influence of additives on the magnetic properties, microstructure and densification of Mn−Zn soft ferrites, Materials Science and Engineering B 141 (2007) 91–107.

[3] H. Shokrollahi, Magnetic properties and densification of manganese–zinc soft ferrites (Mn1−xZnxFe2O4) doped with low melting point oxides, Journal of Magnetism and Magnetic Materials 320 (2008) 463–474.

[4] M. Sangmanee, S. Maensiri, Nanostructures and magnetic properties of cobalt ferrite (CoFe2O4) fabricated by electro spinning, Applied Physics A 97 (2009) 167–177.

[5] G.A. El-Shobaky, A.M. Turky, N.Y. Mostafa, S.K. Mohamed, Effect of preparation conditions on physicochemical, surface and catalytic properties of cobalt ferrite prepared by coprecipitation, Journal of Alloys and Compounds 493 (2010) 415–422.

[6] I. Apostolova, J.M. Wesselinowa, Possible low-TC nanoparticles for use in magnetic hyperthermia treatments, Solid State Communications 149 (2009) 986–990.

[7] P. Kumar, J. Chand, S. Verma, M. Singh, Micro-structural studies of gadolinium doped cobalt ferrites, International Journal of Theoretical and Applied Sciences 3 (2) (2011) 10–12.

[8] O.M. Hemeda, M.Z. Said, M.M. Barakat, Spectral and transport phenomena in Ni ferrite-substituted Gd2O3, Journal of Magnetism and Magnetic Materials 224 (2001) 132–142.

[9] N. Rezlescu, E. Rezlescu, C. Pasnicu, M.L. Craus, Effect of rare earth ions on some properties of a nickel–zinc ferrite, Journal of Physics: Condensed Matter 6 (1994) 5707–5716.

[10] Pranav P. Naik, R.B. Tangsali, S.S. Meena, S.M. Yusuf, Materials Chemistry and Physics, 191 (2017) 215-224

[11] K. Velmurugan, V. S .K. Venkatachalapathy and S. Sendhilnathan, Materials research, 12, (2009), 529 - 534.

[12] Y. Zhang, D. Wen, Influence of RE/Mn (REQLa, Nd and Gd) ratios on the infrared absorption and emission properties of Co–Zn ferrites, Advanced Materials Research 217 (2011) 311–316.

[13] F.-Xiang Cheng, J.-Tao Jia, Zh.-Gang Xu, B. Zhou, Ch.-Sheng Liao, Microstructure, magnetic, and magneto-optical properties of chemical synthesized Co–RE (REQHo, Er, Tm, Yb, Lu) ferrite nanocrystalline films, Journal of Applied Physics 86 (1999) 2727–2732.

[14] M.T. Sebastian, Dielectric Materials for Wireless Communications, 1st edn, Elsevier, UK, 2008.

[15] J. A. Eastman, M. R. Fitzsimmons, L. J. Thompson, A. C. Lawson and R. A. Robinson, Nanostruct. Mater., 1, (1992), 465-470.

[16] D. Oleszak and P. H. Shingu, J. Appl. Phys., 79, (1996), 2975-2980.

[17] J. A. Dean, Lange's handbook of chemistry, McGraw-Hill, New York, 15th edn, 1998.

[18]C. Venkataraju, Applied Physics Research1 (No. 1) (2009) 41-45.

[19] M.M. Haque, M. Huq, M.A. Hakim, Indian J. Phys. 78A (3) (2004) 397-400.

[20] Emad M.M. Ewais, Mahmoud M. Hessien, Abdel-Hady A. El-Geassy, Journal of Australian Ceramic Society, 44 (1) (2008) 57-62.

[21] K. Rama Krishna, K. Vijaya Kumar, Dachepalli Ravinder, Advances in Materials Physics and Chemistry 2, (2012) 185-191.

[22] S. Rana, J. Philip, B. Raj, Micelle based synthesis of cobalt ferrite nanoparticles and its characterization using fourier transform infrared transmission spectrometry and thermogravimetry, Materials Chemistry and Physics 124 (2010) 264–269

[23] Xavier S, Thankachan S, Jacob B P and Mohammed E M 2013 J. Nanomater, Mol. Nanotechnol 2 1.

[24] R. D. Waldron, Phys. Rev., 1955, 99, 1727.

[25] A. Gadkari, T. Shinde, P. Vasambekar, Influence of rare-earth ions on structural and magnetic properties of CdFe2O4 Ferrites, Rare Metals 29 (2010) 168 – 173.

[26] Vasant Naidu, S. Vijayaragavan, R.Legadevi, A, Senthil Kumar, Int. J. Comp. Appl. 30 (2011), 13.

[27] M.M. Rashada, R.M. Mohameda, H. El-Shall, J. Mater. Processing Tech. 198 (2008) 139.
[28] A.K. Nikumbh, R.A. Pawar, D.V. Nighot, G.S. Gugale, M.D. Sangale, M.B. Khanvilkar, A.V. Nagawade, J. Magn. Magn. Mater. 355(2014), 201.

[29].K. Manju, T. Smitha, D. S. Nair, E. K Aswathy, B. Aswathy, T Arathy, Binu, K. T. Krishna, Journal of Advanced Ceramics, 2015, 4(3): 199–205.

[30] L.D. Tung, V. Kolesnichenko, D. Caruntu, N.H. Chou, C.J. O'Connor, L. Spinu, Magnetic properties of ultrafine cobalt ferrite particles, Journal of Applied Physics 93 (2003) 7486–7488.

[31] K. J. Standley, Oxide magnetic materials, Oxford University Press, 1972

[32] G.K.Williamson, W.H. Hall, Acta Metal. 1 (1953) 22

[33] W.J. Nellis, S. Legvold, Phys. Rev. 180 (1969) 581.
[34] P.Kumar,S. K. Sharma, M. Knobel, J. Chand and M. Singh, J. Electroceram., 2011, 27, 51.
[35] J. Jing, L. Liangchao, X. Feng, J.Rare Earth. 25 (2007) 79
[36] S. Singhal, S.K. Barthwal, K. Chandra K, J. Magn. Magn. Mater. 306 (2006) 233.
[37] J. Jiang, Y.M. Yang, L.C. LiL, Physica B 399 (2007) 105.
[38] S. Xavier, S. Thankachan, B.P. Jacob, and E.M. Mohammed, 2013, (2013).
[39] G. Bottoni, D. Candolfo and A. Cecchetti, J. Appl. Phys. 81 (1997) 3794.
[40] K. Nejati and R. Zabihi, Chem. Cent. J. 6, 23, (2012).
[41]. S. Mukherjee, S. Pradip, A.K. Mishra, D. Das, Zn substituted NiFe2O4
with very high saturation magnetization and negligible dielectric loss synthesized via a soft chemical route. Appl. Phys. A 116, 389–393 (2014).
[42]. M.A. Gabal, Y.M. Al Angari, F.A. Al-Agel, Cr-substituted Ni-Zn ferrites via oxalate decomposition. Structural, electrical and magnetic properties. J. Magn. Magn. Mater. 391, 108–115 (2015).
[43] L. Ben Tahar, L.S. Smiri, A.-L. Joudrier, M. Artus, F. Herbst, M.-J. Vaulay, S. Ammar, F. Fie´vet, Mater. Res. Bull. 42 (2007) 1888.

[44] S.S. Jadhav, S.E. Shirsath, B.G. Toksha, S.J. Shukla, K.M. Jadhav, Effect of cation proportion on the structural and magnetic properties of Ni-Zn ferrites nano-size particles prepared by co-precipitation technique. Chin. J. Chem. Phys. 21, 381–386 (2008).

[45] T.J. Shinde, A.B. Gadkari, P.N. Vasambekar, Magnetic properties and cation distribution study of nanocrystalline Ni-Zn ferrites. J. Magn. Magn. Mater. 333, 152–155 (2013).

[46] O.A. Li, C.-R. Lin, H.-Y. Chen, H.-S. Hsu, K.-Y. Shih, I.S. Edelman, K.-W. Wu, Y.-T. Tseng, S.G. Ovchinnikov, J.-S. Lee, Size dependent magnetic and magneto-optical properties of Ni0.2Zn0.8Fe2O4 nanoparticles, J. Magn. Magn. Mater. 408, 206–212 (2016).

[47]. V. Grimal, D. Autissier, L. Longuet, H. Pascard, M. Gervais, Iron, nickel and zinc stoichiometric influences on the dynamic magneto-elastic properties of spinel ferrites, J. Eur. Ceram. Soc. 26, 3687–3693 (2006).

[49]. I. Szczygieł, K. Winiarska, A. Bieńko, K. Suracka, D. GaworskaKoniarek, The effect of the sol-gel autocombustion synthesis conditions on the Mn-Zn ferrite magnetic properties, J. Alloy. Compd. 604, 1–7 (2014).

[50] A.V. Humbe, A.C. Nawle, A.B. Shinde, K.M. Jadhav, Impact of Jahn Teller ion on magnetic and semiconducting behavior of Ni-Zn spinel ferrite synthesized by nitrate-citrate route, J. Alloy. Compd. 691, 343–354 (2017).

[51] I.H. Gul, W. Ahmed, A. Maqsood, Electrical and magnetic characterization of nanocrystalline Ni-Zn ferrite synthesis by co-precipitation route, J. Magn. Magn. Mater. 320, 270–275 (2008).

[52] P.P. Sarangi, S.R. Vadera, M.K. Patra, N.N. Ghosh, Synthesis and characterization of pure single phase Ni-Zn ferrite nanopowders by oxalate based precursor method, Powder Technol. 203, 348– 353 (2010).

[53] E.J.W. Verwey, Electronic conduction of magnetite (Fe3O4) and its transition point at low temperatures, Nature 144, 327–328 (1939).

[54] A.D. Sheikh, V.L. Mathe, Anomalous electrical properties of nanocrystalline Ni–Zn ferrite, J. Mater. Sci. 43, 2018–2025 (2008).

[55] A. Hajalilou, H.M. Kamari, K. Shameli, Dielectric and electrical characteristics of mechanically synthesized Ni-Zn ferrite nanoparticles, J. Alloy. Compd. 708, 813–826 (2017).

[56] M.A. Ali, M.M. Uddin, M.N.I. Khan, F.-U.-Z. Chowdhury, S.M. Haque, Structural, morphological and electrical properties of Snsubstituted Ni-Zn ferrites synthesized by double sintering technique, J. Magn. Magn. Mater. 424, 148–154 (2017).

[57] M. T. Rahman and C.V. Ramana, J. Appl. Phys., 2014, 116, 164108.

[58] Koops C G, Phys.Rev. 83 121, 1951.

[59] Wagner K W 1913 Ann.Phys. 40, 817.

[60] J. C. Maxwell, Electricity and Magnetism, Oxford Univ. Press, London, 1973.

[61] M. Mehedi Hassan, Arham S. Ahmed, M. Chaman, Wasi Khan, A.H. Naqvi, Ameer Azam, Materials Research Bulletin, 47 (2012) 3952–3958.

[62] C. Belkhaoui, Ramzi Lefi, NissafMzabi, Hichem Smaoui, Journal of Materials Science: Materials in Electronics, (2018).

[63] K.Iwauchi, Jpn. J. Appl. Phys., 1971, 10, 1520.

[64] N. Sivakumar, A. Narayanasamy, C. N. Chinnasamy and B. Jeyadevan, J. Phys.: Condens. Matter, 2007, 19, 386201.

[65] A. Rana, O. P. Thakur and V. Kumar, Mater. Lett., 2011, 65, 3191.

[66] Shigeki I and Toshio T 1971 Japan, J. Appl. Phys. 10 260.

[67] R. S. Devan, B. K. Chougule, Journal of Applied Physics 101, (2007)014109. [68] K.M. Batoo, S. Kumar, C.G. Lee, Alimuddin, Curr. Appl Phys. 9 (2009) 826.

[69] A.K. Singh, T.C. Goel, R.G. Mendiratta, O.P. Thankur, C. Prakash, J Appl Phys. 91 (2002) 6626–6629.

[70] M. R. Bryce and Michael C. Petty, Nature 374 (1995) 771-776.

[71] S. Sagadevan, Kaushik Pal, Zaira Zaman Chowdhury, M. Enamul Hoque, J Sol-Gel Sci Technol, (2018).

[72] C. C. Naik, A. V. Salker, Journal of Materials Science: Materials in Electronics (2017).

[73] Waldron, R.D.: Infrared spectra of ferrites, Phys. Rev. 99, 1727– 1735, (1955).

[74] A. G Bhosale and B. K. Chougule Materials Letters 60, (2006), 3912-3915.

[75] D. Ravinder, P. Vijaya and B. Reddy, J. Magn.Magn.Mater, 263, (2003), 127- 133.

CHAPTER 6

Effects of Dy^{+3} doping on Structural, Magnetic and Electrical properties of $CoFe_2O_4$ Nanoparticles.

6.1 Introduction

Ferrites are one of the attractive materials for basic research and technological applications due to their special electric and magnetic properties. Nanotechnology has provided the base for these materials and renewed the interest in spinel ferrites to explore the possibilities of their applications in wider range. The basic goals in this system are to understand how properties changes from bulk level when one or more of its dimensions are reduced to close to atomic level. Nanoparticles have drawn the lots of attention due to the wide range of applications such as drug delivery, magnetic resonance imaging, hyperthermia treatment, data storage, catalysis, biomedical applications etc.. The sizes can be manipulated and with appropriate molecules, the surface can be made functionalized for selective target.

The dysprosium doped cobalt ferrites represent a promising class of magnetic materials with wide range of potential application in various industries across the globe. The tunable magnetic properties and the unique characteristics make them valuable candidates for innovative technology in electronic, communications and energy related fields. Ongoing research and development in this area may uncover even more exciting applications and benefits of these materials in the future.

A remarkable aspect of materials with a spinel structure is their intriguing behavior, stemming from the strong spin exchange interaction among transition metal cations possessing smaller ionic radii. Particularly, cobalt ferrite (CFO) stands out due to its inverse spinel structure denoted by the formula (Fe) A (Co Fe) B, where A and B represent the tetrahedral and octahedral sites, respectively [1-5]. The unique magnetic and electrical properties of CFO arise from the distribution of cations within these sites [6-7].

The distinct characteristics of CFO, such as high coercivity, resistivity, Curie temperature, chemical stability, and mechanical hardness, have garnered significant attention from researchers [8-12]. These properties position the material as a promising candidate for a range of applications, including high-density recording media, transformer cores, sensors, actuators, microwave devices (such as isolators, circulators, and RF circuits), high-quality filters, solid oxide fuels [13-15]. Extensive studies have focused on understanding the unique magnetic behavior of the CFO system and enhancing its properties through doping. The performance of ferrites materials is further improved by doping material with rare earth ions of different types. The concentration of rare earth in doped ferrites and 4fn electronic state of rare earth plays an important role to describe the electrical and magnetic properties of ferrites.

The performance and characteristics of ferrite materials are intricately linked to both the core material chosen and the specific preparation method employed. When delving into the material's characterization, a comprehensive understanding of the process stages, properties, and performance of the sample material is imperative in order to unveil its underlying structure. This structure encompasses atomic arrangement, atomic structure, and macro/micro structure, all of which exert influence on the interatomic bonding and subsequently categorize the material as metals, ceramics, or polymers.

To achieve comprehensive characterization, various probing techniques are employed to interact with the sample material. Once the material's structural details are revealed, the subsequent phase involves an exploration of its diverse properties, including but not limited to mechanical, thermal, optical, physical, and magnetic aspects. Cutting-edge research tools, such as X-ray Diffraction (XRD), Scanning Electron Microscopy (SEM), Transmission Electron Microscopy (TEM), and Electron Dispersive Spectroscopy (EDS), are harnessed to gain both qualitative and quantitative insights into the material's magnetic and electrical attributes.

It is important to note that the properties of a given structure can be modified through adjustments to its composition, processess, or a combination of both factors. Armed with a comprehensive comprehension of a material's structure and composition, a clear direction emerges for its suitable application across various fields.

The investigation of cobalt ferrite samples doped with Dy has been undertaken to comprehensively analyze their structural, magnetic, and electrical attributes. To accomplish this measurement a range of advanced techniques that includes X-ray Diffraction (XRD), Scanning Electron Microscopy (SEM), Transmission Electron Microscopy (TEM), Fourier-Transform Infrared Spectroscopy (FTIR), and Energy-Dispersive Spectroscopy (EDS), have been employed. These techniques collectively enable the meticulous examination of the materials, encompassing aspects such as crystal structure, crystallite size, lattice parameters, structural morphology, and chemical composition. Furthermore, an in-depth investigation into the magnetic and electrical properties of the studied materials has also been carried out.

6.2 Structural Characterization

The sample materials used for characterization are Dy^{+3} doped cobalt ferrites with chemical formula as $CoFe_{2-x}Dy_xO_4$ (x = 0.00, 0.02, 0.04, 0.06, 0.08, 0.10).

Material characterization plays a pivotal role for a multitude of compelling motives. It facilitates a profound grasp of material properties, guarantees the integrity of quality control measures, fine-tunes performance parameters, assists in the judicious selection of materials, identifies and addresses potential shortcomings, and propels the frontiers of research and development. This wealth of information serves as a cornerstone for the effective and efficient design and utilization of materials across diverse industrial applications.

6.2.1 X-ray Diffraction Spectrum

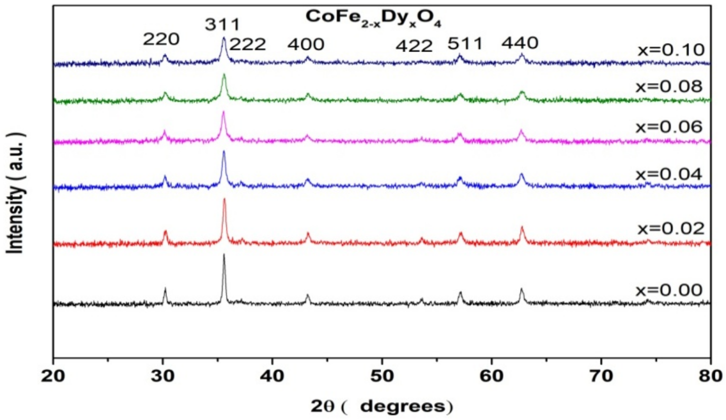

Fig. 6.1: X-ray diffraction pattern for $CoFe_{2-x}Dy_xO_4$ (x = 0.00, 0.02, 0.04, 0.06, 0.08, 0.10).

Figure 6.1 illustrates the X-ray diffraction patterns for a series of samples denoted by the chemical formula $CoFe_{2-x}Dy_xO_4$, with varying dopant concentrations (x = 0.00, 0.02, 0.04, 0.06, 0.08, 0.10). The characterization of these samples was carried out using an XRD Rigaku X-ray diffractometer employing Cu Kα1 radiation (λ = 1.5418 Å).

The dominant peak observed within the XRD pattern is the (311) plane, while all other peaks align coherently with the spinel structure, thereby confirming the absence of impurity phases. This outcome underscores the successful formation of single-phase cubic-structured ferrites material.

Through robust analysis, it was established that all compositions display distinct monophasic characteristics. The determination of this monophasic nature was validated by indexing the major peaks as (220), (311), (222), (400), (422), (511), and (440), in accordance with the characteristic planes of a singular face-centered cubic (f c c) spinel structure. These findings are in agreement with the data from the Joint Committee on Powder Diffraction Standards (JCPDS) Card No. 22-1086, further corroborating the consistent formation of the single-phase FCC cubic spinel structure.

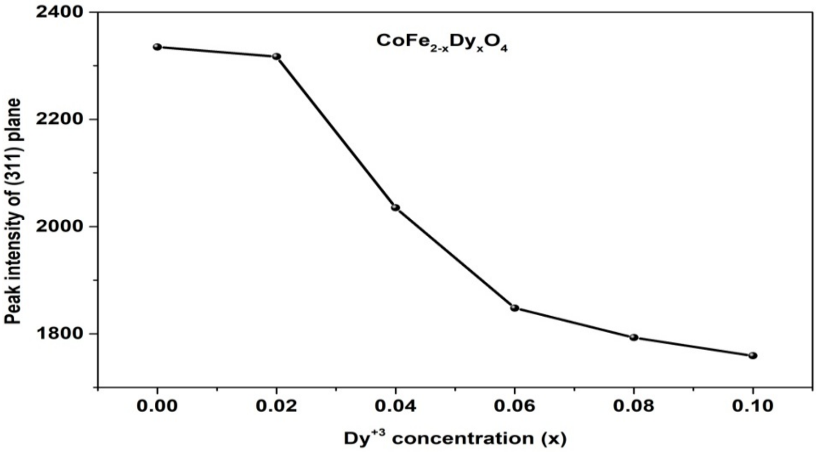

Fig, 6.2: Variation of peak intensity of (311) plane with concentration (x) for

$CoFe_{2-x}Dy_xO_4$

The alteration in peak intensity concerning the (h k l) value, specifically the (311) plane, as depicted in figure 6.2, exhibits a discernible diminishing pattern.

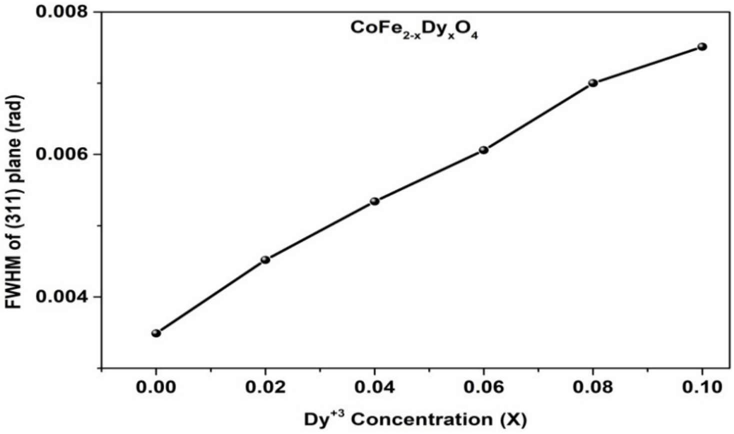

Fig, 6.3: Variation in FWHM of (311) plane withDy^{+3} concentrations for $CoFe_{2-x}Dy_xO_4$

This decline in peak intensity serves as a clear indicator of the diminishing crystalline characteristics within the $CoFe_{2-x}Dy_xO_4$ ferrites lattice, a trend that becomes more pronounced with escalating Dy^{+3} concentration. Furthermore, the Full Width at Half Maximum (FWHM) variation, also observed in correlation with the Dy^{+3} concentrations that illustrates a consistent reduction in crystallite dimensions. This tandem effect of peak intensity and FWHM underscores the direct relationship between increased Dy^{+3} concentrations and the concurrent decrease in both crystalline nature crystallite sizes within the ferrite lattice.

The variation of lattice constant ‘a’ with concentrations of Dy^{+3} for $CoFe_{2-x}Dy_xO_4$ is shown in fig.6.4. Lattice constant increases from 8.375 Å to 8.379 Å as Dy^{+3} concentration increases from x = 0 to x = 0.10.

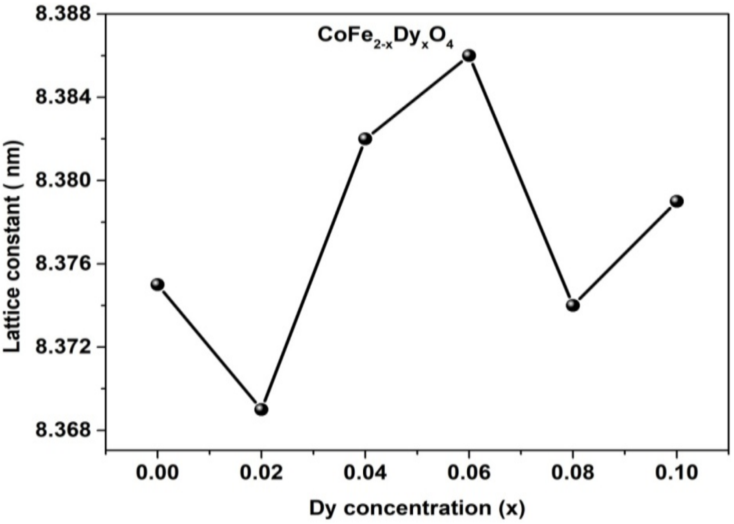

Fig.6.4: Variation of lattice constant ‘a’ with Dy^{+3} concentrations for $CoFe_{2-x}Dy_xO_4$

The increase in lattice constant is due to replacement of larger ionic radii of Dy^{+3}(0.94 Å) by smaller ionic radii of Fe^{+3} (0.64 Å) at octahedral site. This causes expansion of octahedral sub lattice site which results in increase in lattice constant [16]. The crystallite size variation with concentration of Dy^{+3} shows that the crystallite size is found to decrease with increase in Dy^{+3} concentrations in the range from 35 nm to 19 nm. Nano particles do not exhibit identical crystallite size is due to the rate of ferrites formation differ for different composition and favors a different crystallite sizes [17]. The replacement of a larger ionic radii ion by smaller radii ion creates strain in the lattice. Also the presence of Co^{+2} ions with maximum electrostatic shielding by 3d electrons introduces an additional strain. This strain depends on different factors such as lattice defects, larger surface energy, and presence of impurities etc. The micro-strain arises due to larger surface energy involved in larger surface to volume ratio of the sample [18-19]. The decrease in crystallite size is due to inclusion of rare earth ions that develops lattice strain which hinders the crystal growth and is responsible for reduction of crystallite size for these materials. It is noticed that substitution of Dy^{+3} in $CoFe_2O_4$ is restricted; as a result there is a reduction in crystallite size. The reason is Dy^{+3}-O^{-2} bond energy is more than the Fe^{+3}- O^{-2} bond energy, so it required more energy to incorporate Dy^{+3} ions in place of Fe^{+3} ions into octahedral site [20]

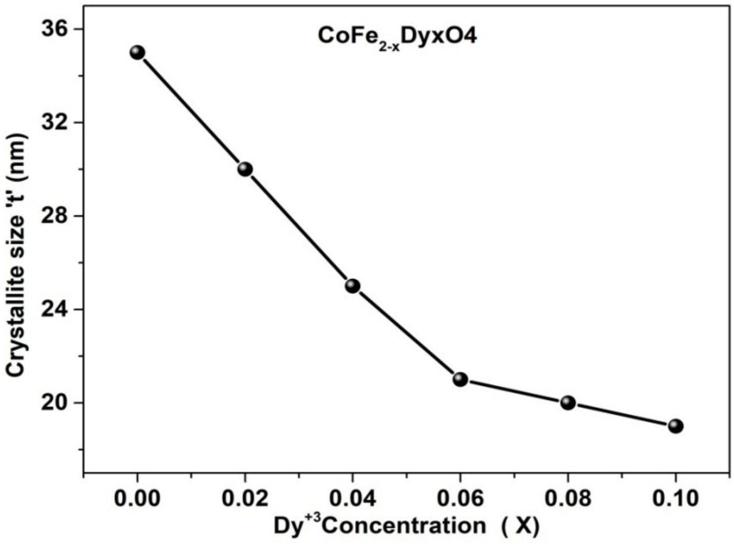

Fig, 6.5 Crystallite size Variation withDy^{+3} concentrations for $CoFe_{2-x}Dy_xO_4$

Table 6.1: lattice constant and crystallite size for various concentrations of Dy^{+3}.

Concentration'x' of Dy^{+3} $CoFe_{2-x}Dy_xO$	**Lattice constant 'a' in Å**	**Crystallite size ' t' in nm**
0.00	8.375	35
0.02	8.369	30
0.04	8.382	25
0.06	8.386	21
0.08	8.374	20
0.10	8.379	19

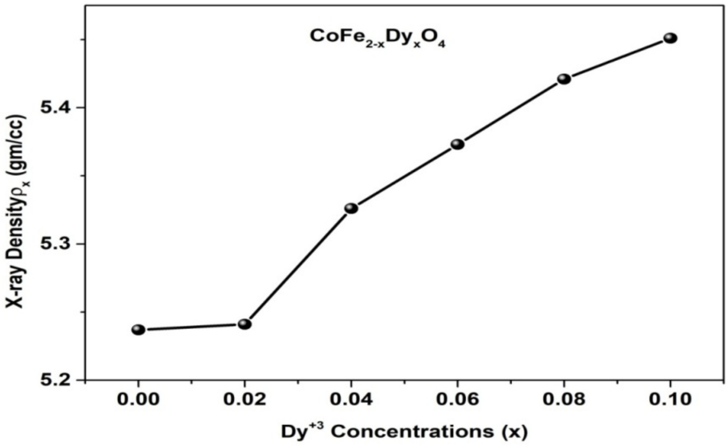

Fig, 6.6: Variation of X-ray density 'ρ_x' with Dy^{+3} concentrations for $CoFe_{2-x}Dy_xO_4$

X-ray density increases with Dy^{+3}concentrations isseenfrom fig6.6 .This can attributed to the fact that atomic weight of Dy^{3+} is 162.5 gm which is greater than that of Fe^{3+} (55.845 gm). This behavior of enhancement in the X-ray density with increase in Dy^{+3}

concentrations also supports effective incorporation of Dy^{+3} into $CoFe_{2-x}$ Dy_xO4 samples. The enhanced value of X-ray density may also due to the improved molecular weight of the samples with dysprosium ions [21- 24].

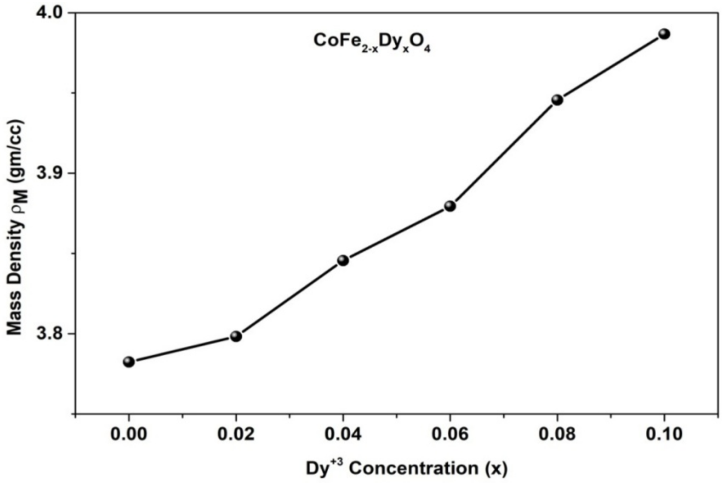

Fig. 6.7: Variation of mass density 'ρ_M' with Dy^{+3} concentrations for $CoFe_{2-x}Dy_xO_4$

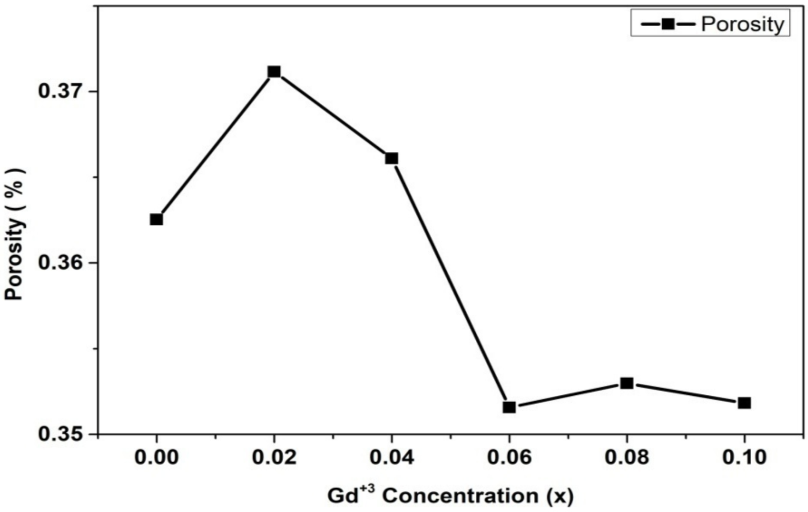

Fig. 6.8 Variation of porosity (%) with Dy^{+3} concentrations for $CoFe_{2-x}Dy_xO_4$

.The mass density is typically expressed in units of grams per cubic centimeter (gm /cm³) or kilograms per cubic meter (kg/m³). For most ferrite materials, the mass density falls in the range of 4.9 to 5.2 gm /cm³, but can be lower or higher value depending on dopants atomic mass and concentrations. The porosity in the ferrites materials can be controlled during fabrication. To achieve a desire level of porosity the techniques used are sintering, hot pressing, Sol-gel method, etc. Fig 6.8 shows the % porosity variation with the concentration of Dy^{+3}.It is observed that initially % porosity increases and then decreases with increase in Gd concentrations.

6.2.2 Fourier Transform Infra red (FTIR) Spectroscopy

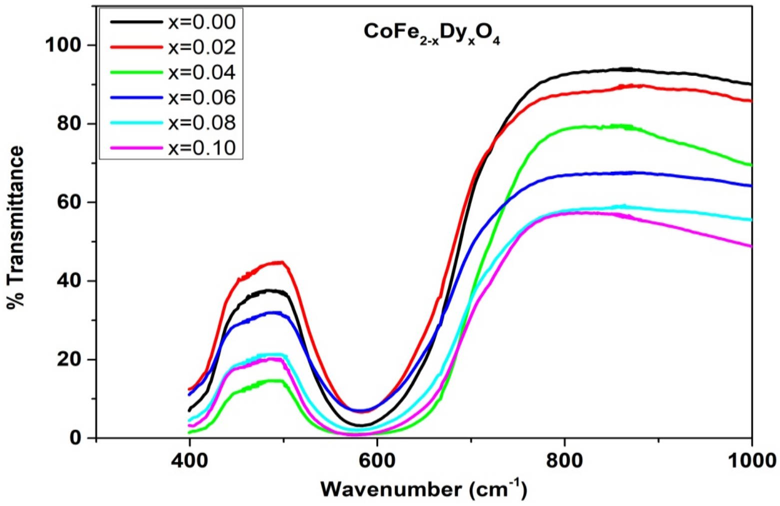

Figure 6.9: FTIR spectra of $CoFe_{2-x}Dy_xO_4$ nano particles.

FTIR spectra of pure and Dy doped $CoFe_2O_4$ nanoparticles samples shows two major absorption band in the wave number range 390 – 700cm^{-1}for all the samples. One band is observed at 390 cm^{-1}- 430cm^{-1}corresponds to stretching vibration of octahedral groups and other band at 550 cm^{-1}- 680 cm^{-1}corresponds to stretching vibration of tetrahedral groups [25]. The two absorption bands are observed, the lower frequency band is about 390 cm^{-1} corresponds to the vibration of metal oxide bond at octahedral site and the one corresponding to about 595 cm^{-1}indicates metal-oxygen vibration at tetrahedral site. These two absorption bands confirm the formation of spinel cobalt ferrites structure material.

6.2.3 Scanning Electron Microscopy (SEM)

The SEM images of pure Co ferrite, 4% Dy doped and 10% Dy doped cobalt ferrites are shown in the fig. 6.10 (a, b, c) respectively.

It is noticed from images that Co ferrites particles are spherical in shape, agglomerated and nano size. The nano particles large agglomerates are formed and this agglomeration increases with doping concentrations of Dy^{+3}. Further the clusters of grain boundaries in nano range are visible. The nano grains particles appears in spherical geometry shape.

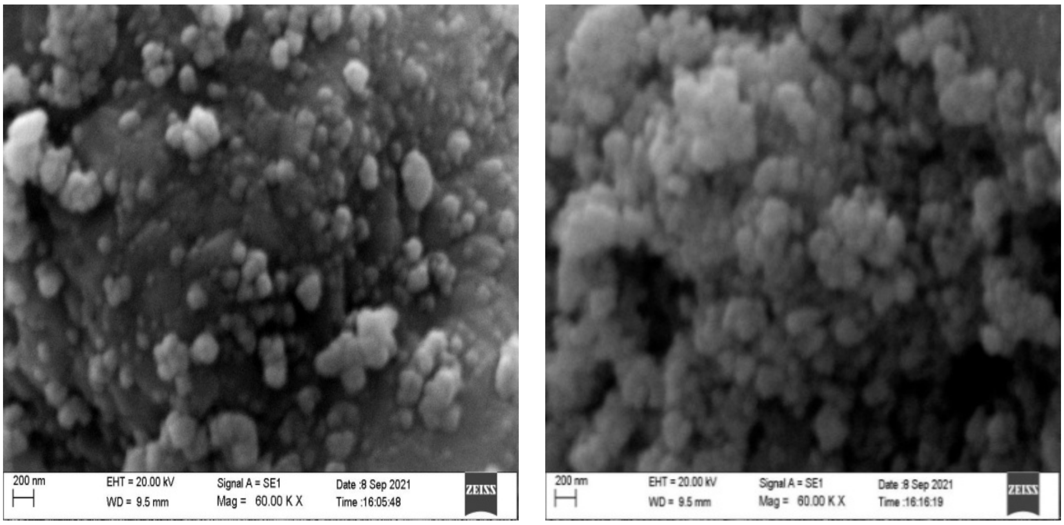

(a) (b)

The surface morphological information of Co ferrite and Dy doped Co ferrite is obtained from SEM images.

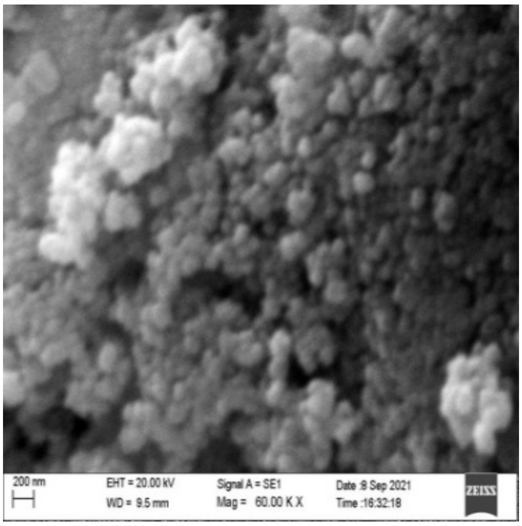

(c)

Fig. 6.10 Scanning Electron Micrograph of (a) $CoFe_2O_4$, (b) $CoFe_{1.96}Dy_{0.04}O_4$ and (c) $CoFe_{1.90}Dy_{0.10}O_4$

The extent of agglomeration increases with doping concentration of Dy^{+3} may be due to the inclusion of Dy ions at octahedral site and also presence of surface charges with other type of forces [26]. The differences in undoped and doped samples were observed.

6.2.4 Energy Dispersive Spectroscopy

Fig.6.11 shows energy dispersive spectroscopy analysis for Co ferrite and Dy doped Co Ferrites samples. The elemental composition of $CoFe_2O_4$ and Dy doped $CoFe_2O_4$ has been analyzed using energy dispersive spectroscopy analysis and table 6.2 shows the experimental and theoretical percentage composition of elements in the samples. The results confirms the presence of Co, Fe, Dy and O elements in the prepared samples and no other impurities are found within the experimental limit of EDS.

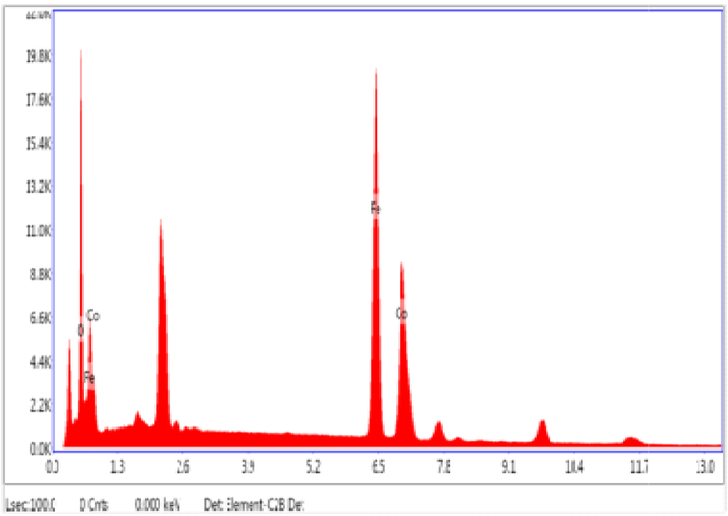

(a)$CoFe_2O_4$

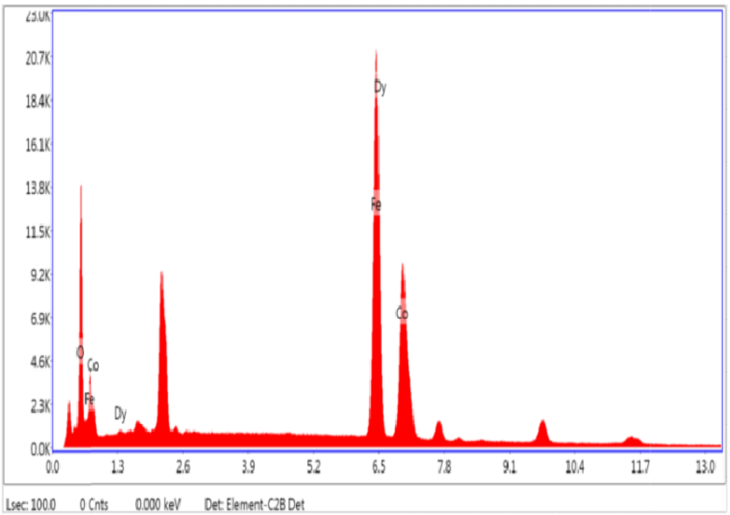

(b) $CoFe_{1.95}Dy_{0.04}O_4$

EDS analysis of (c) $CoFe_{1.90}Nd_{0.10}O_4$ is shown in fig. 6.11 below.

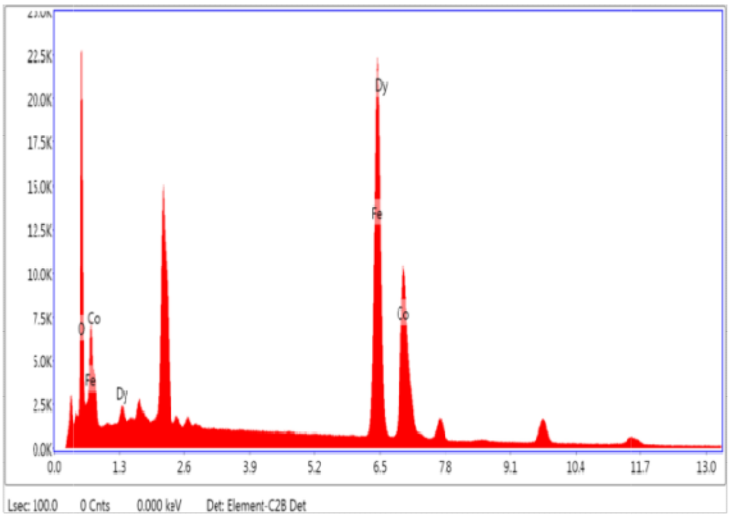

(c) $CoFe_{1.90}Dy_{0.10}O_4$

Fig.6.11: EDS analysis of (a) $CoFe_2O_4$ (b) $CoFe_{1.95}Dy_{0.04}O_4$ (c) $CoFe_{1.90}Dy_{0.10}O_4$

Table 6.2: Experimental and calculated weight percentage value for a) $CoFe_2O_4$ (b) $CoFe_{1.96}Dy_{0.04}O_4$ (c) $CoFe_{1.90}Dy_{0.10}O_4$

Composition	**$CoFe_2O_4$**		**$CoFe_{1.96}Dy_{0.04}O_4$**		**$CoFe_{1.90}Dy_{0.10}O_4$**	
Of Elements	**Exp%**	**Theo%**	**Exp%**	**Theo%**	**Exp%**	**Theo%**
Fe	54.15	47.61	49.75	45.82	50.31	43.26
Co	28.03	25.12	18.85	24.67	17.62	24.03
O	17.82	27.27	26.21	26.78	24.09	26.08
Dy	0	0	5.20	2.72	7.98	6.63
Total	100.00	100.00	100.00	100.00	100.00	100.00

6.2.5 Transmission Electron Micrography

Transmission electron micrograph for $CoFe_{1.96}Dy_{0.04}O_4$ and$CoFe_{1.90}Dy_{0.10}O_4$ shown in fig 6.12 Since Gd^{+3} occupies octahedral site that produces strain in the lattice as well as grain boundaries due to its larger ionic radii which causes hindrance in grain growth that results in the reduction of particle size. The micrograph shows the agglomeration which indicates the strong magnetic nature of Gd^{+3} doped cobalt ferrites.

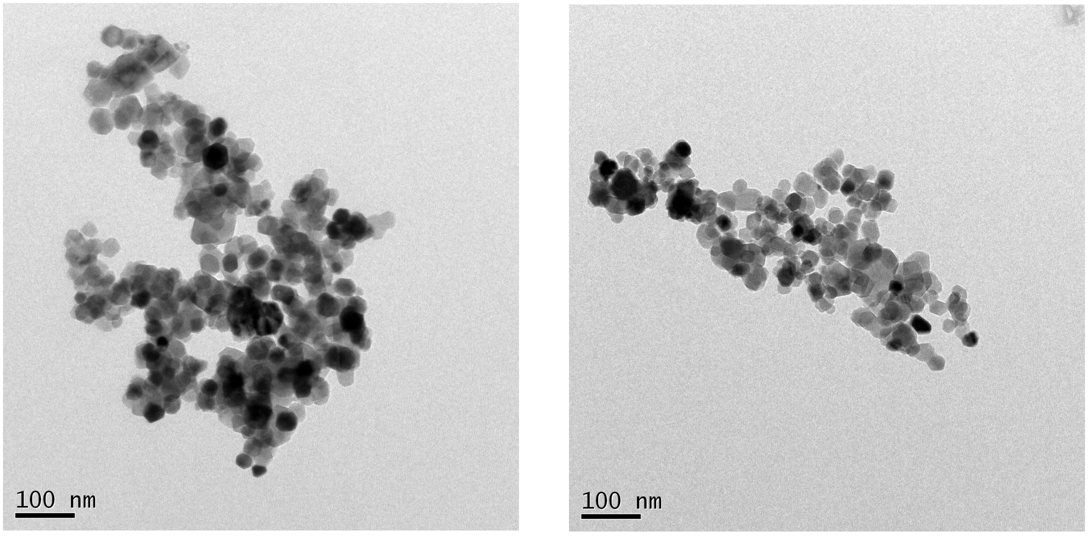

(a) (b)

Fig. 6.12 Transmission Electron Micrograph of (a) $CoFe_{1.96}Dy_{0.04}O_4$ and

(b) $CoFe_{1.90}Dy_{0.10}O_4$

6.3 Magnetic Properties Study

The magnetic properties of samples materials are studied by considering its behaviors changes in presence of external magnetic fields. It has been found that pure cobalt ferrites and Dy^{+3} doped cobalt ferrites shows ferrimagnetic behavior. In the current chapter magnetic measurement studies such as hysteresis for pure and Dy^{+3} doped cobalt ferrites are experimented. Also zero field cooled (ZFC) and field cooled (FC) measurement for constant field has been studied. AC susceptibility measurement to study a Curie temperature of samples has been investigated.

6.3.1 Vibrating Sample Magnetometer (VSM)

Quantum Design's Versa Lab 3Tesla vibrating sample magnetometer (VSM) is used for the magnetic hysteresis loop measurement for cobalt ferrites and Dy^{+3} doped cobalt ferrites samples were carried out for room temperature. The fig. 6.13 shows the hysteresis loops of $CoFe_{2-x}Dy_xO_4$ (x = 0.00, 0.02, 0.04, 0.06, 0.08, 0.10) nanoparticles.

Table 6.3 shows values of the saturation Magnetization (Ms), Coercivity (Hc) and remanence magnetization (Mr) extracted from plot of magnetic moment versus magnetic field.

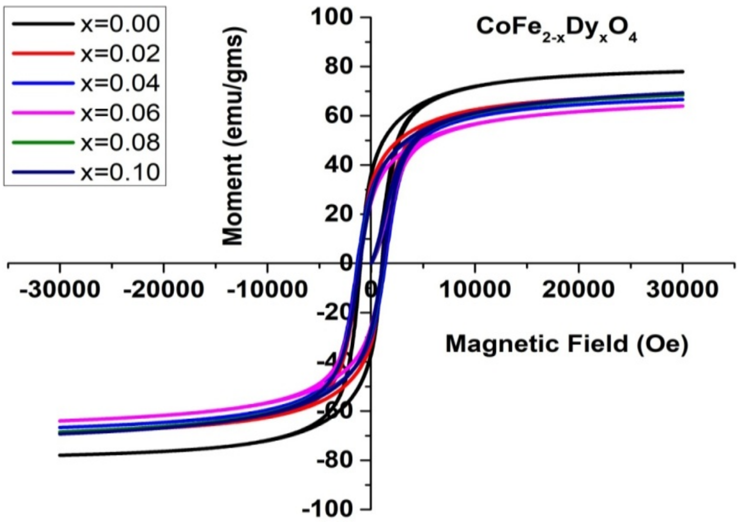

Fig. 6.13 Hysteresis loops for $CoFe_{2-x}Dy_xO_4$ (x = 0.00, 0.02, 0.04, 0.06, 0.08, 0.10) nanoparticles.

It is observed that saturation magnetization decreases with increase in Dy^{+3} concentrations till x= 0.06 and above this value shows increase in saturation magnetization for Dy^{+3} doped Co ferrites sample. The magnetic properties of ferrites are influenced by cation distribution in the spinel lattice sites. As per Neel's sublattice model, three types of interactions i.e. A-A, B-B and A-B exists between tetrahedral site and octahedral site of spinel ferrites. Among these three interactions, A-B interaction is stronger than other two interactions [27, 28]. In rare earth doped ferrites, ion occupies octahedral sitesdue to its larger ionic radius.Also the magnetic moment originate from 4f electrons[29] for Dy^{+3} ions and at room temperature their magnetic dipole orientations are in disorder form hence they contribute very small to net magnetization at room temperature [30,31]. Therefore doping of Dy^{+3} ions in cobalt ferrites lattices is equal to the substitution of non magnetic atom at B sites that result in the reduction of magnetization at B sites.The total magnetization of cobalt ferrites is calculated from the difference of magnetization of B sites and A sites. The A-B interactions become weaker as a concentration of Dy^{+3} increases [32, 33]. Hence the magnetization decreases with increase in Dy^{+3} doping concentrations. The enhancement of saturation magnetization may be due to higher Dy^{+3} doping concentration, in which Co^{+2} ion immigrates in A site accompanied by equivalent Fe^{+3} ion moving from A site to B site. This migration decreases the concentration of Fe^{+3} ions in A site that results into the increase of saturation magnetization for 8% and 10% of Dy^{+3} doped co ferrites. The factors are decrease in Yafetn- kittel angle θ_{YK} between moment of B sites [34] and surface effect [35] due to the surface disorder in which the number of spins increases at surface of rare earth doped ferrites as the crystallite size is reduced [36].

Table 6.3: Magnetic properties of $CoFe_{2-x}Dy_xO_4$: saturation magnetization (Ms), coercivity (Hc), remanent magnetization (Mr) and remanence ratio

Concentration 'x' of $CoFe_{2-x}Dy_xO_4$	**Ms (emu/g)**	**Hc (Oe)**	**Mr (emu/g)**	**Mr/Ms Ratio**
$CoFe_2O_4$	78	1034	35	0.498
$CoFe_{1.98}Dy_{0.02}O_4$	69	1210	30	0.465
$CoFe_{1.96}Dy_{0.04}O_4$	67	1343	25	0.422
$CoFe_{1.94}Dy_{0.06}O_4$	64	1148	21	0.389
$CoFe_{1.92}Dy_{0.08}O_4$	68	1159	20	0.391
$CoFe_{1.90}Dy_{0.1}O_4$	69	1029	19	0.371

The variation of coercivity with Dy^{+3} concentrations are shown in the table 6.3. It is observed that coercivity decreases with Dy^{+3} concentrations. The pure Co ferrites shows coercivity of 1034 Oe and for Dy doped co ferrites sample shows mixed trends for coercivity value for Dy concentrations from x = 0.02 to x = 0.10. The coercivity trend of variation is due to the substitution of large ionic radii Dy^{+3}ion by Fe^{+3} ion in B sites, to compensate for this Co^{+2} ions migrated from B sites to A sites which decreases Co^{+2} cations at B sites. This reduces single Co^{+2} ion anisotropy that results in the reduction of the coercivity. The decrease in coercivity also related to crystallite size in the single domain region according to which coercivity decreases with decrease in crystallite size [37]. The remanent ratio or the loop squareness ratios (Mr/Ms) are presented in the table

6.3 shows on average decrease with increase in Dy^{+3} concentrations. It tells us how domains reorientation of magnetization itself to the easy nearer axis when magnetic field is removed [38]. The low value of remanent ratio indicates the particles interact magneto-statically [39, 40]. The remanent variation indicates the decrease in anisotropy with Dy doped co ferrites samples and is similar to the coercivity.

6.3.2 ZFC and FC Measurement

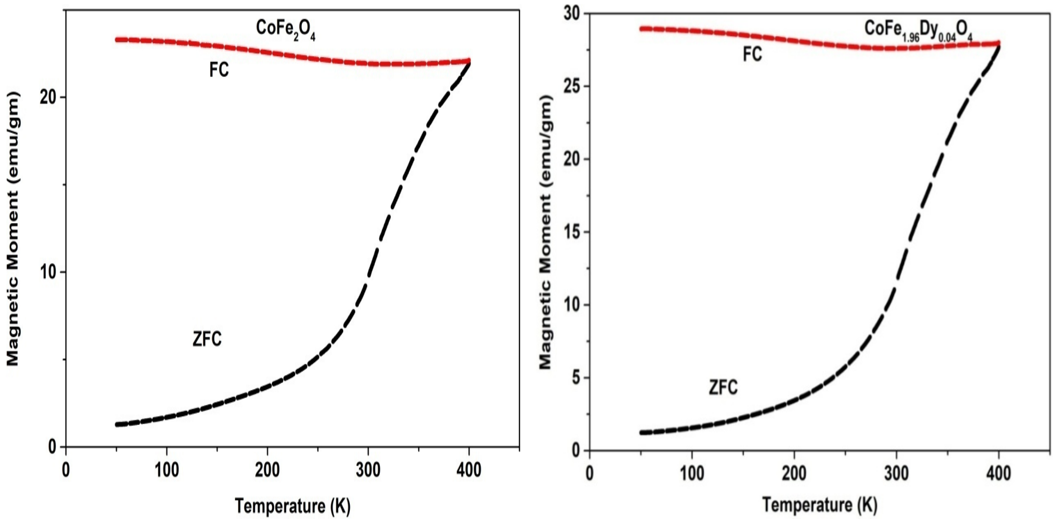

(a) (b)

The magnetic moment variation with temperature (K) for $CoFe_{2-x}Dy_xO_4$

(a) x = 0.00 (b) x = 0.04

The variation of magnetic moment with temperature (K) for $CoFe_{2-x}Dy_xO_4$ (x = 0.10) is shown below.

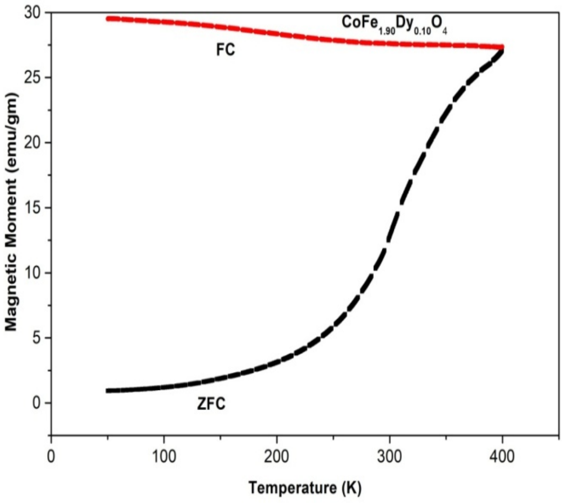

(c)

Fig.6.14: variation of magnetic moment with temperature (K) for $CoFe_{2-x}Dy_xO_4$ (a) x = 0.00, (b) x = 0.04 and (c) x = 0.10)

Figure 6.14 depicts the investigation of magnetization concerning temperature within a 500 Oe applied magnetic field. The study explores the variation in magnetic moment as temperature ranges from 50 K to 400 K. For the Zero Field Cooled (ZFC) measurements, the process involved cooling the sample from 400 K to 50 K without the presence of a magnetic field. Subsequently, the sample was allowed to warm while exposed to a 500 Oe magnetic field, followed by measurement.

In the case of Field Cooled (FC) measurements, both cooling and warming occurred in the presence of the applied magnetic field, and measurements were conducted during the warming phase. The results from Figure 6.14 illustrate that in ZFC measurements, sample magnetization rises as temperature ascends from 50 K to 400 K. Conversely, FC measurements exhibit a gradual decline in magnetization with increasing temperature. This decline can be attributed to thermal activation, which induces randomization of magnetization direction by reducing magnetic anisotropy, subsequently diminishing magnetization magnitude.

During FC cooling, magnetic moments within the particles align with the field direction, resulting in higher magnetization values [41]. It is observed that both T_b and T_{irr} decrease with higher applied magnetic fields, indicative of larger particle blocking phenomena within the sample.

Analysis of Figure 6.14 reveals the presence of an irreversibility temperature in the samples, while the blocking temperature is not discernible. The absence of a blocking temperature for this sample, potentially above 400 K at 500 Oe, could be attributed to an increased quantity of larger particles in comparison to the average particle size within the sample. Literature also suggests that particle agglomeration could contribute to an elevation in blocking temperature [42].

6.3.2 AC Susceptibility

Ac susceptibility refers to the measure of a materials response to an alternating magnetic field. It is one of the important properties in the study of magnetic materials and provides valuable insights into the magnetic behavior. When the magnetic field is applied to a material, it causes the magnetic moment within the material to oscillate. AC susceptibility quantity measures how much materials magnetization changes in the response to this alternating magnetic field and represented as a function of the frequency of the applied AC magnetic field. The AC susceptibility provides valuable information about a material's properties like magnetic phase transitions, magnetic relaxation, super-paramagnetism (sp), magnetic anisotropy etc.

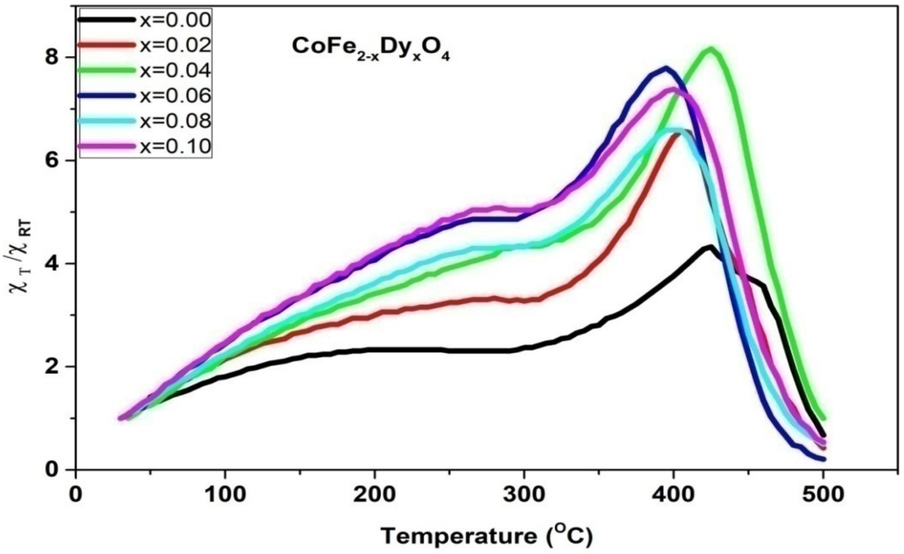

Fig.6.15 The normalized AC susceptibility plot as the function of temperature for $CoFe_{2-x}Dy_xO_4$

The study of AC susceptibility providesinformation about the domain type and the Curie temperature of the ferrites.The ferrites material exhibit three types of domain such as single domain (SD), multi domain (MD) and super-paramagnetic (SP). In multi domain, there are many small domains separated by walls in between and when grain size is of order of wall thickness, unable to support the wall are called single domain. The particles with size smaller than 10 nm exhibits super-paramagnetism nature. Fig.6.15 shows sharp fall in the normalized susceptibility at the particular temperature called

Curie temperature.All the samples exhibit single Curie temperature that indicates ferrite samples are single phase without any impurity in it. The samples are single domain (sp) because as the temperature increases magnetization increases, reaches a maximum value and then there is a sharp fall just before Curie temperature Tc. The region between sharp increase in magnetization and sharp decrease just before Curie temperature, there is a hump in between is called Hopkinson's hump and it is due to Hopkinson's effect. Hopkinson effect is observed in nano- crystalline single domain particles.

Table 6.4: Sample concentration, crystallite size and Curie temperature

Concentrations 'x' of Sample $CoFe_{2-x}Dy_xO_4$	**Dy^{+3} Crystallite Size in nm**	**Curie Temp T_C in ^{O}c**
0.00	35	510
0.02	30	505
0.04	25	503
0.06	21	495
0.08	20	493
0.10	19	488

The curie temperature of the samples obtained from AC susceptibility plot is given in the table 6.4.It is seen from the table 6.4 that the Curie temperature of samples decreases with increase in concentration of $Dy^{+3}$and decrease in crystallite size. It is reported in literature that the variation in Curie temperature can be explained on the bases of variation in their particle size and lattice parameter [42-45]. Sample shows the SD type behavior with the mixture of MD grains. It is also reported that particle with smaller size and higher lattice constant shows higher Curie temperature [46]. But it is observed in our studies that larger particle size ferrites show higher Curie temperature.

AC susceptibility of ferrimagnetic materials is affected by both particle size and lattice constant. However, the relationship is highly complex and depends on the specific material, its crystal structure, the arrangement of magnetic sub-lattices, and the interactions between them.

6.4 Electrical Properties Study

Dysprosium (Dy^{+3}) doped CoFe2O4 are the special magnetic material that exhibits interesting electric and magnetic properties due to the presence of Dy^{+3} ions in the crystal structure. As we know Cobalt ferrites are ferrimagnetic materials, and Dy doping can further modify their electrical characteristics. The specific electrical properties of Dy^{+3} doped cobalt ferrites can vary depending on the doping level, sample preparation techniques, and measurement conditions. The optimization of these parameters is necessary to achieve desired electrical characteristics for specific applications. The study and exploration of these properties are still ongoing; more insights into their properties and potential applications are likely to emerge.The electrical properties of Dy^{+3} doped cobalt ferrites can be tailored by controlling the synthesis methods, annealing conditions, and the concentration of Dy^{+3} dopants. These materials find applications in the fields of electronics, telecommunications, sensors, and magnetic storage devices. The electrical properties such as resistivity, dielectric constant and dielectric loss variation with frequency/temperature, thermo-electric power of Dy^{+3} doped $CoFe_2O_4$ are discussed in the current chapter.

6.4.1 DC Resistivity

The variation of resistivity with temperature for Dy^{+3} doped CoFe2O4 with different concentrations of $Dy^{+3}$are shown in fig. 6.16.The electrical resistivity of Dy^{+3} doped ferrites typically follows a certain temperature dependent trends. The specific temperature dependence of resistivity can vary depending on the type and concentration of the dopants, the crystal structure, density, porosity and the microstructure of the material [47, 48].

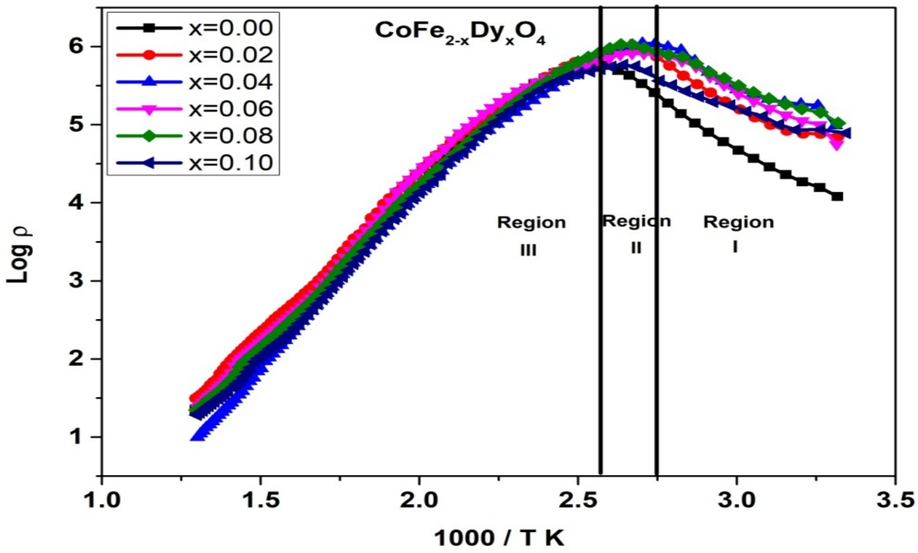

Fig. 6.16 Variation of dc resistivity with (1000/T) of $CoFe_{2-x}Dy_xO_4$(x = 0.0 , 0.02, 0.04, 0.06, 0.08, 0.1)

The resistivity-temperature relationship of a material can provide valuable insights into its electrical behavior and the underlying physical processes.The DC resistivity study was carried out from room temperature to 773 K using two probe method and the plots of log ρ v/s 1000/ T K is shown in Fig. 6.16 For many ferrite materials, including Cobalt ferrites, the resistivity typically decreases with increasing temperature which is the typical behavior of semiconductor. This behavior is associated with the increase in charge carrier mobility due to thermal activation. As the temperature rises, more charge carriers become available for conduction, leading to a lower resistivity. It is seen from the Fig. 6.16 Initially resistivity increases attains maximum, remains constant and then decreases with increase in applied temperature. The resistivity increases in region I from room temperature to 353 K(80^{O}C), remains constant in region II from 353K (80^{O}C) to 380 K (107^{O}C) and then deceases in region III from 380K (107^{O}C) to 773K (500^{O}C). The increase in resistivity in region I is attributed to presence of open pores, loose agglomeration and the entrapped moisture. As the temperature increases, moisture gets evaporated and till all the gets desorption it reaches end of region II in which resistivity remains constant. After desorption of all the moisture in region III, the resistivity fallows the normal trend shown by spinel ferrites i.e. it starts decreasing as temperature increases [49]. The conduction mechanism is based on the Verwey de Boer mechanism [50]. According to this mechanism, the conduction in ferrites is due to exchange of electrons between the ions of same element that exhist with different valence state on the equivalent lattice site. With increase in temperature, the drift mobility in charge carriers leads to the decrease in resistivity [48, 51]. This can be explained as follows: when temperature increases, the vibration of lattice also increases which makes the ions come closer to each other that results in increase of probability of hopping on adjacent ions and thereby increasing the mobility of the charge carriers. The grains are good conducting and grains boundaries are poor conducting so increase in grain size leads to decrease in porosity. There is the relation between porosity and resistivity; increase in porosity gives rise in number of vacancies, scattering centers and pores of electrical charge carriers which increases resistivity [52, 53].

The Arrhenius equation is often applicable for describing the resistivity variation with temperature in materials with thermally activated charge carriers. The activation energy (Ea) characterizes the dependence of resistivity on temperature, and it can be obtained from experimental data by plotting the natural logarithm of resistivity (log ρ) as a function of the reciprocal of temperature (1/T K) and fitting a straight line to the data.

It is also observed that as resistivity decreases with decrease in activation energy [54]. The decrease in activation energy is due to the redistributions of cations in octahedral site. The hopping of electrons is the major responsible for conductivity, hence resistivity. In region III the resistivity decreases as transfer of Fe^{+3} ions from the tetrahedral site to octahedral site increases. It is known that the electron hopping between $Fe^{+2} \Leftrightarrow Fe^{+3}$ ions in octahedral sites are responsible for conduction. As the number of Fe ion increases and ultimately $Fe^{+2} \Leftrightarrow Fe^{+3}$ ion pairs, since the hopping of electrons between $Fe^{+2} \Leftrightarrow Fe^{+3}$ ions are responsible for electrical conduction, an increase in $Fe^{+2} \Leftrightarrow Fe^{+3}$ ions pairs increases the hopping of electrons and also electrical conductivity. Therefore electrical resistivity decreases in region III.

6.4.2 Dielectric Properties

6.4.2.1 Dielectric Constant Variation with Frequency

The variation of dielectric constant with frequencies for $CoFe_{2x}Dy_xO_4$ with x = 0.00, 0.02, 0.04, 0.06, 0.08, 0.10 nanoparticles at room temperature (fig.. The frequency dependence of dielectric constant of pure cobalt ferrites and Dy^{+3} doped cobalt ferrites are measured at room temperature in the frequency range from 20 Hz to 3MHz. It is seen from Fig. 6.17 that the measured value of dielectric constant strongly dependent on the frequency of the applied field.It is observed that initially dielectric constant (Ɛ) decreases abruptlyat low frequencies and at higher frequencies, decrease is gradual and finally become constant for all Dy^{+3} doped Co ferrites samples.

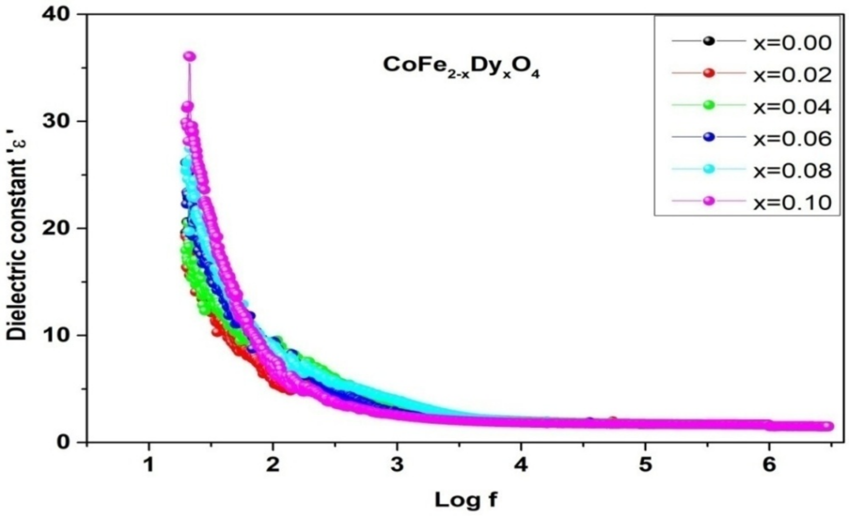

Figure 6.17: Variation of dielectric constant as a function of frequency with Dy^{+3} concentrations

The decrease in dielectric constant at lower frequencies is the characteristic of the dielectric dispersion. The dispersion in dielectric constantis due to the Maxwell-Wagner’s type of interfacial polarization model and is in agreement with Koop’s phenomenological theory [55-57]. According to this model, the dielectric medium consists of conducting grains which are separated by poor conducting grains boundaries.

In the presence of external applied field, the opposite polarity charge carriers moves inside the grains in opposite direction. These moving charges piles up at the poor conducting grain boundaries which acts as the wall. The presence of applied external electric field, the grain functions as an electric dipole which is termed as space charge polarization or interfacial polarization. The space charge polarization shows high dielectric value for the samples at low frequencies [58 - 59]. The polarization mechanism in cobalt ferrites is similar to the conducting process [60], in which electron hopping between $Fe^{+2} \Leftrightarrow Fe^{+3}$ions and hole hopping between $Co^{+2} \Leftrightarrow Co^{+3}$ ions, charge carriers reaching the poor conducting grain boundaries that pile up due high resistance and produces polarization. As the frequency of applied field increases a charge carriers cannot follow the frequency of the alternating applied electric field as a result polarization decreases [61]. Some literature reported [62] that increase in the dielectric constant could be due to the increasing number of Fe^{+3} ions at the octahedral site. This can be explained as follows: The doping of Dy^{+3} ions makes migration of Co^{+2} ions to tetrahedral site in order to relax strain and equal number of Fe^{+3} ions migrate from tetrahedral site to the octahedral site which increases the hopping of electrons between $Fe^{+2} \Leftrightarrow Fe^{+3}$ ions in octahedral sites and increases dielectric constant. For some time dielectric decreases due to the limitation on the migration of Fe^{+3} ions from tetrahedral sites to octahedral sites, the number of Fe ions are decrease and also $Fe^{+2} \Leftrightarrow Fe^{+3}$ion pairs. Thus availability of $Fe^{+2} \Leftrightarrow Fe^{+3}$ ions, and hopping electrons in between $Fe^{+2} \Leftrightarrow Fe^{+3}$decreases in octahedral sites that reduces the dielectric constant value.

6.4.2.2 Dielectric Loss Variation with Frequency

Figure 6.18 shows the variation of dielectric loss (tan δ) with frequencies for $CoFe_{2-x}Dy_xO_4$ with x = 0.00, 0.02, 0.04, 0.06, 0.08, 0.10 nanoparticles at room temperature.

The frequency dependence of dielectric loss of pure cobalt ferrites and Dy^{+3} doped cobalt ferrites are measured at room temperature in the frequency range from 20 Hz to 3MHz.

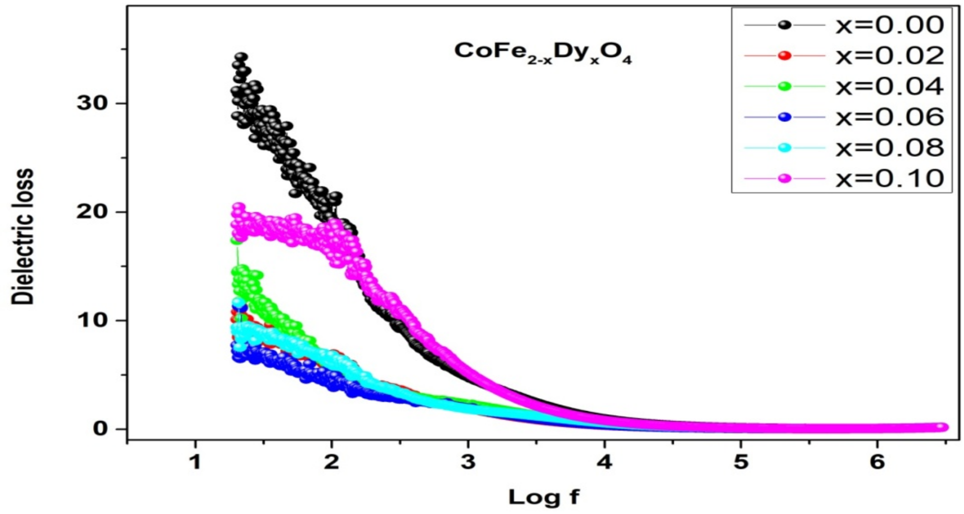

Figure 6.18: Variation of dielectric loss (tan δ) as a function of frequency with Dy^{+3} concentrations.

It is seenfrom fig. 6.18 that initially dielectric loss (tan δ) increaseat very low frequency and as the frequency is increased further it decrease and finally become constant for all Dy^{+3} doped Co ferrites samples. The decreasing trend at higher frequency is similar to dielectric constant. The increase in dielectric loss is due to the limitation in an electronic exchange between Fe^{+2} ions and Fe^{+3}ions due to the lager ionic radii of Dy^{+3} as mentioned in resistivity. The decrease shown in dielectric loss tangent may be the fine particle size results in increase of surface area along with Dy^{+3} ions inclusion that increases the amount of energy require for electronic exchange which is responsible for the dielectric loss. At high frequencies the electronic exchange cannot follow the frequency of applied alternating electrical field and result in the decrease of dielectric loss [63].

The dielectric loss exhibits dispersion with increasing frequency similar to dielectric permittivity and can be explained by Maxwell-Wagner's model [64]. The polarization lags behind applied alternating field due to the presence of defects, structural inhomogeinities in ferrites and hence results in dielectric loss [65]. The dielectric loss decreases with Dy^{+3} substitution and low value loss are observed for higher frequencies which indicate their potential applications in high frequency microwave devices.

6.4.2.3 Dielectric Constant Variation with Temperature as the Function of Frequency

The variation of dielectric constant of a material with frequency is very sensitive to temperature. The measurement of dielectric constant for all the samples was recorded at different frequencies from room temperature to 500 ^{O}C.

The dielectric constant (Ɛ) variation with temperaturefor $CoFe_{2-x}Dy_xO_4$ as a function of frequency for x = 0.0, 0.02, 0.04, 0.06.

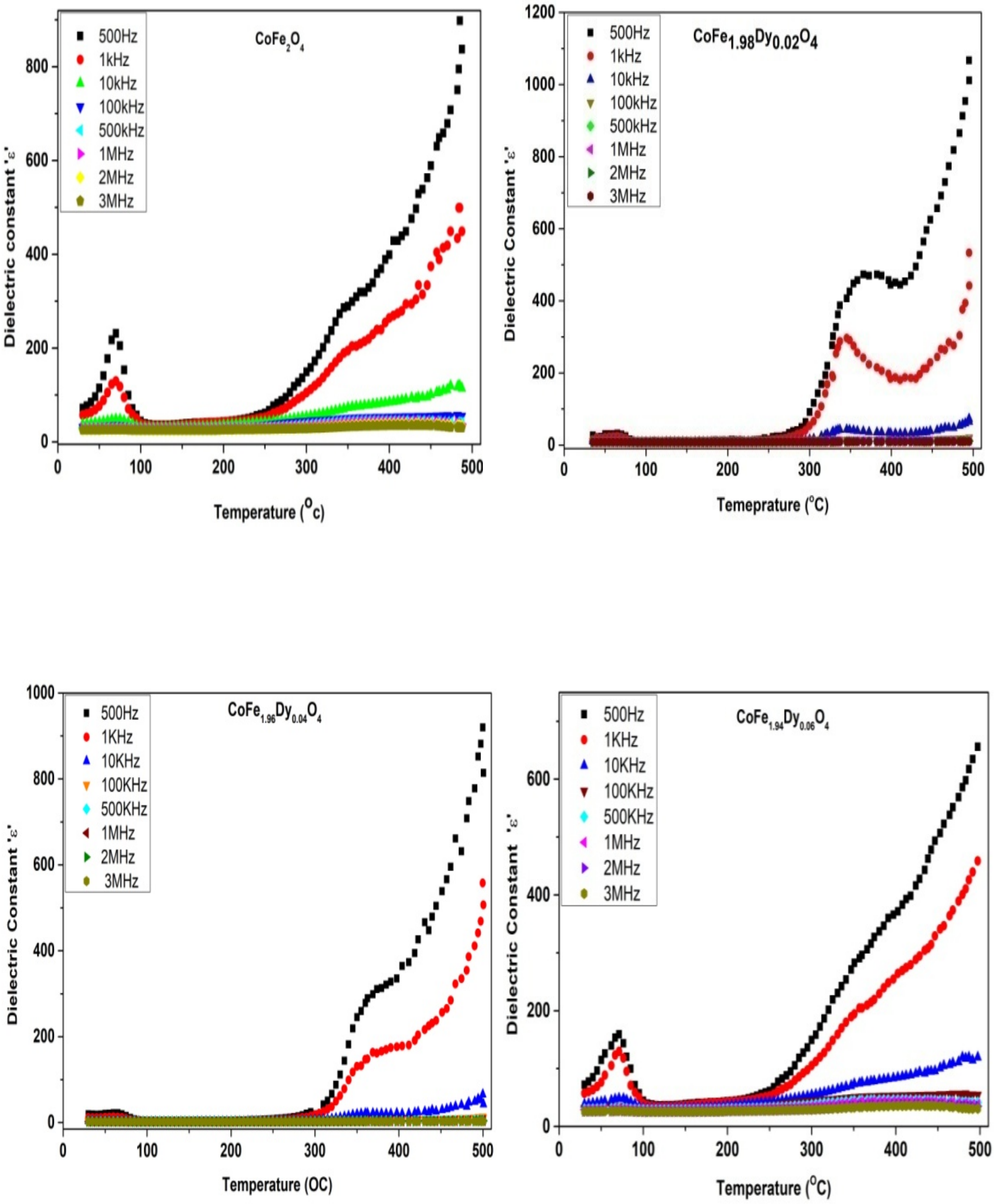

The dielectric constant (Ɛ) variation with temperature for $CoFe_{2-x}Dy_xO_4$ as a function of frequency (x = 0.08 and x = 0.10) is shown in fig. 6.19 below.

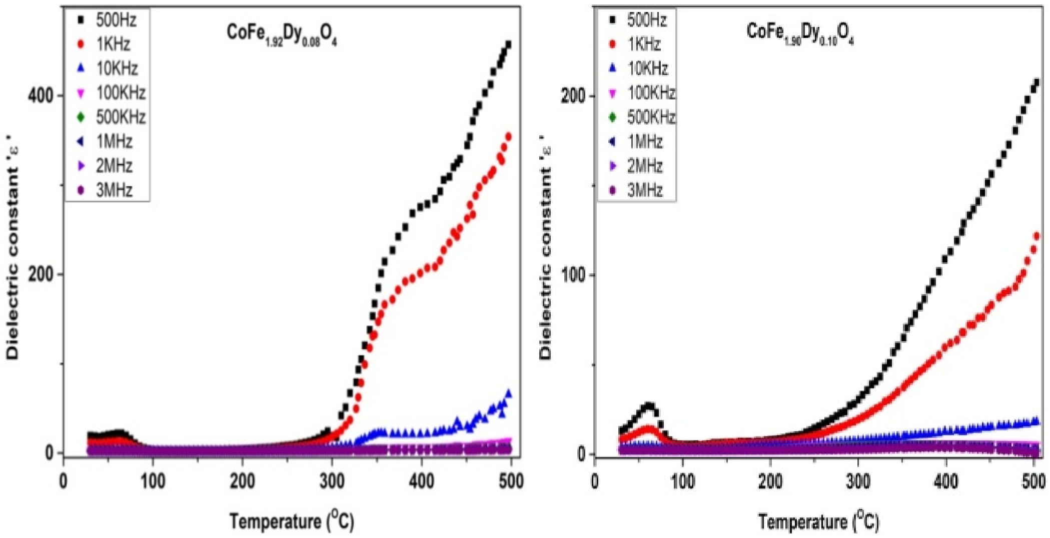

Fig.6.19: Variation of the dielectric constant (Ɛ) with temperaturefor $CoFe_{2-x}Dy_xO_4$ (x= 0. 00, 0.02, 0.04, 0.06, 0.08, 0.10) as a function of frequency.

It is seen from the figure 6.19 that all the samples show peaks behavior in the lower temperature region from 40^{O}C to 90^{O}C over all the frequencies. The structural investigation depicts that the crystallite size is dependent on the Co^{+2} content in the sample and co-relate the link between the particle size and the magnitudes of the peak height. The peaks are the relaxation peaks which are dependent on the frequency. The peaks are produced due to the relaxation time which is the time taken by the electrical dipole to orient in the direction of the applied field. When the frequency of the applied AC field matches with the frequency of the relaxation time, the resonance phenomenon occurs during which maximum energy transfer from the applied AC field occurs. In dielectric constant ‘ε’ variation with temperature as the function of frequency shows peaks behavior between $40^{O}C$ to $90^{O}C$ temperature, relaxation peaks spread and height of dielectric constant decreases with increasing AC field frequency and finally becomes flat for high frequency of 500 KHz. The relaxation peaks at higher frequency and at lower temperature disappear due to charge carrier localization [66, 67]. As the temperature increases, the thermal energy increases which increases hopping rate of charge carrier’s thereby increasing mobility in amplified form that increases the conductivity. There is augmentation of dipole polarization that depends on applied frequency [66, 68] and Co^{+2}content in the sample.

The dielectric constant decreases with increase in Dy^{+3} concentrations in $CoFe_{2-x}Dy_xO_4$. This is due to the substitution of large ionic radii Dy^{+3} ions in octahedral sites which decreases Fe^{+3} ions at octahedral sites of samples. The Dy^{+3} ions at octahedral sites replace Fe^{+3} ions which reduces the rate of hopping of Fe^{+2} and Fe^{+3} ions. Hence polarization decreased with increasing in Dy^{+3} content in the sample which reduces dielectric constant value.

6.4.2.4 Dielectric Loss Variation with Temperature as the Function Of Frequency

The fig. 6.20 shows the variation of dielectric loss with temperature as the function of frequency.It is seen from the figure behavior shown by dielectric loss is similar to the dielectric constant. The peaks in the lower temperature range are not prominent.

The variation of the dielectric loss (tanδ) with temperature for $CoFe_{2-x}Dy_xO_4$ (x= 0.00, 0.02, 0.04, 0.06) as a function of frequency.

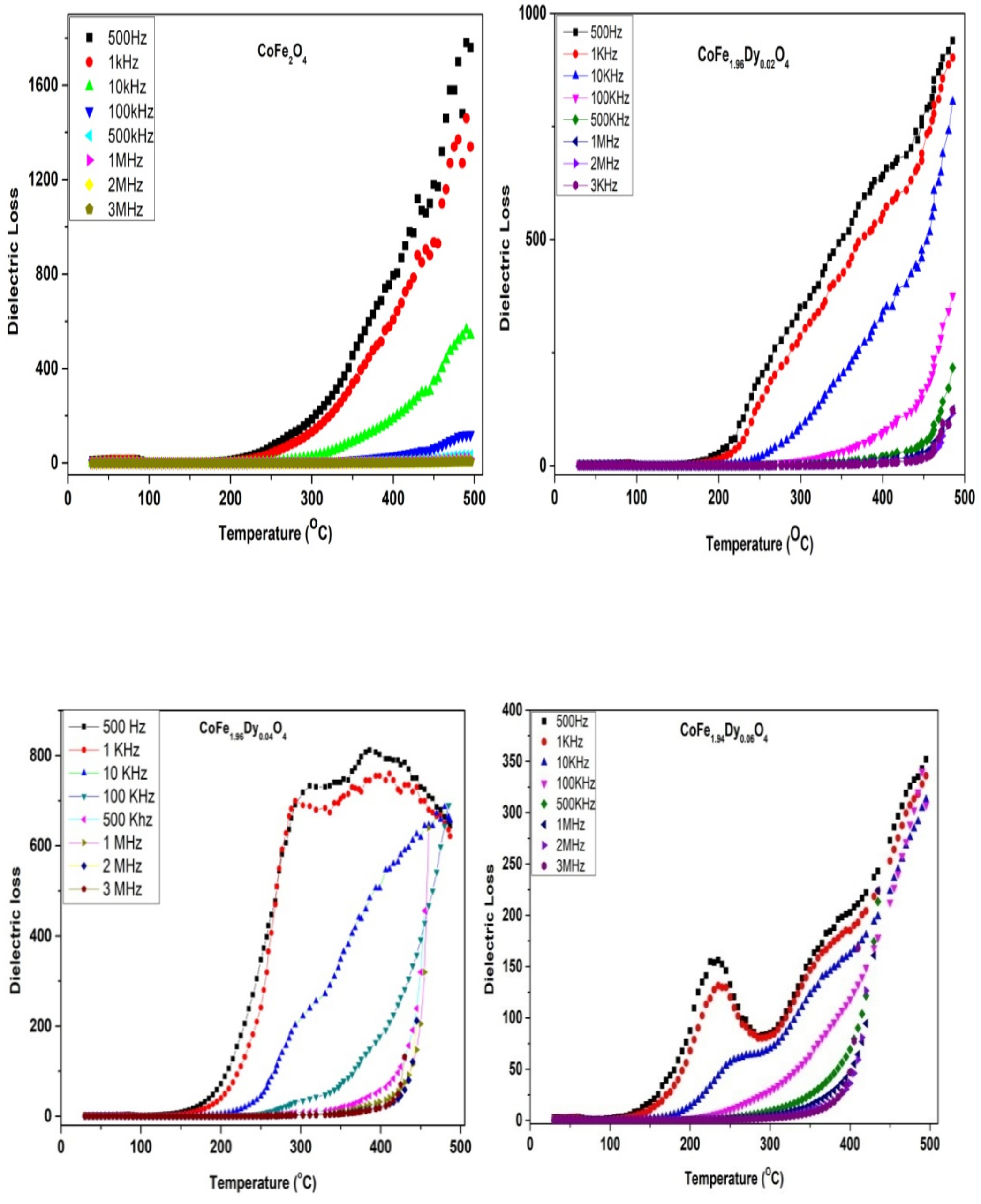

The variation of the dielectric loss (tanδ) with temperature for $CoFe_{2-x}Dy_xO_4$ (x= 0.08, 0.10) as a function of frequency is shown below.

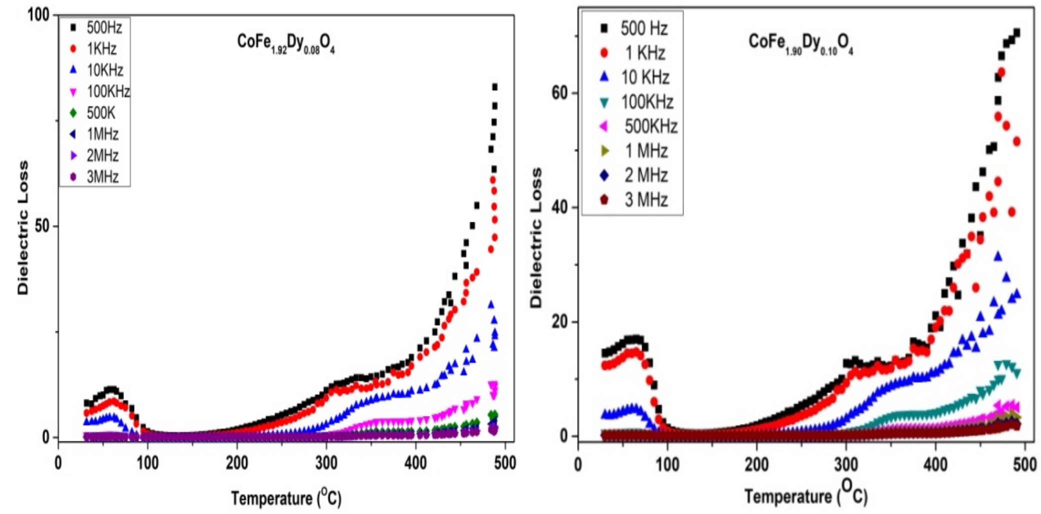

Fig. 6.20: Variation of the dielectric loss (tanδ) with temperature for $CoFe_{2-x}Dy_xO_4$ (x = 0.00, 0.02, 0.04, 0.06, 0.08, 0.10) as a function of frequency.

The peaks in the lower temperature range are not prominent. In the crystalline material,when the dielectric polarization lag behind applied alternating field that results in dielectric loss which occurs due to grain boundary effect. The dielectric property in the case of nano-particle samples may depend on factors such as sample preparation method, structure, size of the crystallite, chemical composition and preparative conditions [68].

6.4.3 Thermoelectric Power

Thermoelectric power or seebeck coefficient of $CoFe_{2-x}Dy_xO_4$ (x= 0.00, 0.02, 0.04, 0.06, 0.08, 0.10) samples was measured in the temperature range of room temperature to 500^OC. Here fig.6.21 shows thermal variation of thermoelectric power of Dy^{+3} dope Cobalt ferrite samples that can be seen that here all the composition have positive thermo electric power at room temperature. As a temperature increases, the positivity of thermoelectric power decreases and changes to negative value at certain temperature, as observed for all the samples.

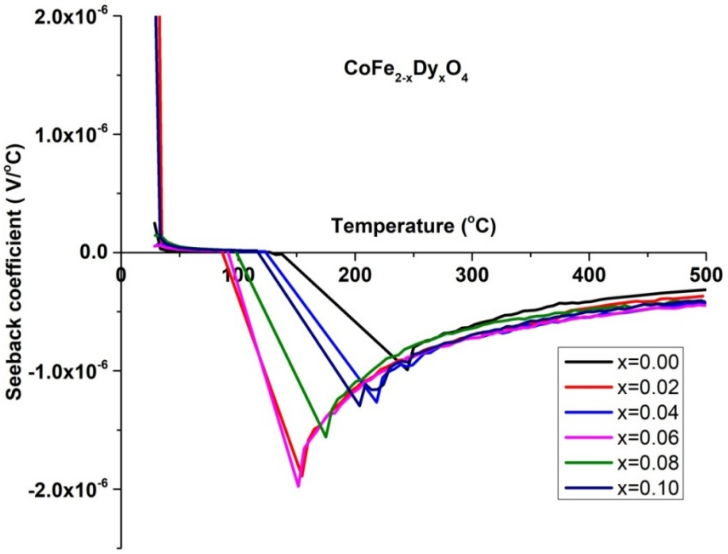

Fig.6.21: Variation of thermoelectric power with temperature of $CoFe_{2-x}Dy_xO_4$ samples.

It is seen from Fig.6.21 that samples shows p-type of semiconductor behavior in low temperature region and n-type of semiconductor in high temperature region. The n-type conduction mechanism in the sample is due to hopping of electrons between Fe^{+2} to Fe^{+3} and p-type of conduction mechanism is due to hopping of holes between $Co^{+3}\Leftrightarrow Co^{+2}$ [69]. The transition from p-type to n-type supports the changes in concentration of Co^{+2} and further predicts that conduction mechanism is due to hopping of electrons between Fe^{+2} and Fe^{+3} [70].

Table 6.5 Transition temperatures T (p-n) of $CoFe_{2-X}Dy_XO_4$ samples.

Concentrations 'x' of $CoFe_{2-x}Dy_xO_4$	**Transition Temperature T p-n (^OC)**
0.00	128
0.02	87
0.04	123
0.06	91
0.08	99
0.10	117

Table 6.5 provides the transition temperature Tp-n of each sample at which thermoelectric power changes from positive to negative i.e. p-type to n-type. The temperature T (p-n) varies in the range of 87^OC to 128 ^OC.

References:

[1] A.K. Giri, E. M.Kirkpatrick, P. Moongkhamklang, and S.A. Majetich, Applied Physics Letters 80 (2002) 2341-2343.

[2] S.J.Lee, C.C.H Lo, P.N.Matlage, S.H.Song, Y.Melikhov, J.E.Snyder, and D.C.Jiles Journal Applied Physics 102 (2007) 073910.

[3] K.Kamal Bharati, R.J. Tackett, C.E.Botez and C.V. Ramana Journal Applied Physics 109 (2011) 07A510.

[4] Simona Burianova, Jana PoltierovaVejpravova, Petr Holec, Jiri Plocek and Daniel Niznansk, Journal Applied Physics 110 (2011) 073902.

[5] K.Vasundhara, S.N. Achary, S.K. Deshpande, P.D. Babu, S. S. Meena and A.K. Tyagi, Journal of Applied Physics 113 (2013) 194101.

[6] A.K. Nikumbh, A.V. Nagawade, V.B.Tadke and P.P. Bakare, Journal of Materials Science 36 (2001), 653.

[7] G.D. Dwivedi, K.F.Tseng, C.L. Chan, P. Shahi, J. Lourembam , B.Chatterjee, A.K. GhoshH.D.Yang and Sandip Chatterjee, Physical review B 82 (2010) 134428.

[8] A.Franco, Jr., and F.C.e Silva, Applied Physics Letters 96 (2010) 172505.

[9] S.J.Lee, S.H.Song, C.C. Lo, S.T. Aldini and D.C. Jiles, Journal Applied Physics 101 (2007), 09C502.

[10] A.Franco Jr., F.L.A Machado, V.S.Zapf and F.W. Fabris, Journal Applied Physics 109, (2011) 07A745.

[11] S.P.Yadav, S.S.Shinde, A.A. Kadam and K.Y.Rajpure, Journal of Alloys and Compounds 555 (2013) 330.

[12] Y. Cedeño Mattei, O. Perales-Perez, M.S.Tomar, F. Roman, P.M Voyles and W. G. Stratton, Journal Applied Physics 103 (2008) 07E512.

[13] A.V.R. Reddy, G. Ranga Mohan, D. Ravinder, B. S. Boyanov, Journal of materials science 34 (1999) 3169.

[14] K. Kamala Bharathi and C.V. Ramana, Journal of Materials Research 26 (2011)584.

[15]G. Dascalu, T.Popescu, M.Feder and O.F.Caltun, Journal of Magnetism and Magnetic Materials 333 (2013) 69. 56.

[16] Pranav P. Naik, R.B. Tangsali, S.S. Meena, S.M. Yusuf, Materials Chemistry and Physics 191, (2017), 215-224.

[17] K.Velmurugan, V.S.K. Venkatachalapathy and S. Sendhilnathan, Materials research, 12, (2009), 529 - 534.

[18] J. A. Eastman, M. R. Fitzsimmons, L. J. Thompson, A. C. Lawson and R. A. Robinson, Nanostruct. Matter. 1, (1992), 465-470.

[19] D. Oleszak and P. H. Shingu, J. Appl. Phys., 79, (1996), 2975-2980.

[20] J. A. Dean, Lange's handbook of chemistry, McGraw-Hill, New York, 15th edn, 1998.

[21] C. Venkataraju, Applied Physics Research1 (No. 1) (2009) 41-45.

[22] M.M. Haque, M. Huq, M.A. Hakim, Indian J. Phys. 78A (3) (2004) 397-400.

[23] Emad M.M. Ewais, Mahmoud M. Hessien, Abdel-Hady A. El-Geassy, Journal of Australian Ceramic Society, 44 (1) (2008) 57-62.

[24] K. Rama Krishna, K. Vijaya Kumar, Dachepalli Ravinder, Advances in Materials Physics and Chemistry 2, (2012) 185-191.

[25] R. D. Waldron, Phys. Rev., 1955, 99, 1727.

[26] K. Manju, T. Smitha, D. S. Nair, E. K Aswathy, B. Aswathy, T Arathy, Binu, K. T. Krishna, Journal of Advanced Ceramics, 2015, 4(3): 199–205.

[27] K. J. Standley, Oxide magnetic materials, Oxford University Press, 1972.

[28] G. K. Williamson, W.H. Hall, Acta Metal. 1 (1953), 22.

[29] W. J.Nellis, S.Legvold, Phys. Rev. 180 (1969) 581.

[30] P.Kumar, S. K. Sharma, M. Knobel, J. Chand and M. Singh, J. Electroceram., 2011, 27, 51.

[31] J. Jing, L. Liangchao, X. Feng, J.Rare Earth. 25 (2007) 79.

[32] S. Singhal, S.K. Barthwal, K. Chandra K, J. Magn. Magn. Mater. 306 (2006) 233.

[33] J. Jiang, Y.M.Yang, L.C. LiL, Physica B 399 (2007) 105.

[34]. A.T. Ngo, P. Bonville, and M.P. Pileni, J. Appl. Phys. 89 (2001) 3370.

[35] K. Maaz, A. Mumtaz, S. K. Hasanain and A. Ceylan, J. Magn. Magn. Mater., 2007, 308, 289.

[36] R. H. Kodama, A. E. Berkowitz, J. E. J. McNiff and S. Foner, Phys. Rev. Lett., 1996, 77, 394.

[37] T. Sodaee, A. Ghasemi, R. Shoja Razavi, J Clust Sci 27, (2016)1239.

[38] G. Bottoni, D. Candolfo and A. Cecchetti, J. Appl. Phys. 81 (1997) 3794.

[39] S. Mukherjee, S. Pradip, A.K. Mishra, D. Das, Zn substitutedNiFe2O4 with very high saturation magnetization andnegligible dielectric loss synthesized via a soft chemical route. Appl. Phys. A 116, 389–393 (2014).

[40]. M.A. Gabal, Y.M. Al Angari, F.A. Al-Agel, Cr-substituted Ni-Zn ferrites via oxalate decomposition. Structural, electrical and magnetic properties. J. Magn. Magn. Mater. 391, 108–115 (2015).

[41] L. Ben Tahar, L.S. Smiri, A.L. Joudrier, M. Artus, F. Herbst, M.-J. Vaulay, S. Ammar, F. Fie´vet, Mater. Res. Bull. 42, (2007), 1888.

[42] S.S. Jadhav, S.E. Shirsath, B.G. Toksha, S.J. Shukla, K.M. Jadhav, Effect of cation proportion on the structural and magnetic properties of Ni-Zn ferrites nano-size particles prepared by co-precipitation technique. Chin. J. Chem. Phys. 21, 381–386 (2008).

[43] T.J. Shinde, A.B. Gadkari, P.N. Vasambekar, Magnetic properties and cation distribution study of nanocrystalline Ni-Zn ferrites. J. Magn. Magn. Mater. 333, 152–155 (2013).

[44]. O.A. Li, C.-R. Lin, H.-Y. Chen, H.-S. Hsu, K.-Y. Shih, I.S. Edelman, K.-W. Wu, Y.-T. Tseng, S.G. Ovchinnikov, J.-S. Lee, Size dependent magnetic and magneto-optical properties of $Ni_{0.2}Zn_{0.8}Fe_2O_4$ nanoparticles. J. Magn. Magn. Mater. 408, 206–212 (2016).

[45]. V. Grimal, D. Autissier, L. Longuet, H. Pascard, M. Gervais, Iron, nickel and zinc stoichiometric influences on the dynamic magneto-elastic properties of spinel ferrites. J. Eur. Ceram. Soc. 26, 3687 – 3693 (2006).

[46] I. Szczygieł, K. Winiarska, A. Bieńko, K. Suracka, D. GaworskaKoniarek, The effect of the sol-gel autocombustion synthesis conditions on the Mn-Zn ferrite magnetic properties. J. Alloy. Compd. 604, 1–7 (2014).

[47] A.V. Humbe, A.C. Nawle, A.B. Shinde, K.M. Jadhav, Impact of Jahn Teller ion on magnetic and semiconducting behavior of Ni-Zn spinel ferrite synthesized by nitrate-citrate route. J. Alloy. Compd. 691, 343–354 (2017).

[48] I.H. Gul, W. Ahmed, A. Maqsood, Electrical and magnetic characterization of nanocrystalline Ni-Zn ferrite synthesis by co-precipitation route. J. Magn. Magn. Mater. 320, 270–275 (2008).

[49] P.P. Sarangi, S.R. Vadera, M.K. Patra, N.N. Ghosh, Synthesis and characterization of pure single phase Ni-Zn ferrite nanopowders by oxalate based precursor method. Powder Technol. 203, 348– 353 (2010).

[50] E.J.W. Verwey, Electronic conduction of magnetite (Fe3O4) and its transition point at low temperatures. Nature 144, 327–328 (1939).

[51] A.D. Sheikh, V.L. Mathe, Anomalous electrical properties of nanocrystalline Ni–Zn ferrite. J. Mater. Sci. 43, 2018–2025 (2008).

[52] A. Hajalilou, H.M. Kamari, K. Shameli, Dielectric and electrical characteristics of mechanically synthesized Ni-Zn ferrite nanoparticles. J. Alloy. Compd. 708, 813–826 (2017).

[53] M.A. Ali, M.M. Uddin, M.N.I. Khan, F.-U.-Z. Chowdhury, S.M. Haque, Structural, morphological and electrical properties of Snsubstituted Ni-Zn ferrites synthesized by double sintering technique. J. Magn. Magn. Mater. 424, 148–154 (2017).

[54] M. T. Rahman and C. V. Ramana, J. Appl. Phys., 2014, 116, 164108.

[55] J. C. Maxwell, Electricity and Magnetism, Oxford Univ. Press, London, 1973.

[56] C. G. Koops, Phys. Rev, 1951, 83, 121.

[57] S. Sharma, Kirti Nanda, R.S. Kundu, R. Punia and N. Kishore, Structural Properties, Conductivity, Journal of Atomic, Molecular, Condensate & Nano Physics, 2 (2015) 15–31.

[58]M. Mehedi Hassan, Arham S. Ahmed, M. Chaman, Wasi Khan, A.H. Naqvi, Ameer Azam, Materials Research Bulletin, 47 (2012) 3952–3958.

[59]C.Belkhaoui, Ramzi Lefi, NissafMzabi, Hichem Smaoui, Journal of Materials Science: Materials in Electronics, (2018).

[60]K.Iwauchi, Jpn. J. Appl. Phys., 1971, 10, 1520.

[61] N. Sivakumar, A. Narayanasamy, C. N. Chinnasamy and B. Jeyadevan, J. Phys.: Condens. Matter, 2007, 19, 386201.

[62] A. Rana, O. P. Thakur and V. Kumar, Mater. Lett., 2011, 65, 3191.

[63] R. S. Devan, B. K. Chougule, Journal of Applied Physics 101, (2007)014109.

[64] K.M. Batoo, S. Kumar, C.G. Lee, Alimuddin, Curr. Applied Phys. 9 (2009) 826.

[65] A.K. Singh, T.C. Goel, R.G. Mendiratta, O.P. Thankur, C. Prakash, J Appl Phys. 91 (2002) 6626–6629.

[66] M. R. Bryce and Michael C. Petty, Nature 374 (1995) 771-776.

[67] S. Sagadevan, Kaushik Pal, Zaira Zaman Chowdhury, M. Enamul Hoque, J Sol-Gel Sci Technol, (2018).

[68] C. C. Naik, A. V. Salker, Journal of Materials Science: Materials in Electronics (2017).

[69] A.G Bhosale and B. K. Chougule Materials Letters 60, (2006), 3912-3915.

[70] D. Ravinder, P. Vijaya and B. Reddy, J. Magn.Magn.Mater, 263, (2003), 127- 133.

Chapter 7

Conclusion

Rare earth-doped ferrites constitute a compelling class of materials that have captured the attention of researchers across various disciplines. These materials, arising from the controlled incorporation of rare earth elements (REEs) into ferrite lattices, exhibit intriguing properties that transcend those of their pristine counterparts. This research aims to elucidate the multifaceted nature of rare earth-doped ferrite materials, encompassing their structural, magnetic and electrical attributes. By harnessing the synergistic effects between REEs and ferrites, researchers have unlocked a wealth of possibilities for tailored applications in industries ranging from electronics to biomedicine.

The introduction of rare earth elements imparts unique attributes to ferrite materials, enriching their intrinsic characteristics. We explore the modification of magnetic properties, including enhanced saturation magnetization, improved coercivity, and tunable magnetic anisotropy. Moreover, the influence of rare earth doping on electrical resistivity, dielectric constants properties is examined in detail. These property enhancements underpin the widespread interest in rare earth-doped ferrites for various technological applications.

In this thesis, synthesis of three series of rare earth elements (Gadolinium (Gd^{+3}), Neodymium (Nd^{+3}), Dysprosium (Dy^{+3})) doped cobalt ferrite with chemical composition $CoFe_{2-x}RE_xO_4$ (x = 0.00, 0.02, 0.04, 0.06, 0.08 and 0.10) has been carried out using combustion method to investigate the effects of rare earth doping on structural , magnetic and electrical properties of Cobalt ferrite.

7.1 Gadolinium (Gd^{+3}) doped $CoFe_2O_4$

The Gadolinium (Gd^{+3}) doped Cobalt ferrites with chemical composition $CoFe_{2-x}Gd_xO_4$ (x = 0.00, 0.02, 0.04, 0.06, 0.08, 0.10) sample series were prepared using combustion method to study the effect of increasing low concentrations on structural, magnetic and electrical properties for these nanomaterials.

From x-ray diffraction pattern, the simple cubic spinel structure is formed without any impurity. The structural parameters such as lattice constant, mass density and x-ray density showed an increase with increasing concentration of Gd^{+3}. The value of lattice constant is seen to increase from 8.3863 Å to 8.3998 Å as the concentration of Gd^{+3} increases from 0.00 to 0.10. The crystallite size is found to decrease from 40 nm to 24 nm as the concentration of Gd^{+3} increases from 0.00 to 0.10. However, the % Porosity of the materials showed a non linear trend with increasing Gd^{+3} concentrations. Fourier transform infrared spectra showed two bands, one at octahedral site and other at tetrahedral site in the wave number range from 390 cm^{-1} – 700 cm^{-1}. These two absorption bands confirm the formation of spinel ferrites structure in the material. Scanning electron micrograph showed spherical shape particle with large agglomeration in the particles and the agglomeration in the particles increases with Gd^{+3} concentration.

Transmission electron micrographs are used to confirmed the reduction in particle sizes with increasing Gd^{+3} concentration and was attributed to the strain introduced in the crystal structure due to incorporation of larger ion Gd^{+3} at the octahedral site. Energy dispersive spectroscopy analysis confirms the presence of Co, Fe, Gd and O elements in the prepared samples and no other impurity elements are found within the experimental limits of the instruments.

The magnetic measurement was recorded for hysteresis loop and magnetic parameters such saturation magnetization (Ms), coercivity (Hc), remanence magnetization (Mr), squarness loop is extracted from hysteresis curve. The study of zero field cooled (ZFC) and field cooled (FC) at constant field for the samples has been carried out. To measure Curie temperature of a sample material, AC susceptibility measurement was recorded.
The saturation magnetization was seen decrease with increasing Gd^{+3} concentrations from x = 0.02 to x = 0.08 and then increases for the concentration at x= 0.10. Coercivity of the materials showed a decrease with increasing Gd^{+3} concentrations.
Remanence magnetization was observed to decrease with increasing Gd^{+3} concentration except for the concentration at x= 0.10. The squareness loop showed a mixed trend with increasing Gd^{+3} concentrations and values lies between 0.392- 0.450. The ZFC and FC measurement with increasing temperature from 50K to 400K at 500 Oe constant magnetic field shows presence of irreversibility temperature but blocking temperature is not observed. The AC susceptibility measurement showed reduction in the curie temperature of the samples with increase in the Gd^{+3} concentrations.

The electric properties such as resistivity, dielectric constant, dielectric loss tangent as function of frequency and temperature has been studied. The thermoelectric power as function of temperature from room temperature to $500^{O}C$ was investigated. The resistivity initially increases in low temperature range from room temperature to $80^{O}C$, and then remains constant in the temperature range from $80^{O}C$ – $107^{O}C$ and finally decreases in the temperature range from $107^{O}C$ - $500^{O}C$. Dielectric constants as a function of frequency decreases with increasing frequencies and remains constant at high frequencies. Dielectric loss as a function of frequency shows slight increase for low frequencies and then decreases with increasing frequencies and remains constant at high frequencies. Dielectric constants variation with temperature as a function of frequency shows peak behavior in low temperature range and then increases with increasing temperature. The value of dielectric constant found to decrease with increase in Gd^{+3} concentrations. Dielectric loss variations with temperature as a function of frequency showed an increase with increasing temperature. The peaks behavior is not prominent in low temperature range and the value of dielectric loss decreases with increase in Gd^{+3} concentrations. The variation of thermoelectric power with temperature shows that initially charge carriers are p-type which changes to n-type charge carriers in the transition temperature range from $67^{O}C$ – $122^{O}C$.

7.2 Neodymium (Nd^{+3}) doped cobalt ferrite

The neodymium (Nd^{+3}) doped Cobalt ferrites with chemical composition $CoFe_{2-x}Nd_xO_4$ (x= 0.00, 0.02, 0.04, 0.06, 0.08, 0.10) sample series were prepared using combustion method to study the effect of increasing low concentrations on structural, magnetic and electrical properties for these nanomaterials.

The X-ray diffraction pattern confirmed the formation of the simple cubic spinel structure without any impurity. The structural parameters such as mass density and x-ray density showed an increase with increasing concentration of Nd^{+3}. The value of lattice constant shows mixed trend, on an average it increases from 8.4064 Å to 8.3944 Å as the concentration of Nd^{+3}increases from 0.00 to 0.10. The crystallite size is found to decrease from 35 nm to 18 nm as the concentration of Nd^{+3}increases from 0.00 to 0.10. The % Porosity of the materials decreases with slight increase at $x = 0.06$ and $x = 0.08$ with increase in Nd^{+3} concentrations. Fourier transform infrared spectra shows two bands, one at octahedral site and other at tetrahedral site in the wave number range from 370 cm^{-1} – 700 cm^{-1}. These two absorption bands confirm the formation of monophasic ferrites structure in the material. Scanning electron micrograph shows spherical shape particle with large agglomeration in the particles and the agglomeration in the particles increases with Nd^{+3} concentration. The reduction in particle size was due to increasing strain caused by Nd doping was confirmed using Transmission electron micrographs. Energy dispersive spectroscopy analysis confirms the presence of Co, Fe, Nd and O elements in the prepared samples and no other impurity elements are found within the experimental limits of the instruments. The saturation magnetization was seen to decrease with increasing Nd^{+3} concentrations.Coercivity of the materials showed a decrease with increasing Nd^{+3} concentrations. Remanence magnetization decreases with increasing Nd^{+3} concentration.The squareness loop showed a decrease with increasing Nd^{+3} concentrations and values lie between 0.501 - 0.342. The ZFC and FC measurement with increasing temperature from 50K to 400K at 500 Oe constant magnetic field shows presence of irreversibility temperature but blocking temperature is not observed. The AC susceptibility measurement shows that the Curie temperature of the samples decreases with increase in the Nd^{+3} concentrations.

The resistivity initially increases in low temperature range from room temperature to $65^{O}C$, and then remains constant in the temperature range from $65^{O}C$ – $97^{O}C$ and finally decreases in the temperature range from $97^{O}C$ -$500^{O}C$. Dielectric constants as a function of frequency shows decrease with increasing frequencies and remain constant at high frequencies. Dielectric loss as a function of frequency shows slight increase or broad peaks for low frequencies and then decreases with increasing frequencies and remains constant at high frequencies.Dielectric constants variation with temperature as a function of frequency shows peak behavior in low temperature range and then increases with increasing temperature. The value of dielectric constant found to decrease with increase in Nd^{+3} concentrations. The intensity of peaks decreases with increase in Nd^{+3} concentrations.Dielectric loss variations with temperature as a function of frequency shows increase with increasing temperature. The peaks behavior is observed in low temperature range and the value of dielectric loss decreases with increase in Nd^{+3} concentrations. The variation of thermoelectric power with temperature shows that initially charge carriers are p-type which changes to n-type charge carriers at the transition temperature which varies between $65^{O}C$ – $128^{O}C$.

7.3 Dy^{+3} doped cobalt ferrites

Rare earth element Dysprosium (Dy^{+3}) doped cobalt ferrites with chemical composition $CoFe_{2-x}Dy_xO_4$ (x = 0.00, 0.02, 0.04, 0.06, 0.08, 0.10) sample series were prepared using combustion method to study the effect of increasing low concentrations on structural, magnetic and electrical properties for these nanomaterials. The x-ray diffraction pattern confirmed the formation of spinel structure without any impurity.

The structural parameters such as lattice constant, mass density and x-ray density showed an increase with increasing concentration of Dy^{+3}. The lattice constant value decreases from 8.375 Å to 8.379 Å as the concentration of Dy^{+3}increases from 0.00 to 0.10. The crystallite size is found to decrease from 35 nm to 19 nm as the concentration of Dy^{+3}increases from 0.00 to 0.10. The % Porosity of the materials decreases with increase in Dy^{+3} concentration.Fourier transform infrared spectra shows two bands, one at octahedral site and other at tetrahedral site in the wave number range from 390 cm^{-1} – 700 cm^{-1}. These two absorption bands confirm the formation of spinel ferrites structure in the material.Scanning electron micrograph shows spherical shape particle with large agglomeration in the particles and the agglomeration in the particles increases with Dy^{+3} concentration. Transmission electron micrographs are used to confirm the reduction in particle size with increasing Dy^{+3} concentrations. Energy dispersive spectroscopy analysis confirms the presence of Co, Fe, Dy and O elements in the prepared samples and no other impurity elements are found within the experimental limits of the instruments.

The saturation magnetization shows decrease with concentrations for Gd^{+3}, Nd^{+3} and Dy^{+3} series from x = 0.02 - 0.06. The Gd series shows increase for x= 0.10 concentration where as in Dy series it increases from x = 0.08 - 0.10. Coercivity of the materials showed a decrease with increasing Dy^{+3}concentrations. Remanence magnetization shows mixed trend with increasing Dy^{+3}concentration. The squareness loop shows decrease with increasing Dy^{+3}concentrations and values lies between 0.498 - 0.371. The ZFC and FC measurement with increasing temperature from 50K to 400K at 500 Oe constant magnetic field shows the presence of irreversibility temperature but blocking temperature is not observed. The AC susceptibility measurement showed that the Curie temperature of the samples decreases with increase in the Dy^{+3}

concentrations.The resistivity initially increases in low temperature range from room temperature to 80^{O}C, and then remains constant in the temperature range from 80^{O}C – 107^{O}C and finally decreases in the temperature range from 107^{O}C -500^{O}C. Dielectric constants as a function of frequency showed decrease with increasing frequencies and remain constant at high frequencies. Dielectric loss as a function of frequency shows slight increase or broad peaks for low frequencies and then decreases with increasing frequencies and remains constant at high frequencies. Dielectric constants variation with temperature as a function of frequency showed peak behavior in low temperature range and then increases with increasing temperature. The value of dielectric constant was found to decrease with increase in Dy^{+3} concentrations. Dielectric loss variation with temperature as a function of frequency shows increase with increasing temperature. The peaks behavior is observed in low temperature range and the value of dielectric loss decreases with increase in Dy^{+3} concentrations. The variation of thermoelectric power with temperature shows that initially charge carriers are p-type which changes to n-type charge carriers at the transition temperature which lies between 87^{O}C – 128^{O}C.

7.4 Comparative study of Gd^{+3} doped Cobalt ferrites, Nd^{+3} doped Cobalt ferrites and Dy^{+3} doped Cobalt ferrite series

From x-ray diffraction pattern, all the three sample series – Gd^{+3}, Nd^{+3} and Dy^{+3} Cobalt ferrites shows the formation of spinel structure without any impurity.

The structural parameters mass density and x-ray density showed an increase with increasing concentration for Gd^{+3}, Nd$^{+3,}$ and Dy^{+3} doped series. The lattice constant increases with increase in concentrations of Gd^{+3} and Dy^{+3} whereas for Nd^{+3} series lattice constant decreases with increase in concentrations.

The crystallite size is found to decrease with increasing concentrations for all three series. The smallest crystallite size obtained is 18 nm for Nd series and the largest value of crystallite size 40 nm is obtained for Gd series. The % Porosity of the materials decreases with increasing concentrations for all three series. Fourier transform infrared spectra shows two bands, one at octahedral site and other at tetrahedral site in the wave number range from 390 cm^{-1} – 700 cm^{-1}. These two absorption bands confirm the formation of spinel ferrites structure in the Gd^{+3} doped, Nd^{+3} doped and Dy^{+3} doped sample materials. Scanning electron micrograph shows spherical shape particles with large agglomeration for all three series. Transmission electron micrographs confirmed the reduction in particle sizes with increasing rare earth concentrations. Energy dispersive spectroscopy analysis confirms the presence of Co, Fe, O and respective rare earth element in all three prepared samples series and no other impurity elements are found within the experimental limits of the instruments. The saturation magnetization shows decrease with Dy^{+3} concentrations up to x=0.06 and increases from x= 0.08 - 0.10. Coercivity of the materials shows decrease with increasing rare earth concentrations. Remanence magnetization shows decrease for Gd and Nd doped series and for Dy^{+3} it shows mixed trend with increasing concentration. The squareness loop decreases with increasing rare earth concentration for Gd^{+3}, Nd^{+3} and Dy^{+3} series. The ZFC and FC measurement with increasing temperature from 50K to 400K at 500 Oe constant magnetic field shows presence of irreversibility temperature but blocking temperature is not observed. The AC susceptibility measurement shows that the curie temperature of the samples decreases with increase in rare earth concentrations.

Initially there is an increase in the resistivity in low temperature region and then it remains constant and finally decreases with increase in the temperature. Dielectric constants as a function of frequency shows decrease with increasing frequencies and remain constant at high frequencies. Dielectric loss as a function of frequency shows slight increase or broad peaks for low frequencies and then decreases with increasing frequencies and remains constant at high frequencies. Dielectric constants variation with temperature as a function of frequency shows peak behavior in low temperature range and then increases with increasing temperature. The value of dielectric constant found to decrease with increase in rare earth concentrations. Dielectric loss variation with temperature as a function of frequency shows increase with increasing temperature. The peaks behavior is observed in low temperature range and the value of dielectric loss decreases with increase in rare earth concentrations. The variation of thermoelectric power with temperature shows that initially charge carriers are p-type which changes to n-type charge carriers at the transition temperature.

7.5 Future Scope of work

The potential for future research endeavors in the realm of rare earth element (REE) doped cobalt ferrites, synthesized through combustion methods, is undeniably promising and poised to make significant contributions across diverse domains. The utilization of combustion synthesis in crafting Cobalt ferrite materials infused with rare earth elements offers the prospect of heightened properties and novel applications. This article explores several compelling trajectories for forthcoming investigations and practical implementations within this domain: To fully harness these promising opportunities, forthcoming research must concentrate on refining the combustion synthesis process or other processes to attain meticulous control over material composition, morphology, and inherent properties. Furthermore, the utilization of comprehensive characterization techniques and theoretical models is imperative to gain deeper insights into the intricate relationships that govern composition, structure, and overall performance. Collaboration amongst diverse disciplines, including materials scientists, chemists, physicists, and engineers, will be pivotal in propelling this field forward and effectively translating these enriched materials into tangible and practical real-world applications.

APPENDIX

➢List of publications

1. “Influence of B- site Gd^{+3} substitutions on various properties of Co - ferrite nanoparticles” Manoj Salgaonkar1, R. S. Gad, Applied Physics A, Materials Science and processing (2021) 127:86

2. “Influence of B-site Dy^{+3} substitutions on structural, magnetic, and electrical properties of cobalt ferrite nanoparticles” ManojSalgaonkar, P.R. Naik, R S Gad (Communicated)

3. Nd^{+3} doped cobalt nanoparticles (Yet to be communicated)

➢PRESENTATION / PARTICIPATION IN NATIONAL / INTERNATIONAL SEMINAR

1.Presented a research paper (oral presentation) on " Effect on Structural, Magnetic And Electrical Properties Of Gd doped cobalt ferriteNanoparticles" in an 4th International conference on Nanoscience and Nanotechnology ICONN- 2017, organised by physics and nanotechnology, SRM university India held during 9th to 11th August 2017 in association with Shizuoka university - Japan, GNS Science - New Zealand and National Chio Tung University - Taiwan co-sponsored by Science and Engineering Research Board (DST-SERB) and Council of Scientific And Industrial Research (CSIR) India.

2. Presented a research paper (presentation) on "Structural and Electrical properties of Nd+3 doped cobalt ferrite nanoparticles prepared using combustion method" in an International conference on Smart Materials and Nanotechnology ICSMN – 2020 held at SPSPM SKN Sinhgad College of Engineering Korti, Pandharpur, Maharashtra, India on January 02-04, 2020.

➢WORKSHOP ATTENDED

1. Attended a two days workshop on **Material Science** between University of Porto, University of Coimbra and Goa University held on November 18th and 19th 2019 at Goa University.